An investigation into the effect of atovaquone on clinical parameters of tumour hypoxia: a window of opportunity study in patients with non-small cell lung carcinoma

A thesis submitted for the degree of Doctor of Philosophy in Oncology

Department of Oncology

Jesus College

University of Oxford

Trinity Term, 2019

Dr Michael Skwarski

BSc (hons) MBChB (hons) MRCP FRCR

ABSTRACT

In no other tumour type is the need to improve tumour radiation response more evident than in non-small cell lung cancer (NSCLC), where exceptionally poor radiotherapy outcomes are part of everyday clinical practice. As tumour hypoxia confers profound resistance to radiation, there is significant interest in developing novel hypoxia modifiers as radiosensitisers.

Previous attempts to address tumour hypoxia have largely focused on improving tumour oxygen supply. However, despite decades of clinical trials combining promising agents with radiotherapy, no hypoxia modifiers are in widespread clinical use. The reasons for this include an absence of clinical studies confirming hypoxia modulation and a lack of validated methods to evaluate tumour hypoxia in order to select patients for treatment.

An entirely new strategy to tackle hypoxia is to reduce tumour oxygen consumption through inhibition of oxidative phosphorylation. Recently, the commonly prescribed antimalarial drug atovaquone has been discovered as the most promising agent for this purpose. The translational research presented in this thesis represents a carefully measured approach in developing atovaquone as a clinical radiosensitiser. The first aim of this work was to design and conduct a clinical trial to confirm that atovaquone reduces tumour hypoxia in patients. The Atovaquone as a Tumour hypOxia Modifier (ATOM) trial was a 'window of opportunity' study in patients with resectable NSCLC and used a multitude of methods to investigate the effect of atovaquone on tumour hypoxia. These included hypoxia PET imaging with FMISO and FAZA PET-CT, perfusion CT and measurement of the endogenous plasma hypoxia markers VEGF, CAIX, OPN and miR-210. Following tumour resection, extensive tumour immunohistochemical analysis was also conducted for CAIX and for exogenous pimonidazole. In recognition of the importance of developing

clinical hypoxia biomarkers, the second aim of this work was to assess the validity of the techniques used by performing correlative analysis of the numerous endpoints of this study.

An exciting finding from this work was that atovaquone treatment rapidly reduced tumour hypoxia in the vast majority of patients, as measured by hypoxia PET imaging. This represents the first clinical confirmation of proof of principle not only for atovaquone as a hypoxia modifier, but also for this new approach in tackling tumour hypoxia by reducing oxygen consumption.

Regarding the evaluation of hypoxia biomarkers, a lack of agreement was generally observed between endogenous hypoxia markers, as well as between such markers and hypoxia PET imaging. This highlights the well-recognised challenge of evaluating tumour hypoxia using surrogate measures. However, correlation between plasma miR-210 expression and hypoxia PET imaging was observed, thus providing provisional support that this recently discovered circulating marker may hold more promise as a clinical hypoxia biomarker in NSCLC.

Given the convincing reduction in tumour hypoxia observed following atovaquone treatment in this study, a new clinical trial has been developed which will combine this agent with chemoradiotherapy in patients with NSCLC.

For patient 10019, who told me his biggest regret was that

he will not have the chance to see the results of this research

ACKNOWLEDGEMENTS

First and foremost, I would like to sincerely thank all the lung cancer patients and their families for taking part in this clinical research project. As I got to know each patient, I became increasingly struck and humbled by their generosity and willingness to contribute at what was an immensely difficult time in their lives.

I am indebted to my supervisors Professor Geoff Higgins and Professor Fergus Gleeson for the opportunity to undertake this DPhil and for their expert guidance throughout. In particular, I would like to acknowledge Geoff's daily supervision, which provided necessary support, direction and freedom in perfect measure. I am also thankful to Geoff for his invaluable career mentorship. I remember being told that my DPhil experience will largely depend upon my supervisor, and I am pleased to say that the last four years have been a pleasure in every respect.

My DPhil project involved running a complex clinical window of opportunity study, the successful delivery of which relied on innumerable clinical and research professionals.

I am especially grateful to Mrs Elizabeth Belcher, Mr Francesco Di Chiara and Mr Dionisio Stavroulias for their enthusiasm for this study and for helping to recruit their patients. In addition, I am thankful to have been welcomed to surgical theatre and to have had the opportunity to witness their surgical wizardry. The research nurse Mrs Jennie Derham played a key role in coordinating trial interventions and provided invaluable support for patients throughout the study.

I would also like to thank Dr Mark McCole for dedicating countless hours for the meticulous processing of resected specimens and for overseeing the immunohistochemical analysis. I would like to acknowledge Mr Marcus Green for his advice about

immunohistochemistry and for the generation of the truly monumental number of tumour sections which enabled extensive analysis to be performed. Dr Philip Macklin, Dr Joshua Bull and Dr Alistair Easton deserve special recognition for their help with tumour immunohistochemical annotation and scoring.

Scheduling patients for multimodality imaging at exceedingly short notice was only made possible by Mrs Lisa Meade and Mr Paul Murphy always managing to accommodate trial patients by reorganising the clinical workload of a busy radiology department. I would like to recognise all the dedicated radiographers who performed the scans and often stayed late into the evening to do so. Special thanks to Dr Daniel McGowan for overseeing all elements of trial imaging and for teaching me the methodology required for imaging analysis. I am extremely grateful to Dr Ruth Macpherson for her patient help with tumour outlining and for orientation of the resected specimens.

Key laboratory personnel included Mrs Lisa Folkes, Mrs Leticia Campo and Dr Remko Prevo who helped with sample analysis and ensured required trial standards were always upheld. I would also like to thank Remko for his support and advice throughout my DPhil and for reviewing this thesis.

I would like to take the time to acknowledge the support I have received from all my family and friends. In particular, I feel fortunate to have been championed in all professional and academic endeavours by my parents and my undertaking of this DPhil was no exception. Lastly, I would like to thank my partner Gastón for inspiring me to become ever more inquisitive and for proof-reading this thesis together under the pine trees of University Parks.

PUBLICATIONS AND AWARDS RELATED TO THESIS

PUBLICATIONS

Skwarski M*, McGowan DR*, Bradley KM, Campo L, Fenwick JD, Gleeson FG, Green M, Horne A, Maughan TS, McCole MG, Mohammed S, Muschel RJ, Ng SM, Panakis N, Prevo R, Strauss VY, Stuart R, Tacconi EMC, Vallis KA, McKenna WG, Macpherson RE, Higgins GS. Buparlisib with thoracic radiotherapy and its effect on tumour hypoxia: a phase I study in patients with advanced non-small cell lung carcinoma. Eur J Cancer 2019;113:87-95. *Joint first authors

Skwarski M and Higgins GS. A new roadmap to improve translation of imaging biomarkers. Br J Cancer 2016;115(12):1443-1444.

Coates JT, **Skwarski M**, Higgins GS. Targeting tumour hypoxia: shifting focus from oxygen supply to demand. Br J Radiol 2018;19:20170843.

McGowan DR, **Skwarski M**, Papież BJ, Macpherson RE, Gleeson FV, Schnabel JA, Higgins GS, Fenwick JD. Whole tumor ^{18}F-fluoromisonidazole dynamic PET kinetic analysis and correlations with perfusion CT blood flow estimates in non-small cell lung cancer patients. EJNMMI 2018;8:73.

Papież BJ, McGowan DR, **Skwarski M**, Higgins GS, Schnabel JA, Brady M. Fast groupwise 4D deformable image registration for irregular breathing motion estimation. Published in the 8th International Workshop on Biomedical Image Registration Conference Proceedings, June 2018.

AWARDS

Innovative Protocol Award for the ARCADIAN clinical trial protocol awarded at the ECCO-AACR-EORTC-ESMO Methods in Clinical Cancer Research Workshop. June 2018, Zeist, Netherlands.

Contributed to the successful application for the **CRUK Trial Award** for the ARCADIAN clinical trial. March 2019.

LIST OF KEY ABBREVIATIONS

AE	Adverse events
ALK	Anaplastic lymphoma kinase
ANCOVA	Analysis of covariance
ARCON	Accelerated radiation, carbogen and nicotinamide
ATOM	Atovaquone as a Tumour hypOxia Modifier
BF	Blood flow
BV	Blood volume
CAIX	Carbonic anhydrase IX
CHART	Continuous hyperfractionated accelerated radiotherapy
CI	Confidence interval
CRT	Chemoradiotherapy
CT	Computed tomography
DAHANCA	Danish Head and Neck Cancer
EGFR	Epidermal growth factor receptor
ELISA	Enzyme-linked immunosorbent assay
ETC	Electron transport chain
FAZA	[^{18}F]-fluoroazomycin arabinoside
FDG	[^{18}F]-fluorodeoxyglucose
FFPE	Formalin-fixed paraffin-embedded
FMISO	[^{18}F]-fluoromisonidazole
HBO	Hyperbaric oxygen
HIF	hypoxia-inducible factor
HNSCC	Head and neck squamous cell carcinoma
HV	Hypoxic volume
hyp-PET	Hypoxia-PET

IHC	Immunohistochemistry
IQR	Interquartile range
LA-NSCLC	Locally advanced non-small cell lung carcinoma
LLQ	Lower level of quantification
LRC	Locoregional control
miRNA	microRNA
MTT	Mean transit time
NSCLC	Non-small cell lung carcinoma
OCR	Oxygen consumption rate
OER	Oxygen enhancement ratio
OPN	Osteopontin
OS	Overall survival
OXPHOS	Oxidative phosphorylation
pCT	Perfusion CT
PD-L1	Programmed death ligand 1
PET	Positron emission tomography
PFS	Progression free survival
PI3K	Phosphoinositide 3-kinase
QC	Quality control
ROS	Reactive oxygen species
SABR	Stereotactic ablative body radiotherapy
SCC	Squamous cell carcinoma
SUV	Standardised uptake value
TBR	Tumour-to-blood ratio
TNM	Tumour, node and metastasis
VEGF	Vascular endothelial growth factor
VHL	von Hippel-Lindau

LIST OF FIGURES

Figure 1.1: Lung cancer survival according to stage of disease at presentation 29

Figure 1.2: Diagram of chronic and acute tumour hypoxia 36

Figure 1.3: The oxygen enhancement ratio 39

Figure 1.4: Illustration of the effect of oxygenation on radiosensitivity 40

Figure 1.5: Diagram of X-ray induced DNA damage and the Oxygen Fixation Hypothesis 42

Figure 1.6: Mechanism of nitroimidazole reduction 46

Figure 1.7: Comparison of HIF-1 α expression with pimonidazole binding 50

Figure 1.8: Diagram of oxidative phosphorylation 59

Figure 1.9: Chemical structure of atovaquone 67

Figure 2.1: The ATOM trial schema 77

Figure 2.2: Photograph of resected lung specimen 88

Figure 3.1: CONSORT diagram for Cohort 1 98

Figure 3.2: CONSORT diagram for Cohort 2 99

Figure 3.3: Atovaquone plasma levels 103

Figure 3.4: Comparison of tumour volume between cohorts and histological subtypes 105

Figure 3.5: Effect of atovaquone on tumour volume 107

Figure 3.6: Waterfall plots showing the effect of atovaquone on tumour volume 107

Figure 3.7: Progression free survival and overall survival for atovaquone treated patients 108

Figure 3.8: Comparison of tumour volume between patients with sufficient and insufficient HV 109

Figure 3.9: NSCLC histological subtypes in patients with sufficient and insufficient baseline HV 110

Figure 3.10: Baseline FDG PET SUV_{max} for patients in Cohort 1 and Cohort 2 111

Figure 3.11: Baseline FDG PET SUV_{max} in patients with sufficient and insufficient baseline hypoxia 111

Figure 4.1: Baseline HV, HV%, TBR_{mean} and TBR_{peak} for Cohort 1 and Cohort 2 124

Figure 4.2: Correlation of tumour volume with HV, HV%, TBR_{mean} and TBR_{peak} 125

Figure 4.3: Comparison of HV, HV%, TBR_{mean} and TBR_{peak} between histological subtypes 126

Figure 4.4: Correlation of FDG PET with HV, HV%, TBR_{mean} and TBR_{peak} 127

Figure 4.5: Waterfall plots demonstrating the effect of atovaquone on tumour HV 128

Figure 4.6: Waterfall plots demonstrating the effect of atovaquone on tumour HV using higher TBR thresholds 129

Figure 4.7: Examples of pre- and post-atovaquone treatment FMISO PET-CT scans 129

Figure 4.8: Correlation of tumour HV measurements per patient 131

Figure 4.9: Effect of atovaquone on tumour HV% 132

Figure 4.10: Waterfall plots demonstrating the effect of atovaquone on tumour HV% 133

Figure 4.11: Change in HV% in atovaquone treated and untreated patients 134

Figure 4.12: Effect of atovaquone on TBR_{mean} and TBR_{peak} 135

Figure 4.13: Change in TBR_{mean} and TBR_{peak} in atovaquone treated and untreated patients 137

Figure 4.14: Correlation of plasma atovaquone levels with change in HV 138

Figure 4.15: Baseline pCT perfusion parameters for patients with paired pCT scans 140

Figure 4.16: Baseline pCT perfusion parameters for patients with paired hyp-PET scans 140

Figure 4.17: Effect of atovaquone on pCT parameters 143

Figure 4.18: Change in pCT parameters following atovaquone treatment 144

Figure 4.19: Change in pCT parameters without atovaquone treatment 144

Figure 4.20: Correlation of pCT with hyp-PET parameters 145

Figure 5.1: Effect of atovaquone on plasma levels of VEGF, CAIX and OPN 156

Figure 5.2: Waterfall plots of the effect of atovaquone on plasma VEGF, CAIX and OPN 157

Figure 5.3: Effect of atovaquone on miR-210 expression 163

Figure 5.4: Waterfall plots of the effect of atovaquone on miR-210 expression 163

Figure 5.5: Effect of sample haemolysis on plasma miR-16 and miR-210 164

Figure 5.6: Effect of atovaquone on miR-210 expression in non-haemolysed plasma samples 165

Figure 5.7: Waterfall plots of the effect of atovaquone on miR-210 expression in non-haemolysed plasma samples 165

Figure 5.8: Correlation of plasma hypoxia markers 167

Figure 5.9: Agreement in change in plasma hypoxia markers per individual atovaquone treated patient 168

Figure 5.10: Agreement in change in plasma hypoxia markers per individual untreated patient 168

Figure 5.11: Correlation of tumour volume with plasma hypoxia markers 170

Figure 5.12: Plasma hypoxia markers and tumour histological subtype 171

Figure 5.13: Plasma hypoxia markers and stage of disease 172

Figure 5.14: Correlation of plasma VEGF levels with hyp-PET parameters 173

Figure 5.15: Correlation of plasma CAIX levels with hyp-PET parameters 174

Figure 5.16: Correlation of plasma OPN levels with hyp-PET parameters 175

Figure 5.17: Correlation of miR-210 expression with hyp-PET 176

Figure 5.18: Plasma miR-210 expression and the presence of sufficient baseline hypoxia 177

Figure 5.19: Examples of pimonidazole IHC staining and automated scoring 178

Figure 5.20: Examples of CAIX IHC staining and automated scoring 179

Figure 5.21: Pimonidazole and CAIX positive and negative IHC controls 180

Figure 5.22: Agreement of manual and automated IHC pimonidazole and CAIX scoring 180

Figure 5.23: Pimonidazole IHC percentage scores per tumour level 181

Figure 5.24: CAIX IHC percentage scores per tumour level 182

Figure 5.25: Effect of atovaquone on tumour pimonidazole IHC 184

Figure 5.26: Effect of atovaquone on tumour CAIX IHC 185

Figure 5.27: Correlation between tumour CAIX and pimonidazole IHC 186

Figure 5.28: Correlation between plasma and tumour CAIX 186

Figure 5.29: Correlation of pimonidazole IHC with hyp-PET 187

Figure 5.30: Correlation of CAIX IHC with hyp-PET 188

Figure 6.1: ARCADIAN trial schema 206

LIST OF TABLES

Table 1.1: 8th edition of TNM staging classification for NSCLC 27

Table 1.2: 8th edition of TNM staging classification clinical stage groupings 28

Table 2.1: Main patient eligibility criteria 75

Table 2.2: ATOM trial tumour hypoxia and perfusion related objectives and endpoints 79

Table 3.1: Baseline patient characteristics 101

Table 3.2: Tumour atovaquone levels 104

Table 3.3: Change in tumour volume in atovaquone treated patients 106

Table 3.4: Change in tumour volume in untreated patients 106

Table 4.1: Summary of hyp-PET derived HV, HV%, TBR_{mean} and TBR_{peak} for Cohort 1 and Cohort 2 123

Table 4.2: Change in HV in atovaquone treated patients 130

Table 4.3: Change in HV in untreated patients 130

Table 4.4: Change in HV% in atovaquone treated patients 133

Table 4.5:Change in HV% in untreated patients 134

Table 4.6: Change in TBR_{mean} and TBR_{peak} in atovaquone treated patients 136

Table 4.7: Change in TBR_{mean} and TBR_{peak} in untreated patients 136

Table 4.8: Summary of baseline pCT perfusion parameters for Cohort 1 139

Table 4.9: Summary of baseline pCT perfusion parameters for Cohort 2 139

Table 4.10: Paired and tumour region matched pCT data for atovaquone treated patients 141

Table 4.11: Paired and tumour region matched pCT data for untreated patients 142

Table 4.12: Summary of change in pCT parameters in atovaquone treated and untreated patients 142

Table 5.1: Plasma levels of VEGF, CAIX and OPN for atovaquone treated patients 158

Table 5.2: Plasma levels of VEGF, CAIX and OPN for untreated patients 159

Table 5.3: Relative expression of miR-210 for Cohort 1 161

Table 5.4: Relative expression of miR-210 for Cohort 2 162

Table 5.5: Tumour pimonidazole and CAIX IHC percentage scores for atovaquone treated patients 183

Table 5.6: Tumour pimonidazole and CAIX IHC percentage scores for untreated patients 184

TABLE OF CONTENTS

ABSTRACT II

ACKNOWLEDGEMENTS V

PUBLICATIONS AND AWARDS RELATED TO THESIS VII

LIST OF KEY ABBREVIATIONS VIII

LIST OF FIGURES X

LIST OF TABLES XIV

1 CHAPTER 1: INTRODUCTION 22

1.1 NON-SMALL CELL LUNG CANCER 23

1.1.1 Epidemiology 23

1.1.2 Histological and molecular classification of NSCLC 23

1.1.3 Diagnosis, staging and prognosis 25

1.1.4 Radical treatment of NSCLC 29

1.1.4.1 Surgery and adjuvant chemotherapy 29

1.1.4.2 Radical (chemo)radiotherapy 30

1.1.5 The importance of locoregional control and improving radiotherapy response in NSCLC 31

1.2 TUMOUR HYPOXIA 33

1.2.1 Normal tissue oxygenation 33

1.2.2 Pathogenesis and classification of tumour hypoxia 35

1.2.3 The cellular response to hypoxia: hypoxia-inducible factors 37

1.3 TUMOUR HYPOXIA AS A BARRIER TO RADIOTHERAPY 39

1.3.1 The oxygen enhancement ratio 39

1.3.2 Tumour hypoxia and poor radiotherapy clinical outcomes 42

1.4 MEASURING TUMOUR HYPOXIA IN THE CLINICAL SETTING 44

1.4.1 Direct measurement with oxygen electrodes 44

1.4.2 Exogenous nitroimidazole based methods 45

1.4.2.1 Hypoxia-dependent reduction and retention of nitroimidazole compounds 45

1.4.2.2 EF5 and pimonidazole immunohistochemistry 47

1.4.2.3 Hypoxia PET imaging 47

1.4.3 Endogenous hypoxia markers 49

1.4.3.1 Tumour tissue hypoxia markers 49

1.4.3.2 Circulating hypoxia markers 50

1.5 PREVIOUS HYPOXIA MODIFICATION STRATEGIES WITH RADIOTHERAPY 52

1.5.1 Increasing tumour oxygenation 52
1.5.1.1 Hyperbaric oxygen 52
1.5.1.2 Correction of anaemia 52
1.5.1.3 ARCON 53
1.5.1.4 Vascular 'normalisation' 54
1.5.1.5 'Oxygen mimetics' 54
1.5.2 Hypoxia-activated cytotoxic prodrugs 55
1.5.3 Summary of past approaches 56
1.6 OXIDATIVE PHOSPHORYLATION AS AN EMERGING TARGET TO TACKLE TUMOUR HYPOXIA 56
1.6.1 Overview of cellular respiration 57
1.6.1.1 Glycolysis and anaerobic respiration 57
1.6.1.2 Aerobic respiration: citric acid cycle 57
1.6.1.3 Aerobic respiration: electron transport chain and oxidative phosphorylation 58
1.6.2 Altered metabolism in cancer and the impact of tumour hypoxia 59
1.6.3 Emergence of the importance of OXPHOS in cancer 61
1.6.4 OCR inhibition to alleviate tumor hypoxia 63
1.6.4.1 Rationale 63
1.6.4.2 Known OCR inhibitors including metformin 64
1.6.4.3 Summary of OCR inhibition as a strategy to alleviate tumour hypoxia 65
1.7 ATOVAQUONE AS A NOVEL TUMOUR HYPOXIA MODIFIER AND POTENTIAL ANTI-CANCER TREATMENT 66
1.7.1 Atovaquone as a commonly used antimicrobial 66
1.7.1.1 Discovery and current clinical uses of atovaquone 66
1.7.1.2 Atovaquone antimicrobial pharmacodynamics 67
1.7.1.3 Atovaquone pharmacokinetics 68
1.7.1.4 Toxicity profile 69
1.7.2 Atovaquone as novel tumour hypoxia modifier and radiosensitiser 69
1.8 SUMMARY AND AIMS OF THESIS 71
1.8.1 Summary 71
1.8.2 Aims 72
2 CHAPTER 2: MATERIALS AND METHODS 73
2.1 THE ATOM CLINICAL TRIAL 74
2.1.1 Overview of study design 74
2.1.2 Patients 74
2.1.3 Trial interventions 75
2.1.3.1 Baseline investigations 75
2.1.3.2 Atovaquone treatment 76

2.1.3.3 Follow-up investigations 76
2.1.3.4 Pimonidazole hydrochloride administration 77
2.1.3.5 Surgery, specimen processing and tumour analysis 77
2.1.3.6 Trial schema 77
2.1.3.7 Additional investigations from the ATOM trial 78
2.1.3.8 Confirmation of patient evaluability 78
2.1.4 Trial objectives and endpoints 78
2.2 TUMOUR IMAGING 80
2.2.1 FMISO and FAZA PET-CT 80
2.2.2 Perfusion CT 81
2.3 CIRCULATING MARKERS OF HYPOXIA 82
2.3.1 Plasma collection 82
2.3.2 Enzyme-linked immunosorbent assays for VEGF, CAIX and OPN 82
2.3.2.1 Assay technique 82
2.3.2.2 Quality control 83
2.3.3 TaqMan RT-PCR for miR-210 84
2.3.3.1 Sample preparation and RNA extraction 84
2.3.3.2 Preparation of QC samples 84
2.3.3.3 cDNA synthesis 85
2.3.3.4 TaqMan PCR 86
2.3.3.5 Quality control 87
2.4 TUMOUR PROCESSING AND IMMUNOHISTOCHEMICAL ANALYSIS FOR PIMONIDAZOLE AND CAIX 87
2.4.1 Generation of orientated formalin-fixed paraffin-embedded tumour blocks 87
2.4.2 Tumour immunohistochemical analysis 89
2.4.2.1 Generation of stained sections 89
2.4.2.2 Immunohistochemical analysis 90
2.4.2.3 Quality control of scoring 91
2.5 MEASUREMENT OF PLASMA AND TUMOUR ATOVAQUONE LEVELS 92
2.6 SAFETY AND CLINICAL OUTCOME ANALYSIS 92
2.7 STATISTICAL ANALYSIS 92
3 CHAPTER 3: CLINICAL DATA 94
3.1 INTRODUCTION 95
3.2 RESULTS 96
3.2.1 Trial recruitment and data collected 96
3.2.2 Baseline patient characteristics 100

3.2.3 Atovaquone treatment, drug levels and safety 102
3.2.3.1 Length of treatment and compliance 102
3.2.3.2 Plasma atovaquone levels 103
3.2.3.3 Atovaquone levels in resected tumour tissue 103
3.2.3.4 Safety and toxicity 104
3.2.4 Baseline tumour volume 105
3.2.5 Effect of atovaquone treatment on tumour volume 105
3.2.6 Clinical outcomes for atovaquone treated patients 108
3.2.7 Can clinicopathological features predict sufficient HV on hyp-PET? 108
3.2.7.1 Tumour volume 109
3.2.7.2 Histology 110
3.2.7.3 Diagnostic FDG PET SUV_{max} 110
3.3 DISCUSSION 112
3.3.1 Baseline clinical characteristics and predicting sufficient baseline tumour HV 112
3.3.2 Atovaquone safety and drug levels 114
3.3.3 Effect of atovaquone on tumour volume and clinical outcomes 116
3.3.4 Study design limitations, challenges encountered and lessons for future studies 117
3.4 CONCLUSION 119
4 Chapter 4: TUMOUR HYPOXIA AND PERFUSION IMAGING 120
4.1 INTRODUCTION 121
4.2 RESULTS 122
4.2.1 Baseline tumour hypoxia as measured by hyp-PET 122
4.2.2 Correlation of hyp-PET parameters with clinicopathological features 124
4.2.2.1 Tumour volume 125
4.2.2.2 Tumour histology 126
4.2.2.3 FDG PET SUV_{max} 127
4.2.3 Atovaquone treatment reduces tumour hypoxia as measured by hyp-PET 128
4.2.3.1 Atovaquone treatment reduces tumour HV 128
4.2.3.2 Atovaquone treatment reduces tumour HV% 132
4.2.3.3 Atovaquone treatment reduces tumour TBR_{mean} and TBR_{peak} 135
4.2.4 Correlation of atovaquone plasma levels with change in HV 137
4.2.5 Baseline tumour perfusion as measured by perfusion CT 138
4.2.6 Atovaquone treatment does not alter tumour perfusion as measured by pCT 141
4.2.7 Correlation of pCT and hyp-PET parameters 145
4.3 DISCUSSION 146
4.3.1 Baseline tumour hypoxia profile 146
4.3.2 Atovaquone treatment reduces tumour hypoxia 148

4.3.3 Atovaquone does not alter tumour perfusion 151

5 CHAPTER 5: PLASMA AND TUMOUR TISSUE HYPOXIA MARKERS 153

5.1 INTRODUCTION 154

5.2 RESULTS 155

5.2.1 Atovaquone treatment does not alter plasma VEGF, CAIX and OPN 155

5.2.2 Atovaquone treatment does not alter plasma miR-210 160

5.2.2.1 Impact of plasma sample haemolysis on miR-210 expression 163

5.2.2.2 Effect of atovaquone on plasma miR-210 excluding haemolysed samples 164

5.2.3 Agreement of plasma hypoxia markers 166

5.2.4 Correlation of plasma hypoxia markers with clinicopathological features 169

5.2.4.1 Tumour volume 169

5.2.4.2 Tumour histology 170

5.2.4.3 Stage of disease 171

5.2.5 Can plasma markers replace hyp-PET in future studies? 172

5.2.5.1 Lack of correlation between plasma VEGF, CAIX and OPN and hyp-PET 173

5.2.5.2 Correlation between plasma miR-210 expression and hyp-PET 175

5.2.6 Tumour pimonidazole and CAIX IHC 177

5.2.7 Intra-tumour heterogeneity in pimonidazole and CAIX IHC 181

5.2.8 Effect of atovaquone on tumour pimonidazole and CAIX IHC 182

5.2.9 Correlation between pimonidazole and CAIX IHC 185

5.2.10 Correlation between plasma and tumour CAIX 186

5.2.11 Correlation between hypoxia IHC with hyp-PET 187

5.3 DISCUSSION 188

5.3.1 Plasma VEGF, CAIX and OPN as hypoxia biomarkers 188

5.3.2 Plasma miR-210 as a potential hypoxia biomarker 192

5.3.3 Tumour tissue IHC based hypoxia biomarkers 194

6 CHAPTER 6: FINAL DISCUSSION AND FUTURE WORK 196

6.1 GENERAL DISCUSSION 197

6.1.1 Tumour hypoxia modification past and present 197

6.1.2 Clinical proof of principle of atovaquone as a tumour hypoxia modifier and anti-cancer treatment 198

6.1.3 Hypoxia biomarker development 202

6.2 CURRENT AND FUTURE WORK 204

6.2.1 Ongoing ATOM trial analysis 204

6.2.2 A new clinical trial combining atovaquone with chemoradiotherapy in NSCLC 204

REFERENCES 207

APPENDIX 231

CHAPTER 1: INTRODUCTION

1.1 NON-SMALL CELL LUNG CANCER

1.1.1 Epidemiology

Lung cancer is the most common cancer worldwide with an estimated two million cases diagnosed in 2018 [1]. In the UK, lung cancer represents the third most common cancer with nearly 50,000 new cases diagnosed annually, accounting for 13% of total cancer registrations [2]. Lung cancer has one of the lowest survival outcomes of any cancer with the overall five-year survival rate largely unchanged over recent decades at around 10%. As a result, lung cancer remains a devastating diagnosis and represents by far the leading cause of cancer-related death nationally, representing nearly 25% of cancer deaths [3–6].

Lung cancer is predominantly a disease of advanced age with incidence rising steeply after 50 years and peaking at 80 years [2]. Over the last decade, the difference between incidence of lung cancer in males and females has continued to narrow with the rate decreasing for males whilst increasing for females. This change reflects changes in the patterns of tobacco smoking over the last three decades which, as first prospectively demonstrated by the seminal work of Sir Richard Doll [7], is the major aetiologic risk factor for the development of lung cancer and known to be responsible for approximately 70% of cases [8]. However, the remainder of lung cancer diagnoses cannot be attributed to tobacco exposure and the incidence of never-smokers with lung cancer is in fact increasing. Other risk factors include exposure to asbestos, silica, air pollutants, radon and ionising radiation, as well as positive family history of lung cancer [9,10].

1.1.2 Histological and molecular classification of NSCLC

Traditionally, lung cancer is classified histologically and clinically into two groups: non-small cell lung cancer (NSCLC) and small cell lung cancer. NSCLC accounts for

approximately 80% of cases and represents a highly diverse and heterogeneous group of tumours, as outlined in the most recent World Health Organisation classification [11]. The most common subtypes of NSCLC are adenocarcinoma, squamous cell carcinoma (SCC) and large cell carcinoma, with adenosquamous carcinoma and giant cell carcinoma less common but well-recognised other subtypes.

Immunohistochemistry (IHC) plays a central role in everyday clinical practice in order to determine the NSCLC subtype, especially in tumours which are poorly differentiated or which have atypical morphological appearances. Typically, adenocarcinomas express TTF1 and NapsinA which together with an absence of squamous markers is diagnostic of adenocarcinoma of lung origin. For SCC, positive markers usually include p40, CK5/6, and p63 with negative staining for TTF-1 or NapsinA. To exclude neuroendocrine differentiation, a panel of markers such as chromogranin, synaptophysin and CD56 are commonly used.

In the last decade, molecular testing of adenocarcinoma for key driver genetic alterations has become part of the standard diagnostic pathway. The prevalence of activating and sensitising mutations in exons 18–21 of epidermal growth factor receptor (EGFR) is 10-20% of the Caucasian population with 90% of the most common mutations comprising of deletions in exon 19 and the L858R substitution mutation in exon 21. For such patients, EGFR tyrosine kinase inhibitors, which include gefitinib or erlotinib, are effective agents and represent first line therapy for advanced disease. Fusion genes involving anaplastic lymphoma kinase (ALK) and a number of partners account for around 3%–8% of lung adenocarcinomas, with ALK-driven tumours sensitive to ALK tyrosine kinase inhibitors such as crizotinib [12].

In the now well-established and rapidly expanding era of immunotherapy, IHC tumour testing for expression of programmed death ligand 1 (PD-L1) has become routine practice. This is as a result of the observed clinical benefit of immune checkpoint inhibitors against programmed death 1 (PD-1)/PD-L1 signalling in metastatic setting [13–15], as well as in combination with concurrent chemoradiotherapy in locally-advanced disease [16].

1.1.3 Diagnosis, staging and prognosis

Accurately establishing a diagnosis of NSCLC and determining the stage of disease is crucial in guiding appropriate clinical decision-making. From the onset, careful assessment of a patient's fitness, and therefore the appropriateness for further investigations and treatments, is of particular relevance given this generally elderly and co-morbid patient population. The diagnostic pathway for NSCLC, especially for patients in which radical treatment is being considered, is arguably one of the longest and most complex with numerous investigations required.

When a lung cancer diagnosis is suspected, chest X-ray and subsequently computed tomography (CT) imaging is performed. For fit patients with potentially radically treatable disease, further imaging with whole-body ^{18}F-fluorodeoxyglucose (FDG) positron emission tomography (PET) has become the standard of care in order to more accurately assess spread of disease. FDG PET relies on the fact that malignant tumours typically have high rates of glucose metabolism and subsequently high rates of cellular uptake of this radiolabelled glucose tracer. Shortly after the widespread availability of this imaging modality, it was shown that FDG PET can diagnose malignant pulmonary lesions with a sensitivity of 96.8% and specificity of 77.8% [17]. Modern imaging methods with co-localisation of uptake with simultaneous CT imaging has increased diagnostic accuracy even further. In addition, FDG PET-CT improves accuracy of NSCLC staging with regards

to predicating loco-regional lymph node involvement as well as the presence of distant metastasis. With regards to distant metastasis, in comparison to CT imaging alone, metastatic lesions are identified in an additional 10% of patients by PET-CT [18], thus limiting the number of patients subjected to aggressive and morbid radical treatments which will ultimately prove futile [19].

Tissue sampling can occur through a variety of means and is guided by imaging findings. For proximal tumours, bronchial biopsy at time of bronchoscopy is usually performed, whereas CT-guided percutaneous biopsy is often used for more peripheral lesions. In cases with suspected loco-regional lymph node involvement, endobronchial ultrasound-guided transbronchial needle aspiration (EBUS-TBNA) has now largely replaced more invasive mediastinoscopy with proven high sensitivity (85%) and negative predictive value (86%) [20]. In patients with metastatic disease, a tissue diagnosis is sought from distal sites of disease to confirm advanced stage disease.

Current staging of NSCLC is according to the 8th Edition of the Union Internationale Contre le Cancer (UICC) and American Joint Committee on Cancer (AJCC) tumour, node and metastasis (TNM) staging classification [21], which is shown in Table 1.1, with the corresponding clinical stage groupings (stage I-IV) shown in Table 1.2.

Table 1.1: 8th edition of TNM staging classification for NSCLC

T (primary tumour)		**Label**
T0	No primary tumour	
Tis	Carcinoma in situ	T*is*
T1	Tumour ≤3 cm	
T1a(mi)	Minimally invasive adeno	T1a *(mi)*
T1a	Superficial tumour in central airways	T1a *SS*
T1a	Tumour ≤1cm	T1a *≤1*
TIb	Tumour >1 but ≤2 cm	T1b *>1-2*
TIc	Tumour >2 but ≤3 cm	T1c *>2-3*
T2	Tumour >3 but ≤5 cm or tumour involving:	
	visceral pleura	T2 *Vis Pl*
	main bronchus (not carina)	T2 *Centr*
T2a	Tumour >3 but ≤4 cm	T2a *>3-4*
T2b	Tumour >4 but ≤5 cm	T2b *>4-5*
T3	Tumour >5 but ≤7 cm	T3 *>5-7*
	or tumour invading chest wall, pericardium or phrenic nerve	T3 *Inv*
	or separate nodule(s) same lobe	T3 *Satell*
T4	Tumour >7 cm	T4 *>7*
	or tumour invading mediastinum, diaphragm, heart, great vessels, recurrent laryngeal nerve, carina, trachea oesophagus or spine	T4 *Inv*
	or tumour nodule(s) in different ipsilateral lobe	T4 *Ipsi Nod*
N (regional lymph nodes)		
N0	No regional node metastasis	
N1	Metastasis in ipsilateral pulmonary or hilar nodes	
N2	Metastasis in ipsilateral mediastinal nodes	
N3	Metastasis in contralateral hilar or mediastinal, or supraclavicular nodes	
M (distant metastasis)		
M0	No distant metastasis	
M1a	Malignant pleural/pericardial effusion and/or nodules	M1a *Pl Dissem*
	or separate nodule in contralateral lung	M1a *Contr Nod*
M1b	Single extrathoracic metastasis	M1b *Single*
M1c	Multiple extrathoracic metastases	M1c *Multi*

Table adapted from that shown in [21]
Abbreviations: T, primary tumour; N, nodal metastasis; M, distant metastasis

Table 1.2: 8th edition of TNM staging classification clinical stage groupings

T/M	Label	N0	N1	N2	N3
T1	T1a *≤1*	IA1	IIB	IIIA	IIIB
	T1b *>1-2*	IA2	IIB	IIIA	IIIB
	T1c *>2-3*	IA3	IIB	IIIA	IIIB
T2	T2a *Cent, Vis Pl*	IB	IIB	IIIA	IIIB
	T2a *>3-4*	IB	IIB	IIIA	IIIB
	T2b *>4-5*	IIA	IIB	IIIA	IIIB
T3	All T3	IIB	IIIA	IIIB	IIIC
T4	All T4	IIIA	IIIA	IIIB	IIIC
M1	M1a, M1b	IVA	IVA	IVA	IVA
	M1c	IVB	IVB	IVB	IVB

Table adapted from that shown in [21]
Abbreviations: T, primary tumour; N, nodal metastasis; M, distant metastasis

Unfortunately, the majority of patients are diagnosed with advanced stage disease at presentation: 50% stage IV, 20% stage III and only 30% with stage I or II disease [22]. This is likely to reflect that symptoms of lung cancer are difficult to differentiate from chronic respiratory symptoms experienced by patients with smoking-related lung disease. At present there is growing pressure for the widespread implementation of lung cancer imaging-based screening based on data from a number of recently published trials showing improvements in rates of early detection and outcomes from such an approach [23,24].

The prognosis for NSCLC is largely dictated by the stage of disease at presentation, as shown in Figure 1.1. In England, the one-year survival for patients diagnosed with stage I disease is 83% but only 17% for patients with stage IV disease [25].

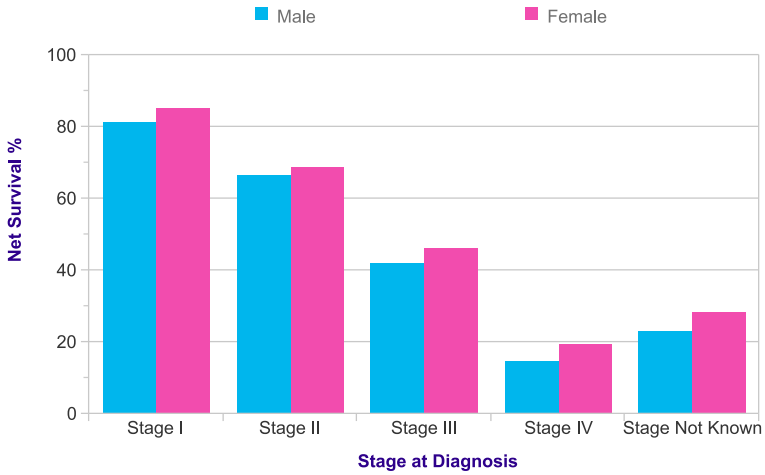


Figure 1.1: Lung cancer survival according to stage of disease at presentation
One-year age standardised net survival by stage for adults in England in 2014. Adapted from [26].

1.1.4 Radical treatment of NSCLC

1.1.4.1 Surgery and adjuvant chemotherapy

Surgery remains the gold standard treatment for medically operable patients with early stage disease (stage I and II). Complete lobectomy, as opposed to sub-lobectomy, has long been the recommended surgical treatment for NSCLC with a solid component due to superior local recurrence and survival outcomes [27]. However, with improvements in surgery and pre-surgical staging, there is growing evidence that for <2 cm lesions such outcomes may be comparable for both surgical approaches [28]. Due to improvements in diagnostic tumour imaging, surgery is increasingly undertaken on a radiological, as opposed to histological diagnosis of lung cancer with benign resection rates widely less than 10% [29].

Following complete resection, adjuvant platinum containing doublet chemotherapy is the standard of care for patients with node positive disease and for patients with tumours ≥ 4 cm due to a proven 4-5% absolute survival benefit at 5 years [30,31].

1.1.4.2 Radical (chemo)radiotherapy

Stereotactic ablative body radiotherapy (SABR) has emerged over the last decade as the treatment of choice in medically inoperable patients with early stage disease which is peripherally located and node negative. SABR typically involves the delivery of 54–60 Gy in three to eight fractions on alternative days with best results observed when the tumour receives >100 Gy equivalent dose in 2 Gy per fraction EQD2 biologically equivalent dose (BED) [32]. As the total treatment length is short and toxicity minimal, SABR has enabled elderly or significantly co-morbid patients to gain access to potentially curative treatment. Long-term follow-up data for SABR has consistently shown excellent five-year local, regional and distant recurrence rates with one notable study reporting such outcomes as 10.5%, 12.7% and 19.9%, respectively [33]. As yet, there is no randomised trial evidence comparing SABR with surgery in early stage disease with numerous prospective and retrospective series reporting similar local control rates and survival outcomes [34,35].

Conventionally fractionated (1.8 to 2 Gy per fraction) radiotherapy to a total dose of 60-66 Gy is the standard of care for adequately fit patients with early stage disease who are medically inoperable and not suitable for SABR or for patients with unresectable locally advanced (stage III) disease. A wide range of radiotherapy dosing and fractionation schedules have been tested over the last few decades. With regards to dose escalation, the Radiation Therapy Oncology Group (RTOG) 0617 randomised phase III clinical trial demonstrated that delivering 74 Gy resulted in inferior survival outcomes with significantly higher rates of toxicity compared with standard dose (60 Gy) radiotherapy [36]. Accelerated hyperfractionated radiotherapy regimes have also been investigated. For example, continuous hyperfractionated accelerated radiotherapy (CHART) which involves delivering 54 Gy in 1.5 Gy fractions three times per day over 12 consecutive days has been

shown to improve local tumour control and OS compared with conventional radiotherapy [37]. However due to only modest benefits observed, concerns regarding toxicity and challenges in practical delivery, hyperfractionated regimes have not been adopted into widespread clinical use.

Specifically for locally advanced disease, multiple meta-analyses have demonstrated a small but clear survival advantage of adding cisplatin doublet chemotherapy to radiation, with concurrent administration shown to be superior to sequential treatment [38,39]. However, concurrent chemoradiotherapy (CRT) is associated with significant treatment-related toxicity, in particular Grade 3 oesophagitis and pneumonitis, and therefore careful assessment of each patient's fitness dictates which specific CRT approach is used in this patient group.

Unfortunately, despite such toxic treatment outcomes have remained exceptionally poor following CRT with five-year overall survival only in the region of 15% [39]. There is, however, growing interest recently in combining immunotherapy to CRT for locally advanced NSCLC. This new approach is based on the highly encouraging results from a recent large randomised phase III study which demonstrated as significant improvement in OS to an unprecedented two-year rate of 65% when the programmed cell death ligand-1 (PD-L1) inhibitor durvalumab was given following completion of CRT [16].

1.1.5 The importance of locoregional control and improving radiotherapy response in NSCLC

It is well-accepted that the poor outcomes following radiotherapy in locally advanced disease are in part due to inadequate local and locoregional control (LRC) [40]. Many CRT studies have demonstrated that despite administration of different regimes, local tumour

control rates are only in the region of 40-66% [41]. Although one could argue that as a significant proportion of this patient population will succumb relatively quickly to distant disease following treatment, and therefore that local disease control is less important, there is Level 1a evidence that LRC directly impacts survival. For example, in the meta-analysis which demonstrated that concurrent CRT improved five-year OS by 5% as compared with sequential treatment, this improvement was associated with an increase in five-year LRC rate of 6% without reducing the frequency of distant metastases [39]. This has led some authors to suggest that there may be a 1:1 ratio linking LRC with OS in this patient population [41]. In fact, with improving systemic therapies such as immunotherapy, which may attenuate the competing risk of death from distant disease, the importance of adequate LRC may become more apparent.

The question naturally arises: what is the best strategy to improve radiotherapy LRC in locally advanced NSCLC (LA-NSCLC)? Firstly, accurate delivery of adequate doses of radiotherapy should be a priority and the excellent LRC control and OS rates for SABR highlight this point well. In LA-NSCLC where SABR is not possible, dose escalation of conventionally fractionated radiotherapy has been shown not to translate into improvements in survival, which is likely to be due to the toxicity associated with delivering such high doses of radiation to large treatment volumes typical for this patient population, especially when using older radiotherapy treatment techniques [36]. In fact, in a recent study of CRT using modern radiotherapy techniques with isotoxic treatment planning, encouraging disease response, survival and toxicity rates were reported [42], thus supporting dose escalation but perhaps only in the context of exceptional quality radiotherapy. However, outside of the clinical trial setting in what is generally a borderline fit for treatment population, it is possible that we have reached the end of the road in exploration of radiation dose escalation for LA-NSCLC.

An alternative strategy to improve tumour response to radiotherapy is through the co-administration of tumour radiosensitising agents. Cytotoxic chemotherapy used concurrently with radiotherapy in LA-NSCLC can be viewed as one class of such agents, with as previously described proven improvements in LRC and OS. Otherwise, currently no other agents are available for this purpose. In recognition that developing such agents in NSCLC represents an urgent unmet clinical need, a collaboration between the National Cancer Research Institute Clinical and Translational Radiotherapy Research Working Group (NCRI CTRad) and Lung Clinical Studies Group (NCRI Lung CSG) has been established in the UK resulting in the development of platform studies testing novel drug and radiotherapy combinations.

When considering which possible approaches can be explored to develop novel tumour radiosensitisers, guidance can be sought by referring back to fundamental radiobiological principles. In 1975 Withers summarised the factors which influence the response of normal tissues and tumours to fractionated radiation describing them as the 'four R's of radiotherapy' consisting of: repair, reassortment, repopulation and reoxygenation [43]. Of these, reoxygenation is of key relevance to the remainder of the body of work presented in this thesis. More specifically, this investigation focuses on a novel strategy to manipulate tumour oxygenation with the aim of increasing tumour radiosensitisation and ultimately improving radiotherapy outcomes for patients with NSCLC.

1.2 TUMOUR HYPOXIA

1.2.1 Normal tissue oxygenation

Oxygen is vital for all living cells and plays a primordial role in key cellular activities. Central in our evolution into large and complex multicellular organisms has been the

development of an intricate vascular system to ensure the adequate supply of oxygen to support cellular function [44]. At the ends of the branching vascular network, capillaries provide the blood-tissue interface for oxygen delivery. In terms of distance, the diffusion limit for oxygen in tissue is in the region of 100-200 μm [45], therefore cells must be within this proximity of a functional vessel to ensure adequate oxygenation. Given the limit of oxygen diffusion, tissue oxygenation is not binary, but rather exists in continuous gradients. Interestingly, the permission of low and near sub-physiological levels of oxygen are important for certain normal tissue functions, such as foetal development, tissue healing and liver zonation [46,47]. However, the presence of such low levels of oxygen in healthy tissue is highly restricted and tightly regulated for specific purposes only.

When discussing tissue oxygenation, it is firstly important to define the units used and the relevant nomenclature. Several units are used to report oxygen levels and include the international system pressure unit the Pascal (Pa) beside millimetre of mercury (mmHg) (1 kPa = 7.5 mmHg) and the percentage of oxygen (1 KPa = 1%), both commonly used in medicine. The term ‘normoxia’ refers to the atmospheric oxygen level of 21% (160 mmHg). ‘Tissue normoxia’, also referred to as ‘physioxia’, varies depending on tissue type and is significantly lower than atmospheric normoxia. For example, in outer layers of skin the oxygen levels are in region of 1% (8 mmHg) [48], whilst in lung tissue they are 6% (42 mmHg) [49] and 10% (72 mmHg) in the kidney [50]. It is important to note that these values are significantly lower than the majority of *in vitro* experiments aimed to replicate tissue normoxia, which are conducted using 95% air and 5% carbon dioxide, and thus performed at around 20% oxygen (150 mmHg). The term ‘hypoxia’ should be reserved for oxygen levels below that of the normoxia range for the tissue in question [51], and generally refers to levels below 1-2% (7.5 to 15 mmHg).

1.2.2 Pathogenesis and classification of tumour hypoxia

In contrast to normal tissues, hypoxia is a common finding in solid tumours. The development of tumour hypoxia can be viewed as an imbalance between oxygen supply and demand. Rapid proliferation and high metabolic rates result in high oxygen consumption which quickly surpasses supply. The subsequent hypoxic microenvironment results in the upregulation of angiogenic factors and thus turns on the 'angiogenic switch' stimulating tumour neovascularisation [52], a phenomenon first described over a century ago [53]. However, despite an abundance of new vessels, the resulting microvasculature is invariably highly dysregulated and 'chaotic' [54]. In particular, the vessels are tortuous, friable and leaky. The highly abnormal endothelium results in non-laminar flow and further leakiness predisposes to thrombosis and oedema, which further impedes perfusion [55,56]. Overall, the tumour vasculature is subfunctional and unable to match the oxygen demand of tumours and therefore, hypoxic regions arise.

The paradox that increased tumour angiogenesis can result in decreased perfusion is well-established [57]. In fact, frequently used anti-angiogenesis therapies, such as for example anti-vascular endothelial growth factor (VEGF) agents including bevacizumab, aim to exploit this phenomenon. These drugs improve tumour perfusion by inhibiting uncontrolled angiogenesis, enabling more regulated vessel development and leading to 'vascular normalisation' [58]. When combined with chemotherapy, as is often the case, this results in improved drug delivery to tumours.

Traditionally, tumour hypoxia is classified as either chronic or acute. Chronic hypoxia occurs in tumour regions located beyond the diffusion capacity of oxygen and is fairly stable. In contrast, acute hypoxia, also referred to as transient or cycling hypoxia, refers to regions of dynamic changes in oxygenation with the potential for reoxygenation [59,60].

Transient hypoxia is commonly observed in tumours with *in vivo* studies demonstrating that up to 20% of the tumour volume may be affected [61], with cycle lengths ranging from seconds to days. It is postulated that high frequency hypoxia cycling arises from alterations in vessel perfusion and red cell flux, whereas remodelling of vasculature is responsible for low frequency cycling occurring over a matter of days [62]. Clinically, in patients with head and neck tumours for example, significant change in the location of hypoxic regions has been observed using hypoxia imaging a short number of days apart [63]. Interestingly, chronic and acute hypoxia result in differing cancer cellular signalling responses, thus further highlighting them as distinct pathophysiological entities. An illustration of the difference between chronic and acute hypoxia is shown in Figure 1.2.

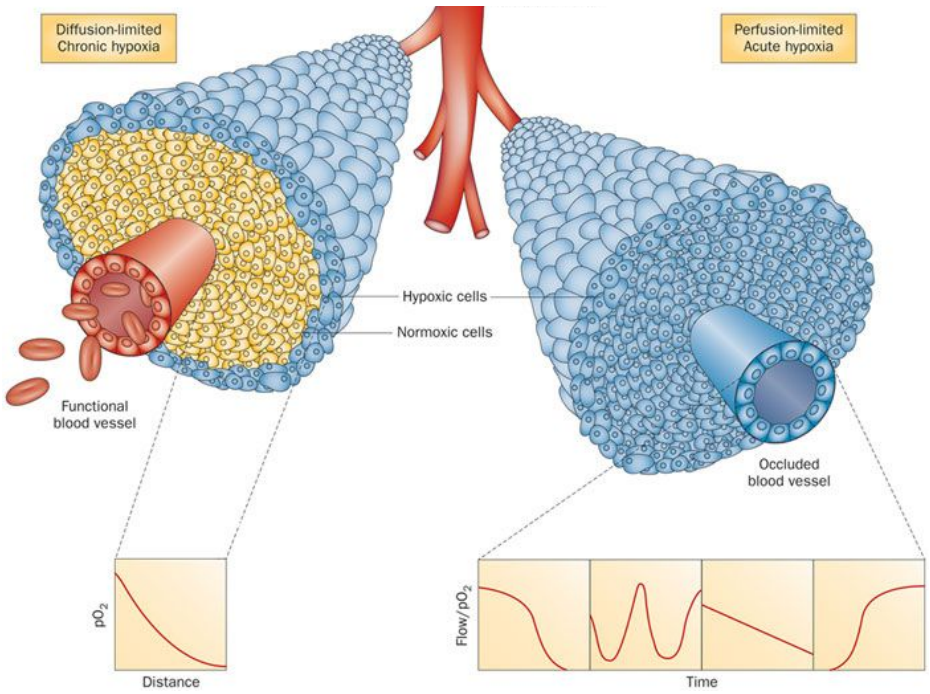


Figure 1.2: Diagram of chronic and acute tumour hypoxia
Tumour cells growing around a functional vessel are shown on the left with oxygen levels falling with increasing distance from the vessel with subsequently hypoxic cells at the outer edge of the tumour cord. Acute hypoxia is shown on the right with hypoxic cells throughout the whole tumour due to vessel occlusion. Possible corresponding changes in blood flow/oxygenation over time are also shown. Adapted from [64], license 4661530558561.

Overall, due to the complex spatiotemporal distribution of tumour hypoxia, accurate characterisation of hypoxia within tumours is challenging with results from sample-based measurement potentially not representative of the tumour as a whole. Nevertheless, the presence of measurable hypoxia is an almost universal feature of tumours. Certain tumour types have consistently been shown to contain higher levels of hypoxia than others [65]. For example, polarographic oxygen electrode measurements in patients with NSCLC have shown median oxygen levels ranging from 14-17 mmHg [49,66], whilst in head and neck squamous cell carcinoma (HNSCC) the average level was 9 mmHg [65,67] and only in the region of 2 mmHg in prostate cancer [68,69], therefore highlighting an additional layer of complexity in the study of tumour hypoxia.

1.2.3 The cellular response to hypoxia: hypoxia-inducible factors

Central to the cellular response to hypoxia are the hypoxia-inducible factors (HIFs) – the principal oxygen sensing machinery. The HIF family of transcription factors includes the well-studied HIF1 and HIF2, as well as HIF3. Each of these factors consists of an oxygen-sensitive and tightly regulated HIF-α subunit (HIF1-α, HIF2-α or HIF3-α, respectively), which forms a heterodimer with a constitutively expressed HIF1-β subunit (also known as ARNT) [70]. The HIF-α subunit contains two highly preserved proline residues (HP402/P564 for HIF1-α and P405/P531 for HIF2-α) which are hydroxylated in the presence of oxygen by prolyl hydroxylase domain-containing proteins (PHDs). This in turn permits binding to the von Hippel-Lindau (VHL) tumour suppressor protein, leading to HIF-α ubiquitination and its targeting for degradation [71,72]. Under hypoxic conditions, HIF-α is stabilised through decreased hydroxylation, allowing binding with HIF1-β and translocation to the nucleus where it recognises and binds to hypoxia-responsive elements (HREs), resulting in the transcription of a multitude of target genes [73].

An additional layer of HIF regulation occurs at the level of recruitment of coactivators. Further oxygen-dependent hydroxylation of HIF1-α, and to a lesser extent HIF2-α, occurs on the C-terminal transactivation domain on aspartate reside 803 by factor inhibiting HIF1 (FIH) [74,75], which results in the inability of HIF1 to transactivate certain target genes [76]. The oxygen tension required to inactivate FIH is lower than that of the PHDs [77], thus enabling a graded transcriptional response dependent upon the severity of hypoxia.

HIF1-α and HIF2-α have differing expression profiles in tissues and tumours, with expression of HIF1-α ubiquitous whereas HIF2-α far more restricted [78]. Together with the difference in their target genes, this provides a differential HIF-responsive transcriptome dependent on tissue and tumour type. Further still, in chronic hypoxia, HIF1-α levels rapidly increase and are stabilised within hours but within days decrease to much lower expression levels [79]. HIF1 has been shown to upregulate PHDs which appear to retain enough activity to hydroxylate HIF1-α even under lower oxygen tensions, resulting in its reinstated degradation [79,80]. In contrast, cycling hypoxia results in an enhanced activity and stabilisation of HIF1-α, at much greater levels than witnessed in chronic hypoxia [81].

The sophisticated regulation of HIF signalling eludes to its importance in regulating wide-ranging aspects of cellular function, with an ever-growing number of HIF target genes identified [82,83]. Perhaps therefore unsurprisingly, hypoxia-related HIF signaling contributes significantly to tumourigenesis by directly contributing to the majority of the hallmarks of cancer, with its effects ranging from stimulation of invasion and metastasis, to promotion of sustained proliferation and immune system evasion [84–86]. Overall, through such means, tumour hypoxia results in an aggressive tumour phenotype.

1.3 TUMOUR HYPOXIA AS A BARRIER TO RADIOTHERAPY

There is overwhelming evidence that tumour hypoxia significantly impedes the tumour radiation response and subsequently leads to poor clinical outcomes in patients treated with radiotherapy.

1.3.1 The oxygen enhancement ratio

As demonstrated nearly three quarters of a century ago by the seminal work of Thomlinson and Gray, the cellular response to ionising radiation is highly dependent upon the presence of oxygen [87–89]. In the majority of cell types studied, the ratio of radiation dose required under severely hypoxic or anoxic conditions versus normoxic conditions to achieve the same biological effect, termed the oxygen enhancement ratio (OER), is typically 2.5 to 3.5 for low linear energy transfer ionising radiation such as X-rays or γ-rays, as shown in Figure 1.3.

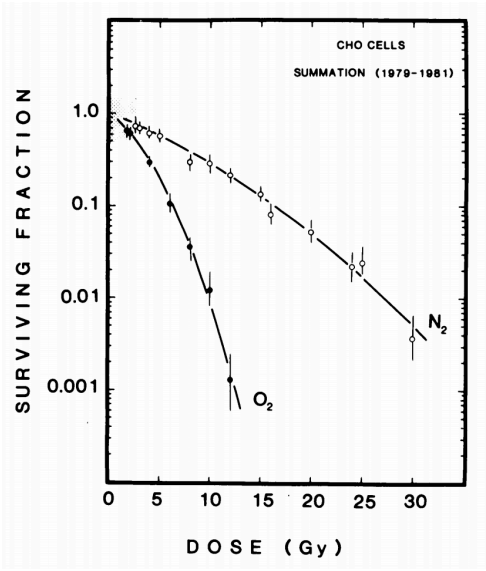


Figure 1.3: The oxygen enhancement ratio
Example of early data demonstrating the difference in radiosensitivity of exponentially grown Chinese Hamster Ovary cells when irradiated using 250 kV X-rays under anoxic (N_2) versus normoxic (O_2) conditions. Figure adapted from [89], license 4733710039834.

Most change in radiosensitivity occurs as oxygen levels increases from 0 to 30 mmHg (0 to 4%), with further increases in oxygenation having little additional effect (Figure 1.4). As a significant proportion of tumour oxygen readings fall within this range, with normal tissue readings normally above this range, this highlights the everyday clinical challenge of treating tumours successfully without causing excessive surrounding normal tissue toxicity.

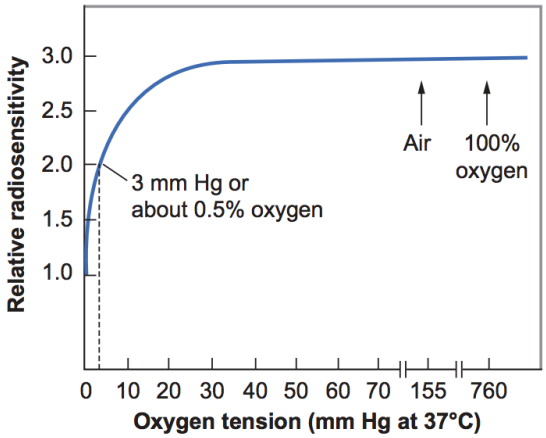
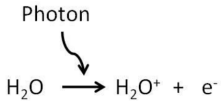


Figure 1.4: Illustration of the effect of oxygenation on radiosensitivity
An idealised representation of the relationship between cellular radiosensitivity and the tension of oxygen present during irradiation. Figure adapted from [90], license 4744891460004.

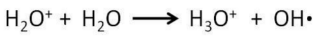
In order to understand how oxygen potentiates cellular radiation response, it is first important to briefly consider how ionising radiation results in cellular damage. Radiation results in damage through its effects on DNA, with DNA double strand breaks being the principle cytotoxic lesions. The effects on DNA can be viewed as either direct or indirect. Direct damage results from ionisation of the DNA without the involvement of intermediate steps, and is the principal way by which high linear energy transfer radiation, such as for example neutrons and α particles, exert their effect [90]. By contrast, megavoltage (MV) X-rays do not produce chemical and biological damage by themselves, but rather predominantly as a result of indirect ionisation when they are absorbed in the material

through which they pass and their energy is transferred to produce fast-moving charged particles that in turn elicit DNA damage [90].

At the energies used by most clinical linear accelerators, the MV photons predominantly interact with 'free' electrons of the absorbing material with some of the photon energy transferred to the electron in the form of kinetic energy and the scattered photon traveling further into the material interacting with more 'free' electrons (Compton Effect) [91]. This ultimately leads to a large number of fast electrons which can ionise other atoms in the irradiated material. As cells are 80% comprised of water, it is important to consider the radiochemistry of water. Following exposure to ionising radiation, water becomes ionised as shown:



H_2O^+ is an ion radical and rapidly interacts with another water molecule to form the highly reactive hydroxyl radical (OH•) as follows:



Such free radicals interact with the DNA molecule and cause damage.

The mechanisms responsible for oxygen increasing cellular radiosensitivity can now be explained as outlined by the Oxygen Fixation Hypothesis first described in the 1950s [92]. Following radiation, DNA damage can be restored through reactions with free radical scavengers such as sulphydryl containing compounds [93,94]. However, in the presence of molecular oxygen, DNA damage can be 'fixed' by the DNA radical reacting with oxygen to form RO2•, which is significantly less amenable to scavenger restoration [95].

Figure 1.5 illustrates direct and indirect damage caused by X-rays and the oxygen fixation hypothesis.

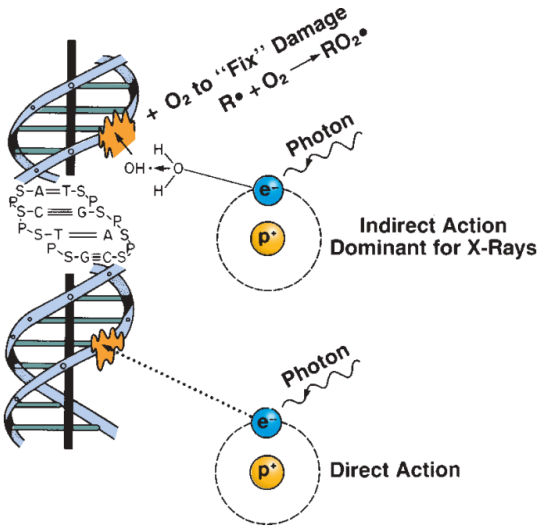


Figure 1.5: Diagram of X-ray induced DNA damage and the Oxygen Fixation Hypothesis
Ionising radiation can cause direct and indirect DNA damage. The majority of DNA damage caused by X-rays occurs through the ionisation of water resulting in free radical damage to DNA which can be fixed in the presence of molecular oxygen. Figure adapted from [90], license 4744891460004.

1.3.2 Tumour hypoxia and poor radiotherapy clinical outcomes

Given the multitude of tumour adaptations to hypoxia contributing to many cancer hallmarks, it is not surprising that the presence of tumour hypoxia has been repeatedly shown to be a negative prognostic factor and to be associated with resistance to therapy regardless of treatment modality used [49,96–98]. However, given that oxygen is a direct 'facilitator' of radiation-induced DNA damage, it is perhaps unsurprising that the impact of hypoxia on radiotherapy outcomes is most profound.

The effect of hypoxia on radiotherapy outcomes has been most studied in patients with HNSCC. In a large analysis of data from numerous HNSCC radiotherapy studies, Nordsmark *et al.* demonstrated that pre-treatment hypoxia directly measured using oxygen

electrodes was a highly significant prognostic factor for overall survival after radiotherapy alone, or in combination with surgery, chemotherapy or a radiosensitiser [67]. Multivariate analysis in this study found that pre-treatment proportion of pO_2 values $\leq$ 2.5 mmHg ($HP_{2.5}$) was independently prognostic for poor survival using a hypoxia threshold of $HP_{2.5}$ <20% (median value).

Furthermore, the negative impact of hypoxia on radiotherapy efficacy can be deduced from the large study of 918 patients with HNSCC randomised to receive CHART versus conventional radiotherapy [99]. Although this study failed to show improved LRC or OS with CHART, a retrospective subgroup analysis of pre-treatment tissue from nearly 200 patients demonstrated that expression of endogenous markers of hypoxia for the HIF-1 and HIF-2 pathway was strongly associated with radiotherapy failure. This led the authors to postulate that hypoxic tumours were resistant to the potential benefit of CHART due to insufficient time for tumour reoxygenation to occur during treatment [100].

In other tumour types, hypoxia has also been shown to predict poor radiotherapy outcomes [101–103]. For example, in patients with NSCLC, higher baseline levels of hypoxia, as determined by multiple hypoxia PET imaging parameters, was predictive of lower rates of local control following radical radiotherapy [102]. In another study in patients with localised prostate cancer receiving radical radiotherapy, direct measurement of tumour oxygenation revealed that the presence of hypoxia, using a HP_{10} cut-off of 63% (median value), was associated with local recurrence within the gland and early biochemical failure [103].

1.4 MEASURING TUMOUR HYPOXIA IN THE CLINICAL SETTING

Over the last few decades, a wide range of methods have been used to study tumour hypoxia in patients, each with specific advantages as well as limitations.

1.4.1 Direct measurement with oxygen electrodes

Direct measurements of tumour oxygenation using glass electrodes began in the 1960s with many early studies demonstrating the relationship between tumor oxygen level and radiation response, especially in cervical cancer and HNSCC [104,105]. However, our understanding of tumour oxygenation increased exponentially in the early 1990s with the introduction of the commercially available Eppendorf pO_2 histograph, also referred to as the polarographic electrode [65]. This technique, which is able to measure oxygen tensions as low as 1-2 mmHg, demonstrated the significant intra- and inter-tumour variability in oxygenation and a large number of clinical studies quickly utilised this technique to demonstrate the correlation between hypoxia and poor clinical outcomes, as previously described.

There were numerous limitations of electrode-based methods for studying tumour oxygenation. Determining oxygen tensions was limited to only accessible tumours and the invasive nature of the procedure, which requires the insertion of the probe along multiple tracks in order to collect sufficient readings, was understandably viewed as somewhat unattractive by patients and clinicians. Furthermore, due to the complex spatiotemporal heterogeneity of hypoxia within tumours, this method was subject to sampling error. Therefore, although this technique is regarded by many as the gold standard for evaluating hypoxia, it has been universally discontinued.

1.4.2 Exogenous nitroimidazole based methods

1.4.2.1 Hypoxia-dependent reduction and retention of nitroimidazole compounds

More recently, the most widely adopted approach for pre-clinical and clinical assessment of hypoxia has become the use of exogenously administered nitroimidazole based agents. Such electron-deficient nitroaromatic compounds are selectively reduced by intracellular nitroreductase enzymes under hypoxic conditions to form reactive products which bind irreversibly to nucleophilic molecules within the cell. Different nitroreductase enzymes in the cytoplasm, mitochondria and microsomes are capable of the reductive metabolism of nitroheterocycles, and include NADPH-cytochrome P450 reductase, cytochrome b5 reductase, xanthine oxidase, aldehyde dehydrogenase, and DT-diaphorase [106]. Although a predominant enzyme in mammalian cells has not been identified, NADPH-cytochrome P450 reductase has been demonstrated to be important in the reductive activation and subsequent hypoxic accumulation of various nitroaromatics [107,108]. The reduction of nitroimidazoles is accomplished by tissue nitroreductases that are plentiful and which do not represent a rate-limiting factor [109], thus enabling repeated evaluation of hypoxia by such agents without reaching enzyme saturation.

Bioreductive activation of nitroimidazole agents involves the addition of the first electron by nitroreducase enzymes to form the nitro radical anion RNO2•-, which is reversible in the presence of molecular oxygen and therefore forms the basis of oxygen-dependence of activation and binding of these agents. However, under low oxygen conditions, another electron reacts with the nitro radical anion first, making a two-electron reduction product which can no longer be reversed by oxygen. Subsequently, the nitroimidazole compound forms an alkylating agent that reacts indiscriminately with intracellular macromolecules,

such as proteins and DNA, and becomes irreversibly trapped [110]. The molecular mechanism underlying nitroimidazole reduction is shown in Figure 1.6.

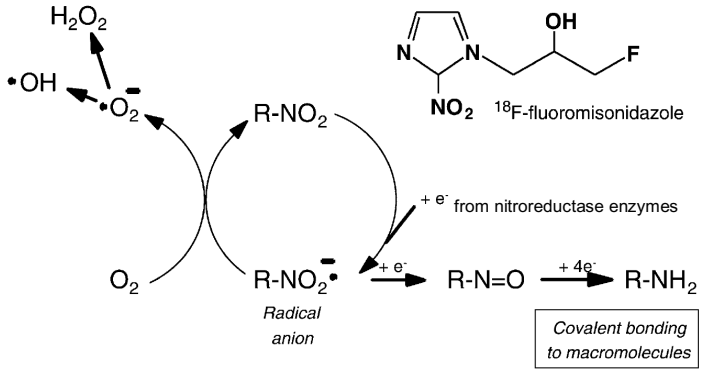


Figure 1.6: Mechanism of nitroimidazole reduction
Mechanism of nitroimidazole compound (R-NO_2) reduction leading to irreversible intracellular retention and the important role of molecular oxygen in this process. An example of a nitroimidazole compound 18F-labelled fluoromisonidazole is shown. Figure adapted from [111].

Importantly, bioreduction and intracellular retention of nitroimidazole compounds is inversely proportional to oxygen levels and requires intact nitroreductase enzymes. As a result, it detects only viable hypoxic cells and does not accumulate in regions of tumour necrosis. Typically, such agents have minimal protein binding, permitting efficient transport from blood into tissues [112] and as they are not actively metabolised, their diffusion distance is significantly greater than that of molecular oxygen [113], and therefore can still reach poorly perfused areas typical of hypoxic regions. Also of importance is that *in vitro* experiments have demonstrated that nitroimidazoles are retained over the same oxygen range at which the OER is observed, with sharply increasing retention below oxygen tensions of 10 mmHg [111], therefore highlighting them as clinically relevant markers for the study of tumour hypoxia in radiation oncology.

1.4.2.2 EF5 and pimonidazole immunohistochemistry

The stability of nitroimidazole adducts in viable hypoxic tissues permits immunohistochemical quantification to be carried out after the administration of nitroimidazole based agents. Such agents have been widely used to study tumour hypoxia and include EF5 [114] and pimonidazole hydrochloride [115]. The degree of immunodetection of such agents has been shown to correlate well with polarographic electrode readings predominantly in pre-clinical studies [115]. However, as with direct measurements, sampling specific tumour regions may be unrepresentative of hypoxia throughout the tumour. In addition, obtaining tissue for this purpose is an invasive procedure, which has associated practical limitations.

1.4.2.3 Hypoxia PET imaging

Nitroimidazoles also provide an exciting and clinically attractive opportunity for the non-invasive evaluation of tumour hypoxia by using PET imaging with radiolabelled nitroimidazole based tracers [116]. [^{18}F]-fluoromisonidazole (FMISO) is the prototypical and most widely used radiotracer for this purpose.

In vitro experiments have demonstrated that the under anoxic conditions, [^{3}H]-FMISO binding was approximately 25-fold greater than normoxic controls with binding reduced to 40% at oxygen pressures of 4 mm Hg [117], thus demonstrating FMISO as a marker of severe and clinically relevant hypoxia. Relevant to measuring hypoxia in tumours, *in vivo* data demonstrates no correlation between regional blood flow and FMISO retention with numerous studies concluding that FMISO uptake is independent of blood flow [118,119].

In vivo, agreement between FMISO and pimonidazole immunohistochemistry (IHC) has been observed [120], however such studies are lacking in patients. In the clinical setting,

numerous studies have demonstrated the ability of FMISO to identify heterogeneously distributed hypoxic tissue within human tumours [121]. Furthermore, in HNSCC, uptake of FMISO and polarographic electrode measurements were well correlated [122].

The partition coefficient describes the lipophilic/hydrophilic nature of molecules and is commonly evaluated as the distribution coefficient between octanol and water. As FMISO partitions nearly equally between octanol and water, once distribution equilibrium is achieved, all tissues should have the same concentration of tracer as blood. Only regions of hypoxia or organs involved in excretion or metabolism will have uptake levels greater than blood. The advantage is that the concentration ratio for normoxic tissue to blood will be very close to one and will be completely independent of blood flow. However, because of such partitioning characteristics of FMISO, whole body clearance is relatively slow, resulting in limited image contrast and requiring imaging following a relatively long period of time after injection of tracer [123]. These limitations have led to the development of newer tracers such as [^{18}F]-fluoroazomycin arabinoside (FAZA), which have higher normal tissue clearance kinetics with improved hypoxia-to-normoxia contrast [124]. However, issues with availability and a lack of experience have limited the use of FAZA to date.

Clinical imaging protocols for using FMISO PET in the study of tumour hypoxia are fairly well established [125,126], with increasing validation and high reproducibility of FMISO demonstrated in NSCLC [127] and HNSCC [128]. This imaging technique enables the assessment of hypoxia heterogeneity within tumours and for multiple measurements per individual patient. However, the limitations are that it is prohibitively expensive for use in large studies, is associated with logistical challenges in terms of tracer supply and subjects patients to not insignificant radiation exposure.

1.4.3 Endogenous hypoxia markers

As our understanding of the complex tumour response to hypoxia continues to improve, methods used for the assessment of hypoxia have shifted to measuring endogenous markers of this response. The majority of such markers are known to be direct transcription targets of HIF-1 as the detection of HIF-1 itself is challenging due to its instability and rapid degradation.

1.4.3.1 Tumour tissue hypoxia markers

In terms of tumour tissue hypoxia analysis, IHC for carbonic anhydrase IX (CAIX) has been commonly performed. CAIX is a transmembrane metalloenzyme that belongs to the family of α-carbonic anhydrases, which catalyse the reversible hydration of carbon dioxide to bicarbonate ions and protons, thereby regulating the cellular and extracellular pH [129]. Sixteen human CA isoforms have been identified, but it is CAIX that is most strongly induced by hypoxia in a broad range of cell types. Expression of CAIX is tightly regulated by HIF-1-dependent HRE and subsequently, levels are highly responsive to hypoxia [130]. High expression of CAIX has consistently been reported in human tumours, including in NSCLC, and shown to predict poor clinical outcomes [131,132]. CAIX expression as detected by IHC has been shown to grossly co-localise with that of HIF-1 as well as pimonidazole staining [133,134], and has also been shown to correlate with direct pO_2 measurements [49].

When considering such endogenous markers of hypoxia, it is important to appreciate that their expression level may be influenced by numerous factors other than oxygen level, such as for example other cellular signalling pathways [135]. In addition, the level of oxygenation and thus severity of hypoxia required to induce HIF signalling (and increase

associated response proteins such as CAIX) differs to that required for the retention of exogenous nitroimidazoles. As shown in Figure 1.7, on detailed inspection of tumour tissue staining, binding of pimonidazole is more restricted to severely hypoxic and peri-necrotic regions as compared to HIF-1 expression [136]. In addition, HIF1 expression and its response proteins can also be found in regions of cycling hypoxia, which are not necessarily positive for nitroimidazole retention at the time of measurement.

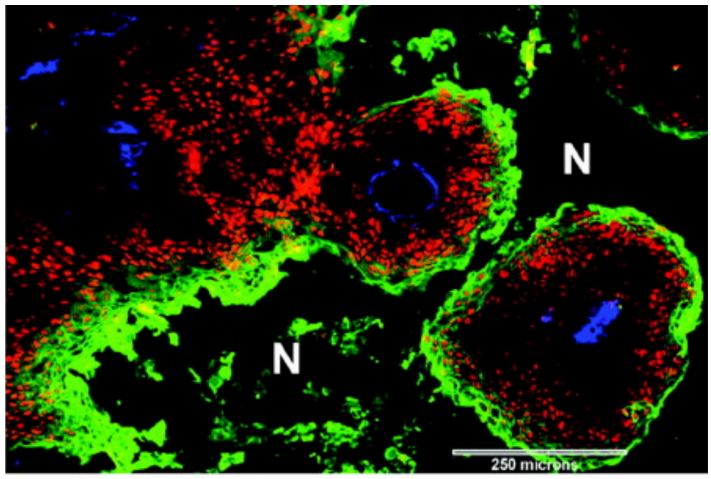


Figure 1.7: Comparison of HIF-1 α expression with pimonidazole binding
Distribution of HIF-1α expression (red) and pimonidazole binding (green) in sections from frozen human cervical cancer biopsies following administration of pimonidazole as detected using immunofluorescence. 'N' represents regions of necrosis and staining for CD31, a vascular marker, is also shown (blue). Adapted from [136], license 4733701142628.

In recognition of the complex tumour response to hypoxia, gene expression profiling is becoming more commonly used to evaluate the transcriptional response to hypoxia with numerous hypoxic metagene signatures now identified and increasingly well-validated [137,138]. For a comprehensive review see Harris *et al*. [139].

1.4.3.2 Circulating hypoxia markers

In addition to tumour tissue-based measurements, endogenous markers of hypoxia also provide the opportunity for identifying circulating hypoxic biomarkers, which may

ultimately function as a plasma hypoxia signature. One of the most well-studied circulating markers to this effect is VEGF. Numerous studies have demonstrated the correlation between plasma VEGF levels and direct tumour oxygen measurements [140], with higher levels predicting poor treatment response and outcomes in numerous tumour types [141]. In addition, high circulating VEGF levels have been shown be associated with poor outcomes in NSCLC [141,142].

Another circulating hypoxia marker which has been studied extensively is osteopontin. This multifunctioning glycoprotein is recognised to play an important role in signalling pathways involved in many aspects of cancer progression including promoting proliferation, angiogenesis and metastasis [143]. Osteopontin is up-regulated under hypoxic conditions by Akt activation and stimulation of the ras-activated enhancer (RAE) in the OPN promoter [144]. Tumour tissue osteopontin expression has been shown to be inversely correlated with direct measurement of oxygen levels in HNSCC [145]. In addition, circulating osteopontin levels have been demonstrated to correlate inversely with polarographic electrode oxygen measurements and function as a prognostic and predictive biomarker with regards to radiotherapy outcomes in NSCLC [49,141] and HNSCC [146–149]. In NSCLC, a recent meta-analysis has demonstrated that osteopontin as measured by both IHC and as a circulating marker, is highly predictive of overall survival [150].

A different class of hypoxia-related circulating biomarkers are microRNAs (miRNAs). These approximately 21 nucleotide non-coding RNAs are key post-transcriptional regulators of gene expression [151]. In the cellular response to hypoxia, and directly targeted by HIF-1α, miR-210 has emerged as the ‘master hypoxiaMIR’ [152]. Shown to correlate with other measures of tumour hypoxia, both tissue and circulating miR-210 have

been reported to be diagnostic, predictive and prognostic hypoxia-related biomarkers in a number of tumour types, including NSCLC [153–156].

1.5 PREVIOUS HYPOXIA MODIFICATION STRATEGIES WITH RADIOTHERAPY

Over the last half century, numerous strategies have been investigated in an attempt to overcome the detrimental effect of tumour hypoxia on radiotherapy outcomes.

1.5.1 Increasing tumour oxygenation

1.5.1.1 Hyperbaric oxygen

Early approaches to address tumour hypoxia focused on increasing tumour oxygen delivery. One such method involved patients breathing 100% oxygen under hyperbaric conditions (HBO). A meta-analysis of HBO in patients with HNSCC treated with radiotherapy demonstrated a small but significant improvement in locoregional control [157]. A comprehensive Cochrane review of 19 clinical trials which delivered HBO concluded that HBO improved local control rates in cervix and head and neck cancer, but these benefits were small and may have only arisen in the context of unconventional fractionation schedules. In addition, HBO was associated with significant adverse effects, including oxygen toxic seizures and severe tissue radiation injury [158]. Given the modest benefit observed, practical inconvenience of treatment delivery and safety concerns, HBO was not adopted into clinical practice.

1.5.1.2 Correction of anaemia

Additional methods aimed at increasing tumour oxygenation have focused on administering blood transfusions to increase haemoglobin levels. Anaemia is a very

common finding in patients presenting for radiotherapy with 40 to 64% of patients being anaemic prior to treatment with anaemia shown to be associated with worse LRC and survival in numerous tumour types [159,160]. However, although the aetiology of anaemia in patients can be multifactorial, it often reflects patients with higher disease burden and therefore those who are more likely to have poor clinical outcomes. Numerous studies, mainly in HNSCC and carcinoma of the cervix, have investigated correcting anaemia with blood transfusions during radiotherapy treatment with overall mixed results observed [161]. An alternative method explored for correcting anaemia during radiotherapy in HNSCC has been erythropoietin injections. However, unfortunately a significant detrimental impact on survival was observed with this approach [162], postulated to be attributable to promoting tumour cell proliferation through stimulation of tumour erythropoietin receptors [163].

1.5.1.3 ARCON

Other studies have aimed to improve oxygen delivery to tumours during radiotherapy by reversing acute hypoxia by combining the vasodilator nicotinamide with inhaled carbogen (95% oxygen and 5% carbon dioxide). This approach has been used as part of the Accelerated Radiation, Carbogen and Nicotinamide (ARCON) regime and has demonstrated promising LRC rates and toxicity in large phase II studies in patients with HNSCC [164] and bladder cancer [165]. Subsequently, in a phase III trial in laryngeal cancer, ARCON was well-tolerated and resulted in improved LRC rates, with the poor regional control seen in more hypoxic tumours specifically addressed by this approach [166]. Furthermore, in bladder cancer the phase III BCON trial demonstrated improvement in LRC and OS using this treatment [167]. However, due to the not insignificant practical challenges involved in delivering this regime, it has not been widely adopted.

1.5.1.4 Vascular 'normalisation'

Intracellular signal transduction pathways are known to play an important role in determining tumour response to radiation with the well-studied EGFR/Ras/PI3K/Akt pathway shown to be of particular importance. Pre-clinical experiments have demonstrated that inhibitors of EGFR, Ras, PI3K and Akt produce marked 'normalisation' of tumour microvasculature with increased perfusion and alleviation of tumour hypoxia [168,169]. Furthermore, in xenograft models it was observed that PI3K inhibition resulted in significant tumour growth delay after radiation because of vascular remodelling, which was independent and synergistic to increasing intrinsic radiosensitivity [170]. Excitingly, just recently the specific PI3K inhibitor buparlisib has been shown to result in a reduction in tumour hypoxia as measured by FMISO PET in patients with advanced NSCLC and to be well-tolerated in combination with palliative thoracic radiotherapy [125], although no assessment of radiation response was possible in this study.

1.5.1.5 'Oxygen mimetics'

An alternative approach to address hypoxia-mediated radioresistance has been to combine drugs which function as 'oxygen mimetics' by promoting the fixation of free radical damage following radiotherapy. These agents belong to the nitroimidazole class of agents, which undergo bioreduction and intracellular trapping under hypoxic conditions, as previously described. Misonidazole was the first of such agents to be shown to result in radiosensitisation *in vitro* [171] and subsequently a number of clinical studies were conducted in many different tumour types combining this agent with radiotherapy [172–176]. With a few exceptions, generally the results did not demonstrate significant improvements in radiotherapy outcomes and this was associated with high toxicity, in

particular with regards to peripheral neuropathy, preventing dose escalation to levels thought to be required to produce tumour radiosensitisation [177].

Subsequently, other nitroimidazoles were developed with more favourable toxicity profiles, of which the 5-nitroimidazole nimorazole has been the most widely studied in combination with radiotherapy. In the large randomised phase III Danish Head and Neck Cancer (DAHANCA) study, nimorazole significantly improved radiotherapy LRC in carcinoma of the supraglottic larynx and pharynx [178]. This study, and others in different tumour sites in the head and neck with the addition of cytotoxic chemotherapy, demonstrated acceptable toxicity [179,180]. Despite such promising results, nimorazole is only routinely used in Denmark, with the lack of demonstrated improvement in overall survival limiting its uptake elsewhere. The results of the randomised nimorazole with radiotherapy versus radiotherapy alone UK phase III study in HNSCC (NIMRAD) are currently awaited [181].

1.5.2 Hypoxia-activated cytotoxic prodrugs

Hypoxia-activated pro-drugs have also been explored in an effort to target hypoxic cells directly. Such agents also become preferentially activated and reduced in low oxygen tensions but this time to form highly cytotoxic species. The most well-known molecule in this class is tirapazamine, which has been shown pre-clinically to be significantly more cytotoxic under hypoxic conditions [182]. Unfortunately, randomised phase III studies using tirapazamine in combination with chemoradiotherapy in carcinoma of the cervix [183] and HNSCC [184] have failed to demonstrate improvement in outcomes.

1.5.3 Summary of past approaches

Over the last three decades a truly wide range of different approaches has been employed to tackle hypoxia-mediated radioresistance and a meta-analysis of such treatments in HNSCC has demonstrated improvement in LRC and OS, thus providing level 1a evidence for hypoxia modification with radiation. However, due to inconsistency of results observed over the years with any outcome improvements only modest at best, no such treatment is widely used. Concerns regarding toxicity and challenges in practical delivery have further curbed enthusiasm. It is now well-recognised that one of the major reasons why hypoxia modification has failed to show significant changes in radiotherapy outcomes is that there has been a complete lack of selecting patients for treatment based on tumour hypoxia and therefore likely to benefit most from such intervention. The reasons for this are largely due to the fact that there is currently no agreement as to which measure of hypoxia should be used for this purpose with many current techniques lacking sufficient validation.

Undeniably, novel and more efficacious hypoxia modification treatments are also required and more recently attention has focused on modulation of tumour metabolism, as will be now discussed and forms the focus of this thesis.

1.6 OXIDATIVE PHOSPHORYLATION AS AN EMERGING TARGET TO TACKLE TUMOUR HYPOXIA

In contrast to previous methods largely aimed at increasing oxygen delivery to tumours, an alternative and exciting novel strategy to tackle tumour hypoxia is to reduce the tumour oxygen consumption rate (OCR), thus addressing the other side of the oxygen supply and demand equation. More specifically, there is growing interest in reducing tumour OCR through inhibition of oxidative phosphorylation (OXPHOS).

1.6.1 Overview of cellular respiration

Cellular respiration describes a series of well characterised metabolic reactions by which cells convert available nutrients into biochemical energy in the form of adenosine triphosphate (ATP). The most readily available source of cellular energy is glucose and molecular oxygen plays a key role in its conversion to ATP.

1.6.1.1 Glycolysis and anaerobic respiration

The first step in cellular respiration in most organisms is glycolysis, also referred to as Embden-Meyerhof-Parnas pathway. This oxygen-independent pathway constitutes a ten step multienzyme process occurring in the cytosol and converts one molecule of glucose into two molecules of pyruvate whilst producing two reduced nicotinamide adenine dinuceotide (NADH) and two ATP molecules (net yield). The fate of pyruvate and cellular respiration hereon is highly dependent on the presence of molecular oxygen [185].

In the absence of oxygen, pyruvate is reduced to lactate by lactate dehydrogenase (LDH). This results in the regeneration of NAD^+ through NADH oxidation and as NAD^+ is required during glycolysis for ATP production, this enables ongoing cellular energy production under anaerobic conditions. Lactate may be converted back to pyruvate by LDH and used for aerobic respiration if oxygenation has increased, or it diffuses into the circulation and can be converted back into glucose by the liver in the Cori cycle.

1.6.1.2 Aerobic respiration: citric acid cycle

In contrast, in the presence of oxygen, pyruvate generated during glycolysis enters the mitochondrial matrix, where it undergoes oxidative decarboxylation by a series of enzymes which make up the pyruvate dehydrogenase complex (PDH) and is converted into acetyl coenzyme A (acetyl CoA). Acetyl CoA enters the citric acid cycle, also known as the Krebs

or tricarboxylic acid cycle, by combining with oxaloacetate to form citrate, which is systematically converted back to oxaloacetate and then combines with acetyl CoA, and so the cycle repeats. Each full cycle produces one guanosine triphosphate (GTP), one reduced flavin adenine dinucleotide ($FADH_2$) and three NADH molecules. $FADH_2$ and NADH move to the inner mitochondrial membrane and facilitate ATP production during the process of OXPHOS [185].

1.6.1.3 Aerobic respiration: electron transport chain and oxidative phosphorylation

The electron transport chain (ETC) uses NADH and $FADH_2$ produced by the Krebs cycle and NADH from glycolysis to produce ATP. Electrons from NADH and $FADH_2$ are released and transferred systematically through protein complexes located in the inner mitochondrial membrane, thus forming the electron transport chain. These inner membrane protein complexes include four enzyme complexes, complex I, complex II, complex III and complex IV, and two coenzymes, ubiquinone (also known as co-enzyme Q) and cytochrome c. As electrons are passed from one electron carrier to another, it results in their reduction and then oxidation, which releases enough energy to pump hydrogen ions across the inner membrane into the space between in the inner and outer mitochondrial membranes. The accumulation of protons in this intermembrane space creates a steep electrochemical gradient across the inner membrane. As protons traverse the protein pore complex ATP synthase embedded in the inner membrane back into the mitochondrial matrix, the shaft of the complex rotates and catalyses the production of ATP by attaching a phosphate to ADP. In total, for every glucose molecule that enters aerobic respiration, a net yield of 36 ATPs is produced.

Once the electrons have passed though the ETC, they are combined with molecular oxygen and hydrogen ions to form water molecules. Therefore, oxygen can be viewed as the

terminal electron acceptor and electron flow through the ETC ceases without oxygen. The ETC couples the transfer of electrons from donor molecules to oxygen with ATP production, thus representing the process known as OXPHOS [186]. Figure 1.8 illustrates the process of ETC and OXPHOS.

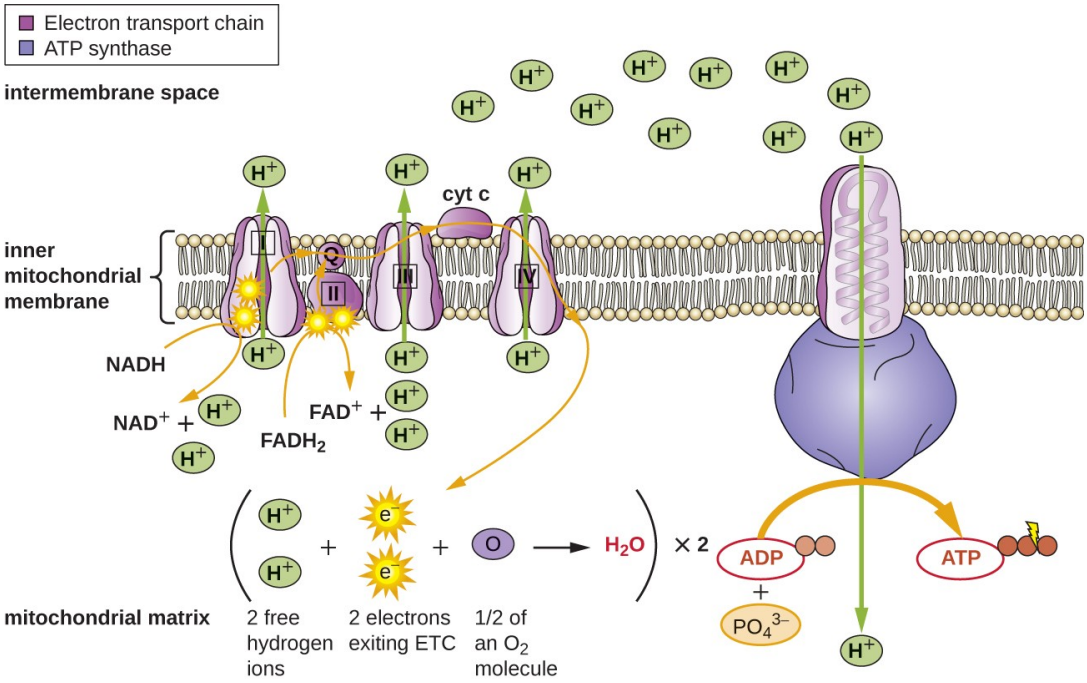


Figure 1.8: Diagram of oxidative phosphorylation
Simplified schematic illustration of the systematic transfer of electrons through protein complexes (complex I-IV) located in the inner mitochondrial membrane constituting the electron transport chain (ETC). The resultant steep proton gradient across the inner mitochondrial membrane is balanced by protons traversing ATP synthase and ATP is produced. The terminal acceptor of electrons from the ETC is oxygen to create water. The process of coupling electron transfer to oxygen with ATP production is known as oxidative phosphorylation. Adapted from [187] under CC licensing.

1.6.2 Altered metabolism in cancer and the impact of tumour hypoxia

A well-established hallmark of cancer is highly abnormal energy metabolism [188,189]. First observed by Otto Warburg in 1920s [190], cancer cells reprogram energy metabolism to predominantly rely on glycolysis, even in the presence of normal oxygenation. This phenomenon of 'aerobic glycolysis' is characterised by marked increase in glucose uptake by cancer cells, largely by upregulation of glucose transporters such as transporter 1

(GLUT1), [188]. Although relying on glycolysis for energy metabolism may seem counterintuitive due to lower yields of ATP per molecule of glucose molecule compared with OXPHOS, the sheer abundance of glucose due to increased uptake results in far greater ATP production and at a faster rate.

Pro-proliferative signal transduction pathways are known to function as glycolytic drivers with increased PI3K/Akt/mTOR signalling and overexpression of RAS and c-myc known to be of key importance [188,191]. For example, AKT has been shown to be perhaps the most important as it appears to be sufficient to drive glycolysis independently [192], whilst c-myc increases transcription of GLUT1, as well as multiple key enzymes involved in glycolysis [193,194].

Tumour hypoxia also plays an important role in fuelling glycolysis, primarily through HIF-1 signalling. For example, HIF-1 upregulates GLUT1 as well as virtually all of the glycolytic enzymes, with key examples being HK, PGI and LDH [195,196]. In addition, HIF-1 also increases expression of PDH kinase 1 which inhibits PDH complex activity, thus preventing the irreversible conversion of pyruvate into acetyl CoA and entry into the citric acid cycle [197], and therefore functions as an important switch between glycolysis and OXPHOS respiration. Within the mitochondria itself, HIF-1 tightly regulates the expression of different isoforms of subunit COX4 and the function of ETC complex IV of the electron transport chain, thus impacting on ATP production and oxygen consumption [198]. More recently, it is increasingly recognised that HIF-1 also regulates the expression of a wide range of miRNAs which fine tune metabolic pathways, as outlined in a comprehensive review [199].

In terms of OXPHOS activity in cancer, downregulation has been demonstrated in several tumour types and attributed to mitochondrial DNA (mtDNA) mutations, or reduced

mtDNA content, given that mtDNA codes for many of the subunits of OXPHOS protein complexes I to V [200]. Such downregulation of OXPHOS has been demonstrated to correlate with poor clinical outcomes in many cancers, and shown to be associated with invasive and metastatic tumour phenotypes [201].

1.6.3 Emergence of the importance of OXPHOS in cancer

Because of the observation that glycolysis is upregulated and OXPHOS is downregulated in tumours, it has become a long-held belief that OXPHOS is largely redundant in cancer and thus has been largely forgotten. However, more recently it has been demonstrated that in a number of tumour types mitochondrial metabolism is not downregulated, including pancreatic and endometrial cancer as well as in lymphoma and high OXPHOS subtype melanoma [202,203]. In addition, it has increasingly become recognised that OXPHOS is indeed active in cancer cells and does in fact contribute, although to a varying degree, to cellular energy production [204]. Such is the higher yield of ATP production with OXPHOS compared with glycolysis, that it has been shown that when OXPHOS activity is reduced as low as 6%, it still contributes to 50% of the cell's energy requirements [205]. In a meta-analysis of normal cell types and cancer cell lines, the average contribution of OXPHOS to ATP production was 80% in normal cells and 83% in cancer cells [204]. Despite the often severely hypoxic conditions within tumours, the level of oxygen, the key determinant of the oxygen consumption rate (OCR) [206,207], is generally above that which would impair mitochondrial respiration as the K_{mO2} of COX is as low as 0.1–0.8 μM in different biological systems [202].

The previous explanation that decreased OXPHOS in cancer is attributable to significantly decreased or mutated mtDNA is controversial. In fact, many types of cancer have increased mtDNA content relative to normal tissue [200,208]. With regards to mtDNA mutations,

analysis of paired tumour and normal tissue samples has revealed deleterious somatic tumour-specific mtDNA mutations in the majority of rectal and colon adenocarcinomas [209]. Furthermore, such mutations were identified in all mtDNA genes many of which were predicted to impair OXPHOS. Interestingly, it has been shown that cancer cells with these mutations in OXPHOS related genes such as complex I subunits, have much higher sensitivity to complex I inhibitors [210], indicating these mutations play an important role in cancer cell function.

Further still, *in vitro* experiments using ethidium bromide to deplete mitochondrial DNA have demonstrated that reduction of mitochondrial respiration dramatically changes the behaviour of cancer cells and decreases tumorigenic potential [211]. This is supported by a number of different cancer cell *in vivo* models, which have demonstrated that depletion of mitochondrial respiratory complexes results in delayed tumour formation following transplantation and an inability of cancer cells to metastasise [212]. Interestingly, when tumours did eventually form and disseminate, they showed marked reactivation of OXPHOS due to acquisition of host mitochondrial DNA. There is also growing evidence that reliance on OXPHOS, and in fact impaired glycolysis, is a key feature of cancer stem cells and quiescent cancer cells resistant to standard therapies and responsible for repopulation of tumours after treatment [213].

Perhaps one important role of OXPHOS in carcinogenesis is the production of reactive oxygen species (ROS). High levels of ROS production has long been recognised to be a classical feature of tumours [214] with many early studies focused on the DNA damaging effects of reactive oxygen species, which is believed to be tumorigenic by promoting genomic instability [215]. However, more recently a paradigm shift has occurred in our understanding of ROS with a more nuanced view of the importance of ROS as signaling

pathway molecules, promoting tumorigenesis by regulation of cellular proliferation, metabolic alterations and angiogenesis [216].

Therefore, after decades of disregard, OXPHOS has re-emerged as a functioning and important part of cancer cellular function. As OXPHOS consumes significant quantities of oxygen, inhibition of this process is a novel approach to reduce tumour oxygen consumption and therefore tackle tumour hypoxia.

1.6.4 OCR inhibition to alleviate tumor hypoxia

1.6.4.1 Rationale

Over the last few years there has been growing interest in using OXPHOS inhibitors to reduce tumour OCR. Such an approach would permit unconsumed oxygen to diffuse into adjacent low oxygen regions and therefore alleviate tumour hypoxia. Indeed, 3D multicellular spheroid studies have demonstrated that OCR reduction alleviates central hypoxic regions by increasing the availability of free oxygen [217,218]. In support of this approach, mathematical modeling suggests that only a 30% decrease in OCR would abolish severe hypoxia [218] and that reduction in OCR is likely to be a more effective strategy to reduce hypoxia than previous methods aimed at increasing oxygen supply [217].

Inhibition of OXPHOS has been shown to reduce OCR in many different cancer cell types, indicating potential wide applicability [219]. Also this approach is thought less susceptible to poor tumour perfusion as such inhibitors would initially target OXPHOS in well-perfused and non-hypoxic regions, which would then result in oxygen rapidly diffusing to adjacent regions of chronic hypoxia, thus targeting ‘hard to reach’ tumour regions indirectly [220].

1.6.4.2 Known OCR inhibitors including metformin

A number of FDA approved drugs are known to inhibit OXPHOS through off-target effects and have gained attention as potentially clinically useful OCR inhibitors [220]. In particular, the anti-diabetic medication Metformin has been most studied in this context. This biguanide is the most widely prescribed medication for treatment of type II diabetes mellitus and exerts its glucose-lowering effect through inhibition of hepatic gluconeogenesis [221]. The potential of metformin as an anti-cancer agent first came to light when large epidemiological and retrospective studies demonstrated that diabetic patients taking metformin had significantly lower incidence of cancer and better clinical outcomes following treatment, including in the context of radiotherapy, than patients with diabetes taking alternative medication [222–224]. The observed benefits of metformin have been attributed to a number of its effects, including systemically lowered insulin/insulin-like growth factor-1 (IGF-1) as well as potential inhibition of mammalian target of rapamycin (mTOR), activation of AMP-activated kinase (AMPK) and reduction in ROS [225–227].

The mechanism by which metformin reduces OCR is through inhibition of complex I of the ETC [228]. Pre-clinical data has shown that metformin reduces OCR in numerous cancer cell lines leading to alleviation of hypoxia in spheroids as well as in xenograft models with corresponding improvement in radiation response [219,229,230].

However, unfortunately despite such promise, clinically achievable concentrations of metformin are significantly lower than those required in pre-clinical models to result in meaningful OCR reduction, and thus unlikely to be a good anti-hypoxia agent. Furthermore, in a number of cell types, metformin was shown to be ineffective at inhibiting OCR, suggesting potential limited applicability [219]. A recent clinical study in breast

cancer has demonstrated that metformin does alter tumour metabolism, switching it to a glycolytic phenotype [231], suggesting sufficient tumour metabolism modulatory activity in patients; however, no hypoxia measures were utilised. A recent randomised study of concurrent CRT with or without metformin in LA-NSCLC failed to demonstrate improvement in outcomes [232]. A number of clinical studies are currently underway to investigate the effect of metformin on tumour hypoxia with no reported results as of yet.

Numerous other FDA approved drugs, as well as new experimental agents, have been shown to inhibit OXPHOS pre-clinically but several have significant toxicity and unfavourable pharmacokinetics, and are thus unattractive candidates [219]. In one early phase study of the novel complex I inhibitor BAY87-2243, the trial was terminated early due to unexpected toxicity [233], demonstrating the importance of carefully assessing the safety of such agents, especially when combined with chemotherapy or radiotherapy. Another complex I inhibitor papaverine had also been shown to reduce hypoxia and improve tumour radiation response pre-clinically [234] and is undergoing phase I testing in combination with SABR in NSCLC but unfortunately, once again, no hypoxia readouts have been included in the study design.

1.6.4.3 Summary of OCR inhibition as a strategy to alleviate tumour hypoxia

Overall, pre-clinical data is highly encouraging for developing OXPHOS inhibitors in order to reduce OCR and thus tumour hypoxia. However, the translation of such agents into the clinical setting has proven challenging with no clinical evidence to date of alleviation of tumour hypoxia. Any agent being developed for this purpose must not only have strong pre-clinical data to support its effect on OCR and hypoxia, but do so at clinically relevant concentrations and with favourable toxicity profile.

The recent discovery that the commonly prescribed and well-tolerated antimalarial drug atovaquone meets all such criteria is of great promise. The work presented in this thesis represents the translation of this exciting finding into the clinical setting, in order to establish clinical proof of principle of not only this drug as a hypoxia modifier, but for the concept of OCR inhibition more widely.

1.7 ATOVAQUONE AS A NOVEL TUMOUR HYPOXIA MODIFIER AND POTENTIAL ANTI-CANCER TREATMENT

1.7.1 Atovaquone as a commonly used antimicrobial

1.7.1.1 Discovery and current clinical uses of atovaquone

Atovaquone is an FDA approved drug in widespread clinical use for over 20 years. It is currently used as a single agent for the treatment of the *Pneumocystis* pneumonia caused by the opportunistic fungus *Pneumocystis jirovecii*, and in combination with proguanil for the prophylaxis and treatment of malaria caused by the protozoa *Plasmodium falciparum.*

Atovaquone (2-[trans-4-(4'-chlorophenyl) cyclohexyl]-3-hydroxy-1,4-naphthoquinone, 566C80) is a ubiquinone (co-enzyme Q10) analogue which emerged in 1991 as the leading compound with efficacy against malaria and opportunistic infections such as *Pneumocystis* pneumonia in immunosuppressed patients with favourable pharmacokinetic properties [235]. The chemical structure of atovaquone is shown in Figure 1.9.

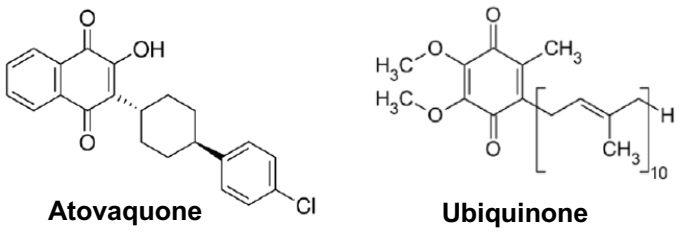


Figure 1.9: Chemical structure of atovaquone
The chemical structure of atovaquone and its similarity with that of ubiquinone. Adapted from [236] under CC licensing.

Following required improvements in synthesis methodology, atovaquone became a commonly used antimicrobial in patients from the mid 1990s. Today, in combination with proguanil, atovaquone accounts for over 70% of malarial prophylaxis prescriptions in the US [237].

1.7.1.2 Atovaquone antimicrobial pharmacodynamics

The mechanism of action of atovaquone against *Plasmodium falciparum* is mediated through inhibition of mitochondrial complex III [238,239], whereas the mechanism responsible for atovaquone's activity against *Pneumocystis* species still remains unknown. Complex III, also known as cytochrome bc_1 complex or co-enzyme Q cytochrome c reductase, is a multi-subunit transmembrane protein located in the inner mitochondrial membrane which couples the electron transfer from ubiquinol, the reduced form of ubiquinone or co-enzyme Q, to cytochrome *c,* resulting in the movement of four protons across the lipid bilayer and thereby contributing significantly to ATP production. Atovaquone binds to the catalytic Q_o site through hydrogen bonding to the Rieske iron-sulfur proteins which form the most important catalytic subunit of complex III required for transfer of electrons from ubiquinol during the ETC [240,241]. By disrupting mitochondrial respiration in this way, atovaquone significantly prevents energy

production in parasites. In addition, atovaquone also acts by blocking essential pyrimidine biosynthesis, which has been shown to be the predominant metabolic function of complex III in *Plasmodium falciparum* [242].

1.7.1.3 Atovaquone pharmacokinetics

Atovaquone is highly lipophilic with very low aqueous solubility. The bioavailability is variable and highly dependent upon the formulation used and whether it is administered together with food. When used as a single agent for the treatment of *Pneumocystis* pneumonia, atovaquone tablet formulations have been largely replaced with micronised particle suspensions, which have been shown to increase bioavailability two-fold. Administration of atovaquone with high fat-content food significantly enhances absorption further by again approximately two-fold and is therefore recommended.

The dose of atovaquone for the treatment of mild to moderate pneumocystis pneumonia is 750 mg twice daily, with higher doses previously used in severe infections. Studies using atovaquone suspension at this dose in patients with HIV and *Pneumocystis* pneumonia have demonstrated average plasma atovaquone concentrations in the region of 21-22 μg/mL (57-60 μM) with steady-state plasma levels achieved after approximately six to seven days of drug administration. Atovaquone is extensively bound to plasma proteins (99.9%) over the concentration range of 1 to 90 μg/mL and the half-life is two to three days. This long half-life is due to lack of metabolism of atovaquone and extensive enterohepatic cycling. The vast majority (>90%) of atovaquone is excreted unchanged in faeces [243,244].

1.7.1.4 Toxicity profile

Atovaquone causes very few side effects and has an excellent safety profile. Adverse events which have potentially been attributed to atovaquone are generally very mild and most commonly include rash, fever, vomiting, diarrhoea, abdominal pain and headache [243,244]. Encouragingly, an overdose of atovaquone with 31,500 mg resulted in no observed toxicity [245].

1.7.2 Atovaquone as novel tumour hypoxia modifier and radiosensitiser

Using a Seahorse XF analyser, Ashton *et al*. [219] conducted a high-throughput screen of 1697 FDA approved drugs to assess their effect on OCR in FaDu hypopharyngeal cancer cells. A number of compounds were identified to cause a decrease in OCR, the majority of which were excluded from further evaluation based on pragmatic criteria that included known unacceptable toxicity, poor pharmacokinetics and agents where the achievable concentration in patients is below that required for OCR reduction. As atovaquone reduced OCR at easily achievable concentrations clinically and has an excellent safety profile, it proved to be the best agent to take forward for further evaluation as potential tumour hypoxia modifier.

Subsequently, it was demonstrated that 10 μM atovaquone dramatically reduced OCR by approximately 80-90% in A549 lung cancer, H1299 lung cancer, H460 large cell lung cancer, HCT116 colorectal cancer, DLD-1 colorectal cancer, MCF7 breast cancer and T24 bladder cancer cells. A lesser but still impressive reduction of 58% in OCR was seen in PSN-1 pancreatic cancer cells. Furthermore, the effect on OCR was dose-dependent with smaller but still significant decreases in OCR observed at 2 μM [219]. Atovaquone was then demonstrated to completely alleviate hypoxia in 3D spheroids of FaDu, H1299 and

HCT116 3D cells, again at clinically achievable concentrations. Combination of atovaquone treatment and radiation in FaDu spheroids resulted in increased growth delay following irradiation.

In vivo experiments provided further support for atovaquone as a tumour hypoxia modifier and radiosensitiser. Using FaDu and HT116 mice xenograft models, seven days of atovaquone treatment was shown to eradicate tumour hypoxia as detected by tumour EF5 staining, with mean mice plasma levels comparable to those seen in patients. There was no effect on tumour growth in FaDu xenografts with atovaquone treatment alone, but marked tumour growth delay was observed when combined with radiation [219].

Mechanistic experiments in FaDu cells demonstrated that, as per its antimicrobial mode of action, atovaquone specifically inhibits mitochondrial complex III. With regards to radiosensitisation, colony formation assays performed under different oxygen conditions revealed that atovaquone did not alter radiosensitivity, indicating that atovaquone is not an intrinsic radiosensitiser [219].

Overall, this data provides compelling evidence that atovaquone decreases OCR through mitochondrial complex III inhibition, which results in a reduction in tumour hypoxia and in turn results in tumour radiosensitisation. Given that hypoxia is predominantly a tumour-specific phenomenon, is it hypothesised that atovaquone would preferentially sensitise tumours and not normal tissues to radiation and thus improve the therapeutic index for radiotherapy. As atovaquone is safe, well tolerated and inexpensive, it represents a truly ideal agent to take into clinical testing as a novel hypoxia modifier.

1.8 SUMMARY AND AIMS OF THESIS

1.8.1 Summary

Lung cancer is a devastating disease with novel radiosensitisers urgently needed to improve poor radiotherapy outcomes. Since its discovery over half a century ago, tumour hypoxia is perhaps the best validated target in oncology given its key role in tumorigenesis and treatment resistance leading to poor clinical outcomes. This is especially pertinent for patients receiving radiotherapy treatment, given the profound tumour radioresistance under hypoxic conditions.

Previous attempts to tackle hypoxia have largely focused on improving tumour oxygen supply. However, despite decades of clinical trials combining promising agents with radiotherapy, no hypoxia modifiers are in widespread clinical use to date. The reasons for this are multifactorial but undoubtedly include a lack of clinical studies confirming such agents modify hypoxia in patients and an inability to select patients for treatment due to an absence of sufficiently validated hypoxia biomarkers.

An exciting new strategy to tackle tumour hypoxia is reprogramming cellular metabolism through inhibition of OXPHOS to reduce tumour OCR. The commonly prescribed antimicrobial drug atovaquone has emerged as the most promising agent for this purpose. However, before embarking on studies combining atovaquone with radiotherapy, it is important to demonstrate tumour hypoxia modification in the clinical setting and strive to develop hypoxia biomarkers to inform the design of any future atovaquone and radiotherapy combination studies. The work presented in this thesis specifically addresses both of these points.

1.8.2 Aims

The aims of this DPhil project were as follows:

1) To design and conduct a clinical proof of principle trial to investigate the effect of atovaquone on tumour hypoxia in patients with NSCLC.
2) To further develop candidate hypoxia biomarkers to inform the design of future hypoxia modification clinical studies.

CHAPTER 2: MATERIALS AND METHODS

2.1 THE ATOM CLINICAL TRIAL

2.1.1 Overview of study design

The Atovaquone as a Tumour hypOxia Modifier (ATOM) trial (NCT02628080) was a phase 0, single-centre (Oxford University Hospitals NHS Foundation Trust), open-label, window-of-opportunity study, which primarily investigated whether a short course of atovaquone treatment reduces tumour hypoxia in patients with resectable NSCLC. All patients provided written informed consent and the conduct of the trial complied fully with the Declaration of Helsinki. Ethical approval was obtained prior to study opening from the National Research Ethics Service Committee South Central Berkshire B (16/SC/0012).

The trial was designed to recruit 30 patients to two cohorts sequentially: 15 patients to Cohort 1 receiving atovaquone treatment and 15 patients to Cohort 2 not receiving treatment. Patients attended for two study visits during which multiple investigations were performed to assess tumour hypoxia, as well as tumour perfusion. Shortly following the second investigation visit, patients proceeded to surgery as originally planned at which point tumour tissue was collected for analysis from the resected specimen.

2.1.2 Patients

Patients with resectable NSCLC and deemed fit for surgery were identified in cardiothoracic outpatient clinics and invited to participate in the study. The main patient eligibility criteria are shown in Table 2.1.

Table 2.1: Main patient eligibility criteria

Inclusion criteria	Exclusion criteria
• Confirmed or suspected NSCLC considered suitable for surgical resection by the Lung Cancer Multidisciplinary Team • Age ≥ 18 years • Eastern Cooperative Oncology Group performance status of 0-2 • At least one measurable lesion >2 cm in maximal length on diagnostic imaging performed within 60 days of trial screening • Haematological and biochemical blood indices within the specified range • Written informed consent • Willing and able to comply with trial protocol	• Previous systemic chemotherapy or biological therapy within 21 days of commencing atovaquone treatment • Treatment with other investigational agent, or participation in another interventional clinical trial within 28 days of recruitment • Known previous adverse reaction to atovaquone or its excipients • Co-administration of known electron transport chain inhibitors (including metformin) • Impaired gastrointestinal function that may significantly alter absorption of atovaquone • Administration of warfarin in the 14 days prior to starting atovaquone • Active hepatitis, gallbladder disease or pancreatitis

2.1.3 Trial interventions

2.1.3.1 Baseline investigations

During the baseline study visit (Visit 1), FMISO PET-CT was conducted to quantify the tumour hypoxic volume (HV), as well as other hypoxia PET imaging parameters as outlined in section 2.2.1. FAZA PET-CT was used in the event that FMISO was unavailable. Tumour perfusion was also measured using perfusion CT (pCT) and performed immediately following completion of hypoxia PET (hyp-PET) imaging. In addition to imaging, levels of the candidate hypoxia plasma markers were measured which included VEGF, CAIX, osteopontin (OPN) and miR-210. The methodology for each of these techniques is described in detail later in this chapter.

2.1.3.2 Atovaquone treatment

Patients in Cohort 1 received 7 to 16 days of 750 mg twice-daily oral atovaquone treatment (Wellvone 750 mg/5 mL oral micronised suspension, GlaxoSmithKline UK) starting immediately after completion of all baseline investigations with the last dose of atovaquone administered the evening prior to surgery. Whenever possible, the maximum length of treatment was administered, however the treatment length was shorter for patients for whom the time interval prior to surgery required this, with a minimum of seven days treatment mandated as this is the length of treatment required to achieve stable plasma levels.

2.1.3.3 Follow-up investigations

During the follow-up visit (Visit 2), all patients underwent identical investigations to those described for the baseline visit. In addition, plasma atovaquone levels were measured for Cohort 1 patients. The interval between the baseline and follow-up visits was maximised (16 days) whenever possible with the minimum of seven days for Cohort 1 and two days for Cohort 2.

During Visit 2, full clinical assessment was performed as well as routine haematology and biochemistry blood tests were taken to assess for toxicity. Given the established favourable toxicity profile of atovaquone, only CTCAE grade ≥ 3 or unexpected adverse events (AEs) were reported. Completion of Visit 2 investigations marked the end of study participation.

2.1.3.4 Pimonidazole hydrochloride administration

All patients were provided with 500 mg/m^2 oral pimonidazole hydrochloride (Hydroxyprobe-1, Natural Pharmacia International, Inc.), an exogenous nitroimidazole hypoxia marker, for self-administration 16 to 24 hours prior to surgery.

2.1.3.5 Surgery, specimen processing and tumour analysis

Surgery was not delayed for any patient. Immediately following resection, the specimen (usually lobectomy or pneumonectomy) was inflated and fixed with formalin. Subsequently, the specimen underwent cut-up and tumour tissue was embedded in paraffin blocks, as per standard clinical practice. For the purposes of this study, the whole tumour was collected and stored. Tumour IHC for pimonidazole and CAIX, as well as measurement of tumour atovaquone levels (Cohort 1 only) was conducted.

2.1.3.6 Trial schema

The ATOM trial schema showing all trial interventions is shown in Figure 2.1.

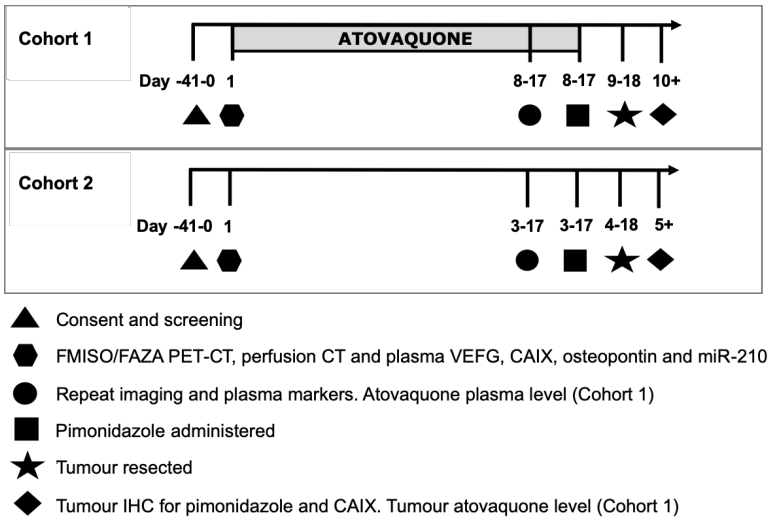


Figure 2.1: The ATOM trial schema

2.1.3.7 Additional investigations from the ATOM trial

In addition to the above hypoxia and perfusion measures, additional investigations were performed as part of the ATOM trial. For completion, these investigations included additional tumour imaging to assess tumour perfusion using DCE and DWI MRI as well as dynamic FMISO or FAZA PET-CT. Also, tumour tissue hypoxia metagene and mutational analysis is underway, as is IHC for the vascular markers CD31 and CD146. These investigations are currently being analysed and therefore lie outwith the scope of this thesis.

2.1.3.8 Confirmation of patient evaluability

Patients were deemed evaluable if >75% of the prescribed atovaquone dose was taken (Cohort 1) and if two sets of interpretable hypoxia PET-CT scans were obtained. Patients with insufficient hypoxia (HV <1.5 mL) on baseline imaging to reliably measure change in hypoxia were deemed unevaluable and were replaced, however their data was still used for correlation with other trial endpoints. This volume of hypoxia, which corresponds to 62 PET voxels, was pragmatically chosen and implemented following discussion with trial radiologists and physicists as it was felt to represent a sufficient volume to reliably compare between PET scans above the background 'noise' of this imaging modality.

Patients who did not take pimonidazole or patients who did not undergo surgery were still evaluable for the study as long as a histological diagnosis of NSCLC was available.

2.1.4 Trial objectives and endpoints

The primary, secondary and tertiary trial objectives and corresponding endpoint measures which are relevant for this thesis are shown in Table 2.2.

Table 2.2: ATOM trial tumour hypoxia and perfusion related objectives and endpoints

Primary objective	**Endpoint measures**	**Cohorts and timepoint(s)**
To assess whether atovaquone reduces tumour hypoxia	FMISO/FAZA PET Plasma CAIX, OPN and VEGF	Cohort 1 and between Cohort 1 and 2 (Visit 1 and 2)
	Pimonidazole IHC	Between Cohort 1 and 2 (post-surgery)
Secondary objectives		
To further assess whether atovaquone reduces tumour hypoxia	Plasma miR-210	Cohort 1 and between Cohort 1 and 2 (Visit 1 and 2)
To assess whether atovaquone changes tumour perfusion	Perfusion CT	Cohort 1 and between Cohort 1 and 2 (Visit 1 and 2)
To assess whether plasma hypoxia markers correlate with FMISO/FAZA PET and one another	Plasma CAIX, OPN, VEGF and miR-210 FMISO/FAZA PET	Cohort 1 and 2 combined (Visit 1)
Tertiary objectives		
To assess whether plasma and tumour atovaquone levels predict change in hypoxia	Plasma and tumour atovaquone levels FMISO/FAZA PET	Cohort 1 (Visit 1 and 2 and post-surgery)
To assess correlation between FMISO/FAZA PET and hypoxia assessed by IHC	FMISO/FAZA PET Pimonidazole and CAIX IHC	Cohort 1 and 2 combined (Visit 2 and post-surgery)
To assess correlation between plasma hypoxia marker and hypoxia assessed by IHC	Plasma and IHC CAIX	Cohort 1 and 2 combined (Visit 2 and post-surgery)
To assess atovaquone toxicity	Clinical assessment	Cohort 1 (Visit 2)

Abbreviations: FMISO, [^{18}F]-fluoromisonidazole; FAZA, [^{18}F]-fluoroazomycin arabinoside; PET, positron emission tomography; CT, computed tomography; VEGF, vascular endothelial growth factor; CAIX, carbonic anhydrase IX; OPN, osteopontin; IHC, immunohistochemistry.

In addition to these objectives, for the purposes of this thesis it was also investigated whether clinicopathological features such as tumour size, stage of disease, histology subtype and diagnostic FDG PET avidity were predictive of tumour hypoxia and perfusion. The effect of atovaquone on tumour volume and survival (PFS and OS) was also described.

2.2 TUMOUR IMAGING

2.2.1 FMISO and FAZA PET-CT

FMISO or FAZA hypoxia PET (hyp-PET) imaging was performed to visualise and quantify tumour hypoxia. Patients were imaged in the supine position with arms above head (if possible) in a single bed position using a GE Discovery 690 or 710 PET-CT scanner (GE Healthcare, USA). An activity of 370 MBq of FMISO (University of Cambridge) or FAZA (University of Manchester) was injected and a 10-minute PET acquisition image was acquired 4 hours post-injection. CT was performed for localisation and PET attenuation correction. It was mandated that each patient underwent scanning using the same tracer and PET-CT scanner for both imaging visits.

Analysis of the 4-hour hyp-PET images was performed using Hermes Hybrid Viewer software (Hermes Medical Solutions AB, Sweden). Tumours were outlined on each CT image and the volumes were transferred to the corresponding PET images (PET and CT images were hard-registered by the PET-CT imaging system). If any metastases or involved nodes were identified within the PET field of view, they were also outlined and included in the analysis. Prior diagnostic imaging was used to guide tumour outlining and all outlines were reviewed and approved by an experienced consultant PET radiologist. A volume of blood in the centre of the descending aorta was outlined using 10 consecutive PET images to provide the background mean standardised uptake value (SUV_{mean}). Next, to determine the tumour hypoxic volume (HV), voxel-by-voxel SUVs were divided by the background SUV_{mean} to provide tumour-to-blood ratio (TBR) values for each tumour voxel and voxels with TBR ≥1.4 were classified as hypoxic, as previously described [126]. Volumes of hypoxic voxels before and after atovaquone were compared and ≥10% reduction in HV from baseline defined as a meaningful change. This cut-off was based on

FMISO reproducibility test-retest data [128] and used the minimum detectable change (MDC) method [246]. Okamoto et al. demonstrated a mean difference of 2.7% and SD 14% in tumour-to-muscle (TMR) volumes from FMISO scans repeated within 48 hours (n=9, excluding two patients with TMR volumes <1.5 mL) [128]. MDC is the minimum change at 95% confidence and is defined as the standard error (4.7) multiplied by 1.96, giving 9.2%. The ≥10% threshold was previously ratified by the University's independent Early Phase Trial Oversight Committee in combination with external radiology advice and our group has recently published another clinical trial using this threshold [125]. Patients with an insufficient HV (<1.5 mL) on baseline imaging to reliably measure change in HV were deemed unevaluable and were replaced.

Other hyp-PET parameters used for analysis were the percentage of the tumour volume which was defined as hypoxic (HV%), the mean tumour TBR (TBR_{mean}) and the highest TBR_{mean} value for a contiguous 1 cm^3 volume of tumour (TBR_{peak}), as previously published [127,247].

2.2.2 Perfusion CT

pCT was performed immediately following the hyp-PET using the same PET-CT scanner with patients in the same position. A pre-contrast CT was initially performed to determine the location for the pCT scan. The pCT was limited to a 4 cm region of the tumour in the superior to inferior direction due to high temporal resolution (one image per second) and CT detector width. This meant that for large tumours the tumour was not fully imaged during the pCT scan. When the change in pCT parameters was investigated between imaging visits per individual patient, only data from matched tumour regions was used, whereas for correlation with other trial endpoints unmatched data was used, as this was more representative of the whole tumour. Images were acquired in cine mode (120 kV, 60

mA) with 70 mL iodinated contrast (Omnipaque 300) injected at 5 mL/s followed by a 25 mL water flush at 5 mL/s. The scan duration was 45 seconds, during which time patients were instructed to hold their breath in inspiration for as long as possible and to breathe out slowly, if needed. As any movement during the scan is of concern for pCT analysis as the voxel size is very small (0.7 mm), motion correction was performed using software developed by our Engineering Department [248]. The motion-corrected pCT data was then processed voxel-by-voxel using the commercial software GE Perfusion 4D (GE Healthcare, USA) using an input function obtained from the mean of a selected region in the descending aorta to provide tumour blood flow (BF), blood volume (BV) and mean transit time (MTT) parameters. A meaningful change in these parameters was classed as ≥25% change from baseline, consistent with previously published data [249].

2.3 CIRCULATING MARKERS OF HYPOXIA

2.3.1 Plasma collection

Plasma was collected for VEGF, CAIX, OPN and miR-210 on arrival at Visit 1 and Visit 2. For each patient, 2 x 10 mL EDTA vacutainers were filled with blood, inverted a number of times and placed on ice with subsequent processing occurring within 30 minutes. The samples were centrifuged at 2000 x g for 10 minutes at 4°C after which the plasma layer was transferred into fresh collection tubes and centrifuged again at the same conditions. The plasma was then aliquoted into cryovials and stored at -80°C.

2.3.2 Enzyme-linked immunosorbent assays for VEGF, CAIX and OPN

2.3.2.1 Assay technique

Frozen plasma samples were defrosted, mixed and spun before being assayed using Human Carbonic Anhydrase IX, VEGF or Osteopontin Quantikine ELISA Kits (R&D Systems,

USA, DCA900, DVE00 and DOST00, respectively) according to the manufacturer's instructions. Samples were assayed in duplicate alongside seven standards (prepared on the day) and three quality controls (QCs) generated previously from recombinant protein (R&D Systems, USA). One set of standards and two sets of QCs were assayed for each 96 well plate.

Plates were measured for absorbance at 450 and 570 nm using the FLUOstar Omega Plate Reader (BMG LABTECH, Germany). Blank corrected readings at 570 nm were subtracted from blank corrected readings at 450 nm using MARS Data Analysis Software (BMG LABTECH, Germany). MasterPlex Readerfit Software (MiraiBio Group of Hitachi Solutions America, Ltd) was used to generate a 4-parameter fit curve (weighted with $1/y^2$) from the blank corrected 450-570 nm subtracted MARS data to determine concentration values from optical density. Using Microsoft Excel, mean concentration, standard deviation and percentage coefficient of variation (%CV) were generated for each duplicate.

2.3.2.2 Quality control

As previously determined by validation experiments conducted by Good Clinical Practice (GCP) Laboratory, University of Oxford, for other clinical studies, the mean value of at least 4 of 6 QC concentrations on each plate were required to be within 20% (for high and medium QC) or 25% (for low QC) of the expected concentration. In addition, for the standards the mean readings needed to be within 15% of expected value, except for the lowest standard, which needed to be within 25%. Mrs Lisa Folkes and Mrs Leticia Campo (GCP Labortatory) assisted with sample analysis.

2.3.3 TaqMan RT-PCR for miR-210

Plasma levels of miR-210 were quantified relative to the endogenous reference miRNA miR-16, as well as to a synthetic 'spike-in' miR-Cel-39. miR-16 is a commonly used reference miRNA when measuring circulating miRNAs and has been shown to be highly stable in patients with a range of different cancers, including NSCLC [250–252]. A synthetic spike-in miRNA, not endogenously expressed in humans, was added to the plasma samples prior to processing. This permitted correction of differences in RNA extraction efficiencies between samples [253]. Optimisation of the methodology used was conducted by Dr Remko Prevo (Higgins Laboratory Manager) who also assisted with sample analysis.

2.3.3.1 Sample preparation and RNA extraction

Plasma samples were defrosted at room temperature, mixed and centrifuged at 12000 x g for 15 minutes to pellet any cell debris and 500 µl of supernatant was used for analysis. Proteinase K digestion and RNA extraction was undertaken using Quick-cfRNA Serum & Plasma Kit (Zymo Research, USA, R1059), as per the manufacturer's instructions, with one additional step prior proteinase K digestion, which involved a 15-minute incubation at 55°C to improve subsequent proteinase K digestion. Subsequently, 5 µl of 0.03 nM miR-Cel-39 spike-in (Life Technologies, USA) was added to each sample prior to incubation with proteinase K.

2.3.3.2 Preparation of QC samples

miR-210, miR-16 and cel-miR-39 miRNA QCs were prepared in advance using purchased synthetic custom-made miRNAs (Life Technologies, USA) and pooled together at 50 µM concentration (each) and stored at -80°C. On the day of sample processing, for each batch

of samples a QC was defrosted and diluted using yeast tRNA water (RNA carrier), 5 μg/ml aliquots of which were prepared in advance and stored at -80°C. Final concentrations of all miRNAs used for cDNA synthesis were 50 pM.

2.3.3.3 cDNA synthesis

cDNA synthesis was performed using TaqMan microRNA Reverse Transcription Kit (Life Technologies, USA) according to the manufacturer's instructions. A cDNA Mastermix was prepared and contained the following components for each individual reaction:

Reagent	**Volume per reaction (μl)**
dNTP mix	0.15
Multiscribe RT enzyme	1.00
10 x RT Buffer	1.50
RNase Inhibitor	0.19
Nuclease free water	4.16
Total	**7.00**

Each cDNA synthesis reaction was performed in a final volume of 15 μl, which contained:

Reagent	**Volume per reaction (μl)**
cDNA Mastermix	7
Sample or QC miRNA	5
Specific miRNA cDNA RT primer	3
Total	**15**

The specific miRNA cDNA RT primers were part of TaqMan MicroRNA Assays: hsa-miR-210, hsa-miR-16 and cel-miR-39 (Thermo Fisher Scientific, USA). cDNA synthesis was performed using a DNA Engine Tetrad PCR Thermal Cycler (Bio-Rad Laboratories, USA) which was programmed as follows: 16°C for 30 minutes, 42°C for 30 minutes, 85°C for 5 minutes and hold at 4°C.

2.3.3.4 TaqMan PCR

TaqMan PCR was performed in duplicate in a final volume of 20 µl per individual reaction, which contained:

Reagent	**Volume per reaction (µl)**
TaqMan Universal Master Mix II	10
Specific TaqMan assay miRNA probe	1
Nuclease free water	4
cDNA template (or water control)	5
Total	**20**

The specific miRNA cDNA TaqMan probes were part of TaqMan MicroRNA Assays: hsa-miR-210, hsa-miR-16 and cel-miR-39 (Thermo Fisher Scientific, USA). Nuclease free water (Thermo Fisher Scientific, USA) was used as the no-template control. Each cDNA template was diluted 3.3-fold using PCR water prior to use. For the PCR reaction, the Step-One Real Time PCR machine (Thermo Fisher Scientific, USA) was used with the following thermocycling parameters: 95°C for 10 mins and then 40 cycles of 95°C for 15 seconds and 60°C for 1 minute.

The Step-One Real Time PCR machine software generates the mean cycle threshold (Ct) values for the targets which are transferred into Microsoft Excel to calculate the relative miR-210 expression in each plasma sample using delta-delta Ct method using the exogenous (Cel-miR-39) and endogenous (miR-16) miRNAs as combined reference miRNAs.

2.3.3.5 Quality control

The following acceptance criteria were mandated based on comprehensive validation experiments of this technique conducted by Dr Remko Prevo (Laboratory Manager, Higgins group, University of Oxford):

- Ct values for individual miRNAs must lie between 12 and 34.
- The mean Ct value for the negative controls (water template) for each TaqMan probe must be at least 35 or not detectable.
- The miRNA recovery rate of the RNA purification step must be > 10%, which will correspond to a maximum Ct value of 26.4 for the spike-in miRNA.
- The %CV for Ct values from duplicate PCR reactions on sample cDNA must be < 2 %
- The Ct values for the positive controls (QCs; 50 pM synthetic miRNA pool) must lie between 14 and 18 for Cel-miR-39 and between 15.5 and 19.5 for miR-210 and miR-16.

2.4 TUMOUR PROCESSING AND IMMUNOHISTOCHEMICAL ANALYSIS FOR PIMONIDAZOLE AND CAIX

2.4.1 Generation of orientated formalin-fixed paraffin-embedded tumour blocks

Immediately following surgical resection, the lung specimen (usually lobectomy or pneumonectomy) containing the tumour was inflated with standard clinical grade 10% neutral buffered formalin and left to fix at room temperature. As this was a diagnostic clinical specimen, the length of fixation before specimen cut-up was variable and dictated by clinical resources including the histopathologist's availability. The length of fixation varied from 1 to 12 days. During the cut-up, the specimen was oriented by a Consultant Radiologist using pre-surgical imaging and specimen orientation sutures placed by the

surgeon at the time of resection. The reason for orientating the specimen prior to cut-up was to ensure that the tumour sections generated were in the same axial plane as the hyp-PET images to allow ongoing work investigating whether there is spatiotemporal agreement between hypoxia imaging, IHC and gene expression within tumours.

The resected specimen was sliced from superior to inferior in 4 to 5 mm thick slices (Figure 2.2) and the surrounding normal lung trimmed and discarded. Following clinical annotation, each slice was subdivided in order to fit into standard size cassettes, if required. Prior to loading of tissue into cassettes, the tissue edges were inked with different coloured dye to permit orientation of IHC sections.



Figure 2.2: Photograph of resected lung specimen
Thirteen consecutive 5 mm slices of a formalin inflated and fixed right upper lobe (patient 10004) revealing that it is almost entirely replaced by an 8 x 5 cm (maximum diameter) adenocarcinoma. Note the significant central regions of necrosis in certain slices (arrow).

The entire tumour was loaded into cassettes with careful annotation of which slice level corresponds to which unique cassette ID, and subsequently tissue processing and paraffin embedding was performed as per standard clinical procedure. The generated formalin-

fixed paraffin-embedded (FFPE) blocks required for clinical analysis were stored in the John Radcliffe Hospital clinical sample archives, whereas the remainder of the tumour blocks were stored in the Oxford Radcliffe Biobank.

All FFPE blocks per individual patient were reviewed and three levels per tumour were selected for IHC analysis, based on presence of ample tumour tissue from one level located near the top, middle and bottom of the tumour. The number of blocks which constituted a tumour level varied depending upon the size of the tumour and ranged from 1 to 12.

2.4.2 Tumour immunohistochemical analysis

2.4.2.1 Generation of stained sections

From each FFPE block, three 4 μM thick sections were cut using a microtome and mounted onto charged slides. One slide underwent haematoxylin and eosin staining whilst the other two sections were used for IHC analysis for pimonidazole and CAIX. In addition, two further sections were generated for IHC analysis of CD31 and CD146 and also one 10 μM section for taken for hypoxia metagene analysis as part of ongoing work as previously described.

All IHC staining was automated and performed using the Leica BOND-MAX Autostainer (Leica Biosystems, Germany) to ensure high-throughput and technical consistency. All stains had been previously optimised and validated by the Translational Histopathology Laboratory, University of Oxford, for previous pre-clinical and clinical studies. The following conditions were used: antigen retrieval at 100ºC for 20 minutes with Epitope Retrieval Solution 1 or 2 (Leica Biosystems, Germany), primary antibody incubation for 30 minutes and then detection using horseradish peroxidase enzyme-based BOND

Polymer Refine Detection System (Leica Biosystems, Germany), as per manufacturer's instructions.

For pimonidazole IHC, the primary antibody used was Hypoxyprobe-1 MAb1 Anti-pimonidazole mouse IgG1 monoclonal antibody (Natural Pharmacia International, USA, 4.3.11.3) at 1/1000 dilution. For a positive control, FFPE tissue from a mouse xenograft pilot 1 L1 model treated with pimonidazole was kindly donated by Professor Len Seymour's group, University of Oxford. CAIX IHC was performed using a rabbit polyclonal CAIX antibody (Abcam, UK, 15086) at 1/2000 dilution. For CAIX positive controls, a tissue microarray was used which was prepared by the Translational Histopathology Laboratory, University of Oxford, from multiple tumour and normal tissues purchased from ProteoGenex, USA. For pimonidazole and CAIX negative controls, mouse IgG (Abcam, UK, ab37355) and rabbit IgG (Genetex gtx47478) were used at the equivalent primary antibody concentrations, respectively. The quality of staining was reviewed and approved by Dr Mark McCole (Trial Consultant Histopathologist).

2.4.2.2 Immunohistochemical analysis

The analysis of IHC for this study involved establishing a collaboration between Dr Mark McCole, Dr Philip Macklin (Clinical Research Fellow, Nuffield Department of Medicine, University of Oxford), Dr Joshua Bull (Post-doctoral Researcher, Wolfson Centre for Mathematical Biology, University of Oxford) and Dr Alistair Easton (Consultant Histopathologist and Translational Histopathology Laboratory Lead, University of Oxford). Collaboratively, an automated IHC scoring method was developed due to the large number of IHC slides generated by this project (1250 in total) to ensure feasible throughput and IHC scoring consistency.

Stained slides were scanned at x 200 magnification using a NanoZoomer S210 digital slide scanner (Hamamatsu, Japan) to generate whole slide images. All subsequent analyses were conducted using MATLAB software (MathWorks, USA), using custom-made analysis scripts developed by Dr Joshua Bull. Each slide was annotated by Dr Philip Macklin with oversight by Dr Mark McCole at x 2.5 magnification power to demarcate the edge of the tissue section, the tumour boundary and any areas of processing artefacts. Detection of each IHC stain was conducted within the annotated tumour region of each image at x10 magnification using a bespoke imaging pipeline. This pipeline used the Simple Linear Iterative Clustering (SLIC) algorithm to generate superpixels with a size of approximately 30 pixels per superpixel. A support vector machine (SVM) classifier then was used to distinguish positively stained from negatively stained superpixels. Each SVM classifier was 'trained' by Dr Mark McCole and Dr Philip Macklin using images from a large number of patients by identifying regions of positive and negative staining. The proportion of stained tissue within the annotated tumour, that is without differentiation of scoring between the tumour epithelial and stromal compartments since this permits direct comparison with hyp-PET data and is routine practice in histopathology studies [254], was then reported as a percentage score. The percentage score per level, and subsequently per whole tumour was reported and used for trial endpoint analysis.

2.4.2.3 Quality control of scoring

The SMV classifiers were tested on images in which all positively stained superpixels have been previously manually annotated by Dr Philip Macklin ('ground truth data') and demonstrated good sensitivity and specificity. The classifier scoring was also tested against manual scores from Dr Alistair Easton who was independent to pipeline development on a randomly selected set of validation images (one image from each trial patient) with very

strong positive correlation ($r > 0.7$) mandated in order to permit the use of this methodology for scoring the trial sections.

2.5 MEASUREMENT OF PLASMA AND TUMOUR ATOVAQUONE LEVELS

Plasma and tumour tissue atovaquone levels were measured by high performance liquid chromatography (HPLC) using absorbance detection by Dr Lisa Folkes, Senior Bioanalysis Scientist, Bioanalysis Core, CRUK/MRC Oxford Institute for Radiation Oncology and Biology. For tumour HPLC, a piece of formalin-fixed tumour tissue was taken at the time of tumour cut-up (prior to tissue processing and paraffin embedding) and stored at -80°C prior to analysis.

2.6 SAFETY AND CLINICAL OUTCOME ANALYSIS

Given the already well-established excellent safety profile of atovaquone, only grade ≥3 adverse events (AEs) or grade ≥2 AEs related to atovaquone were reportable.

Twelve-month PFS and OS data was determined from review of patient medical records. This was data was available for all patients in Cohort 1 but only for a few patients in Cohort 2 due to official closure of the study.

2.7 STATISTICAL ANALYSIS

All data analysis was performed using GraphPad Prism software version 8.0 (GraphPad Software, USA). Descriptive statistics were used for describing baseline demographic and clinicopathological data, as well as for baseline hypoxia and perfusion parameters per cohort. No statistical analysis was performed to compare cohorts as the patient population studied was the same.

As the vast majority of data collected was not normally distributed, non-parametric tests were used to investigate the effect of atovaquone treatment on specific measures of interest: Wilcoxon signed-rank test was used to assess intra-patient changes per cohort and the Mann-Whitney U test was used for inter-cohort analyses, unless otherwise stated. For correlation analysis between data from different trial endpoints Spearman's rho correlation coefficient was used. Results from statistical testing was deemed significant if $p < 0.05$, with two-sided tests of significance performed.

Kaplan-Meier curves were generated for PFS and OS for patients for whom such data was available and 1-year rates were compared with historical data.

It is important to note that no formal power calculations were made for this study and no correction performed for multiple statistical testing. Therefore, all analyses performed and p values generated should be used for guidance purposes only and for hypothesis generation at best.

CHAPTER 3: CLINICAL DATA

3.1 INTRODUCTION

Clinical 'window of opportunity' studies describe trials in which patients undergo experimental intervention(s) in the time period between cancer diagnosis and initiation of standard treatment, typically surgery. Such studies generally include treatment naïve patients and provide a unique opportunity to conduct translational research in order to assess the effect of novel agents, and thus confirm clinical proof of principle, in biologically unaltered disease. Furthermore, such trials enable the development of specific disease-related biomarkers.

However, window of opportunity studies are notoriously difficult to conduct with generally high failure rates [255]. The obvious major challenge is the limited time available to undertake such research given that definitive treatment cannot be delayed, especially in the era of increasingly stringent clinical targets. Such studies require patient recruitment and mobilisation of numerous resources at exceedingly short notice. The successful delivery of such studies therefore heavily relies upon a highly motivated multidisciplinary team of clinical and research collaborators, as well as detailed upfront logistical planning.

The results now presented demonstrate the feasibility of conducting a complex and ambitious clinical proof of principle window of opportunity study in patients with operable NSCLC. The Atovaquone as a Tumour hypOxia Modifier (ATOM) trial was designed to recruit 30 patients to two cohorts sequentially: 15 patients to Cohort 1 receiving atovaquone treatment and 15 patients to Cohort 2 not receiving treatment. For both cohorts, baseline hypoxia FMISO or FAZA PET-CT (hyp-PET) was conducted and repeated following approximately two weeks and the tumour hypoxic volume (HV), as well as other hyp-PET derived parameters, were measured. In addition, during both visits the level of candidate hypoxia plasma markers were measured which included VEGF, CAIX, OPN

and miR-210. Furthermore, extensive resected tumour IHC analysis was conducted for endogenous CAIX as well as for the exogenous hypoxia marker pimonidazole. This trial primarily investigated whether a short course of atovaquone treatment reduced tumour hypoxia in patients with resectable NSCLC. Through correlative analysis of generated data, additional endpoints aimed to further validate such methods in the clinical assessment of tumour hypoxia and thus to contribute to the development of hypoxia biomarkers.

In this chapter, important clinical data will be presented to provide the necessary clinical context for interpreting the effect of atovaquone on tumour hypoxia as well as for hypoxia biomarker correlative analysis. In addition, atovaquone compliance, pharmacokinetics and toxicity will be presented. The effect of atovaquone on clinical outcomes such as a tumour volume as well as PFS and OS will also be examined. Finally, an assessment of whether readily available clinicopathological features can predict patients with sufficient baseline HV on hyp-PET to reliably measure change in this parameter using such imaging will be conducted, thus aiming to inform the design of future hyp-PET studies.

3.2 RESULTS

3.2.1 Trial recruitment and data collected

The ATOM trial opened in June 2016 and closed ahead of schedule in September 2018. In total, 46 patients were recruited. As planned, 30 patients were evaluable for primary endpoint hyp-PET analysis, 15 patients in the atovaquone treatment group (Cohort 1) and 15 patients in the untreated group (Cohort 2). The reasons why patients were unevaluable for hyp-PET analysis and were therefore replaced were: insufficient (<1.5 mL) baseline tumour HV to reliably assess change in this parameter using such imaging (n=13), uninterpretable FAZA PET-CT scan (n=1), FMISO production failure (n=1) and surgery

brought forward for clinical reasons (n=1). Patients who were deemed unevaluable on this basis prior to Visit 2 (n=14) did not attend for further investigations and did not receive atovaquone treatment or pimonidazole hydrochloride.

Thirty-two patients attended for both trial visits and were evaluable for assessing change in levels of VEGF, CAIX, OPN and miR-210, 17 patients in Cohort 1 and 15 patients in Cohort 2. Forty-four patients had both baseline plasma hypoxia markers and hypoxia PET data for correlative analysis.

Except for one patient for whom surgery was cancelled due to disease progression, all patients proceeded to surgery and the primary tumour was resected. Of the patients who attended for Visit 2, pimonidazole hydrochloride was administered within the required timeframe prior to surgery (16-24 hours) in 26 patients, 15 in Cohort 1 and 11 in Cohort 2. Reasons why patients did not receive pimonidazole hydrochloride, or did so but outwith the required treatment time window, were: rescheduling of surgery on the morning of the operation due to limited theatre or critical care bed availability (n=5) and cancellation of surgery in advance due to disease progression (n=1). Correlation between Visit 2 hypoxia PET and pimonidazole or CAIX IHC was possible for 25 (both cohorts) and 14 (Cohort 2) patients, respectively. Correlation of CAIX IHC and Visit 2 plasma CAIX levels was possible for 14 patients (Cohort 2).

Consolidated Standards of Reporting Trials (CONSORT) diagrams showing the recruitment and evaluability of patients for primary trial endpoints for Cohort 1 and Cohort 2 are shown in Figure 3.1 and Figure 3.2, respectively.

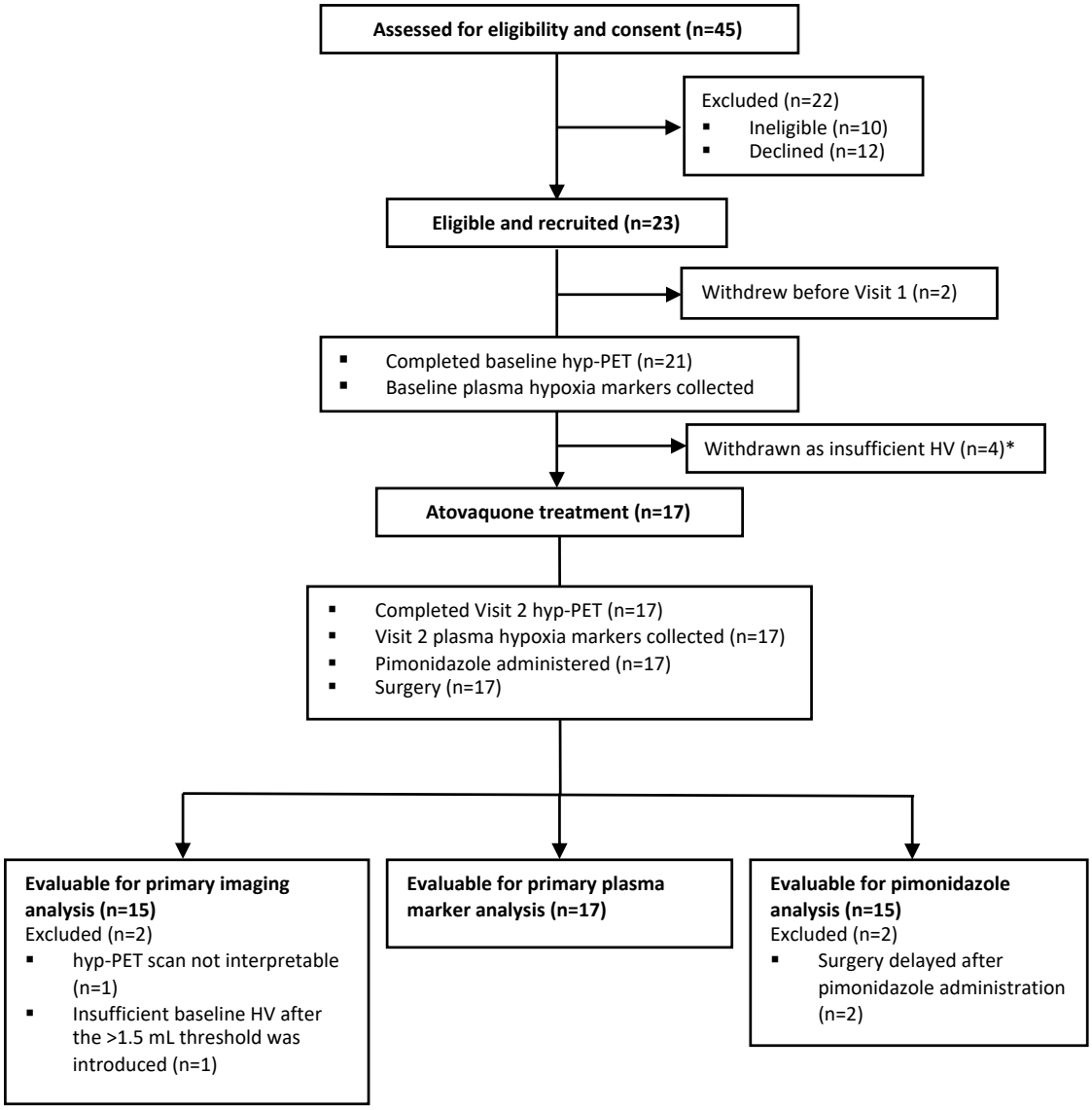


Figure 3.1: CONSORT diagram for Cohort 1
Recruitment and eligibility of patients for primary endpoints in Cohort 1. *One of the four patients with insufficient HV at baseline received atovaquone, this patient is not included in the number of patients treated with atovaquone. All four patients went on to have surgery but are not included in the number who had surgery in this diagram. Abbreviations: hyp-PET, hypoxia FMISO or FAZA positron emission tomography; HV, hypoxic volume.

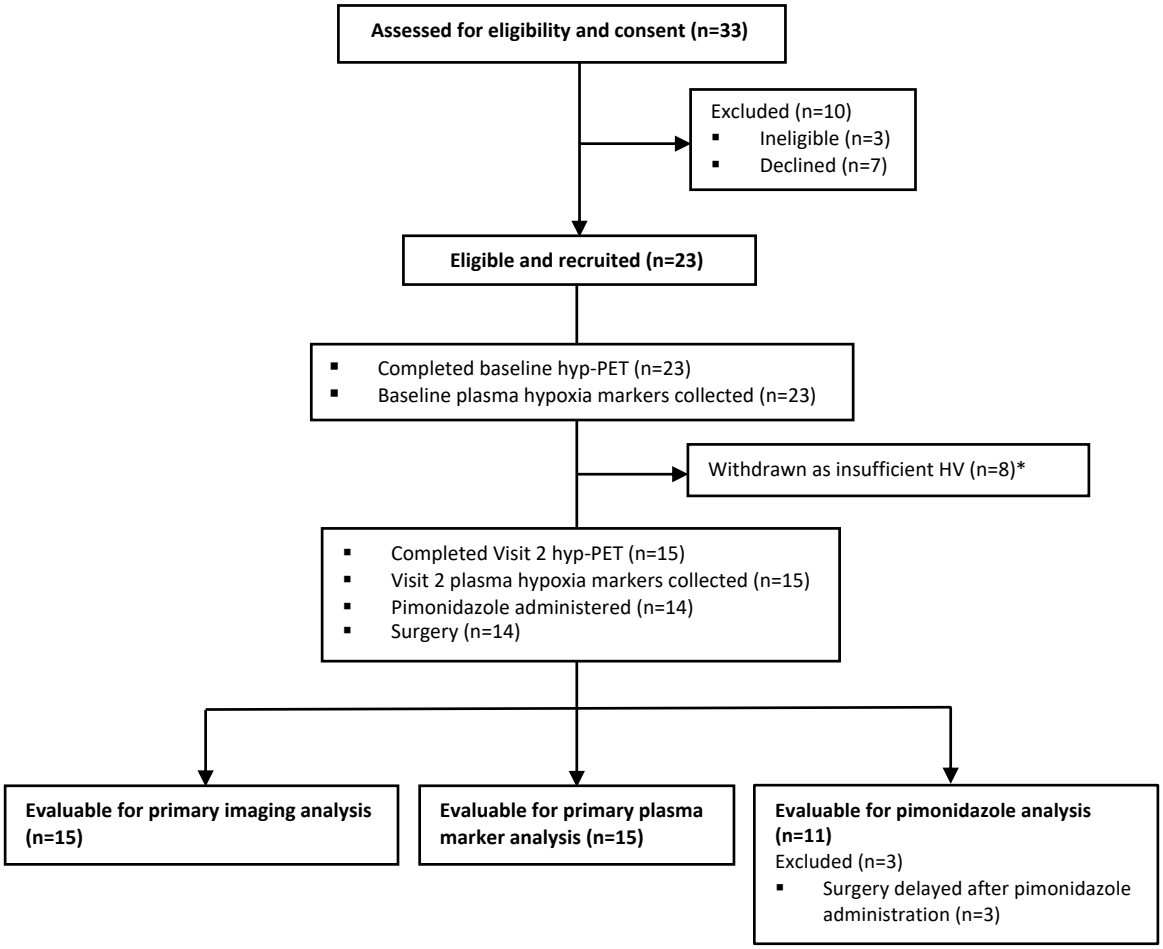


Figure 3.2: CONSORT diagram for Cohort 2
Recruitment and eligibility of patients for primary endpoints in Cohort 2. *All 8 patients with insufficient hypoxia at baseline went on to have surgery but are not included in the number who had surgery in this diagram. Abbreviations: hyp-PET, hypoxia FMISO positron emission tomography; HV, hypoxic volume.

Twenty-two patients were evaluable for assessing change in tumour perfusion using pCT, 16 patients in Cohort 1 and six patients in Cohort 2. Of the patients who attended for both study visits, six patients could not undergo paired pCT scans due to: inability to accommodate such scans due to lack of scanner availability (n=3), iodine contrast allergy (n=1), renal impairment (n=1) and contrast already administered on the day of pCT for clinical reasons (n=1). Technical differences between paired pCT scans resulted in four additional patients classed as unevaluable for this endpoint.

Plasma atovaquone levels were measured for all patients in Cohort 1 who attended for Visit 2 (n=17) and tumour atovaquone levels were measured in 14 patients in Cohort 1. The reason why no tumour tissue was collected for atovaquone measurement for three patients was: tumour too small to sample without impacting IHC analysis (n=1) and no trial personnel present to obtain this sample at time of resected specimen cut-up (n=2).

3.2.2 Baseline patient characteristics

The baseline clinical characteristics for all trial patients is shown in Table 3.1.

Table 3.1: Baseline patient characteristics

Characteristics	Cohort 1 (n=23)	Cohort 2 (n=23)
Age (years)	69.7 (58.5 – 74.1)	68.6 (62.4 – 71.4)
Sex		
Male	11 (47.8)	17 (73.9)
Female	12 (52.2)	6 (26.1)
Ethnicity		
White British	22 (95.7)	21 (91.3)
Other white background	1 (4.4)	1 (4.4)
Irish	0 (0.0)	1 (4.4)
Smoking Status		
Never smoker	0 (0.0)	2 (8.7)
Ex-smoker	22 (95.7)	21 (91.3)
Current smoker	1 (4.4)	0 (0.0)
ECOG performance status		
0	16 (69.6)	16 (69.6)
1	7 (30.4)	7 (30.4)
Histology[1]		
Adenocarcinoma	15 (65.2)	11 (47.8)
Squamous cell carcinoma	7 (30.4)	8 (34.8)
Adenosquamous carcinoma	1 (4.4)	0 (0.0)
Large cell	0 (0.0)	1 (4.4)
Giant cell carcinoma	0 (0.0)	1 (4.4)
Pleomorphic carcinoma	0 (0.0)	1 (4.4)
Not otherwise specified	0 (0.0)	1 (4.4)
TNM stage[2]		
T1b	0 (0.0)	1 (4.4)
T1c	2 (8.7)	1 (4.4)
$T2_{vis}$	1 (4.4)	2 (8.7)
T2a	3 (13.0)	4 (17.4)
T2b	5 (21.7)	3 (13.0)
T3	7 (30.4)	5 (21.7)
T4	5 (21.7)	7 (30.5)
N0	13 (56.5)	12 (52.2)
N1	7 (30.4)	8 (34.8)
N2	3 (13.0)	3 (13.0)
M0	23 (100.0)	22 (95.6)
M1b	0 (0.0)	1 (4.4)
Tumour maximum diameter (mm)	45 (33 – 60)	44 (29 – 60)
TNM stage grouping[2]		
Stage Ia	2 (8.7)	1 (4.4)
Stage IB	1 (4.4)	3 (13.0)
Stage IIa	5 (21.7)	1 (4.4)
Stage IIb	7 (30.4)	7 (30.4)
Stage IIIa	6 (26.1)	8 (34.8)
Stage IIIb	2 (8.7)	2 (8.7)
Stage IVa	0 (0.0)	1 (4.4)
Haemoglobin (g/dL)	13.2 (12.0 – 14.3)	13.9 (12.9 – 14.7)

Data shown as patient number with percentage, or mean with interquartile range. [1]Histology and [2]staging are following resection unless this was not performed in which case diagnostic histology and imaging were used, respectively. 8th edition of the TNM staging classification was used. Abbreviations: ECOG, Eastern Cooperative Oncology Group; TNM, tumour, node and metastasis.

Overall, the cohorts were well-balanced in terms of patient age, ethnicity, smoking status, performance status, stage of disease and baseline haemoglobin level. A significant

proportion of patients in both cohorts had locally-advanced (stage III) disease, and one patient had oligometastatic disease, which is in-keeping with changing cardiothoracic surgical practice at high volume centres. Tumour size was comparable between cohorts and a detailed assessment of baseline tumour volume is presented below in section 3.2.4.

There were more male patients in Cohort 2 compared with Cohort 1. As expected, adenocarcinoma was the most common subtype of NSCLC in both cohorts with SCC next most common. However, in Cohort 2 the proportion of patients with adenocarcinoma was less than Cohort 1 and included some additional less common histological subtypes, including giant cell carcinoma, pleomorphic carcinoma and large cell carcinoma. All patients who underwent surgery had clear resection margins and no significant intraoperative complications were experienced.

3.2.3 Atovaquone treatment, drug levels and safety

3.2.3.1 Length of treatment and compliance

Eighteen patients in Cohort 1 received oral atovaquone 750 mg twice daily. The median total number of days that atovaquone was taken was 14 (IQR 12 to 15) days.

Out of the 18 patients who took atovaquone, 15 were evaluable for primary imaging analysis with hypoxia PET imaging with a median of 12 (IQR 7 to 13) days of treatment between scans. The 17 patients evaluable for plasma marker analysis took a median of 12 (IQR 8 to 13) days between measurements and for the 15 patients evaluable for pimonidazole analysis the median was 14 (IQR 12 to 15) days. Treatment compliance was very high with only a total of eight missed doses in six patients.

3.2.3.2 Plasma atovaquone levels

For atovaquone treated patients (n=17), the median atovaquone plasma level was 62.3 μM with large variation in values ranging from 29.4 μM to 113 μM. No correlation was observed between length of treatment and plasma atovaquone levels ($r_s = 0.17$, $p = 0.505$). This data demonstrates that all patients had plasma atovaquone levels at or above that shown to reduce OCR pre-clinically (30 μM) [219] and that the length of treatment was sufficient for all patients to achieve this desirable level (Figure 3.3).

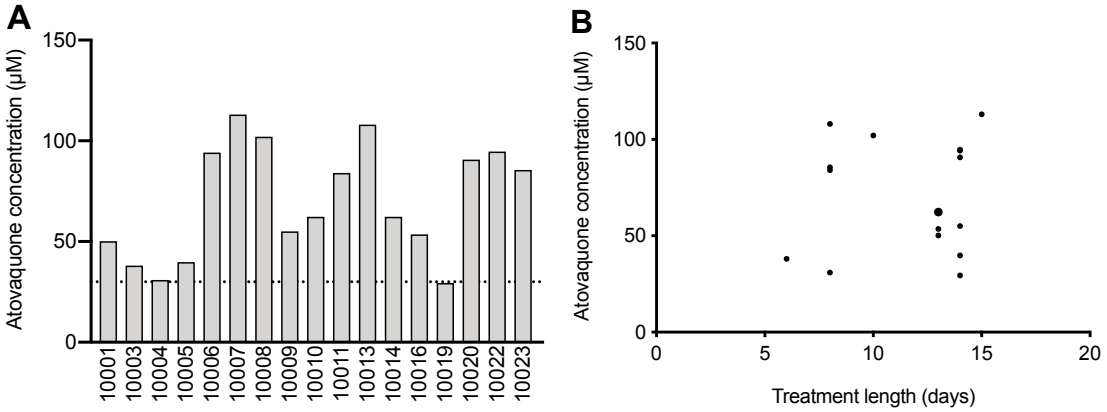


Figure 3.3: Atovaquone plasma levels
A) Plasma concentration of atovaquone for all Cohort 1 patients who completed treatment. The dotted line represents the concentration of atovaquone shown preclinically to result in OCR inhibition. B) Lack of correlation between length of atovaquone treatment and plasma atovaquone concentration. The larger data point represents two overlapping points.

3.2.3.3 Atovaquone levels in resected tumour tissue

Atovaquone levels in formalin-fixed tumour tissue are shown in Table 3.2.

Table 3.2: Tumour atovaquone levels

Patient	Atovaquone concentration (μM)*
10001	13
10003	3
10004	<LLQ
10005	2
10006	12
10007	8
10008	1
10009	2
10010	17
10011	10
10014	<LLQ
10016	2
10019	<LLQ
10020	4

*Estimated levels only. Abbreviation: LLQ, lower limit of quantification

The tumour atovaquone levels should be interpreted with significant caution and used as rough estimates at most. Firstly, the tumour samples taken from the resected formalin-fixed tumour proved extremely difficult to homogenise sufficiently and thus drug extraction was undoubtedly suboptimal. Secondly, the long fixation period of the resulted lung tissue prior to obtain samples, up to 12 days in certain cases, may have resulted in washing out of drug from the tumour. Given these concerns regarding accuracy of levels measured in tumours, it was unsurprising that no correlation was observed between plasma and tumour levels of atovaquone per patient (data not shown).

3.2.3.4 Safety and toxicity

Only one patient in the atovaquone treatment group experienced a reportable AE during the study, grade 3 hypertension, which was deemed unrelated to atovaquone as it occurred prior to starting treatment. The lack of AEs observed is consistent with the already well-established excellent safety profile of atovaquone.

3.2.4 Baseline tumour volume

The baseline tumour volumes for Cohort 1 and Cohort 2 patients evaluable for hyp-PET analysis, as well as the difference in tumour volume between adenocarcinoma and SCC histological subtypes is shown in Figure 3.4. There was a wide range of tumour volumes in this study ranging from 5.3 mL to 371.1 mL. The median tumour volume in both cohorts was similar: 59.3 (IQR 32.0 to 134.5) mL in Cohort 1 and 43.7 mL (IQR 45.8 to 69.1) mL in Cohort 2. There was no significant difference in tumour volume between adenocarcinoma and SCC histology in this study ($p = 0.505$).

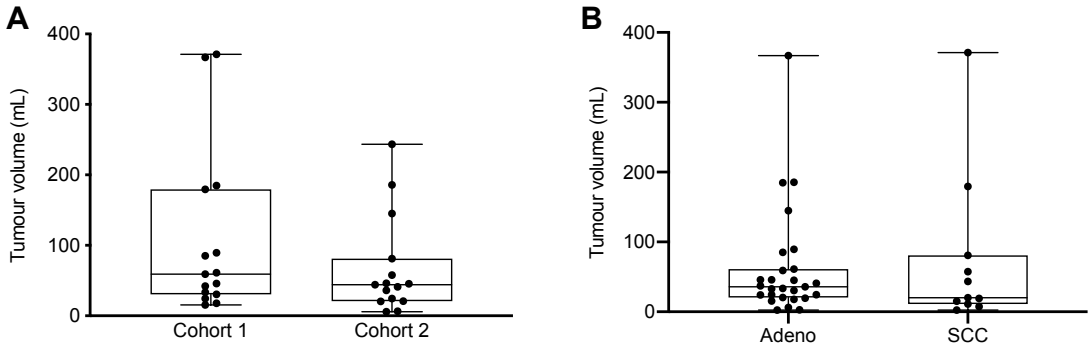


Figure 3.4: Comparison of tumour volume between cohorts and histological subtypes
Box and whisker plots showing tumour volumes for patients evaluable for hyp-PET imaging analysis with relation to A) cohort and B) adenocarcinoma or SCC histology. Tumour volume was obtained from the outlined tumour volumes of interest using hyp-PET scans. Medians with interquartile and absolute ranges are shown. Abbreviations: adeno, adenocarcinoma; SCC, squamous cell carcinoma. Difference in tumour volume between adenocarcinoma and SCC histology is not significant (Mann-Whitney U test).

3.2.5 Effect of atovaquone treatment on tumour volume

Individual patient paired tumour volume data along with the absolute and percentage change from baseline for atovaquone treated and untreated patients is shown in Table 3.3 and Table 3.4, respectively.

Table 3.3: Change in tumour volume in atovaquone treated patients

Patient	Pre volume (mL)	Post volume (mL)	Change (mL)	%Δ
10001	89.5	97.8	8.3	9.3
10004	184.9	193.9	9.0	4.9
10005	61.0	53.7	-7.3	-11.9
10006	179.5	186.6	7.1	4.0
10007*	19.4	19.1	-0.3	-1.4
10008	17.8	17.5	-0.3	-1.8
10009	59.3	60.4	1.1	1.9
10010	371.1	376.2	5.0	1.4
10011	24.6	27.8	3.2	12.9
10013	15.5	14.7	-0.8	-5.3
10014	42.2	44.5	2.3	5.5
10016	30.6	28.5	-2.1	-6.9
10019	366.9	399.2	32.3	8.8
10020	85.3	82.7	-2.6	-3.0
10022	45.9	47.7	1.9	4.0
10023	33.4	35.6	2.1	6.4
Median (IQR)	**52.6** (26.1 – 157.0)	**50.7** (28.0 –164.4)		
Median (95% CI)			**2.0** (-0.8 – 7.1)	**3.0** (-3.0 – 6.4)

Abbreviations: pre, pre-atovaquone treatment; post, post-atovaquone treatment; IQR, interquartile range; CI, confidence interval. *Patient 1007 was not evaluable for hyp-PET analysis but is evaluable for assessing change in tumour volume following atovaquone treatment.

Table 3.4: Change in tumour volume in untreated patients

Patient	Visit 1 volume (mL)	Visit 2 volume (mL)	Change (mL)	%Δ
10024	45.8	43.8	-2.0	-4.5
10025	40.8	38.8	-2.0	-4.9
10028	20.6	22.0	1.4	6.6
10029	24.1	23.8	-0.3	-1.3
10030	243.0	279.4	36.4	15.0
10031	5.4	5.5	0.1	2.0
10033	6.3	7.5	1.2	18.4
10034	43.7	51.9	8.2	18.9
10036	35.9	37.6	1.7	4.7
10039	144.8	159.2	14.4	9.9
10041	20.0	23.1	3.1	15.4
10043	80.7	79.3	-1.4	-1.8
10044	45.3	45.7	0.4	0.9
10045	185.4	185.7	0.3	0.2
10046	57.5	56.2	-1.3	-2.3
Median (IQR)	**43.7** (20.6 – 80.7)	**43.8** (23.1 – 79.3)		
Median (95% CI)			**0.4** (-1.3 – 3.1)	**2.0** (-1.8 –15)

Abbreviations: pre, pre-atovaquone treatment; post, post-atovaquone treatment; IQR, interquartile range; CI, confidence interval

The absolute change in tumour volume for atovaquone treated and untreated patients is shown in Figure 3.5 with volumes logarithmically (natural base) transformed to aid

visualisation. Analysis of non-transformed data showed that there was no significant change in tumour volume in both atovaquone treated (p = 0.083) and untreated (p = 0.208) patients.

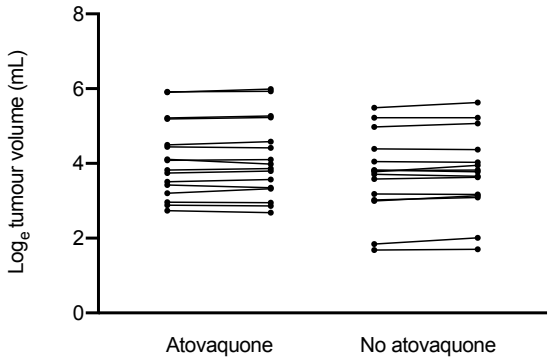


Figure 3.5: Effect of atovaquone on tumour volume
Changes in tumour volume for atovaquone treated and untreated patients. The tumour volume data is logarithmically (natural base) transformed to aid visualisation. Differences are not significant (Wilcoxon signed-rank test).

The median percentage change in tumour volume was 3.0 (95% CI -3.0 to 6.4) % for atovaquone treated patients and 2.0 (95% CI -1.8 to 15) % in untreated patients. This data is shown as waterfall plots in Figure 3.6 and illustrates the small and comparable changes in tumour volume in both cohorts.

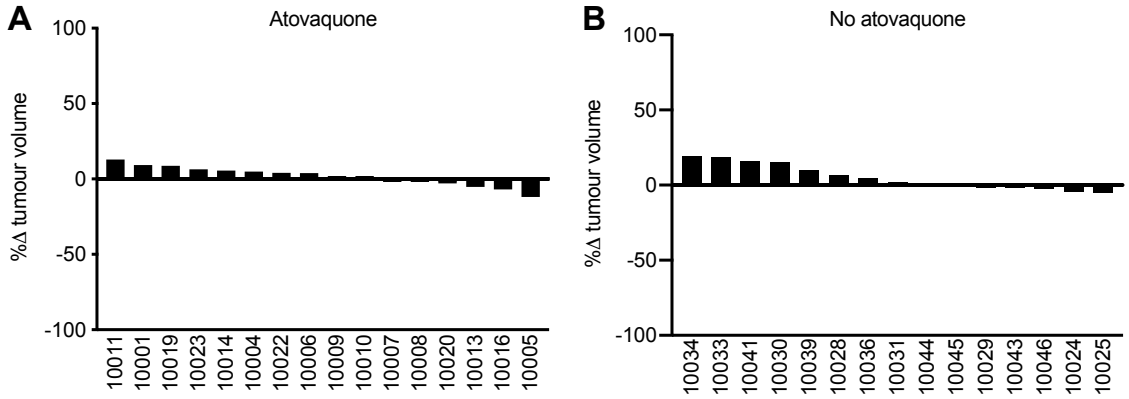


Figure 3.6: Waterfall plots showing the effect of atovaquone on tumour volume
Percentage changes from baseline in tumour volume for A) atovaquone treated and B) untreated patients.

3.2.6 Clinical outcomes for atovaquone treated patients

For patients who received atovaquone treatment in Cohort 1 (n=17) the median follow-up was 23 months with median PFS and OS not reached at the time the study closed. The one-year PFS rate was 51.3% and OS rate was 76.0%. All deaths were disease-related therefore the disease-specific one-year OS rate was also 76.0%. This survival analysis is shown using Kaplan-Meier curves in Figure 3.7. This data was not mature for Cohort 2 when the study closed.

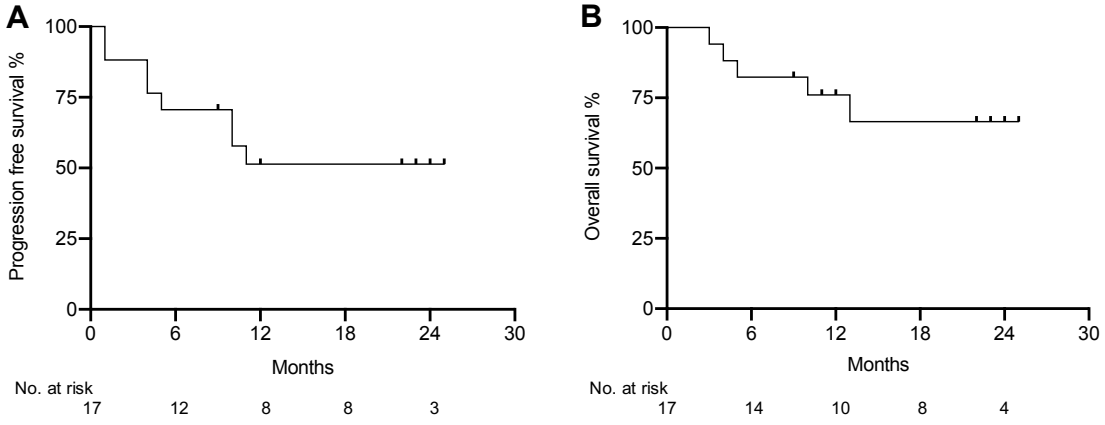


Figure 3.7: Progression free survival and overall survival for atovaquone treated patients
Kaplan-Meier curves for A) progression free survival and B) overall survival for patients who received atovaquone treatment prior to surgical resection. Censored patients are shown on each curve.

3.2.7 Can clinicopathological features predict sufficient HV on hyp-PET?

As described in section 2.1.3.8, a minimum threshold of 1.5 mL for tumour HV on baseline hyp-PET was implemented to determine whether patients were evaluable for assessing change in HV. Thirteen (30%) of 43 recruited patients who had interpretable baseline FMISO PET scans were found to have insufficient HV and were consequently replaced. The PET data from these patients was still used for correlation with numerous other trial endpoints.

The data presented below represents a brief investigation whether tumour volume, histology subtype or diagnostic FDG PET avidity was predictive of whether patients had sufficient baseline HV, as per the >1.5 mL cut-off used in this study.

3.2.7.1 Tumour volume

As shown in Figure 3.8, for patients with insufficient baseline HV the median tumour volume was 19.1 (IQR 5.2 to 30.3) mL which was significantly lower than that for patients with sufficient baseline HV 45.5 (IQR 24.5 to 103.3) mL, ($p < 0.001$). In addition, the range in tumour volume was much less for patients with insufficient HV with the maximum volume of only 43.4 mL, compared with 371.1 mL in patients with sufficient HV.

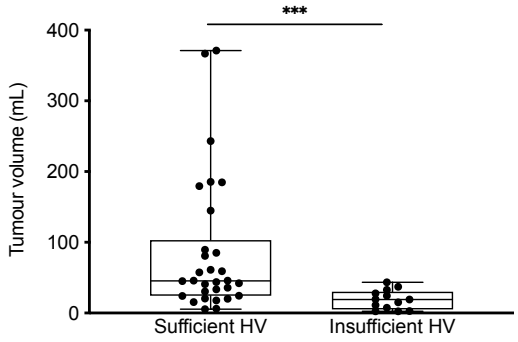


Figure 3.8: Comparison of tumour volume between patients with sufficient and insufficient HV
Box and whisker plots demonstrating the difference in baseline tumour volume between patients with sufficient (≥1.5 mL) and insufficient (<1.5 mL) HV as determined by hyp-PET imaging. The median level with interquartile and absolute ranges are shown. Abbreviations: HV, hypoxic volume. ***$p < 0.001$ (Mann-Whitney U test).

Full correlation analysis between tumour volume and HV is conducted in Chapter 4, however with regards to the threshold for sufficient HV used in this study this data suggests that tumour volume may be predictive for this.

3.2.7.2 Histology

In the 13 patients with insufficient baseline HV, six (46%) had adenocarcinoma, six (46%) had SCC histological subtype and one (7%) had giant cell carcinoma. The proportion of patients with SCC was higher in patients with insufficient HV than compared to patients with sufficient HV (46% vs 17%). The histological subtypes of patients with sufficient and insufficient hypoxia are shown in Figure 3.9.

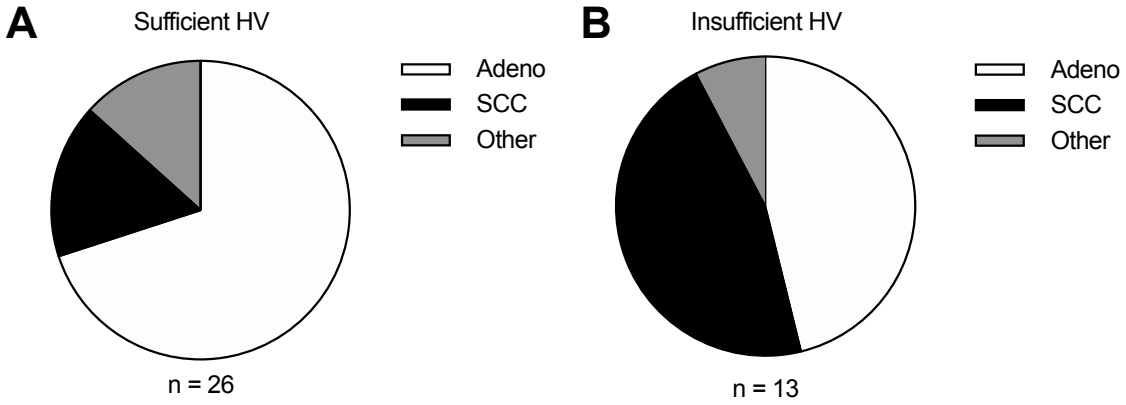


Figure 3.9: NSCLC histological subtypes in patients with sufficient and insufficient baseline HV
Pie charts showing the proportion of adenocarcinoma, SCC or other histological subtypes in patients with A) sufficient and B) insufficient HV as determined by baseline hyp-PET. Abbreviations: HV, hypoxic volume; Adeno, adenocarcinoma; SCC, squamous cell carcinoma.

3.2.7.3 Diagnostic FDG PET SUV_{max}

The median baseline FDG PET SUV_{max} for all Cohort 1 patients was 16.7 (IQR 12.4 to 23.3) and was 14.4 (IQR 11.8 to 18.6) for Cohort 2. For patients with sufficient baseline HV in Cohort 1 the median value was 20.9 (IQR 12.5 to 24.5) and for Cohort 2 patients was 15.5 (IQR 12.2 to 18.9). Figure 3.10 shows the baseline FDG PET SUV_{max} values for both cohorts. This data demonstrates that there was a large range in FDG PET SUV_{max} values in both cohorts.

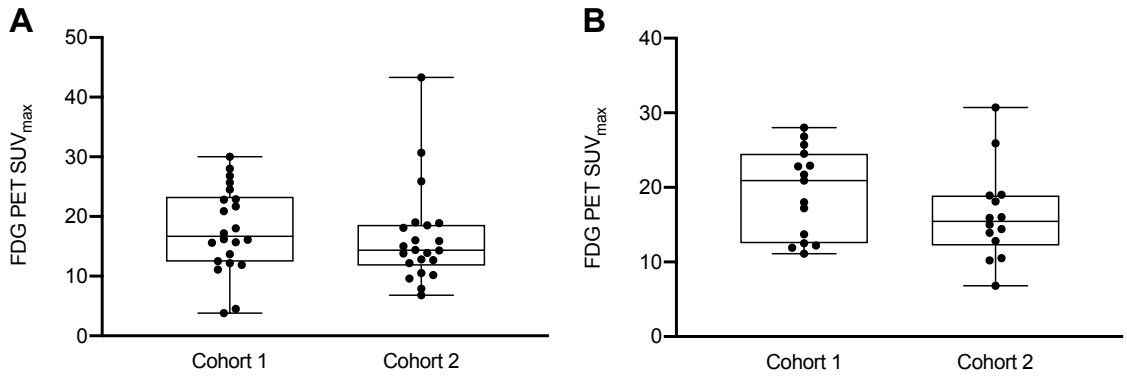


Figure 3.10: Baseline FDG PET SUV_{max} for patients in Cohort 1 and Cohort 2
Box and whisker plots comparing the baseline diagnostic FDG PET SUV_{max} values for Cohort 1 and Cohort 2 for A) all patients and B) patients with sufficient (≥1.5 mL) baseline HV as determined by hyp-PET. The median level with interquartile and absolute ranges are shown. Abbreviations: FDG, fluorodeoxyglucose; PET, positron emission tomography; SUV_{max}, maximum standardised uptake value.

For all patients with sufficient baseline HV, the median SUV_{max} value was 17.2 (IQR 12.7 to 22.9) and for patients with insufficient hypoxia it was 13.8 (IQR 8.8 to17.1), which was not significantly different (p = 0.123) (Figure 3.11).

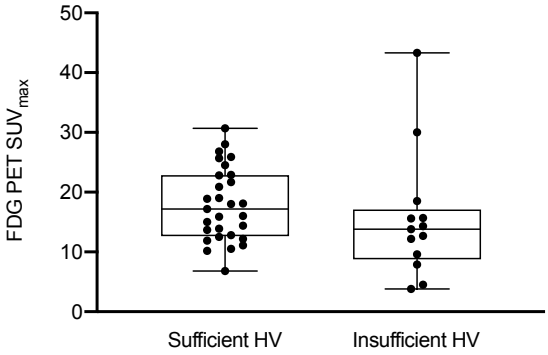


Figure 3.11: Baseline FDG PET SUV_{max} in patients with sufficient and insufficient baseline hypoxia
Box and whisker plots comparing the baseline diagnostic FDG PET SUV_{max} values for patients with sufficient (≥1.5 mL) and insufficient (<1.5 mL) baseline HV as determined by hyp-PET. The median level with interquartile and absolute ranges are shown. Abbreviations: HV, hypoxic volume; FDG, fluorodeoxyglucose; PET, positron emission tomography; SUV, standardised uptake value. Difference is not significant (Mann-Whitney U test).

Full correlation analysis between baseline tumour FDG PET SUV_{max} and hyp-PET imaging parameters is presented in Chapter 4, however, with regards to the threshold for sufficient HV used in this study it appears that FDG PET is not predictive.

3.3 DISCUSSION

Overall, the ATOM trial demonstrates the feasibility of conducting a complex and ambitious window of opportunity study in patients with operable NSCLC. This study generated a large amount of data permitting a detailed assessment of the effect of atovaquone on tumour hypoxia, which is presented in the following chapters. In addition, the data collected provides the possibility for correlative analysis of numerous hypoxia endpoints, thus contributing to the assessment of their validity as clinical hypoxia biomarkers.

3.3.1 Baseline clinical characteristics and predicting sufficient baseline tumour HV

The baseline patient characteristics in this study were typical of an operable NSCLC population with atovaquone treated and untreated patients generally well-balanced in terms of key features such as histological subtype, tumour volume, haemoglobin and FDG PET avidity. Despite this being a surgical patient cohort, a significant proportion of patients had advanced disease, including stage IIIB and IV disease, in keeping with changing cardiothoracic surgical practice especially in large volume centres. The large range in tumour size observed is reflective of the heterogeneous nature of NSCLC.

It was felt that in order to reliably measure the effect of atovaquone on tumour HV using hyp-PET there needed to be detectable hypoxia and in sufficient quantity at baseline to accurately measure any change above background measurement error. Therefore, a minimum 1.5 mL HV threshold was implemented and only patients meeting this cut-off were eligible to continue with the study. Although this approach was necessary, it resulted in almost a third of patients being replaced, which was somewhat unexpected and significantly impacted on trial recruitment, as well as cost.

Although some small studies have shown higher rates of detection of tumour hypoxia in patients with NSCLC using FMISO [256], most studies have demonstrated similar rates to that observed in this one of the largest of such studies. For example in LA-NSCLC, 35% of patients were found to have undetectable tumour hypoxia using FAZA PET [257] and in another study in advanced NSCLC, 42% of patients had undetectable hypoxia using the same tracer [258]. It must be noted that higher rates would have likely been reported in these other studies had a threshold been used, instead of just any detectable volume of hypoxia reported. In this trial, only seven (16%) patients had completely undetectable hypoxia. Also, inclusion criteria in this study mandated that tumours had to be at least 2 cm in diameter, whereas other trials did not stipulate this, and this was therefore likely to further decrease our reported rate of insufficient hypoxia comparatively. Overall, all these findings are consistent with direct oxygen measurements in NSCLC, which demonstrate variability in oxygenation with measured levels often above 10 mmHg, the level above which nitroimidazole-based hypoxia tracers such as FMISO and FAZA do not accumulate [111]. For example, in one study in patients with operable NSCLC the median oxygen pressure has been demonstrated to be 16.6 mmHg (range 0.7 to 46 mmHg) [49] and in murine xenograft *in situ* NSCLC models, only the minority of tumours had oxygen levels <10mmH in more than 20% of measurements [259].

Therefore, in future studies using hyp-PET to measure change in tumour hypoxia, it would be being advantageous to be able to predict which patient are likely to have insufficient hypoxia as this could inform setting of eligibility criteria. In this study, it appeared that tumour volume was most predictive of whether patients had sufficient hypoxia and therefore having a minimum tumour size cut-off as part of the inclusion criteria appears justified. With a 2 cm tumour diameter requirement, some of the smallest tumours were approximately 2.5 ml which was just above the 1.5 ml HV cut-off and some of these

tumours did contain sufficient hypoxia. Setting a higher size limit would have resulted in lower rates of patient replacement but significantly impacted on recruitment. Given that baseline data from patients with insufficient hypoxia was used for correlation with other hypoxia measures, this increase in study participants in fact strengthened the hypoxia biomarker validation element of this study, albeit as significant additional cost. Overall, in this study, a pragmatic inclusion criterion of minimum tumour size of 2 cm proved to be a good decision, balancing adequate recruitment, biomarker data collection and use of resources.

Interestingly, baseline diagnostic FDG PET avidity did not appear to predict whether patients had sufficient baseline hypoxia. Full correlation of FDG avidity and hypoxia PET parameters is presented in Chapter 4, but this data would suggest that this imaging modality may not be helpful for identifying patients with sufficient hypoxia. With regards to histological subtype, a higher proportion of patients with insufficient baseline hypoxia had SCC. On review of the literature there is no consistent evidence that there is a difference between these subtypes in hypoxia as measured by hyp-PET and given the small numbers of patients in this study with SCC, although interesting this does not provide convincing evidence of a clear difference.

3.3.2 Atovaquone safety and drug levels

As expected, atovaquone treatment was extremely well tolerated in this study with no significant side effects reported and subsequently a high rate of compliance observed.

Encouragingly, plasma levels of atovaquone for all patients were at or above the level shown preclinically to reduce OCR and tumour hypoxia [219]. There was a large range in levels consistent with the known variable bioavailability of this drug with plasma

concentrations in this study comparable to that reported in other studies using atovaquone at this dose for antimicrobial purposes [244]. As atovaquone levels are known to reach steady plasma state after approximately six days of treatment, it was unsurprising to observe that patients with longer treatment length did not have higher plasma levels. Together these data confirm that all patients had sufficient and comparable atovaquone levels and could therefore contribute equally to investigating the effect of atovaquone on tumour hypoxia.

In contrast, assessing atovaquone levels within the resected tumour proved troublesome, showing very low and variable yields. The samples of formalin-fixed tumour tissue were extremely difficult to homogenise sufficiently, which is likely to have impeded drug extraction. In addition, it is conceivable that the extended bathing of the resected lung specimen in formalin (in some cases for almost two weeks prior to obtaining tumour tissue) may have significantly reduced drug levels within the tumour, especially given the highly lipophilic properties of this drug. The methodology for resected specimen clinical processing and tumour sampling was dictated by local clinical protocol and although the time prior to cut up was limited whenever possible, it was outwith the full control of this study. Furthermore, it may have been the case for some samples that tissue which was obtained was not viable and taken from predominantly necrotic regions. There is no published data measuring atovaquone levels in formalin-fixed tumours and no data on the effect of the fixation process on atovaquone detection. In fact, there is very little data on measuring drug levels in fixed tumour tissue in general. Unpublished data from the Higgins Group and the Bioanalysis Core HPLC Laboratory, Department of Oncology, has previously compared atovaquone levels in murine xenograft tumours processed as either fresh frozen or formalin-fixed just for 24 hours and observed significantly lower levels in fixed tumours, with levels on average 25% lower and in certain cases significantly less so.

The data in this study does demonstrate that atovaquone was detectable within the tumour in the majority of cases, which was encouraging even though the quantification of the exact level was not possible.

3.3.3 Effect of atovaquone on tumour volume and clinical outcomes

In keeping with preclinical data, atovaquone treatment did not significantly alter tumour volume with any small changes observed likely to reflect differences in tumour imaging due to CT slice thickness, phase of the respiratory cycle, differences in tumour outlining and change in tumour appearance due to surrounding consolidation. All changes reported are below what would be considered significant by conventional RECIST criteria [260]. In order to definitively establish whether atovaquone alters tumour growth and size, significantly longer treatment duration that the average two weeks used in this study would be required.

For patients who received atovaquone prior to surgical resection, the one-year PFS and OS rates were 51% and 76%, respectively. This survival data is comparable to other published NSCLC surgical series as well as locally and nationally reported surgical outcomes [261], especially when the significant proportion of patients with locally advanced disease in this study is taken into consideration. In addition, the uptake of adjuvant chemotherapy was not known which could have impacted on survival especially given that many patients in this study met the criteria for such treatment. It was unfortunately not possible to collect clinical outcome data for longer due to closure of the study and therefore the median PFS and OS were not reached. Furthermore, a comparison with untreated patients was not possible as the trial closed within one year of recruitment of the first untreated patient in Cohort 2.

Overall, the data presented supports preclinical data that atovaquone as a single agent is likely to have little impact on disease progression.

3.3.4 Study design limitations, challenges encountered and lessons for future studies

This study had a number of shortcomings. Firstly, as this was a single centre study with a non-treatment cohort there were concerns that recruitment may be a challenge and therefore the decision was made not to randomise patients and to prioritise recruitment to the treatment cohort. In retrospect, recruitment to both cohorts was such that randomisation would have been possible resulting in a more statistically robust study design. Secondly, although not unreasonable in comparison to other window-of-opportunity and proof of principle studies, the patient numbers in this study were clearly relatively small and this must be considered when drawing conclusions. As this study was primarily designed to test whether atovaquone alters tumour hypoxia, the patient numbers were felt to be sufficient to assess for any early signal of this.

Despite the successful running of this study, some logistical challenges were encountered which were specific to this patient population. Although the recruitment rate was high, with approximately 50% of approached patients electing to participate in the study, the most common reason patients declined to participate was that they did not wish to have additional hospital visits and scans. This reflects the fact that patients with operable NSCLC have arguably one of the longest diagnostic and staging pathways, which requires numerous hospital visits for investigations, which not uncommonly can last a number of months.

The last-minute rescheduling of surgery, often on the morning of the operation, was an additional challenge in this study and occurred in six patients. This inevitable occurrence

reflects the ‘real world’ clinical setting and is an important consideration for any surgical window study, especially when using an exogenous marker of hypoxia such as pimonidazole, which needs to be administered within a specific timeframe prior to surgery.

Conducting imaging studies using radioactive tracers such as FMISO or FAZA, which are not widely available, is known to be challenging due to problems with tracer availability and higher rates of tracer production failure, as reported by other studies [125,262]. In this study this resulted in the withdrawal of only one patient, however rescheduling of scans was required for a number of patients due to tracer production failures. A ‘backup’ tracer, FAZA in the case of this study, ensured the study remained open when FMISO became unexpectedly unavailable for a period of time at the beginning of this study.

pCT proved difficult with uninterpretable paired scans in four patients due to 1) differences observed in rate of contrast injection despite this being administered through an automated pump system 2) tumour movement with respiration and 3) signal interference from adjacent hilar and mediastinal vessels. Furthermore, due to the large tumour size in many cases and limited pCT detector width, in the majority of cases only part of the tumour was imaged. As a result, careful tumour region matching of scans was required in order to assess change in perfusion for individual patients with data from non-matched tumour regions discarded. Overall, this highlights the difficulty of performing high quality pCT imaging in this patient population.

Lastly, it was important that pathological confirmation of NSCLC was not mandated as part of this study’s inclusion criteria as the majority of patients proceeded to surgery on a radiological diagnosis alone. The decision was made that a suspected diagnosis of NSCLC was sufficient for trial eligibility in recognition of the high diagnostic accuracy of modern-day diagnostic imaging and subsequently changing clinical practice. Furthermore,

performing a biopsy to confirm diagnosis prior to study entry would not have been feasible given the short window of time available prior to surgery and would have likely had negative impact on recruitment. All patients in this study were ultimately confirmed to have a diagnosis of NSCLC following histopathological assessment of the resected specimen justifying the strategy adopted. However, this approach was only acceptable given that treatment in this trial was short and non-toxic and that the tumour was eventually resected for diagnostic purposes. A significant disadvantage of not mandating upfront diagnostic tissue was that it was not possible to compare pre- and post-atovaquone treatment tumour tissue, which would have been of significant interest.

3.4 CONCLUSION

Overall, the ATOM trial was a success and generated a large amount of data to evaluate the effect of atovaquone on tumour hypoxia and validate tumour hypoxia biomarkers. The clinical data presented in this chapter demonstrated patients in this study were representative of the wider NSCLC population, with both atovaquone treated and untreated cohorts well balanced in key clinical features of interest when conducting hypoxia-orientated clinical research. As expected, atovaquone was well tolerated with adequate plasma levels achieved for all patients. The lack of effect of this agent when used in isolation on tumour size and surgical outcomes was as to be expected as the true potential of this agent lies as a tumour hypoxia modifier in order to improve radiotherapy outcomes. With this clinical context in place, data presented in the following two chapters investigates whether this proof of principle can be established.

CHAPTER 4: TUMOUR HYPOXIA AND PERFUSION IMAGING

4.1 INTRODUCTION

This chapter investigates the effect of atovaquone on tumour hypoxia and perfusion using non-invasive tumour imaging. As outlined in Chapter 1, hyp-PET using radiolabelled nitroimidazole compounds such as FMISO and FAZA has become the modern-day standard for the evaluation of tumour hypoxia in clinical research. Imaging protocols and reported parameters are increasingly well established, with high accuracy and reproducibility demonstrated by numerous studies [126–128]. Imaging hypoxia in this way reduces the risk of sampling error whilst enabling exploration of the heterogeneous nature of tumour hypoxia. In addition, it does not rely on surrogate endogenous markers of hypoxia and therefore can be viewed as a more 'direct' measure of hypoxia. Such imaging techniques also provide the opportunity for evaluating hypoxia at multiple time points per individual patient, making it clinically acceptable for assessing changes in tumour hypoxia over time. Hyp-PET was therefore an obvious primary endpoint measure to evaluate the effect of atovaquone on tumour hypoxia in the ATOM study.

When interpreting results from any study using hyp-PET, it is important to first fully characterise the baseline hypoxic profile of tumours in question. In clinical trials there is often significant variation between the baseline characteristics of patients and this may impact on results. This is of particular importance for proof of principle studies such as this, in which patient numbers are relatively small and where full understanding of tumour biology is of paramount importance and interest. As presented in the last chapter, there was a large range of tumour size, histological subtypes, disease stage and other clinical features observed in this study population, which was expected given that NSCLC is a truly heterogeneous disease entity in the clinical setting. Fully characterising the baseline hypoxic profile of tumours by hyp-PET is also of key importance for the planned tumour

hypoxia IHC data analysis as there was no pre-treatment tissue collected and therefore the imaging baseline data will guide inter-cohort comparison of IHC results. Furthermore, such data will also be used for correlation with sample-based hypoxia endpoints in order to further validate such methods in the study of tumour hypoxia, as presented in Chapter 5.

Assessment of tumour hypoxia and any potential treatment-related changes in hypoxia would be incomplete without parallel measurement of tumour perfusion. Although imaging hypoxia with hyp-PET is unlikely to be affected by poor perfusion, as previously described, it is nevertheless still important to fully evaluate tumour perfusion for a number of reasons. As with hypoxia imaging, it is important to investigate for any gross baseline differences between patient cohorts, which may impact results. Therefore, this data is presented prior to assessing any changes in perfusion following atovaquone treatment. Furthermore, as preclinical data indicated that atovaquone reduced tumour hypoxia through inhibition of OCR, excluding changes in perfusion would help further support this mechanism of action. This is important as there is no published data of the effect of atovaquone on tumour perfusion.

4.2 RESULTS

4.2.1 Baseline tumour hypoxia as measured by hyp-PET

FMISO or FAZA hypoxia PET (hyp-PET) imaging was performed to visualise and quantify tumour hypoxia. A volume of blood in the centre of the descending aorta was outlined to provide the background mean standardised uptake (SUV_{mean}). To determine the tumour hypoxic volume (HV), voxel-by-voxel SUVs were divided by the background SUV_{mean} to provide tumour-to-blood ratio (TBR) values for each tumour voxel and voxels

with TBR ≥1.4 were classified as hypoxic, as previously described [126]. A minimal baseline level of tumour hypoxia was set at HV ≥1.5 mL and patients with a lower value were deemed unevaluable for the trial and were replaced.

Other hyp-PET parameters used for analysis were the percentage of the tumour volume which was defined as hypoxic (HV%), the mean tumour TBR (TBR_{mean}) and the highest TBR_{mean} value for a contiguous 1cm^3 volume of tumour (TBR_{peak}), as previously published [127,247].

The complete baseline hyp-PET derived hypoxic parameters together for all patients is shown in Appendix Table 1 and is summarised below in Table 4.1. An inter-cohort comparison for each of these hypoxia imaging parameters for patients with sufficient baseline HV is shown in Figure 4.1.

Table 4.1: Summary of hyp-PET derived HV, HV%, TBR_{mean} and TBR_{peak} for Cohort 1 and Cohort 2

	n	HV (mL)	HV% (%)	TBR_{mean}	TBR_{peak}
Cohort 1 (all)	**20**	**6.8** (0.9 – 34.9)	**21.3** (3.9 – 48.4)	**1.2** (1.0 – 1.4)	**1.9** (1.5 – 2.4)
Cohort 1, HV ≥1.5 mL	**15**	**28.9** (5.4 – 50.8)	**34.8 (**13.4 – 52.8)	**1.3** (1.1 – 1.5)	**2.0** (1.7 – 2.5)
Cohort 2 (all)	**23**	**2.6** (0.2 – 21.7)	**18.2** (3.4 – 35.2)	**1.1** (0.9 – 1.3)	**1.7** (1.3 – 2.2)
Cohort 2, HV ≥1.5 mL	**15**	**11.4** (2.6 – 34.0)	**23.5** (12.0 – 50.2)	**1.2** (1.1 – 1.5)	**2.1** (1.6 – 2.3)

Data shown are median values with interquartile ranges. Abbreviations: HV, hypoxic volume; HV%, hypoxic volume percentage; TBR, tumour-to-blood ratio.

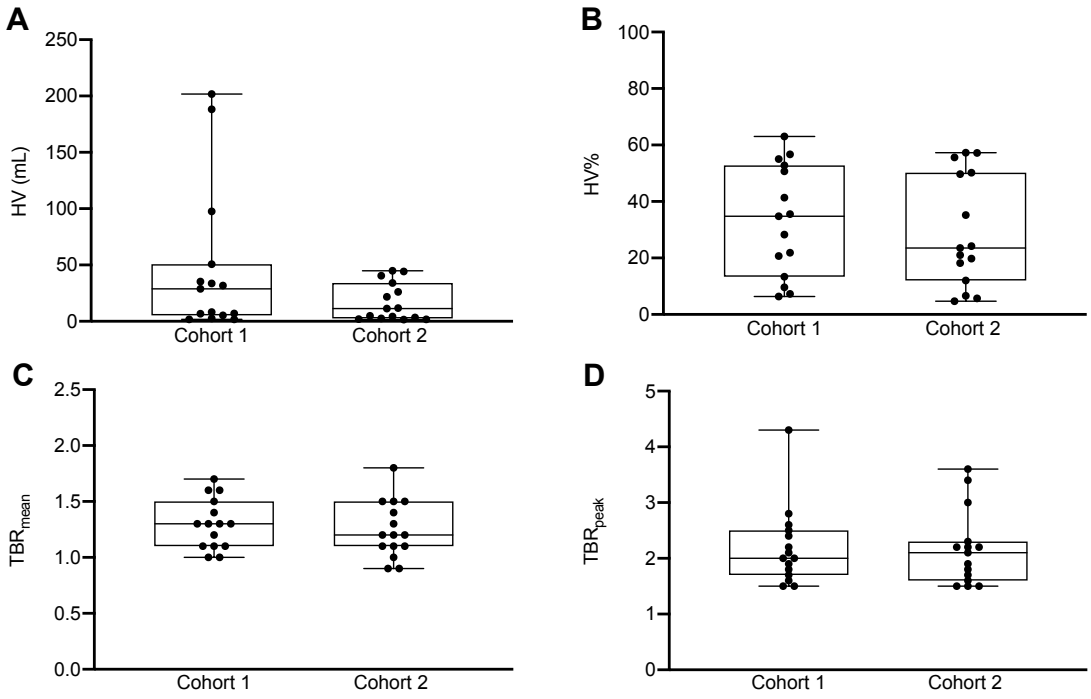


Figure 4.1: Baseline HV, HV%, TBR_{mean} and TBR_{peak} for Cohort 1 and Cohort 2
Box and whisker plots demonstrating the difference in baseline A) HV, B) HV%, C) TBR_{mean} and D) TBR_{peak} between patients in Cohort 1 and Cohort 2 with sufficient HV (≥1.5 mL). Medians with interquartile and absolute ranges are shown. Abbreviations: HV, hypoxic volume; HV%, hypoxic volume percentage; TBR, tumour-to-blood ratio.

There was a large range in values for baseline hyp-PET parameters in both cohorts. When comparing cohorts, the potentially most relevant observation was that the median HV value in atovaquone treated patients in Cohort 1 was more than twice that for untreated patients in Cohort 2 (29.4 mL vs 11.4 mL). In addition, the median value for HV% and TBR_{mean} were also higher in the atovaquone treated group.

4.2.2 Correlation of hyp-PET parameters with clinicopathological features

Next, to further characterise the baseline hypoxic profile of tumours, correlative analyses between baseline hyp-PET parameters and tumour volume and FDG PET SUV_{max} was conducted. Differences in hyp-PET parameters between NSCLC histological subtypes was also explored.

4.2.2.1 Tumour volume

The data presented in Chapter 3 demonstrated that tumour volume appeared to be predictive of whether patients had sufficient baseline HV, as per the ≥1.5 mL threshold. As now shown in Figure 4.2, there was a strong positive correlation between tumour volume and HV (r_s = 0.79, p < 0.001) and a moderate strength positive correlation with HV% (r_s = 0.43, p = 0.004), TBR_{mean} (r_s = 0.47, p = 0.001) and TBR_{peak} (r_s = 0.59, p < 0.001) for all trial patients. Overall, this data demonstrated that larger tumours in this study were more hypoxic not only in terms of absolute hypoxic volume, but also with regards to average and maximum based hyp-PET parameters.

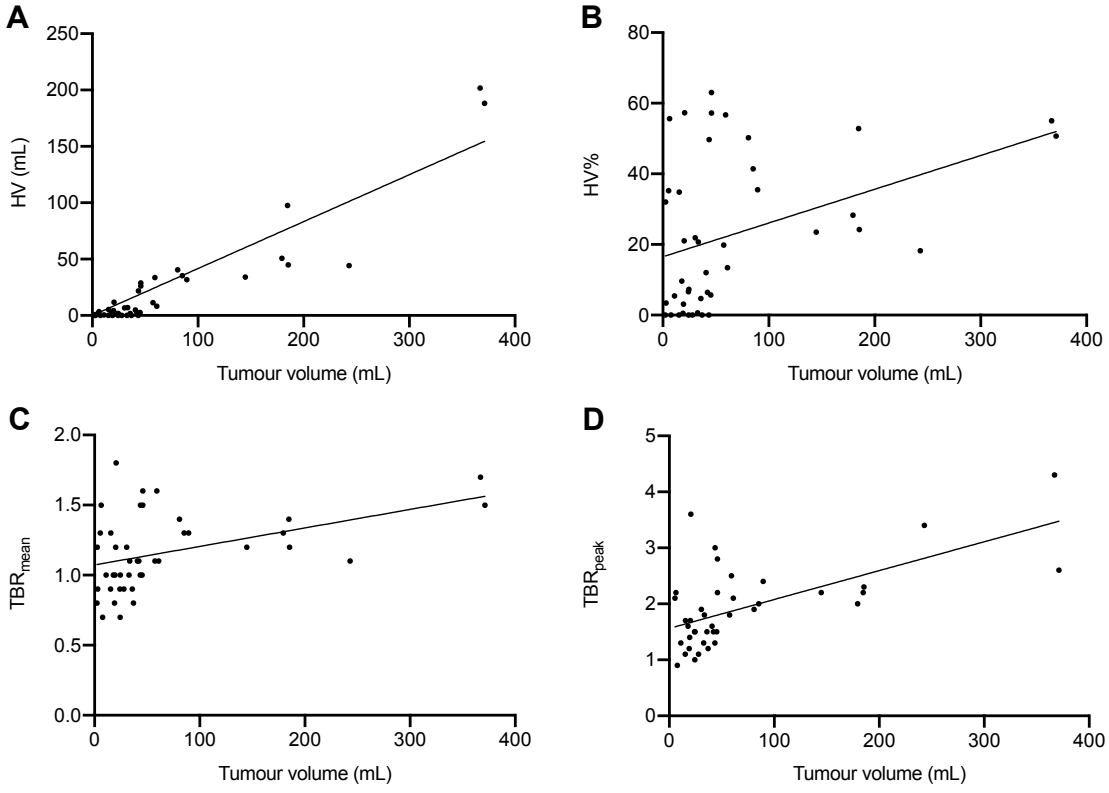


Figure 4.2: Correlation of tumour volume with HV, HV%, TBR_{mean} and TBR_{peak}
Scatter plots showing correlation between baseline tumour volume and hyp-PET derived tumour A) HV, B) HV%, C) TBR_{mean} and D) TBR_{peak} for all patients. Abbreviations: HV, hypoxic volume; HV%, hypoxic volume percentage; TBR, tumour-to-blood ratio. Lines of best fit are shown for correlated data (Spearman's rho correlation coefficient with p < 0.05).

4.2.2.2 Tumour histology

Given that tumour volume correlates with tumour hypoxia, prior to assessing differences in hypoxia between adenocarcinoma and SCC histology it was important to compare these histological subtypes in this study in terms of size. As was shown previously in Figure 3.4 in Chapter 3, tumour size was comparable for both adenocarcinomas and SCC in this study. Subsequently, the difference in baseline hyp-PET derived parameters between adenocarcinoma and squamous histology was assessed and is shown in Figure 4.3. There was no significant difference observed between the two histology subtypes in terms of HV ($p = 0.288$), HV% ($p = 0.075$), TBR_{mean} ($p = 0.213$) and TBR_{peak} ($p = 0.084$).

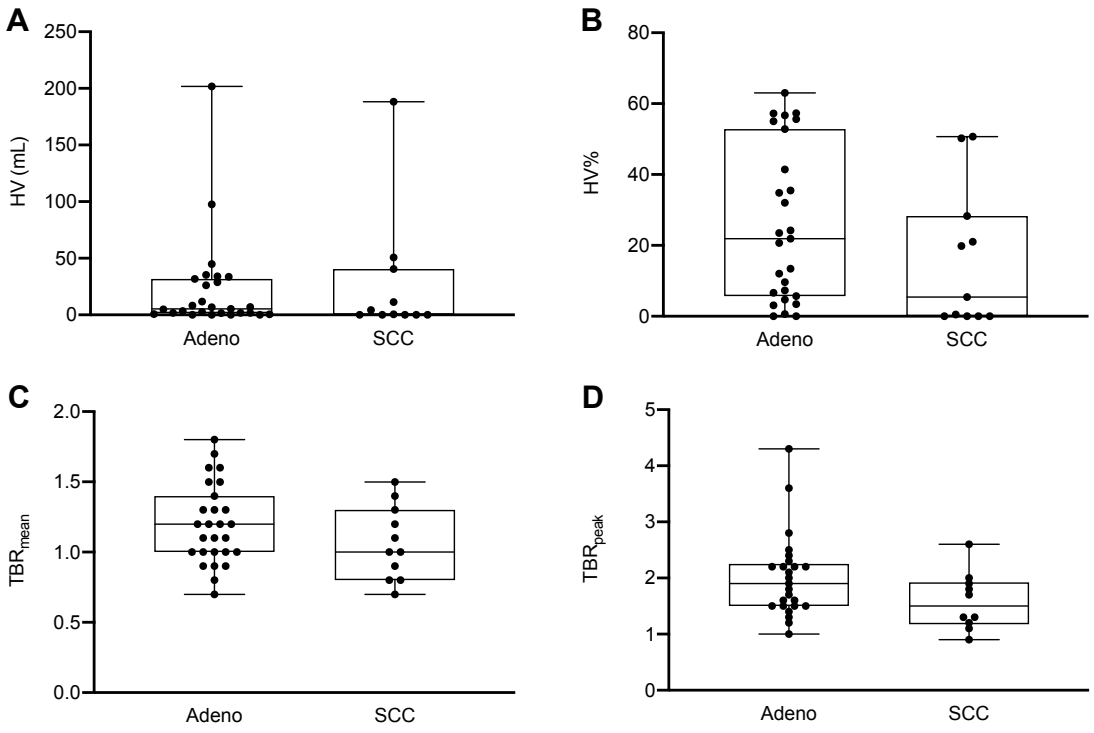


Figure 4.3: Comparison of HV, HV%, TBR_{mean} and TBR_{peak} between histological subtypes
Box and whisker plots showing the difference in baseline hyp-PET derived tumour A) HV, B) HV%, C) TBR_{mean} and D) TBR_{peak} between adenocarcinoma and squamous histological subtypes for all patients. Medians with interquartile and absolute ranges are shown. Abbreviations: HV, hypoxic volume; HV%, hypoxic volume percentage; TBR, tumour-to-blood ratio. Differences between groups are not significant (Mann-Whitney U test).

4.2.2.3 FDG PET SUV_{max}

Data presented in Chapter 3 demonstrated that FDG PET SUV_{max} did not appear to predict whether patients had sufficient baseline HV, as per the ≥1.5 mL study threshold. Interestingly, on full correlative analysis between FDG PET SUV_{max} and hyp-PET parameters (Figure 4.4) there was a weak positive correlation observed with HV ($r_s = 0.35$, $p = 0.025$) and TBR_{mean} ($r_s = 0.33$, $p = 0.032$). However, there was no correlation observed with HV% ($r_s = 0.27$, $p = 0.081$) and TBR_{peak} ($r_s = 0.27$, $p = 0.098$).

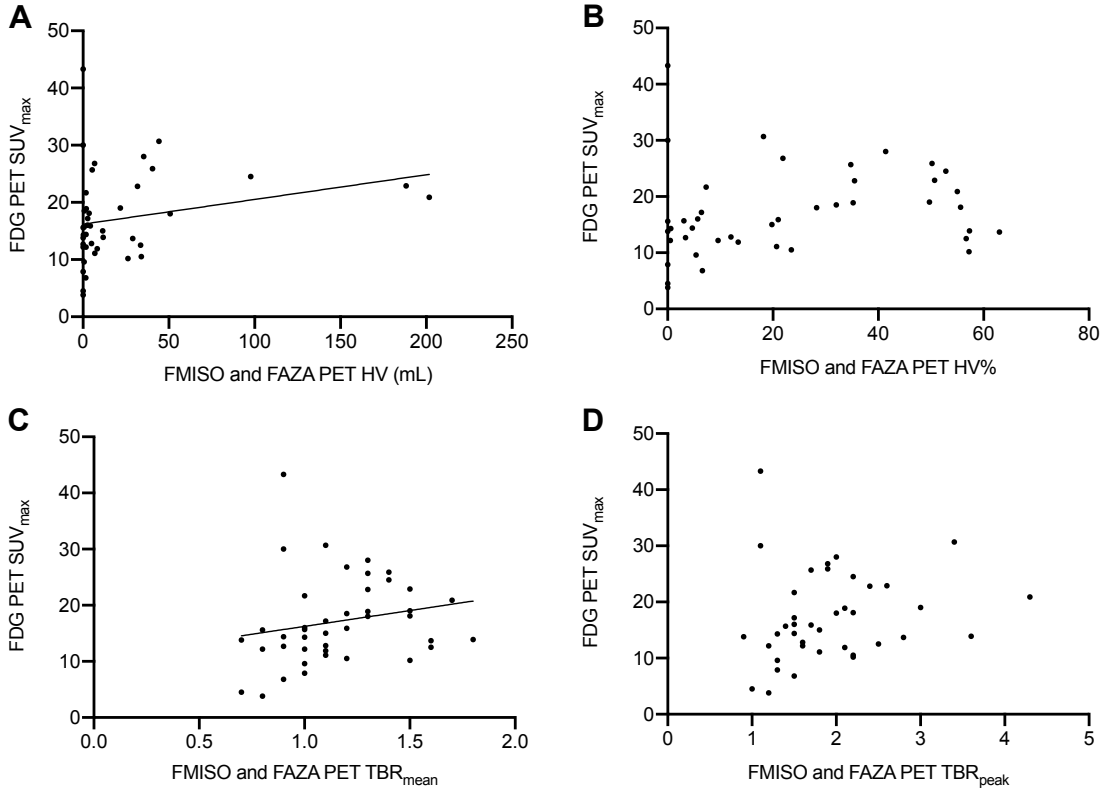


Figure 4.4: Correlation of FDG PET with HV, HV%, TBR_{mean} and TBR_{peak}
Scatter plots showing the correlation between diagnostic FDG PET SUV_{max} and baseline hyp-PET derived tumour A) HV, B) HV%, C) TBR_{mean} and D) TBR_{peak} for all patients. Abbreviations: HV, hypoxic volume; HV%, hypoxic volume percentage; TBR, tumour-to-blood ratio. Lines of best fit are shown for correlated data (Spearman's rho correlation coefficient with $p < 0.05$).

4.2.3 Atovaquone treatment reduces tumour hypoxia as measured by hyp-PET

4.2.3.1 Atovaquone treatment reduces tumour HV

The percentage change in HV from baseline for each patient is shown as waterfall plots in Figure 4.5, with a striking difference observed between atovaquone treated and untreated patients. Eleven (73.3%) of 15 treated patients had >10% reduction in HV, and therefore were classed as responders, compared with only 2 (13.3%) of 15 untreated patients.

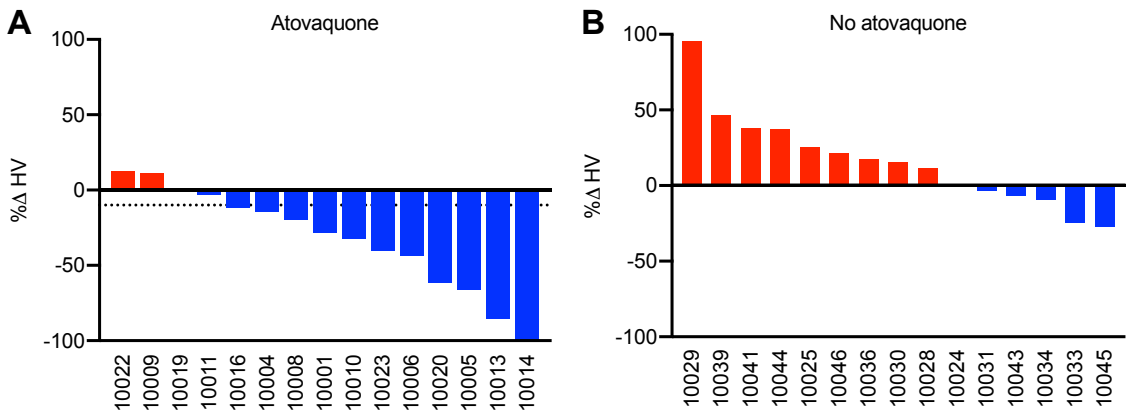


Figure 4.5: Waterfall plots demonstrating the effect of atovaquone on tumour HV
Percentage changes from baseline in hyp-PET derived tumour HV for A) atovaquone treated and B) untreated individual patients. Red bars represent patients with an increase in HV whilst blue bars represent patients with a decrease in HV. The dotted line represents the minumum threshold of >10% reduction in HV required for patients to be classed as responders to atovaquone treatment. Abbreviation: HV, hypoxic volume.

Interestingly, if higher thresholds were set for determining whether hyp-PET tumour voxels were hypoxic, such as for example TBR ≥1.6 and ≥1.8, even more pronounced reductions in HV were observed following atovaquone treatment (Figure 4.6).

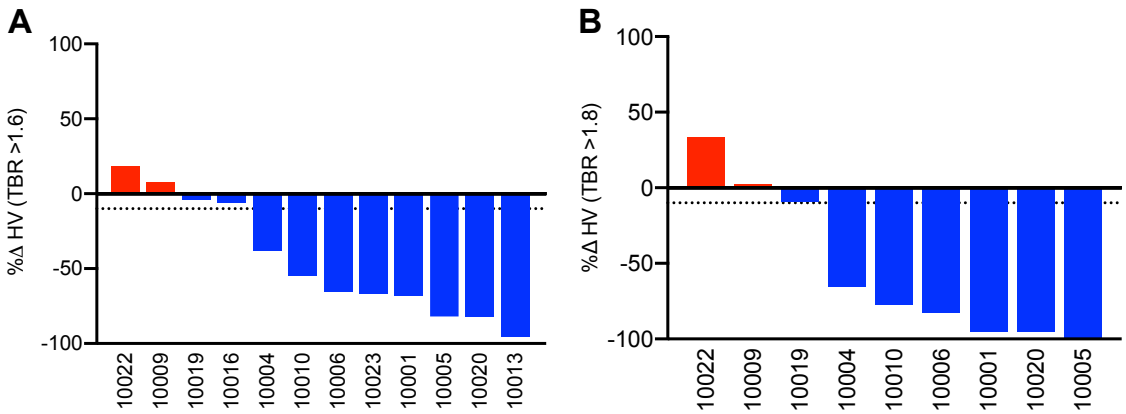


Figure 4.6: Waterfall plots demonstrating the effect of atovaquone on tumour HV using higher TBR thresholds
Percentage changes from baseline in hyp-PET derived tumour HV for atovaquone treated patients when using A) TBR ≥1.6 and B) TBR ≥1.8 as thresholds for defining HV. Red bars represent patients with an increase in HV whilst blue bars represent patients with a decrease in HV. The dotted line represents the minumum >10% reduction in HV cut-off required for patients to be classed as responders to atovaquone treatment. Abbreviations: HV, hypoxic volume; TBR, tumour-to-blood ratio.

Representative pre- and post-atovaquone treatment FMISO PET-CT scans for two patients classed as responders to treatment are shown in Figure 4.7.

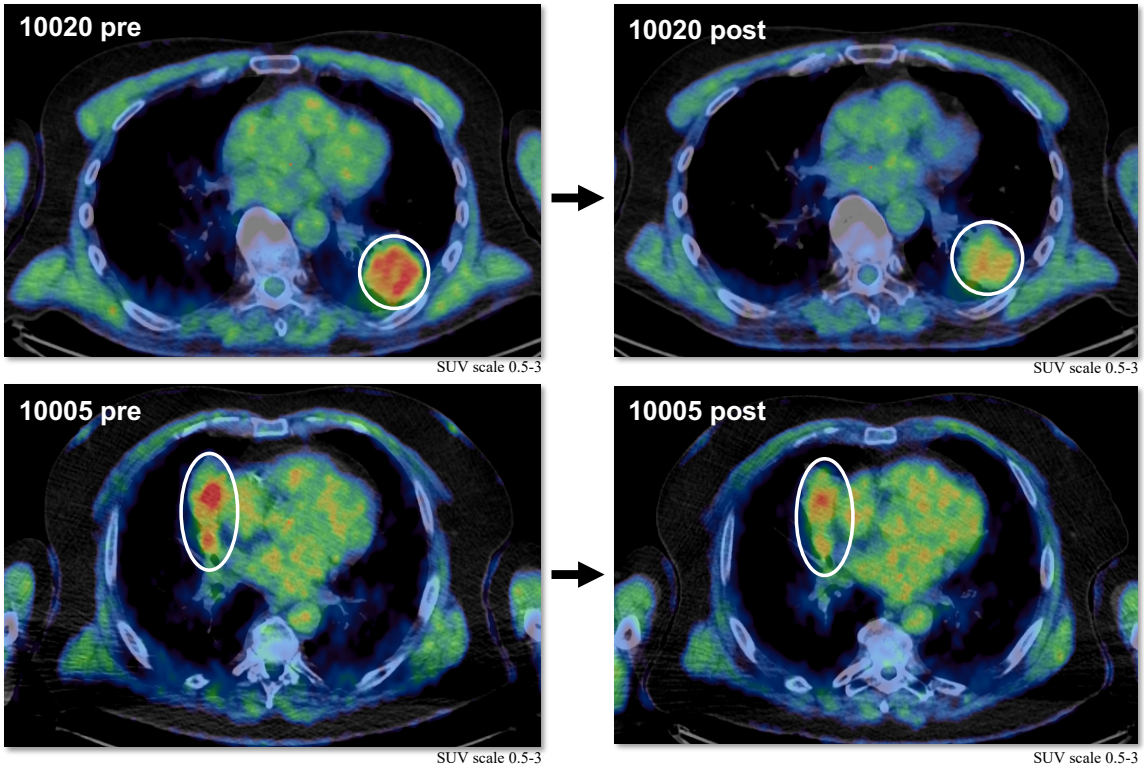


Figure 4.7: Examples of pre- and post-atovaquone treatment FMISO PET-CT scans
Representative examples of A) pre and B) post-atovaquone treatment FMISO PET-CT scans for two patients (10005 and 10020). The tumour regions of interest are circled in white with avid (red) regions representing regions of tumour hypoxia. For patient 10020 there was a 61.3% reduction in HV and for patient 10005 there was a 65.9% reduction in HV.

Paired HV data for individual patients and the change in this parameter for atovaquone treated and untreated patients are shown in Table 4.2 and Table 4.3, respectively.

Table 4.2: Change in HV in atovaquone treated patients

Patient	Pre HV (mL)	Post HV (mL)	Δ (mL)	%Δ
10001	31.8	22.9	-8.9	-28.0
10004	97.7	83.6	-14.2	-14.5
10005	8.2	2.8	-5.4	-65.9
10006	50.8	28.5	-22.2	-43.8
10008	1.7	1.4	-0.3	-19.9
10009	33.6	37.4	3.8	11.2
10010	188.3	127.2	-61.1	-32.4
10011	1.8	1.7	-0.0	-2.8
10013	5.4	0.8	-4.7	-85.5
10014	2.7	0.0	-2.7	-100.0
10016	6.7	5.9	-0.8	-11.6
10019	201.7	202.6	0.9	0.4
10020	35.3	13.7	-21.7	-61.3
10022	28.9	32.4	3.5	12.2
10023	6.9	4.1	-2.8	-40.4
Median (IQR)	**28.9** (5.4 – 50.8)	**13.7** (1.7 – 37.4)		
Median (95% CI)			**-2.8** (-14.2 – -0.1)	**-28.0** (-61.3 – -2.8)

Abbreviations: HV, hypoxic volume; pre, pre-atovaquone treatment; post, post-atovaquone treatment; IQR, interquartile range; CI, confidence interval.

Table 4.3: Change in HV in untreated patients

Patient	Visit 1 HV (mL)	Visit 2 HV (mL)	Δ (mL)	%Δ
10024	26.2	26.0	-0.2	-0.7
10025	4.9	6.2	1.3	25.4
10028	11.8	13.1	1.4	11.5
10029	1.6	3.2	1.6	95.1
10030	44.2	51.0	6.8	15.5
10031	1.9	1.9	-0.1	-3.6
10033	3.5	2.6	-0.9	-24.9
10034	21.7	19.6	-2.1	-9.4
10036	1.7	2.1	0.4	21.1
10039	34.0	49.8	15.8	46.5
10041	4.2	5.8	1.6	38.2
10043	40.5	37.7	-2.9	-7.1
10044	2.6	3.5	1.0	37.7
10045	44.8	32.7	-12.2	-27.1
10046	11.4	13.9	2.5	21.8
Median (IQR)	**11.4** (2.6 – 34.0)	**13.1** (3.2 – 32.7)		
Median (95% CI)			**1.0** (-0.9 – 1.6)	**15.5** (-7.1 – 37.7)

Abbreviations: HV, hypoxic volume; Pre, pre-atovaquone treatment; post, post-atovaquone treatment; IQR, interquartile range; CI, confidence interval.

For atovaquone treated patients, the pre-treatment median HV was 28.9 (IQR 5.4 to 50.4) mL and post-treatment was 13.7 (IQR 1.7 to 37.4) mL. The median absolute change was -2.8 mL (95% CI -14.2 to -0.1) mL and the median percentage change was -28.0% (95% CI -61.3 to -2.8). For patients who did not receive atovaquone treatment the median HV at baseline was 11.4 (IQR 2.6 to 34.0) mL and was 13.1 (IQR 3.2 to 32.7) mL for visit 2. The median absolute change was 1.0 (95% CI -0.9 to 1.6) mL and the median percentage change was 15.5% (95% CI -7.1 to 37.7).

Next, an analysis of covariance (ANCOVA) model was fitted with HV following treatment as the outcome adjusting for treatment cohort and baseline HV. The decision to correct for baseline hypoxia was taken due to the observation that tumours in treated patients appeared to be more hypoxic at baseline and that some of the largest absolute HV changes following atovaquone treatment where seen in patients with larger tumours and that larger percentage changes in HV were seen in the smallest tumours. In addition, and as shown in Figure 4.8, HV values at Visit 1 and Visit 2 were very strongly correlated in both cohorts ($r_s = 0.9$, $p < 0.001$), indicating that a large predictor of the HV value at Visit 2 was the baseline HV. The HV data was log transformed as for ANCOVA analysis transformation improved the model's validity due to normality of residuals.

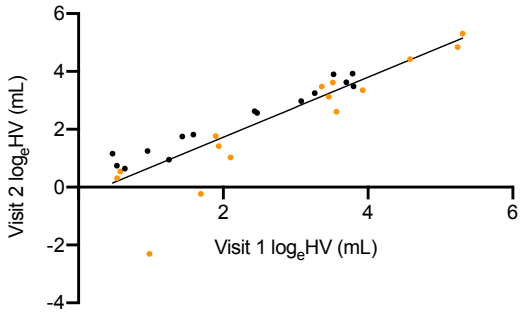


Figure 4.8: Correlation of tumour HV measurements per patient
Scatter plot showing the correlation between natural log transformed hyp-PET derived tumour HV measured at Visit 1 and Visit 2 for each trial patient. Orange data points represent atovaquone treated patients and black data points represent untreated patients. Abbreviation: HV, hypoxic volume. Line of best fit is shown to signify positive correlation (Spearman's rho correlation coefficient with $p < 0.05$).

Using ANCOVA analysis, with the post-treatment HV value for one patient (10014) changed from 0 to 0.1 to ensure all patients were included in the analysis, the treatment estimate was 0.8 (95% CI 0.3 to 1.3, p = 0.003), and thus the expected geometric mean of HV was 2.2 times higher (more hypoxic) following no treatment than compared with atovaquone treatment.

4.2.3.2 Atovaquone treatment reduces tumour HV%

In contrast to absolute HV, HV% represents an average-based tumour hyp-PET parameter taking into consideration the whole tumour volume. This alternative measure of hypoxia not only provides an additional parameter to use to study the effect of atovaquone on hypoxia, but also will be used for upcoming correlation with other mean-based endpoints, such as percentage pimonidazole staining in IHC analysis.

The absolute change in HV% from baseline for each patient is shown in Figure 4.9 and illustrates a significant reduction for atovaquone treated patients (p = 0.003), with no significant change observed for untreated patients (p = 0.56).

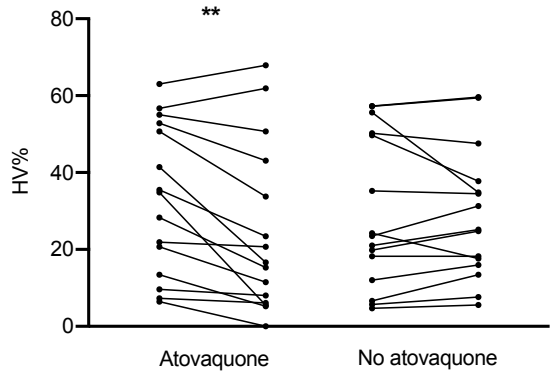


Figure 4.9: Effect of atovaquone on tumour HV%
Absolute changes in hyp-PET derived tumour HV% for atovaquone treated and untreated patients. Abbreviation: HV%, hypoxic volume percentage. **p < 0.01 (Wilcoxon signed-rank test).

The change in HV% from baseline for each atovaquone treated and untreated patient is also shown as waterfall plots in Figure 4.10. A reduction in this parameter was observed

in 13 (86.7%) of 15 atovaquone treated patients whilst in 10 (66.7%) of 15 untreated patients there was an increase.

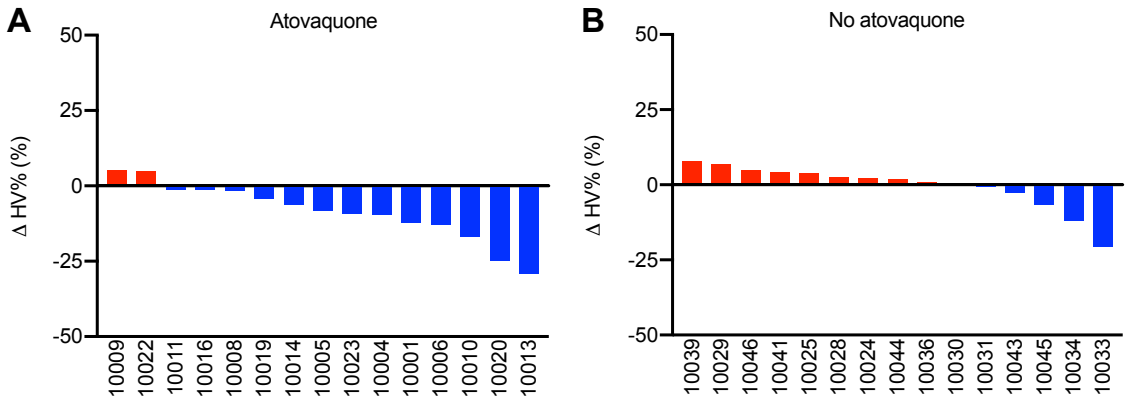


Figure 4.10: Waterfall plots demonstrating the effect of atovaquone on tumour HV%
Absolute changes from baseline in hyp-PET derived tumour HV% for A) atovaquone treated and B) untreated patients. Red bars represent patients with an increase in HV% whilst blue bars represent patients with a decrease in HV%. Abbreviations: HV%, hypoxic volume percentage.

Paired HV% data and the change in this parameter for atovaquone treated and untreated patients are shown in Table 4.4 and Table 4.5, respectively.

Table 4.4: Change in HV% in atovaquone treated patients

Patient	Pre HV%	Post HV%	Δ (%)
10001	35.5	23.4	-12.1
10004	52.8	43.1	-9.7
10005	13.4	5.2	-8.2
10006	28.3	15.3	-13.0
10008	9.6	8.0	-1.6
10009	56.7	61.9	5.2
10010	50.7	33.8	-16.9
10011	7.3	6.1	-1.2
10013	34.8	5.5	-29.3
10014	6.4	0.0	-6.4
10016	21.9	20.7	-1.2
10019	55	50.7	-4.3
10020	41.4	16.6	-24.8
10022	63	67.9	4.9
10023	20.7	11.5	-9.2
Median (IQR)	**34.8** (13.4 – 52.8)	**16.6** (6.1 – 43.1)	
Median (95% CI)			**-8.2** (-13.0 – -1.2)

Abbreviations: HV%, hypoxic volume percentage; pre, pre-atovaquone treatment; post, post-atovaquone treatment; IQR, interquartile range; CI, confidence interval.

Table 4.5:Change in HV% in untreated patients

Patient	Visit 1 HV%	Visit 2 HV%	Δ (%)
10024	57.2	59.4	2.2
10025	12	16.0	4.0
10028	57.3	59.6	2.3
10029	6.6	13.4	6.8
10030	18.2	18.3	0.1
10031	35.2	34.5	-0.7
10033	55.6	34.9	-20.7
10034	49.7	37.7	-12.0
10036	4.7	5.6	0.9
10039	23.5	31.3	7.8
10041	21	25.1	4.1
10043	50.2	47.6	-2.6
10044	5.7	7.7	2.0
10045	24.2	17.6	-6.6
10046	19.8	24.7	4.9
Median (IQR)	**23.5** (12 – 50.2)	**25.1** (16.0 – 37.7)	
Median (95% CI)			**2.0** (-2.6 – 4.1)

Abbreviations: HV%, hypoxic volume percentage; IQR, interquartile range; CI, confidence interval

There was a significant difference in the median change from baseline in HV% between atovaquone treated and untreated patients (p = 0.001), as shown in Figure 4.11.

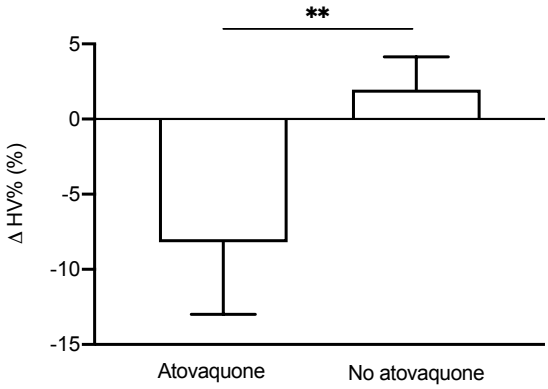


Figure 4.11: Change in HV% in atovaquone treated and untreated patients
Comparison of the median change in hyp-PET derived tumour HV% from baseline between atovaquone treated and untreated patients. Data shown is median change with 95% CI. Abbreviation: HV%, hypoxic volume percentage. **p < 0.01 (Mann-Whitney U test).

4.2.3.3 Atovaquone treatment reduces tumour TBR_{mean} and TBR_{peak}

TBR_{mean} is another mean-based tumour hypoxia parameter whereas TBR_{peak} gives an indication of the maximum severity of hypoxia.

Figure 4.12 shows the absolute change in TBR_{mean} and TBR_{peak} for each patient with both parameters significantly lower following atovaquone treatment (TBR_{mean} p = 0.005, TBR_{peak} p = 0.003) but not significantly different between imaging visits for untreated patients (TBR_{mean} p = 0.836, TBR_{peak} p = 0.720). Paired TBR_{mean} and TBR_{peak} values and the change in these parameters for atovaquone treated and untreated patients are shown in Table 4.6 and Table 4.7, respectively.

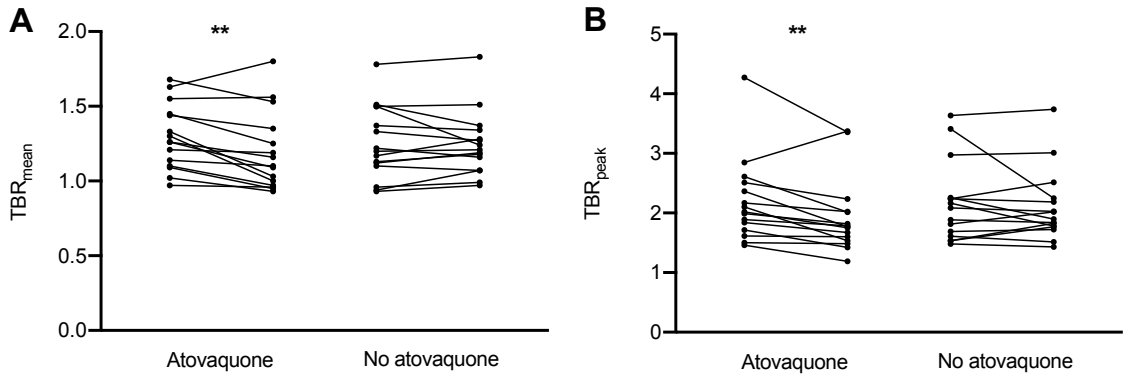


Figure 4.12: Effect of atovaquone on TBR_{mean} and TBR_{peak}
Changes in hyp-PET derived tumour A) TBR_{mean} and B) TBR_{peak} from baseline for atovaquone treated and untreated patients. Abbreviation: TBR, tumour-to-blood ratio. **p < 0.01 (Wilcoxon signed-rank test).

Table 4.6: Change in TBR_{mean} and TBR_{peak} in atovaquone treated patients

Patient	Pre TBR_{mean}	Post TBR_{mean}	Δ TBR_{mean}	Pre TBR_{peak}	Post TBR_{peak}	Δ TBR_{peak}
10001	1.26	1.16	-0.1	2.37	1.77	-0.60
10004	1.44	1.35	-0.09	2.17	2.02	-0.15
10005	1.1	0.97	-0.13	2.10	1.54	-0.57
10006	1.26	1.09	-0.17	1.99	1.82	-0.17
10008	1.02	0.93	-0.09	1.61	1.60	-0.01
10009	1.55	1.56	0.01	2.51	2.24	-0.27
10010	1.45	1.25	-0.20	2.61	2.02	-0.60
10011	0.97	0.96	-0.01	1.50	1.48	-0.02
10013	1.3	1	-0.30	1.71	1.42	-0.29
10014	1.09	0.95	-0.14	1.46	1.19	-0.27
10016	1.21	1.19	-0.02	1.89	1.79	-0.10
10019	1.68	1.53	-0.15	4.27	3.36	-0.92
10020	1.33	1.03	-0.30	2.02	1.75	-0.27
10022	1.63	1.8	0.17	2.85	3.37	0.52
10023	1.14	1.1	-0.04	1.84	1.67	-0.17
Median (IQR)	**1.26** (1.10 – 1.45)	**1.10** (0.97 – 1.35)		**2.02** (1.71 – 2.51)	**1.77** (1.54 – 2.02)	
Median (95% CI)			**-0.10** (-0.17 – -0.02)			**-0.27** (-0.57 – -0.10)

Abbreviations: Pre, pre-atovaquone; post, post-atovaquone; TBR, tumour-to-blood ratio; IQR, interquartile range; CI, confidence interval.

Table 4.7: Change in TBR_{mean} and TBR_{peak} in untreated patients

Patient	Visit 1 TBR_{mean}	Visit 2 TBR_{mean}	Δ TBR_{mean}	Visit 1 TBR_{peak}	Visit 2 TBR_{peak}	Δ TBR_{peak}
10024	1.5	1.51	0.01	2.24	2.18	-0.05
10025	1.13	1.18	0.05	1.61	1.52	-0.09
10028	1.78	1.83	0.05	3.64	3.74	0.10
10029	0.94	1.07	0.13	1.54	1.77	0.23
10030	1.1	1.07	-0.03	3.41	2.25	-1.16
10031	1.33	1.27	-0.06	2.08	2.03	-0.06
10033	1.5	1.24	-0.26	2.17	1.78	-0.38
10034	1.51	1.37	-0.14	2.97	3.01	0.04
10036	0.93	0.97	0.04	1.48	1.43	-0.05
10039	1.17	1.28	0.11	2.24	2.51	0.28
10041	1.2	1.21	0.01	1.69	1.72	0.04
10043	1.37	1.34	-0.03	1.88	1.84	-0.04
10044	0.96	0.99	0.03	1.54	1.83	0.29
10045	1.22	1.16	-0.06	2.25	1.90	-0.36
10046	1.12	1.19	0.07	1.82	2.02	0.20
Median (IQR)	**1.20** (1.10 – 1.50)	**1.21** (1.07 – 1.34)		**2.08** (1.61 – 2.25)	**1.90** (1.77 – 2.25)	
Median (95% CI)			**0.01** (-0.06 – 0.05)			**-0.04** (-0.09 – 0.20)

Abbreviations: TBR, tumour-to-blood ratio; IQR, interquartile range; CI, confidence interval.

There was a significant reduction in TBR_{mean} (p = 0.009) and TBR_{peak} (p = 0.030) in atovaquone treated patients when compared with untreated patients (Figure 4.13).

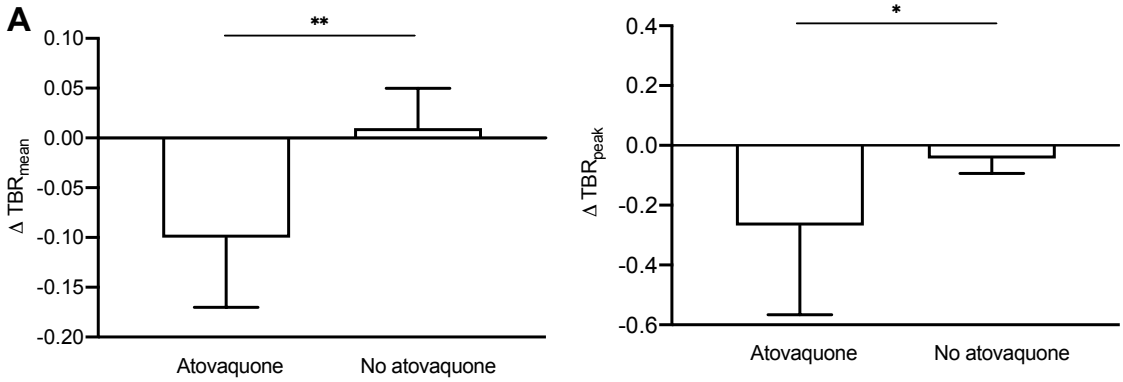


Figure 4.13: Change in TBR_{mean} and TBR_{peak} in atovaquone treated and untreated patients
Comparison of the median change in hyp-PET derived tumour A) TBR_{mean} and B) TBR_{peak} between atovaquone treated and untreated patients. Data shown is median change with 95% CI. Abbreviation: TBR, tumour-to-blood ratio. *p < 0.05, **p < 0.01 (Mann-Whitney U test).

4.2.4 Correlation of atovaquone plasma levels with change in HV

As was shown in Chapter 3, plasma levels of atovaquone for all patients were at or above the level previously shown pre-clinically to reduce tumour hypoxia. However, as there was a large range in levels between patients (29.4 μM to 113 μM) it was next investigated whether plasma levels correlated with the degree of reduction in tumour hypoxia. As shown in Figure 4.14 there was no correlation observed between atovaquone plasma levels and both percentage (r_s = -0.22, p = 0.401) and absolute (r_s = 0.00, p = 0.999) change in HV. In addition, there was no correlation between atovaquone plasma levels and change in HV% (r_s = -0.17, p = 0.541), TBR_{mean} (r_s = -0.11, p = 0.705) and TBR_{peak} (r_s = 0.46, p = 0.999).

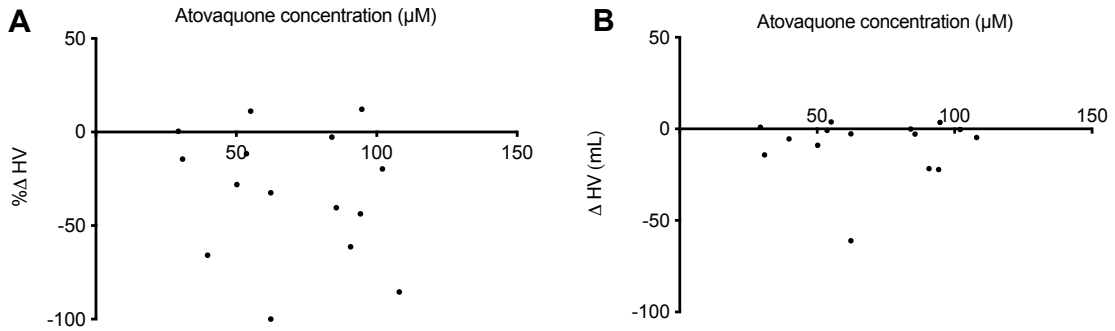


Figure 4.14: Correlation of plasma atovaquone levels with change in HV
Scatter plots showing lack of correlation between atovaquone plasma levels and A) percentage and B) absolute change from baseline in hyp-PET derived tumour HV. Abbreviation: HV, hypoxic volume.

4.2.5 Baseline tumour perfusion as measured by perfusion CT

pCT was performed in parallel to hyp-PET imaging for all patients to further characterise the tumour hypoxic profile and to investigate whether any reduction in hypoxia following atovaquone treatment may be due to changes in perfusion.

The complete pCT data collected for Cohort 1 and Cohort 2 is presented in Appendix Table 2 and Appendix Table 3, respectively. As described in Chapter 2, due to the limited size of the pCT imaging field some tumours were incompletely imaged and therefore only data from matched tumour regions on both scans per patient were used. However, as unmatched data provides the most representative estimate of whole tumour perfusion (as no data is discarded for matching purposes) this data was used to evaluate baseline tumour perfusion and for correlation with hyp-PET parameters at baseline.

A summary of unmatched baseline pCT data for all patients, as well as for patients with paired pCT and hyp-PET scans and therefore evaluable for measuring change in perfusion and hypoxia, is shown in Table 4.8 and Table 4.9, for Cohort 1 and Cohort 2 respectively.

Table 4.8: Summary of baseline pCT perfusion parameters for Cohort 1

	n	Baseline BF (mL/100 g/min)	Baseline BV (mL/100 g)	Baseline MTT (s)
All	**20**	**96.6** (63.5 – 114.7)	**5.8** (4.8 – 7.6)	**6.1** (4.8 –7.5)
Paired pCT	**16**	**84.4** (63.5 – 114.7)	**6.4** (5.0 – 7.6)	**6.5** (5.0 – 7.5)
Paired hyp-PET	**14**	**79.2** (59.6 – 112.4)	**6.1** (4.7 – 7.8)	**6.5** (5.4 – 7.6)

Data shown are median values with interquartile ranges. Abbreviations: BF, blood flow; BV, blood volume; MTT, mean transit time; pCT, perfusion CT.

Table 4.9: Summary of baseline pCT perfusion parameters for Cohort 2

	n	Baseline BF (mL/100 g/min)	Baseline BV (mL/100 g)	Baseline MTT (s)
All	**19**	**80.0** (43.2 – 106.0)	**4.5** (3.2 – 6.4)	**5.9** (4.3 – 7.1)
Paired pCT	**6**	**61.4** (39.1 – 76.4)	**5.1** (3.0 – 7.0)	**7.7** (5.9 – 9.5)
Paired hyp-PET	**11**	**71.1** (43.2 – 92.0)	**4.5** (3.2 –6.4)	**6.0** (5.9 – 8.4)

Data shown are median values with interquartile ranges. Abbreviations: BF, blood flow; BV, blood volume; MTT, mean transit time; pCT, perfusion CT.

A comparison in baseline pCT parameters between cohorts for patients evaluable for measuring change in perfusion and hypoxia are shown in Figure 4.15 and Figure 4.16, respectively.

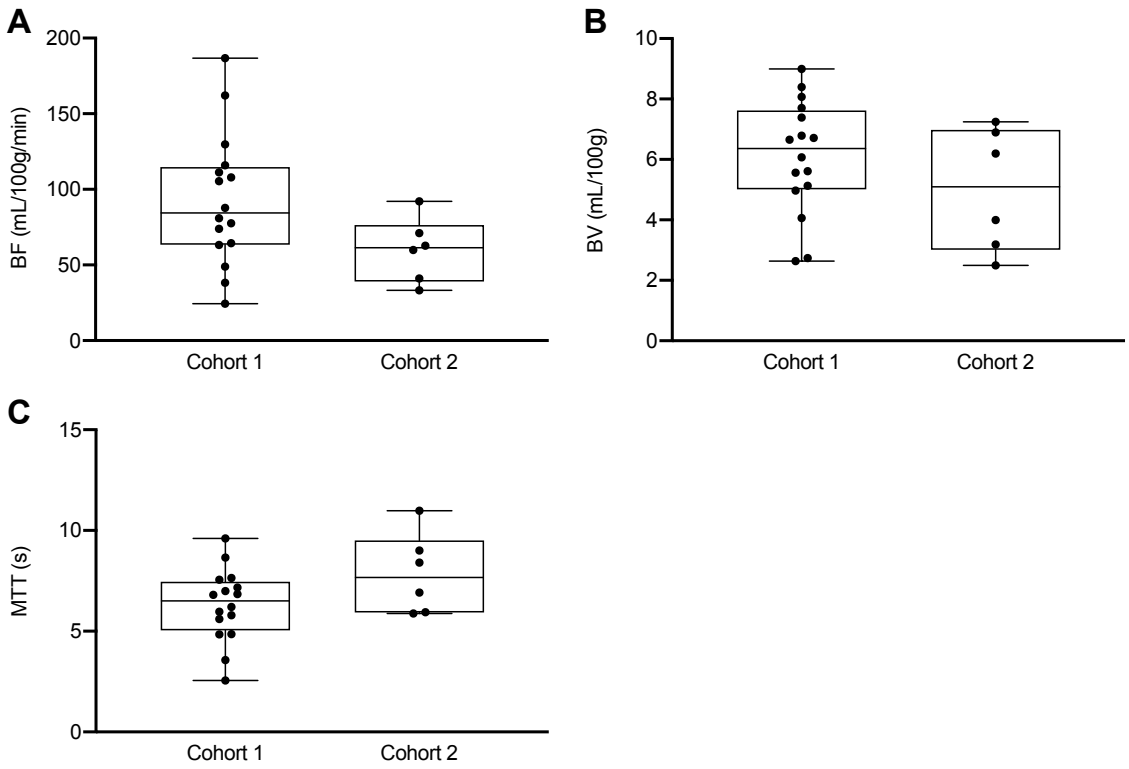


Figure 4.15: Baseline pCT perfusion parameters for patients with paired pCT scans
Box and whisker plots comparing baseline pCT derived tumour A) BF, B) BV and C) MTT between patients with paired pCT scans in Cohort 1 and Cohort 2. Median levels with interquartile and absolute ranges are shown. Abbreviations: BF, blood flow; BV, blood volume; MTT, mean transit time.

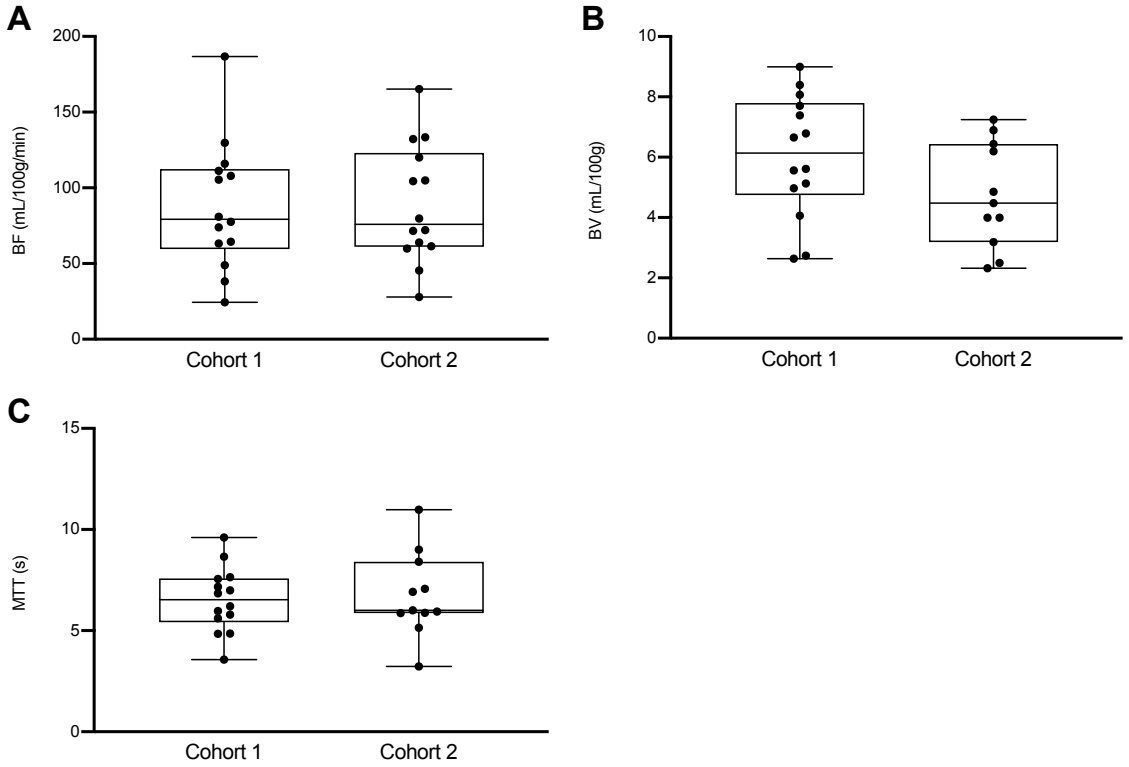


Figure 4.16: Baseline pCT perfusion parameters for patients with paired hyp-PET scans
Box and whisker plots comparing baseline pCT derived tumour A) BF, B) BV and C) MTT between patients with paired hyp-PET scans in Cohort 1 and Cohort 2. Median levels with interquartile and absolute ranges are shown. Abbreviations: BF, blood flow; BV, blood volume; MTT, mean transit time.

This data demonstrated that there was a large range in BF, BV and MTT in patients in this study. For patients with paired pCT scans and therefore used to assess change in tumour perfusion, it appears that patients in Cohort 1 who went on to receive atovaquone treatment had higher baseline BF and BV and lower MTT than Cohort 2 patients who received no treatment, therefore suggesting Cohort 1 tumours were better perfused at baseline. With regards to patients with paired hyp-PET scans and who were therefore evaluable for assessing changes in hypoxia, collectively there was less of a clear difference observed between baseline tumour perfusion between cohorts.

4.2.6 Atovaquone treatment does not alter tumour perfusion as measured by pCT

Paired and tumour region matched pCT data for atovaquone treated and untreated patients is shown in Table 4.10 and Table 4.11, respectively. Summary of the absolute and percentage change for each parameter for both cohorts is shown in Table 4.12.

Table 4.10: Paired and tumour region matched pCT data for atovaquone treated patients

Patient	Pre BF (mL/100 g/min)	Pre BV (mL/100 g)	Pre MTT (s)	Post BF (mL/100 g/min)	Post BV (mL/100 g)	Post MTT (s)
10001	107.9	9.0	6.2	120.2	9.3	7.3
10003	162.0	6.1	2.6	93.8	4.0	2.5
10004	63.2	6.7	8.7	61.5	7.5	10.1
10005	38.3	2.6	6.0	71.5	4.3	5.7
10006	77.6	5.0	6.8	79.8	4.8	6.3
10007	87.8	6.7	6.8	80.4	6.3	8.4
10008	115.9	5.6	5.8	133.4	5.6	4.7
10009	105.5	5.1	4.8	132.2	5.8	4.3
10010	23.3	2.7	9.8	26.5	2.5	8.7
10011	111.3	8.4	7.2	104.4	8.1	8.6
10014	198.1	7.8	3.2	165.2	7.9	5.2
10016	70.5	3.7	5.4	63.9	3.3	5.3
10019	49.5	7.4	4.9	59.5	7.3	4.9
10020	80.9	6.8	7.0	72.0	5.1	6.7
10022	64.9	5.7	7.7	45.2	5.4	10.7
10023	112.0	7.7	7.9	104.9	6.6	6.6
Median (IQR)	**84.4** (63.6 – 11.8)	**6.4** (5.0 – 7.6)	**6.5** (5.0 –7.5)	**80.1** (62.1 – 116.3)	**5.7** (4.4 – 7.4)	**6.5** (5.0 – 8.6)

Abbreviations: pre, pre-atovaquone treatment; post, post-atovaquone treatment; BF, blood flow; BV, blood volume; MTT, mean transit time; pCT, perfusion CT; IQR, interquartile range.

Table 4.11: Paired and tumour region matched pCT data for untreated patients

Patient	Visit 1 BF (mL/100 g/min)	Visit 1 BV (mL/100 g)	Visit 1 MTT (s)	Visit 2 BF (mL/100 g/min)	Visit 2 BV (mL/100 g)	Visit 2 MTT (s)
10024	33.5	2.5	11.0	30.1	2.6	10.2
10025	48.2	3.5	6.0	44.5	3.3	4.7
10028	62.8	6.2	8.4	70.8	6.4	7.4
10030	42.1	3.1	6.7	44.8	3.9	6.5
10043	98.6	6.8	5.3	65.3	6.5	8.5
10044	72.1	7.3	8.9	71.2	7.2	9.3
Median (IQR)	**55.5** (40.0 – 78.7)	**4.8** (3.0 – 6.9)	**7.6** (5.8 – 9.5)	**55.0** (40.9 – 70.9)	**5.2** (3.1 – 6.6)	**8.0** (6.1 – 9.5)

Abbreviations: BF, blood flow; BV, blood volume; MTT, mean transit time; pCT, perfusion CT; IQR, interquartile range.

Table 4.12: Summary of change in pCT parameters in atovaquone treated and untreated patients

	n	BF (mL/100 g/min)	BV (mL/100 g)	MTT(s)
Atovaquone treatment	**16**			
Δ		**-4.2** (-8.9 – 12.3)	**-0.2** (-0.4 – 0.3)	**-0.1** (-0.6 – 1.5)
%Δ		**-4.5** (-11.0 – 15.1)	**-3.6** (-11.4 – 3.3)	**-2.8** (-11.0 – 20.4)
No treatment	**6**			
Δ		**-2.2** (-33.3 – 8.0)	**0.0** (-0.4 – 0.8)	**-0.5** (-1.3 – 3.3)
%Δ		**-4.4** (-33.8 – 12.7)	**1.0** (-5.9 – 26.5)	**-5.1** (-22.2 – 62.5)

Data shown are median values with 95% confidence intervals. Abbreviations: BF, blood flow; BV, blood volume; MTT, mean transit time; pCT, perfusion CT

Individual patient absolute changes in each pCT perfusion parameter for atovaquone treated and untreated patients are shown in Figure 4.17. For atovaquone treated patients there was no significant change in BF ($p = 0.820$), BV ($p = 0.298$) and MTT ($p = 0.528$). No statistical analysis was performed for untreated patients due to the small number of patients with paired scans.

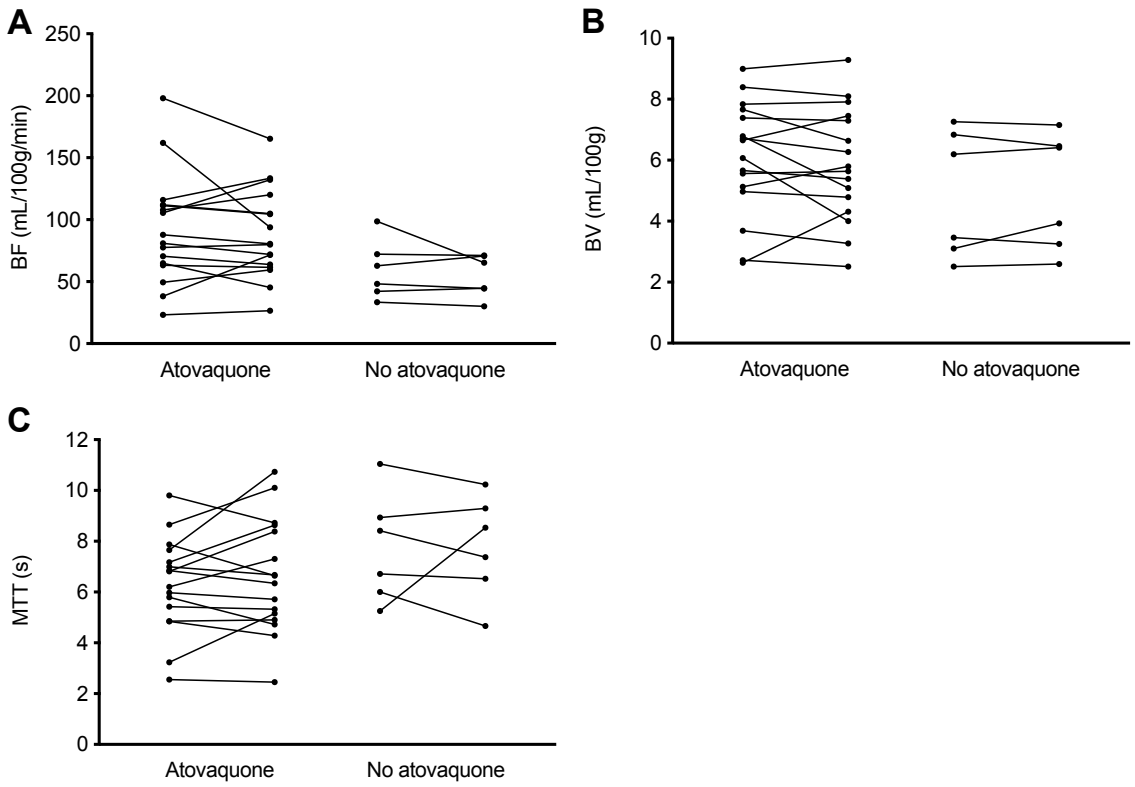


Figure 4.17: Effect of atovaquone on pCT parameters
Changes in pCT derived tumour A) BF, B) BV and C) MTT for atovaquone treated and untreated patients. Abbreviations: BF, blood flow; BV, blood volume; MTT, mean transit time. Changes observed in the atovaquone treated group were not significant (Wilcoxon signed-rank test).

The percentage change from baseline in all pCT parameters per individual atovaquone treated and untreated patient are shown in Figure 4.18 and Figure 4.19, respectively. Overall, this data demonstrates that for the vast majority of patients the percentage change for all parameters was within the accepted 25% error range for measuring change using this imaging modality [263].

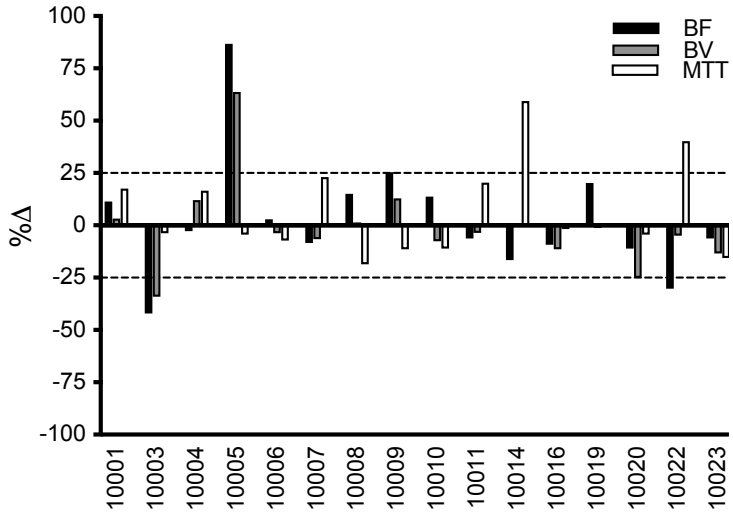


Figure 4.18: Change in pCT parameters following atovaquone treatment
Percentage change from baseline in pCT derived tumour BF, BV and MTT following atovaquone treatment. The dotted lines represent the error margin for measuring change in these parameters using pCT. Abbreviations: BF, blood flow; BV, blood volume; MTT, mean transit time.

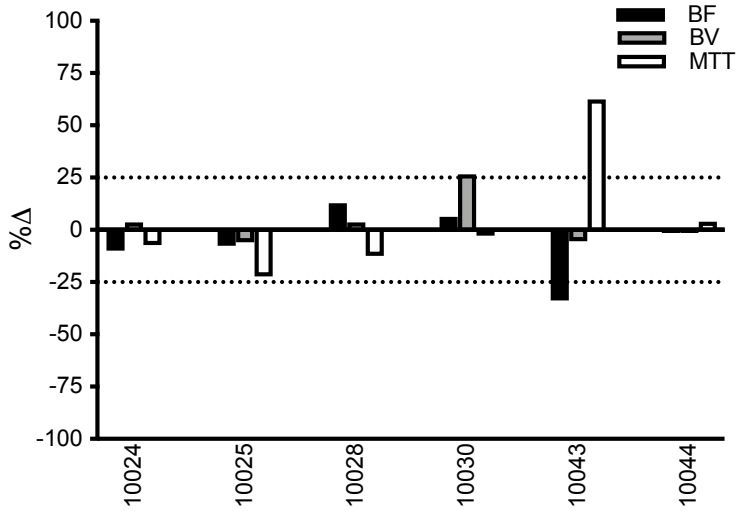


Figure 4.19: Change in pCT parameters without atovaquone treatment
Percentage change from baseline in pCT derived tumour BF, BV and MTT in untreated patients. The dotted lines represent the error margin for measuring change in these parameters using pCT. Abbreviations: BF, blood flow; BV, blood volume; MTT, mean transit time.

4.2.7 Correlation of pCT and hyp-PET parameters

For all patients with a both interpretable pCT and hyp-PET scans at baseline, or at Visit 2 for untreated patients in Cohort 2 if the Visit 1 pCT scan was not performed or was uninterpretable, correlation analysis between pCT derived tumour BF and hyp-PET derived HV, HV%, TBR_{mean} and TBR_{peak} was conducted. As shown in Figure 4.20, there was a moderate negative correlation between BF and HV (r_s = -0.40, p = 0.009) and TBR_{peak} (r_s = -0.47, p = 0.002) and a weak negative correlation with HV% (r_s = -0.36, p = 0.021) and TBR_{mean} (r_s = -0.35, p =0.023).

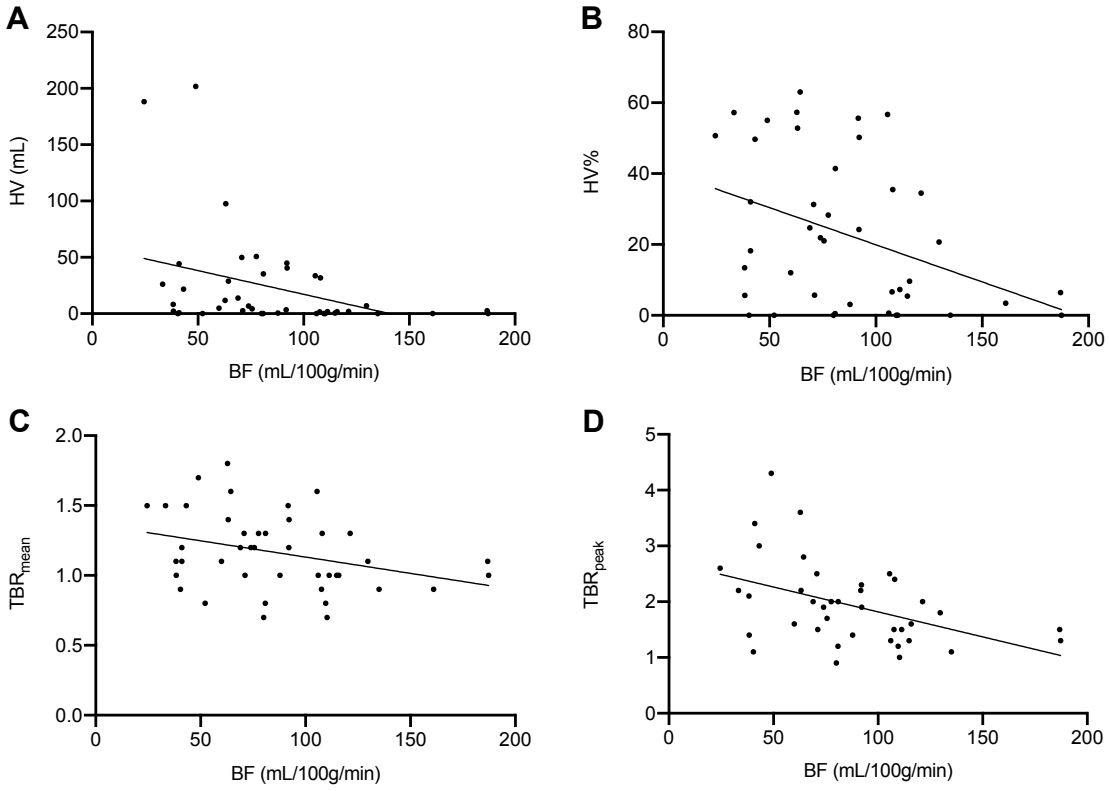


Figure 4.20: Correlation of pCT with hyp-PET parameters
Scatter plots showing the correlation of pCT derived tumour BF with hyp-PET derived tumour A) HV, B) HV%, C) TBR_{mean} and D) TBR_{peak}. Abbreviations: BF, blood flow; HV, hypoxic volume; HV%, hypoxic volume percentage; TBR, tumour-to-blood ratio. Lines of best fit are shown for correlated data (Spearman's rho correlation coefficient with $p < 0.05$).

4.3 DISCUSSION

4.3.1 Baseline tumour hypoxia profile

The comparison of baseline hypoxic profiles showed that tumours in the atovaquone treated cohort were more hypoxic at baseline. This was somewhat of a surprising finding given that there was no large difference between cohorts in terms of tumour volume, and especially as tumour volume and hypoxia appeared strongly correlated. It is possible that this difference was due to the large range in tumour size and degrees of hypoxia observed, as well as possibly due to the relatively small patient numbers in each cohort. It is also possible that tumour necrosis may have played a role as many tumours often contained large regions of necrosis (Figure 2.2) and thus the relationship between tumour size and HV is not straightforward. Given the highly heterogeneous nature of NSCLC, even in a resectable patient population, this large variability in tumour size and hypoxia was largely unavoidable and is in keeping with other published trials in this tumour type [125,127,264].

Interestingly, other clinical features such as histological subtype and diagnostic FDG PET avidity did not appear convincingly predictive of baseline hypoxia, further demonstrating the unpredictability of tumour hypoxia. With regards to FDG PET, although a weak correlation was observed between FDG PET SUV_{max} and both HV and TBR_{mean}, there was no correlation with HV% and TBR_{peak}. In agreement, data presented in Chapter 3 demonstrated that FDG PET was not predictive of the presence of sufficient baseline hypoxia. Tumour imaging with FDG PET relies on high rates of tracer uptake due to upregulation of the glycolytic pathway, a common feature of tumours. As this is the predominant metabolic pathway under anaerobic conditions, this has naturally lead to the hypothesis that FDG uptake may be a surrogate marker of hypoxia [265]. However, the

mixed results in this study echo the established debate in the literature as to whether FDG uptake is a good marker of tumour hypoxia, or not [264,266,267].

However, perhaps in the context of developing OCR inhibitors as hypoxia modifiers, FDG PET could potentially play an important future role. In a recent study in breast cancer patients, FDG PET was used as one of the outcome measures which demonstrated the shift in metabolism from OXPHOS to glycolysis following treatment with the known OCR inhibitor metformin [231]. Therefore, perhaps FDG PET may be a useful tool in future studies developing OCR inhibitors as hypoxia modifiers in order to investigate the metabolic tumour phenotype and thus of any change in metabolism following treatment with such agents, instead of being a marker of tumour hypoxia *per se*.

Overall, the baseline hypoxia data in this chapter does not support that clinical parameters such as tumour size, histology and FDG PET avidity can reliably predict the degree of tumour hypoxia as measured by hyp-PET. Therefore, matching patients based on such parameters, as was initially considered in this study, would unlikely have ensured the same hypoxic profile of both cohorts. This data supports that in hypoxia imaging studies it is important to carefully assess for differences in hypoxia at baseline given its high degree of unpredictability.

The finding of non-equivalence between cohorts in baseline hypoxia is of importance in this particular study for two reasons. Firstly, it informed the decision to correct for baseline HV in the primary analysis of the effect of atovaquone on tumour hypoxia. Secondly, it informed the comparison of resected tumour hypoxia IHC results between atovaquone treated and untreated patients (Chapter 5).

4.3.2 Atovaquone treatment reduces tumour hypoxia

The most exciting finding from this study is the dramatic reduction in tumour hypoxia following atovaquone treatment as assessed by all hyp-PET parameters. This is the first trial to show that an OCR inhibitor reduces hypoxia in the clinical setting and therefore represents a crucial clinical proof of principle not only for this agent but as well as for this emerging hypoxia modification strategy. Further still, the reduction in the most severe regions of hypoxia was even more pronounced, with near complete resolution of these hypoxic regions in a number of cases. As such intensely hypoxic regions are likely to represent more radiobiologically resistant disease, this therefore suggests that this approach may hold real clinical promise and provides further impetus for further developing this agent as a novel tumour radiosensitiser.

Although the degree of hypoxic change observed in this study was impressive, due to the lack of previous proof of principle clinical studies to confirm efficacy of hypoxia modifiers it is somewhat difficult to contextualise the magnitude of the effect observed. In the only other study to test the effect of a specific hypoxia modifier using hyp-PET in NSCLC, changes following buparlisib, a specific PI3K inhibitor, were less than observed following atovaquone treatment [125]. In the small imaging sub-study of the ARCII trial in pancreatic cancer, the PI3K/Akt inhibitor nelfinavir was also shown to reduce hypoxia, however, because dynamic FMISO PET imaging was used, a comparison of the size of effect is not possible. For nelfinavir, which has proven proof of principle with reduction in hypoxia, promising outcomes following combination with radiotherapy in pancreatic cancer [268], rectal cancer [269] and NSCLC [270] have been observed, although it needs to be appreciated that this drug is also known to increase tumour intrinsic radiosensitivity.

It is also not known what magnitude of change in hypoxia is required to translate to meaningful reduction in radioresistance, and therefore improvement in radiotherapy outcomes. As hyp-PET tracers such as FMISO and FAZA accumulate at oxygen levels far below the threshold at which the OER becomes a feature [90,111], theoretically any reduction in the uptake of these tracers should improve tumour radiation response. However whether this reduction in uptake translates in meaningful clinical benefit is of course a different question altogether.

Many studies using hyp-PET have demonstrated reductions in tumour hypoxia during standard fractionated radiotherapy in numerous tumour types, including NSCLC [271]. It has repeatedly been shown in HNSCC that a lack of decrease in hypoxia tracer uptake during the early stages of radiotherapy correlates with poor LRC [272,273]. However, a number of other studies have shown that a not insignificant proportion of patients with complete resolution of hypoxia during radiotherapy still developed loco-regional failure [101,274]. For NSCLC, such studies linking hypoxia change during radiotherapy with outcomes in NSCLC are lacking.

However, these studies did not test the effect of hypoxia modification prior to radiotherapy; the change in hypoxia during radiotherapy may reflect the intrinsic radiosensitivity of disease, as opposed to the effect of the presence of hypoxia. It is likely that the answer to what change in hypoxia is required to improve radiotherapy outcomes is multifactorial and dependent upon tumour-specific factors such as size, intrinsic tumour radiosensitivity and severity of baseline hypoxia, as well as treatment-specific factors including the exact (chemo)radiotherapy regime in question.

The diametrically opposite patterns of hypoxia change observed between atovaquone treated and untreated patients further supports that atovaquone reduces hypoxia. However,

it was interesting to observe that hypoxia increased in untreated patients between the imaging time points, and so significantly. Although it is intuitive that hypoxia would worsen over time, the degree of increase in hypoxia in this on average two-week period was surprising, especially given that there were no significant changes in tumour volume. On review of the literature there is an absence of clinical studies conducting hyp-PET over a comparable timeframe in NSCLC without intervention. Hyp-PET test-retest studies investigating reproducibility repeated scans within much shorter time periods, typically only 24 to 48 hours [127,128].

Perhaps some of the largest increases in hypoxia observed in untreated patients could be due to acute (cycling or transient) hypoxia. The phenomenon of sizable fluctuations in tumour hypoxia due to occlusion or impaired function of tumour vasculature has been shown in numerous clinical studies [60,275–277]. In this study, the importance of perfusion in determining hypoxia was observed by the strong negative correlation between hypoxic parameters and blood flow. Further still, perhaps tumours in the lung may be may be more prone to such fluctuations due to the unique and complex physiological properties of this particular organ in which ventilation and perfusion are intricately coupled [278]. It is not inconceivable that minor tumour growth could result in worsening bronchial obstruction and thus decreased ventilation and subsequently decreased perfusion of that region of lung. In fact, for hilar tumours, as many cases in this study were, tumour-related reduction in ventilation and subsequently perfusion has been reported [279]. Unfortunately in this study, the untreated patients with the largest increases in hypoxia were not evaluable for paired perfusion CT analysis and therefore it was not possible to investigate for underlying changes in tumour perfusion. However, overall if in the natural history of hypoxia in NSCLC is for such an increase over even a short period of time, then the reduction observed following atovaquone treatment in this study is all the more impressive.

4.3.3 Atovaquone does not alter tumour perfusion

The data from pCT imaging in this study demonstrated that atovaquone treatment does not result in large changes in tumour perfusion. This was important to assess as there is no clinical or even preclinical data on the effect of this agent on tumour vasculature [219]. In addition, PI3K and AKT inhibitors have been shown to reduce tumour hypoxia through improved tumour perfusion following comparable short treatment length [125,268]. Given the established large margin for error when measuring perfusion with pCT [263] it may be that small changes would not have been detected using this technique. However, the lack of any gross changes in perfusion following atovaquone treatment provides further support that this drug reduces tumour hypoxia through OCR inhibition. To further confirm that atovaquone inhibits OXPHOS, tumour gene expression analysis focusing metabolic gene signatures has been initiated and a collaboration to investigate the effect of atovaquone on the tumour metabolomic profile has also been established.

A number of technical and practical challenges were encountered in this study with regards to performing pCT. Firstly, tumours were often very large and only partially imaged due to the limited scan detector width and therefore perfusion data may not have been representative of the whole tumour. Furthermore, to assess change in perfusion parameters very careful matching of scans was required with removal of any unmatched data. Secondly, although data was motion corrected, movement of the tumour due to respiration was a problem and 45 second breath holds for patients with underlying poor lung function was not always achievable. Third, numerous scans were technically not interpretable due to variations in the rate of injection as measured by the analysis input function and interference of signal form adjacent normal structures such as heart and great vessels which was particularly a challenge for centrally located tumours. Overall, it is

acknowledged that performing high quality pCT imaging in NSCLC patients is a significant challenge.

CHAPTER 5: PLASMA AND TUMOUR TISSUE HYPOXIA MARKERS

5.1 INTRODUCTION

Data presented in this chapter represents an investigation into the effect of atovaquone on tumour hypoxia as measured by plasma hypoxia markers and by performing tumour immunohistochemical analysis. As described in Chapter 1, numerous such sample-based methods have been used over the last couple of decades to assess tumour hypoxia, each reflective of different elements of the hypoxic cellular response. By incorporating such methods alongside non-invasive tumour imaging, a comprehensive analysis of the effect of atovaquone on tumour hypoxia was endeavoured whilst simultaneously aiming to further validate such techniques.

The plasma markers investigated were VEGF, CAIX and OPN as measured by ELISA and miRNA miR210 as measured by PCR. VEGF, CAIX and OPN have been widely used as endogenous surrogate markers of tumour hypoxia. Fairly consistently, high levels have been shown to predict poor clinical outcomes, especially following radiotherapy in numerous tumour types including NSCLC [150,280]. These markers have previously been shown to correlate with one another in NSCLC [280] and to agree with polarographic electrode measurements of hypoxia [140,280], thus identifying them as attractive candidate hypoxia biomarkers for clinical studies.

In addition to these well-known markers, the effect of atovaquone on plasma levels of the miRNA miR-210 will be presented. miR-210 has recently emerged as the ‘master hypoxiaMIR’ responsible for fine-tuning the hypoxic cellular response [152,281]. Levels of miR-210 are detectable in a range of bodily fluids, including plasma, and have been shown to remarkably stable. Given its promise as a hypoxia biomarker, the effect of atovaquone on plasma levels of this marker was assessed and its correlation with other measures of hypoxia examined. Furthermore, as plasma miR-210 has been increasingly

recognised as a sensitive diagnostic biomarker for NSCLC [155,156], its association with clinicopathological features will also be explored. Important technical challenges of measuring plasma miR-210 will also be discussed, in particular with regards to sample haemolysis.

Hyp-PET has become the most widely used method to study hypoxia, however its use is highly restricted due to poor tracer availability and high cost. Therefore, the agreement of plasma markers with such imaging will be presented in order to investigate whether such markers may potentially replace hyp-PET in future studies.

In addition to circulating markers, resected tumour immunohistochemical analysis for the exogenous nitroimidazole-based hypoxia marker pimonidazole hydrochloride, as well as for the endogenous hypoxia marker CAIX, was also performed and such data from atovaquone treated and untreated patients will be compared. Furthermore, agreement of both IHC markers, as well as correlation with hyp-PET imaging will be explored in order to further validate these techniques as clinical measures of tumour hypoxia. To reduce the risk of sampling error, extensive IHC was performed on multiple whole tumour levels, which also provided the opportunity to assess heterogeneity of tumour hypoxia using IHC.

5.2 RESULTS

5.2.1 Atovaquone treatment does not alter plasma VEGF, CAIX and OPN

Six (26%) of 23 patients in Cohort 1 and eight (35%) of 23 patients in Cohort 2 had baseline VEGF levels below the lower level of quantification (LLQ), thus impacting on the number of patients in whom the baseline level and therefore change in level for this analyte could be determined. This was also the case for CAIX for one patient in Cohort 1.

As shown in Figure 5.1, depicting absolute change in level of each marker per individual patient, there was no significant change observed in levels of VEGF, CAIX and OPN between visits for both atovaquone treated and untreated patients (atovaquone treated VEGF p = 0.340, CAIX p = 0.900 and OPN p = 0.556; untreated VEGF p = 0.820, CAIX p = 0.121 and OPN p = 0.561). The percentage change from baseline for each plasma marker per patient is shown as waterfall plots in Figure 5.2. A full list of values for Cohort 1 and Cohort 2 patients and the median change per cohort is presented in Table 5.1 and Table 5.2, respectively.

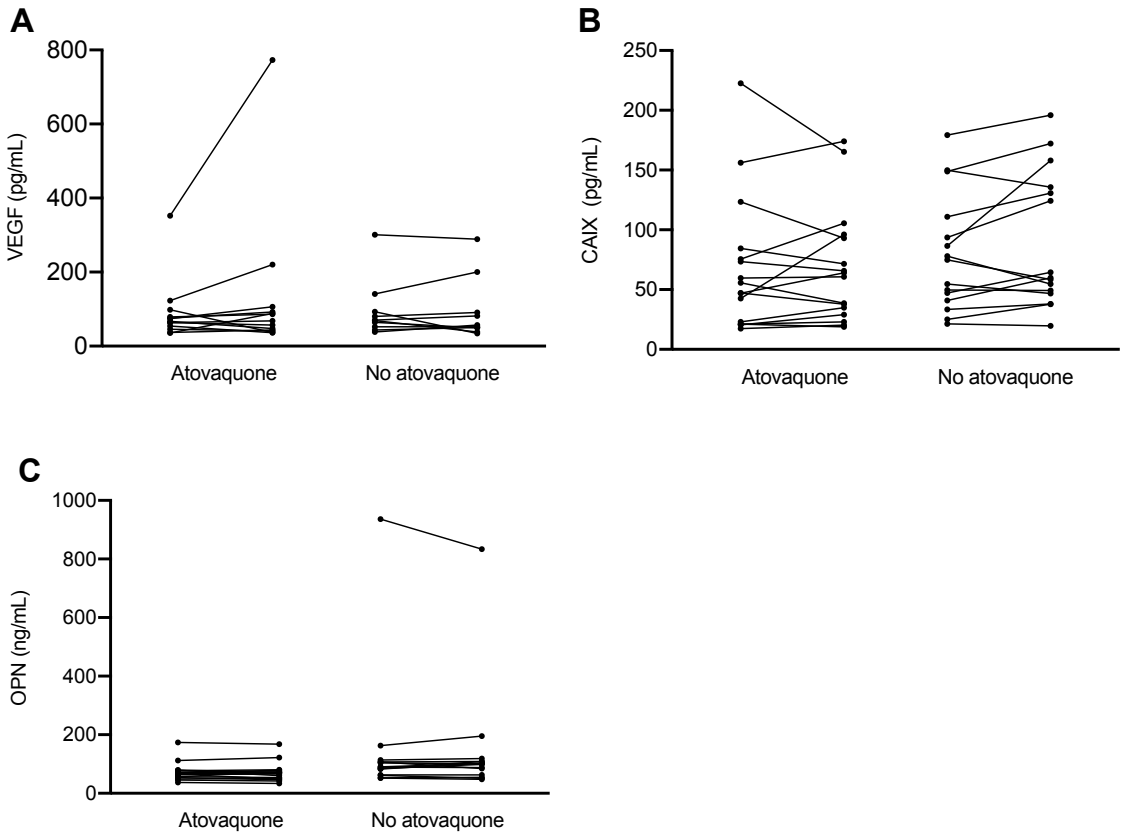


Figure 5.1: Effect of atovaquone on plasma levels of VEGF, CAIX and OPN
Absolute change in plasma levels of A) VEGF, B) CAIX and C) OPN between visits for atovaquone treated and untreated patients. Abbreviations: VEGF, vascular endothelial growth factor; CAIX, carbonic anhydrase IX; OPN, osteopontin. Changes in analyte per cohort were not significant (Wilcoxon signed-rank test).

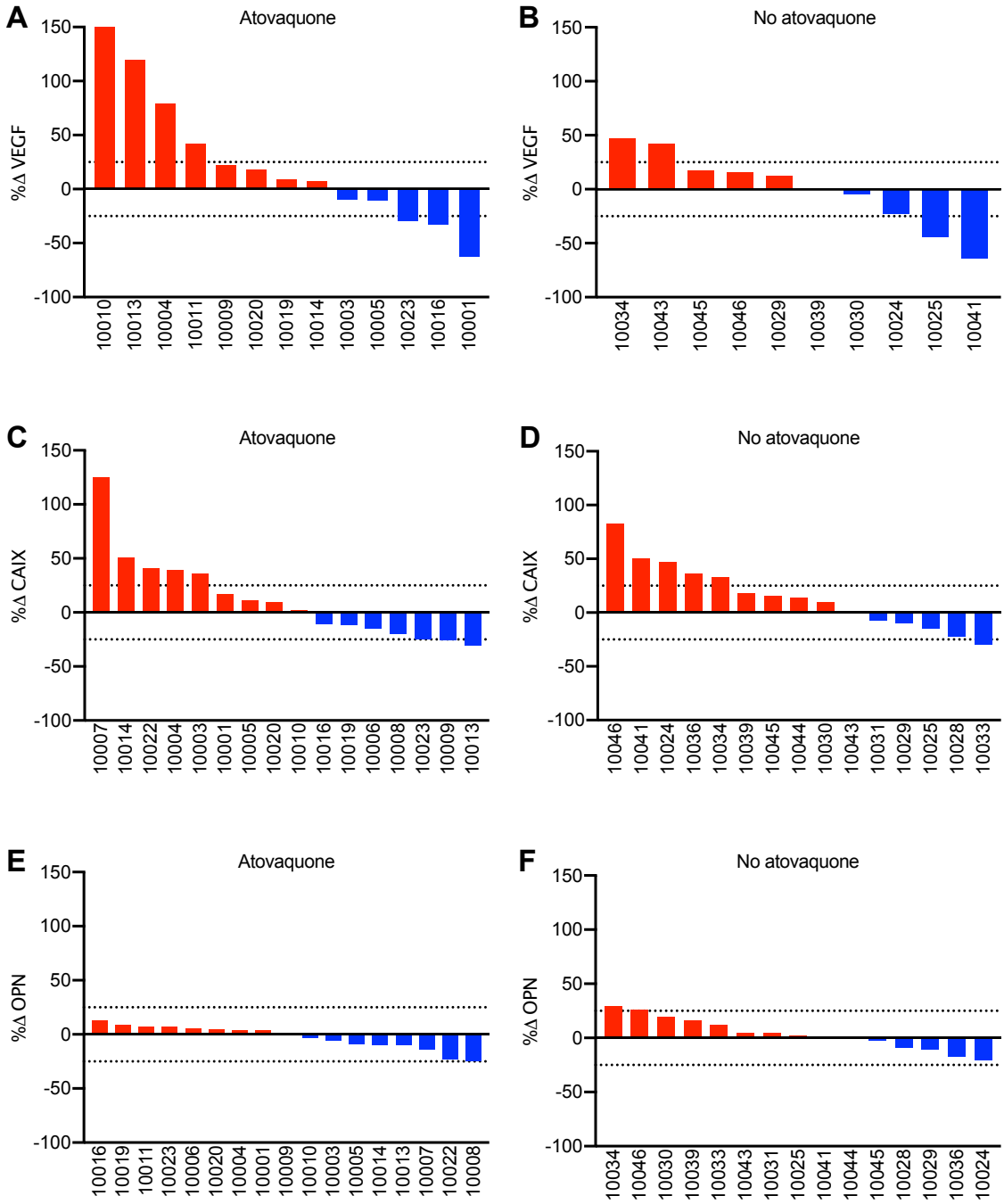


Figure 5.2: Waterfall plots of the effect of atovaquone on plasma VEGF, CAIX and OPN
Percentage change from baseline in plasma A) VEGF in Cohort 1, B) VEGF in Cohort 2, C) CAIX in Cohort 1, D) CAIX in Cohort 2, E) OPN in Cohort 1 and F) OPN in Cohort 2, per individual patient. Red bars represent patients with a rise in marker level and blue bars represent patients with a decrease in marker level. Dotted lines indicate the margin of error (25%) when measuring percentage change using ELISA. Abbreviations: VEGF, vascular endothelial growth factor; CAIX, carbonic anhydrase IX; OPN, osteopontin.

Table 5.1: Plasma levels of VEGF, CAIX and OPN for atovaquone treated patients

Patient	VEGF (pg/mL)			CAIX (pg/mL)			OPN (ng/mL)		
	Pre	**Post**	**%Δ**	**Pre**	**Post**	**%Δ**	**Pre**	**Post**	**%Δ**
10001	98.3	36.8	-62.6	17.4	20.4	17.3	64.0	66.2	3.4
10002	115.0			54.0			40.5		
10003	45.5	41.3	-9.2	47.0	64.0	36.2	57.2	54.1	-5.4
10004	123.0	220.0	78.9	75.6	105.5	39.6	77.4	80.1	3.5
10005	63.8	57.1	-10.5	156.1	174.0	11.5	45.6	41.7	-8.6
10006	<LLQ	45.5		84.5	71.6	-15.3	64.7	68.0	5.1
10007	<LLQ	37.8		42.7	96.1	125.2	53.5	45.9	-14.2
10008	<LLQ	<LLQ		47.3	37.8	-20.0	65.3	49.0	-25.0
10009	75.9	92.4	21.7	222.6	165.3	-25.7	72.1	72.9	1.1
10010	35.5	88.6	149.6	59.7	60.8	1.8	174.0	168.0	-3.4
10011	74.6	106.0	42.1	<LLQ	44.3		48.8	52.3	7.2
10012	<LLQ			137.1			74.1		
10013	352.0	773.0	119.6	55.6	38.6	-30.6	79.3	71.5	-9.8
10014	63.4	68.1	7.4	23.1	34.8	50.6	37.0	33.5	-9.5
10015	<LLQ			81.0			68.8		
10016	54.4	36.5	-32.9	73.5	65.6	-10.6	70.1	79.0	12.7
10017	43.3			273.1			62.9		
10018	67.1			104.2			51.5		
10019	79.3	86.2	8.7	21.2	18.8	-11.6	112.0	122.0	8.9
10020	36.9	43.5	17.9	21.1	23.1	9.8	69.8	73.1	4.7
10022	<LLQ	54.7		20.6	29.1	41.2	78.6	60.1	-23.5
10023	67.0	47.6	-29.0	123.5	93.0	-24.7	66.2	70.9	7.1
Median (IQR)	**67.1** (47.7–93.6)	**55.9** (41.9–91.5)		**59.7** (32.9–113.9)	**60.8** (32.0–94.5)		**65.8** (53.0–74.9)	**68.0** (50.7–76.1)	
Median paired (IQR)	**67.0** (50.0–88.8)	**68.1** (42.4–99.2)		**51.5** (21.7–82.3)	**62.4** (30.5–95.3)		**66.2** (55.4–78.0)	**68.0** (50.7–76.1)	
Median (95%CI)			**8.7** (-29.0–78.9)			**5.8** (-2.0–39.6)			**1.1** (-9.5–6.1)

Abbreviations: VEGF, vascular endothelial growth factor; CAIX, carbonic anhydrase IX; OPN, osteopontin; pre, pre-atovaquone treatment; post, post-atovaquone treatment; IQR, interquartile range; CI, confidence interval; LLQ, lower level of quantification.

Table 5.2: Plasma levels of VEGF, CAIX and OPN for untreated patients

Patient	VEGF (pg/mL)			CAIX (pg/mL)			OPN (ng/mL)		
	Visit 1	**Visit 2**	**%Δ**	**Visit 1**	**Visit 2**	**%Δ**	**Visit 1**	**Visit 2**	**%Δ**
10024	64.3	49.6	-22.9	40.9	60.0	46.7	107.0	84.5	-21.0
10025	68.8	38.6	-43.9	54.6	46.8	-14.4	107.0	109.0	1.9
10026	79.5			21.4			71.9		
10027	60.6			55.5			104.0		
10028	<LLQ	62.6		74.9	58.4	-22.0	52.2	47.5	-9.0
10029	80.6	90.8	12.7	149.8	135.7	-9.4	936.0	834.0	-10.9
10030	301.2	288.8	-4.1	179.2	195.9	9.3	163.0	195.0	19.6
10031	<LLQ	<LLQ		21.4	19.7	-7.7	52.5	54.8	4.4
10032	<LLQ			58.2			97.6		
10033	<LLQ	81.8		78.0	54.6	-29.9	90.4	101.0	11.7
10034	38.6	56.7	46.9	93.6	124.3	32.7	84.3	109.0	29.3
10035	<LLQ			68.0			83.4		
10036	<LLQ	36.1		47.2	64.4	36.5	61.4	50.9	-17.1
10037	98.3			46.5			87.7		
10038	<LLQ			49.7			81.9		
10039	52.3	52.3	0.0	111.0	130.6	17.6	84.6	98.4	16.3
10040	98.4			406.9			64.7		
10041	93.3	34.0	-63.6	25.1	37.7	50.4	63.2	63.0	-0.3
10042	33.4			69.8			110.0		
10043	140.9	200.0	41.9	49.7	49.2	-0.9	114.0	119.0	4.4
10044	<LLQ	<LLQ		33.4	37.9	13.7	89.3	88.3	-1.1
10045	70.1	81.9	16.8	148.8	172.2	15.8	104.0	101.0	-2.9
10046	43.5	50.3	15.6	86.5	158.0	82.6	82.5	104.0	26.1
Median (IQR)	**70.1** (52.3–98.3)	**56.7** (44.1–86.4)		**58.2** (46.5–93.6)	**60.0** (46.8–135.7)		**87.7** (71.9–107.0)	**101.0** (63.0–109.0)	
Median paired (IQR)	**69.5** (50.1–105.2)	**54.5** (46.9–118.1)		**74.9** (40.9–111.0)	**59.9** (46.8–135.7)		**89.3** (63.2–107.0)	**101.0** (63.0–109.0)	
Median (95% CI)			**6.3** (-28.1–23.1)			**13.7** (9.4–36.5)			**1.9** (-9.0–16.3)

Abbreviations: VEGF, vascular endothelial growth factor; CAIX, carbonic anhydrase IX; OPN, osteopontin; IQR, interquartile range; CI, confidence interval; LLQ, lower level of quantification.

This data demonstrates that generally there were few patients with a greater than 25% increase or decrease in plasma VEGF, CAIX or OPN which is the accepted margin for error when measuring changes in plasma protein levels using ELISA.

For VEGF, four (31%) of 13 patients had a significant rise in plasma levels following atovaquone treatment whereas three (23%) patients had a decrease. Due to fewer untreated patients having detectable and thus paired VEGF levels, comparison between atovaquone treated and untreated patients is difficult, however, no gross differences were observed.

Three patients in both cohorts who had undetectable baseline levels of VEGF had detectable levels at Visit 2, of whom two in both cohorts had levels greater than 25% of the lower level of quantification, therefore signifying a significant rise of unknown magnitude.

For CAIX, similar changes in plasma levels were observed in both cohorts. Five (31%) of 16 atovaquone treated patients and five (33%) of 15 untreated patients had a significant rise in levels. Two (13%) of 16 atovaquone treated patients in Cohort 1 and one (7%) of 15 untreated patients had a significant decrease in plasma CAIX.

For OPN, only one atovaquone treated patient had a significant rise in the plasma level of this marker, with non-significant changes in levels observed for all other patients.

5.2.2 Atovaquone treatment does not alter plasma miR-210

Plasma miR-210 levels for Cohort 1 and Cohort 2 patients were measured using qRT-PCR and reported as expression ratios relative to the internal control miR-16, as shown in Table 5.3 and Table 5.4, respectively, together with median levels and change per cohort.

Table 5.3: Relative expression of miR-210 for Cohort 1

Patient	Pre miR-210 ($x10^{-3}$)	Post miR-210 ($x10^{-3}$)	%Δ
10001	0.77	0.76	-2.1
10002	0.81 (H)		
10003	1.27	0.94	-26.3
10004	2.83	1.22	-56.9
10005	0.77 (H)	0.77 (H)	-0.1
10006	0.70	0.64	-8.2
10007	0.98	1.32	34.9
10008	1.21	2.09	72.5
10009	1.44	0.60 (H)	-58.7
10010	1.22	0.83 (H)	-31.7
10011	1.40	1.10	-21.6
10012	0.52		
10013	0.67	0.66	-0.8
10014	2.10	1.14	-45.7
10015	0.74		
10016	1.55	2.51	62.1
10017	1.17		
10018	1.34		
10019	2.88	0.95 (H)	-66.9
10020	0.74	0.92 (H)	24.5
10022	1.67	2.42 (H)	45.2
10023	1.22	0.85 (H)	-30.4
Median all (IQR)	**1.22** (0.76 – 1.47)	**0.94** (0.77 – 1.27)	
Median paired (IQR)	1.**22** (0.77 – 1.61)	**0.94** (0.77 – 1.27)	
Median (95% CI)			**-8.3** (-31.7 – 24.5)

Abbreviations: pre, pre-atovaquone treatment; post, post-atovaquone treatment; IQR, interquartile range; CI, confidence interval; H, haemolysis.

Table 5.4: Relative expression of miR-210 for Cohort 2

Patient	Visit 1 miR-210 ($x10^{-3}$)	Visit 2 miR-210 ($x10^{-3}$)	%Δ
10024	0.93	0.87	-5.8
10025	1.71	1.00	-41.4
10026	1.16		
10027	0.83 (H)		
10028	0.71	0.66 (H)	-7.8
10029	0.58 (H)	0.58 (H)	-0.6
10030	1.09	1.26	16.0
10031	1.12	0.66	-41.2
10032	0.83		
10033	0.53 (H)	0.54 (H)	0.7
10034	1.35	0.86 (H)	-36.5
10035	0.55		
10036	1.44 (H)	1.18 (H)	-18.0
10037	0.69		
10038	0.87		
10039	1.77	1.41	-20.2
10040	0.56		
10041	0.77 (H)	1.12	46.0
10042	0.60 (H)		
10043	2.83	1.10 (H)	-61.3
10044	1.18	1.04	-11.6
10045	2.46	1.64 (H)	-33.3
10046	1.00	0.91	-9.1
Median all (IQR)	**0.93** (0.69 – 1.35)	**1.00** (0.66 – 1.18)	
Median paired (IQR)	**1.12** (0.77 – 1.71)	**1.00** (0.66 – 1.18)	
Median (95% CI)			**-11.6** (-36.5 – -0.65)

Abbreviations: IQR, interquartile range; CI, confidence interval; H, haemolysis.

The change in plasma relative expression of miR-210 for each patient between visits is shown in Figure 5.3. There was no significant change in miR-210 expression observed in patients receiving atovaquone ($p = 0.244$), however, rather surprisingly there was a reduction of statistical significance in patients who did not receive treatment ($p = 0.012$). The percentage change form baseline miR-210 expression per individual patient is shown as waterfall plots in Figure 5.4. There was a reduction in miR-210 expression in 11 (65%) of 17 patients who received atovaquone and in 12 (80%) of 15 patients who did not receive treatment.

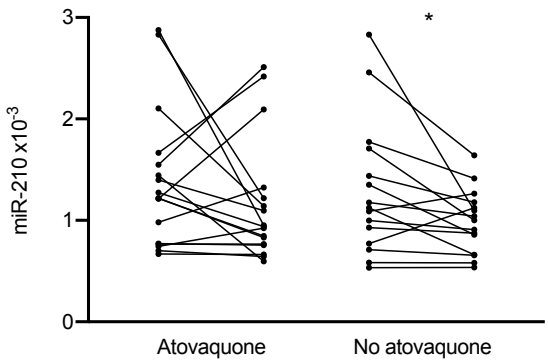


Figure 5.3: Effect of atovaquone on miR-210 expression
Changes in plasma miR-210 expression between trial visits for atovaquone treated and untreated patients. miR-210 is reported as an expression ratio relative to the internal control miR-16. *p < 0.05 (Wilcoxon signed-rank test).

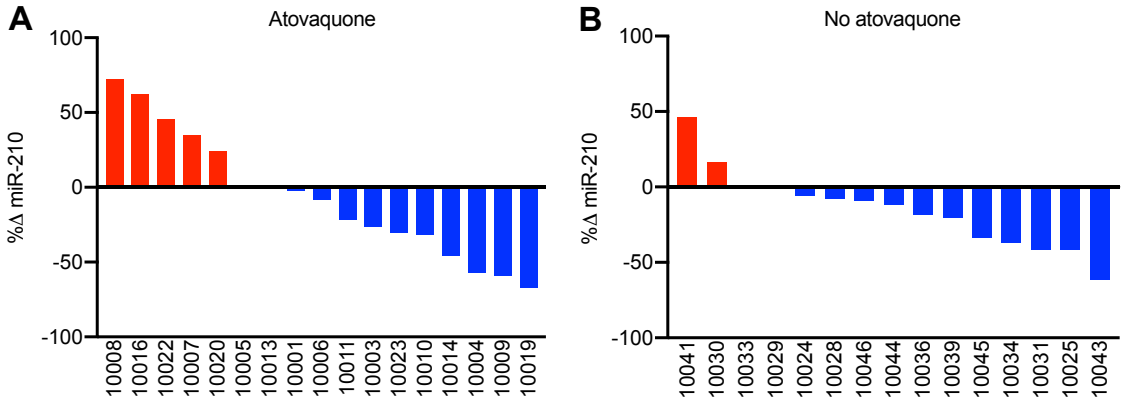


Figure 5.4: Waterfall plots of the effect of atovaquone on miR-210 expression
Percentage change from baseline in plasma miR-210 expression relative to the internal control miR-16 for A) atovaquone treated and B) untreated individual patients. Red bars represent patients with a rise in expression whilst blue bars represent patients with a decrease in expression.

5.2.2.1 Impact of plasma sample haemolysis on miR-210 expression

As recent reports have demonstrated that sample haemolysis may impact on the accuracy of measurement of expression of numerous plasma miRNAs, including miR-16 and miR-210 [282], this was also assessed in this study. As shown in Table 5.3 and Table 5.4, the baseline plasma collected from two patients in Cohort 1 and six patients in Cohort 2 had

evidence of haemolysis on visual inspection of the samples. As shown in Figure 5.5, the haemolysed baseline samples (n=8) had significantly higher miR-16 expression than compared with non-haemolysed samples (n=37) ($p < 0.0001$) and significantly lower miR-210 expression relative to miR-16 ($p = 0.023$).

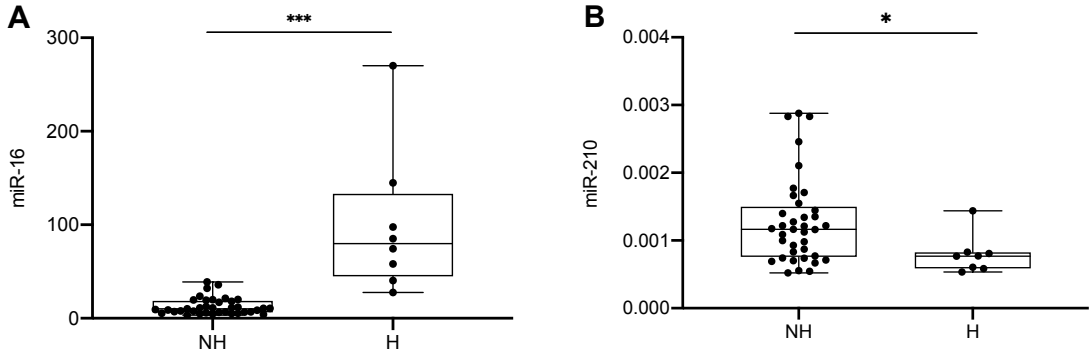


Figure 5.5: Effect of sample haemolysis on plasma miR-16 and miR-210
Box and whisker plots showing the difference between haemolysed and non-haemolysed baseline plasma samples for A) miR-16 and B) miR-210 expression. miR-16 expression is reported as an expression ratio relative to exogenous miR-Cel-39 spike-in and miR-210 is reported as an expression ratio relative to miR-16. Medians with interquartile and absolute ranges are shown. Abbreviations: NH, non-haemolysed; H, haemolysed. *$p < 0.05$, ***$p < 0.0001$ (Mann-Whitney U test).

As this data indicates that plasma sample haemolysis may affect the accuracy of measurement of miR-16, and consequently relative miR-210 expression, the data were reanalysed excluding all patients with haemolysis in either or both Visit 1 and Visit 2 samples. In addition, the decision was made that for upcoming correlative analysis of miR-210 expression with other hypoxia measures, only data from non-haemolysed samples would be used.

5.2.2.2 Effect of atovaquone on plasma miR-210 excluding haemolysed samples

The change in relative miR-210 expression for each patient is shown in Figure 5.6 and the percentage change from baseline is shown as waterfall plots in Figure 5.7. Interpretation

of these results should be performed with some caution given the small patient numbers, however, as before this data demonstrates that atovaquone does not appear to reduce plasma miR-210 (p = 0.56), with on this occasion no significant change observed in untreated patients (p = 0.11).

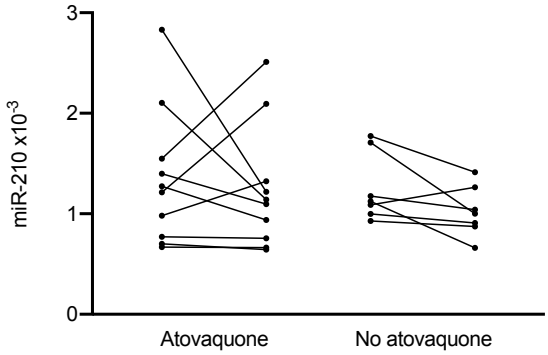


Figure 5.6: Effect of atovaquone on miR-210 expression in non-haemolysed plasma samples
Data shown are changes in plasma miR-210 expression between trial visits for atovaquone treated and untreated patients. miR-210 data is reported as an expression ratio relative to the internal control miR-16. Changes in analyte per cohort were not significant (Wilcoxon signed-rank test).

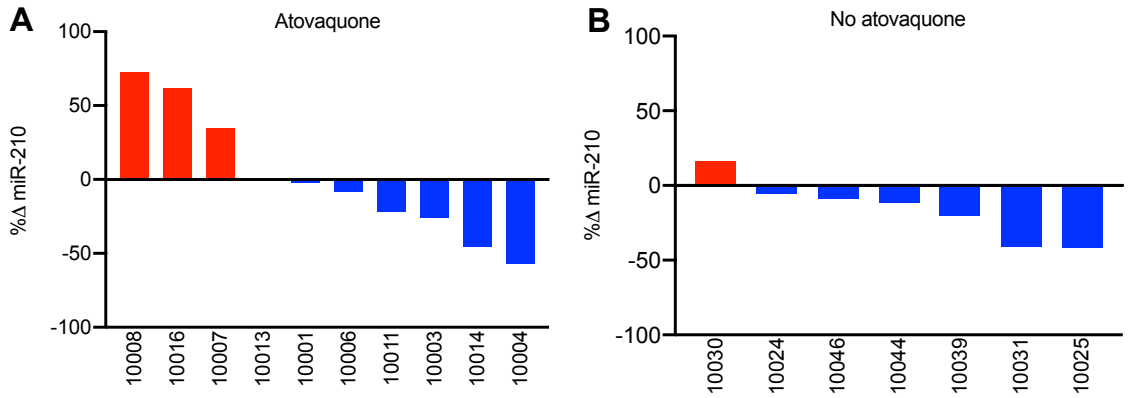


Figure 5.7: Waterfall plots of the effect of atovaquone on miR-210 expression in non-haemolysed plasma samples
Data shown are percentage change from baseline in plasma miR-210 expression relative to miR-16 for A) atovaquone treated and B) untreated individual patients. Red bars represent patients with a rise in expression whilst blue bars represent patients with a decrease in expression.

5.2.3 Agreement of plasma hypoxia markers

Next, to investigate whether there was agreement between plasma VEGF, CAIX, OPN and miR-210, correlation analysis between the levels of each marker at baseline was conducted. This data is shown in Figure 5.8 and demonstrates lack of correlation between any markers: VEGF vs CAIX, r_s = -0.04, p = 0.84; VEGF vs OPN, r_s = 0.03, p = 0.86; VEGF vs miR-210, r_s = -0.04, p = 0.84; CAIX vs OPN, r_s = 0.09, p = 0.56; CAIX vs miR-210, r_s = -0.05, p = 0.76; OPN vs miR-210, r_s = 0.17, p = 0.32.

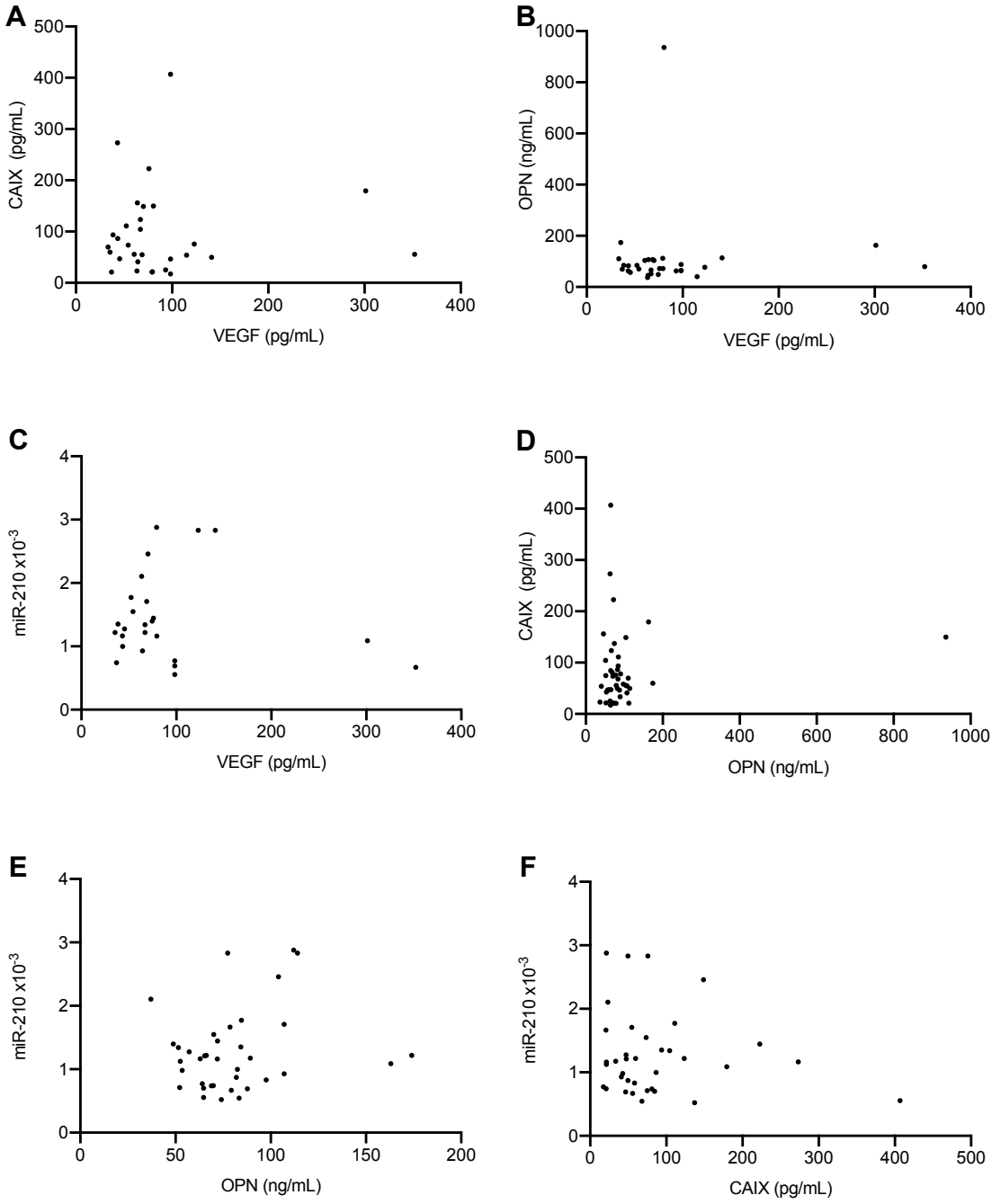


Figure 5.8: Correlation of plasma hypoxia markers
Scatter plots showing lack of correlation between plasma levels of VEGF, CAIX, OPN and miR-210 taken at baseline for all trial patients. Plasma miR-210 data is reported as an expression ratio relative to internal control miR-16. Abbreviations: VEGF, vascular endothelial growth factor; CAIX, carbonic anhydrase IX; OPN, osteopontin.

In addition, in the majority of cases there was no agreement in the direction of change in marker level per individual patient for both atovaquone treated and untreated patients, as shown in Figure 5.9 and Figure 5.10, respectively.

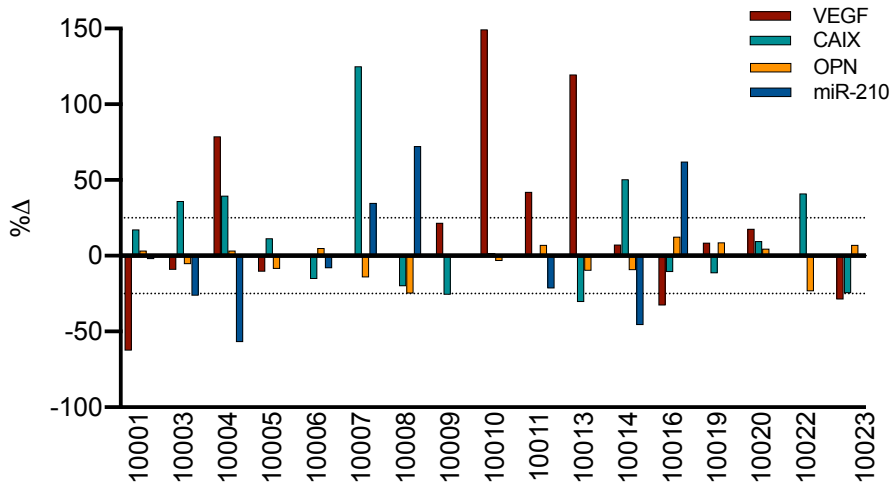


Figure 5.9: Agreement in change in plasma hypoxia markers per individual atovaquone treated patient
Percentage change from baseline in plasma VEGF, CAIX, OPN and miR-210 per individual patients receiving atovaquone treatment. Dotted line indicates the margin of error when measuring percentage change in VEGF, CAIX and OPN using ELISA. Abbreviations: VEGF, vascular endothelial growth factor; CAIX, carbonic anhydrase IX; OPN, osteopontin.

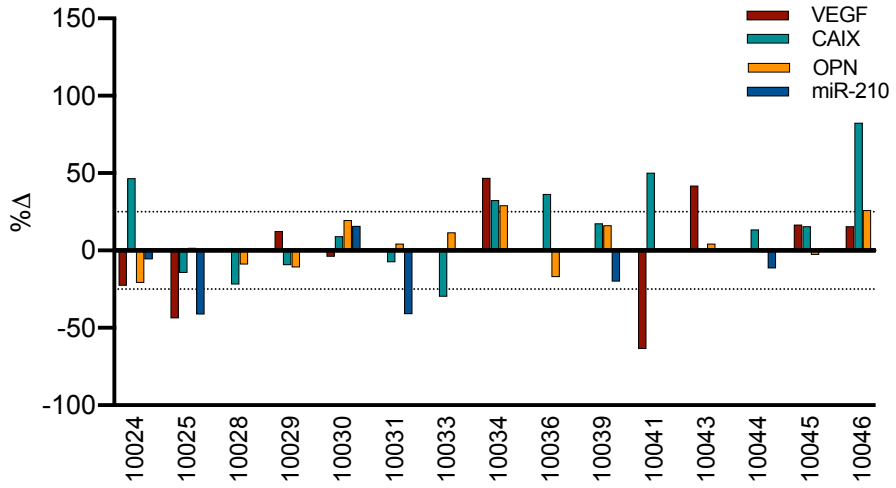


Figure 5.10: Agreement in change in plasma hypoxia markers per individual untreated patient
Percentage change from baseline in plasma VEGF, CAIX, OPN and miR-210 per individual patients not receiving atovaquone treatment. Dotted line indicates the margin of error when measuring percentage change in VEGF, CAIX and OPN using ELISA. Abbreviations: VEGF, vascular endothelial growth factor; CAIX, carbonic anhydrase IX; OPN, osteopontin.

5.2.4 Correlation of plasma hypoxia markers with clinicopathological features

5.2.4.1 Tumour volume

Correlation between tumour volume and baseline plasma VEGF, CAIX, OPN and miR-210 is shown in Figure 5.11. There was a moderate positive correlation between tumour volume and miR-210 ($r_s = 0.49$, $p = 0.003$) but no correlation between tumour volume and VEGF ($r_s = -0.05$, $p = 0.82$), CAIX ($r_s = -0.05$, $p = 0.75$) and OPN ($r_s = 0.30$, $p = 0.05$).

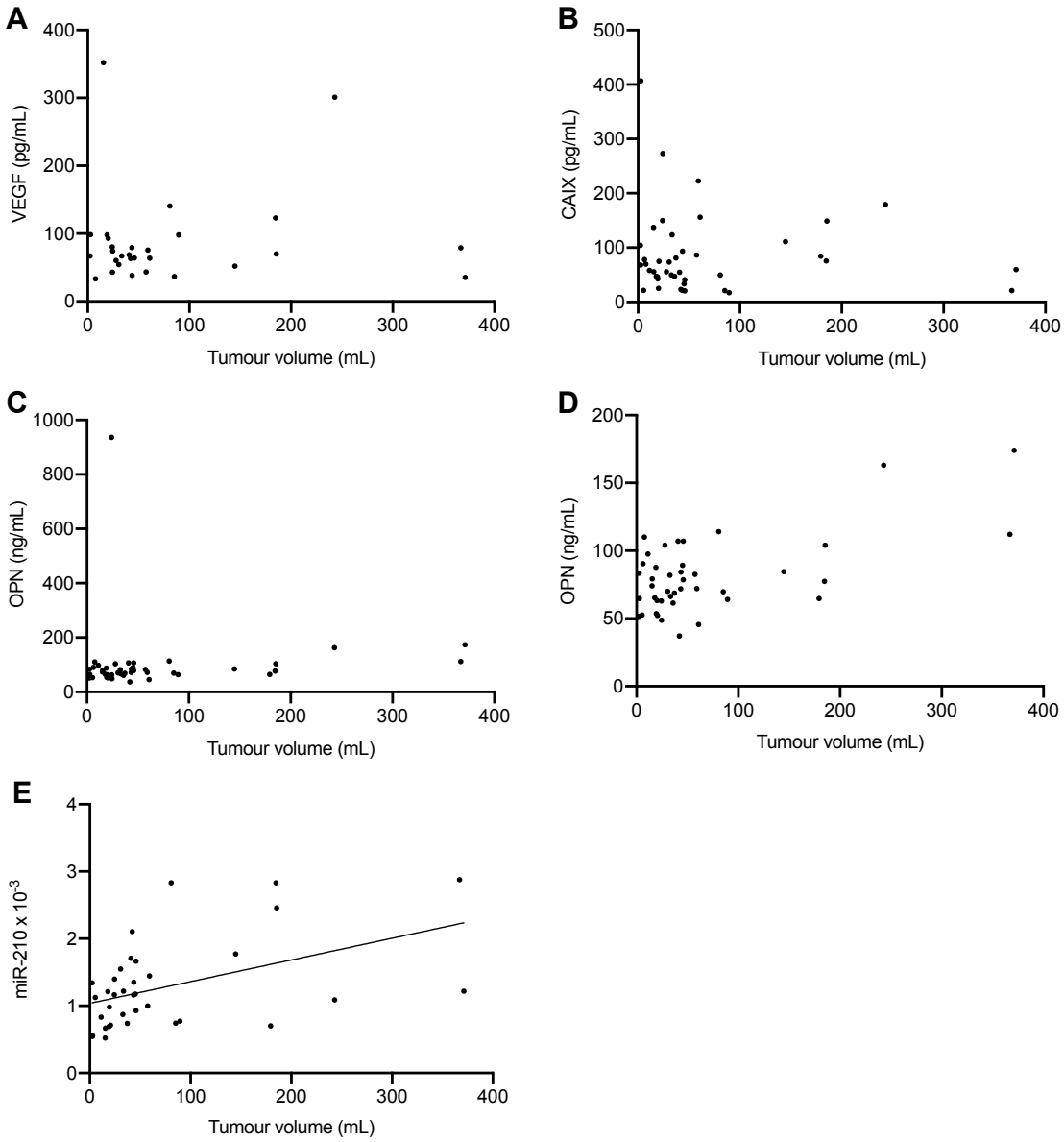


Figure 5.11: Correlation of tumour volume with plasma hypoxia markers
Scatter plots showing the correlation between tumour volume and baseline plasma levels of A) VEGF, B) CAIX, C) OPN, D) OPN with one outlier (patient 10029) removed to aid visualisation and E) miR-210. Plasma miR-210 data is reported as an expression ratio relative to internal control miR-16 and only shows patients with non-haemolysed samples. Abbreviations: VEGF, vascular endothelial growth factor; CAIX, carbonic anhydrase IX; OPN, osteopontin. Line of best fit is shown for correlated data (Spearman's rho correlation coefficient with $p < 0.05$).

5.2.4.2 Tumour histology

The differences in baseline plasma VEGF, CAIX, OPN and miR-210 between adenocarcinoma and squamous histology are shown in Figure 5.12. There was no

significant difference in plasma levels between the two types of histology for VEGF (p = 0.99), CAIX (p = 0.97), OPN (p = 0.68) and miR-210 (p = 0.50).

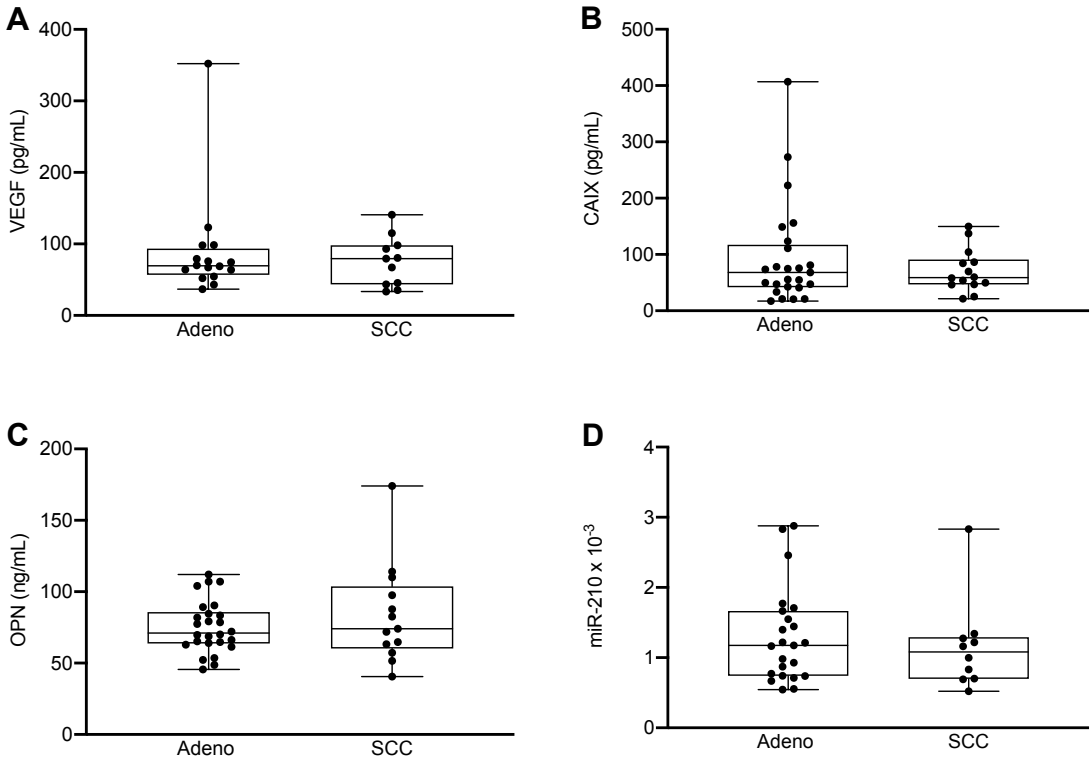


Figure 5.12: Plasma hypoxia markers and tumour histological subtype
Box and whisker plots comparing baseline plasma A) VEGF, B) CAIX, C) OPN and D) miR-210 between adenocarcinoma and squamous tumour histology. For OPN one outlier (patient 10029) is excluded to aid visualisation. Median levels with interquartile and absolute ranges are shown. Plasma miR-210 data is reported as an expression ratio relative to internal control miR-16 and only shows patients with non-haemolysed samples. Abbreviations: adeno, adenocarcinoma; CAIX, carbonic anhydrase IX; OPN, osteopontin; SCC, squamous cell carcinoma; VEGF, vascular endothelial growth factor. Differences between groups were not significant (Mann-Whitney U test).

5.2.4.3 Stage of disease

The difference in baseline plasma levels of VEGF, CAIX, OPN and miR-210 between patients with different stages of disease is shown in Figure 5.13. Due to small patient numbers in certain stage groups, statistical analysis was not performed. On inspection of the data, no clear differences in plasma VEGF, CAIX and OPN levels were observed between different stages of disease. However, for miR-210, the data suggests that plasma

levels may increase with increasing stage of disease, a finding which is consistent with the positive correlation between plasma miR-210 and tumour volume presented in 5.2.4.1.

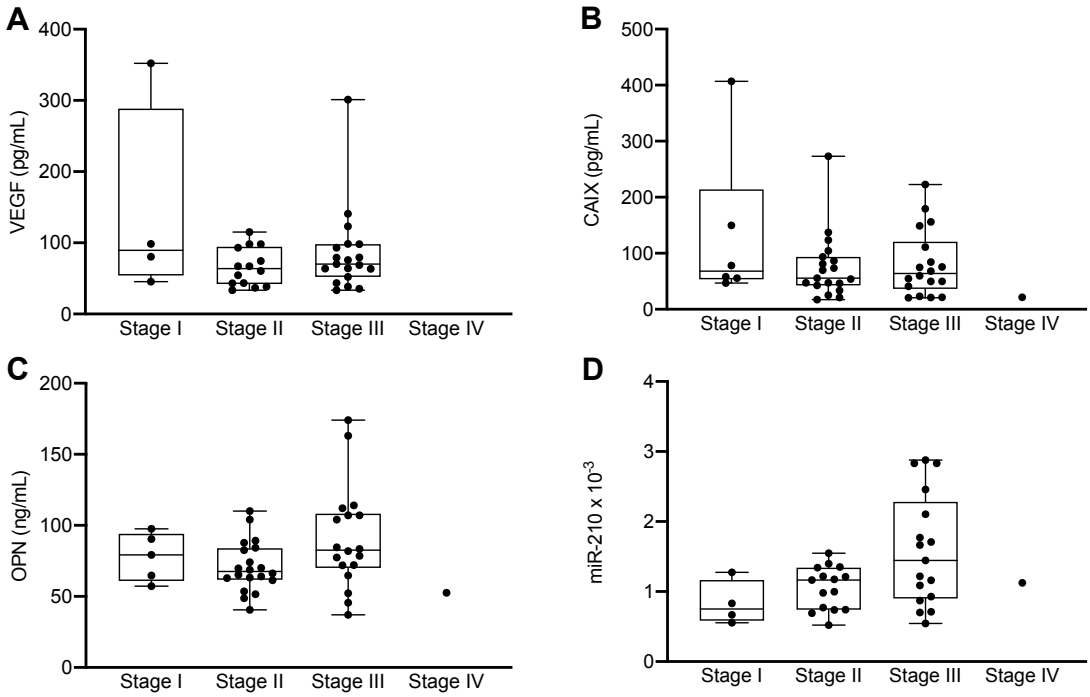


Figure 5.13: Plasma hypoxia markers and stage of disease
Box and whisker plots demonstrating the difference in baseline plasma levels of A) VEGF, B) CAIX, C) OPN and D) miR-210 between different stages of disease. For OPN one outlier (patient 10029) is excluded to aid visualisation. Plasma miR-210 data is reported as an expression ratio relative to internal control miR-16 and only shows patients with non-haemolysed samples. Median levels with interquartile and absolute ranges are shown. Abbreviations: CAIX, carbonic anhydrase IX; OPN, osteopontin; VEGF, vascular endothelial growth factor. No statistical testing performed.

5.2.5 Can plasma markers replace hyp-PET in future studies?

Next, to investigate whether plasma hypoxia markers could potentially replace hyp-PET in future hypoxia studies, correlation analysis between baseline plasma markers and baseline FMISO and FAZA PET-derived hypoxia parameters was conducted.

5.2.5.1 Lack of correlation between plasma VEGF, CAIX and OPN and hyp-PET

As shown in Figure 5.14, no correlation was observed between plasma VEGF levels and hyp-PET derived HV ($r_s = 0.09$, $p = 0.635$), HV% ($r_s = 0.10$, $p = 0.600$), TBR_{mean} ($r_s = 0.08$, $p = 0.685$) and TBR_{peak} ($r_s = 0.10$, $p = 0.623$).

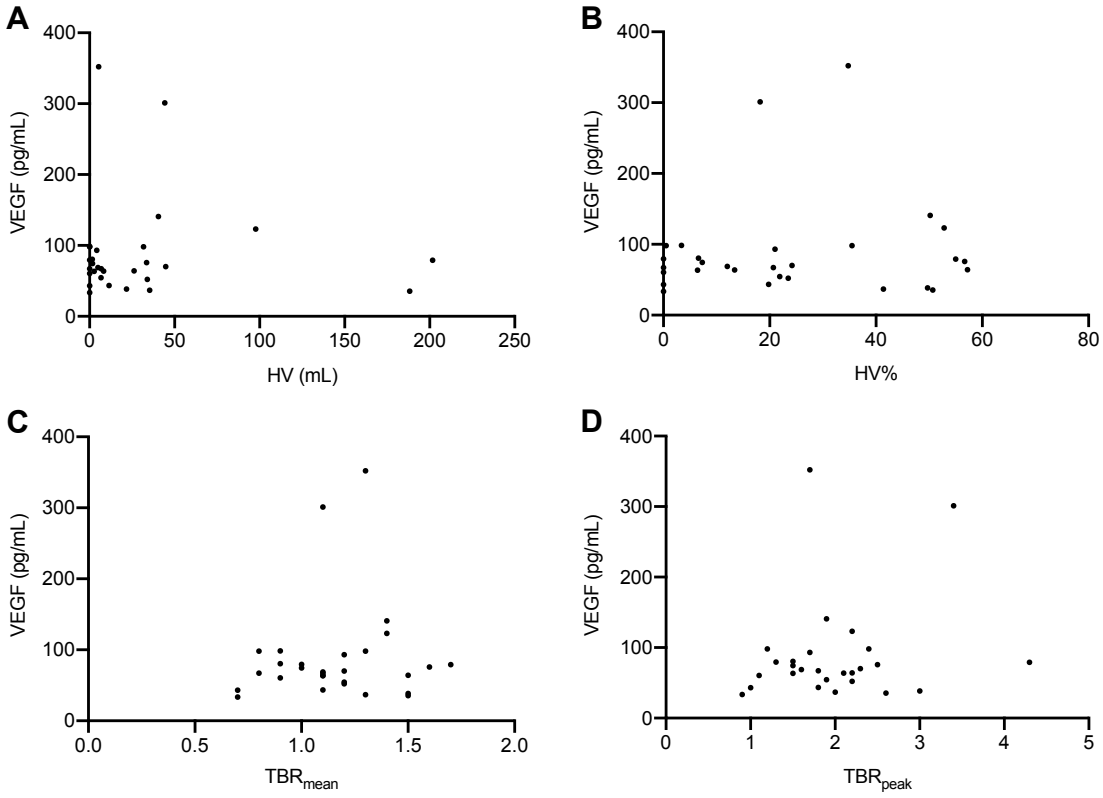


Figure 5.14: Correlation of plasma VEGF levels with hyp-PET parameters
Scatter plots showing a lack of correlation between baseline VEGF levels and baseline hyp-PET derived A) HV, B) HV%, C) TBR_{mean} and D) TBR_{peak} for all trial patients. Abbreviations: VEGF, vascular endothelial growth factor; HV, hypoxic volume; HV%, hypoxic volume percentage; TBR, tumour-to-blood ratio.

Similarly for CAIX, no correlation between plasma levels and HV ($r_s = -0.04$, $p = 0.798$), HV% ($r_s = -0.16$, $p = 0.310$), TBR_{mean} ($r_s = -0.22$, $p = 0.168$) and TBR_{peak} ($r_s = 0.03$, $p = 0.853$) was observed (Figure 5.15).

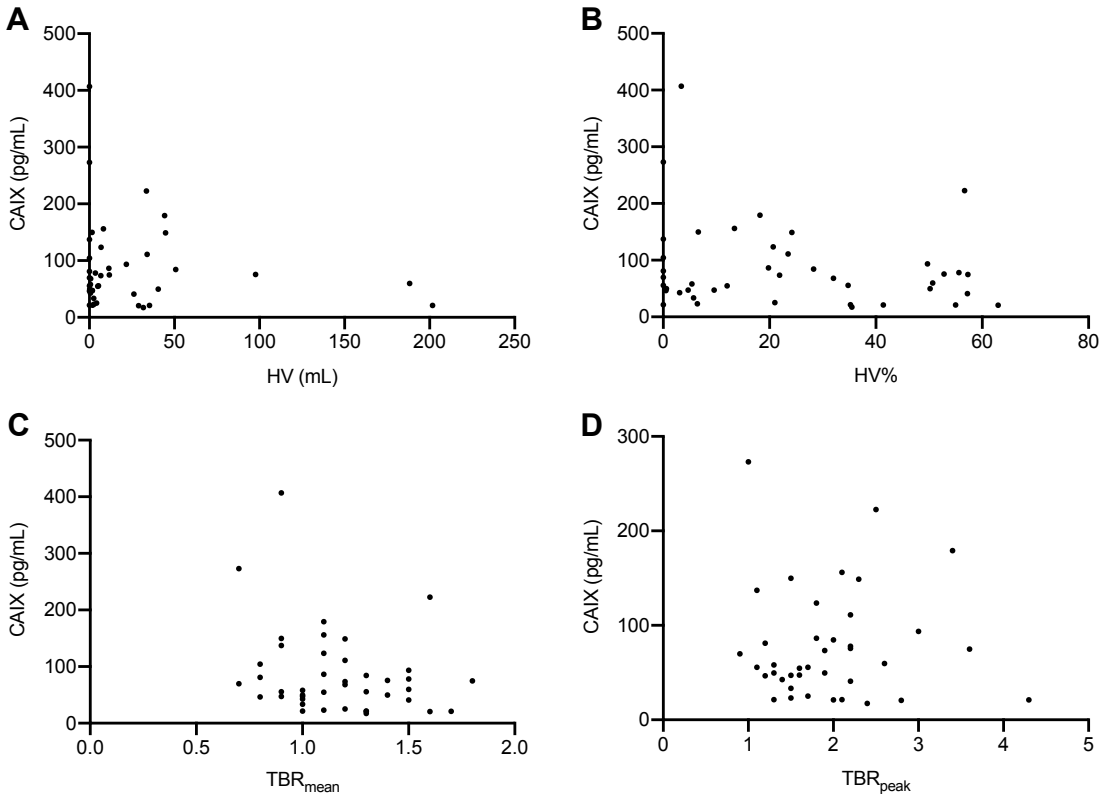


Figure 5.15: Correlation of plasma CAIX levels with hyp-PET parameters
Scatter plots showing a lack of correlation between baseline CAIX levels and baseline hyp-PET derived A) HV, B) HV%, C) TBR_{mean} and D) TBR_{peak} for all trial patients. Abbreviations: CAIX, carbonic anhydrase IX; HV, hypoxic volume; HV%, hypoxic volume percentage; TBR, tumour-to-blood ratio.

For OPN, once again no correlation was observed between plasma levels and HV (r_s = 0.28, p = 0.071), HV% (r_s = 0.20, p = 0.205), TBR_{mean} (r_s = 0.20, p = 0.203) and TBR_{peak} (r_s = 0.16, p = 0.346), as shown in Figure 5.16.

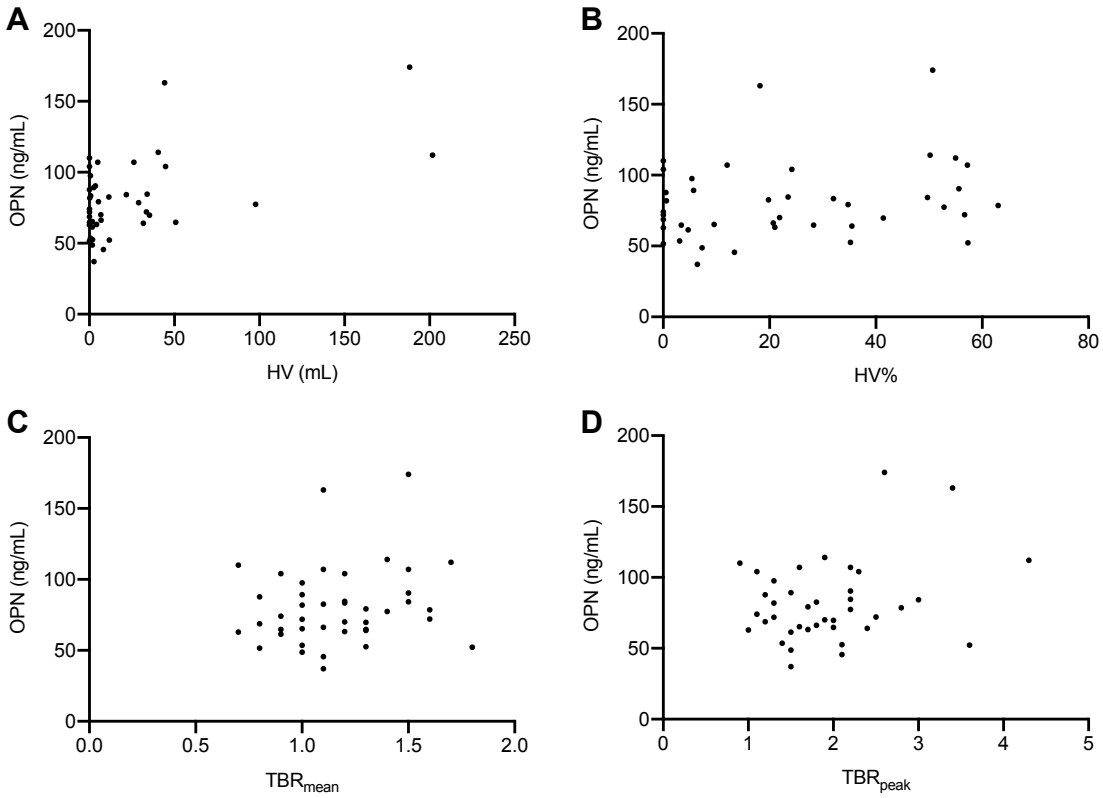


Figure 5.16: Correlation of plasma OPN levels with hyp-PET parameters
Scatter plots showing a lack of correlation between baseline OPN levels and baseline hyp-PET-derived A) HV, B) HV%, C) TBR_{mean} and D) TBR_{peak} for all trial patients. One outlier (patient 10029) is excluded to aid visualisation Abbreviations: OPN, osteopontin; HV, hypoxic volume; HV%, hypoxic volume percentage; TBR, tumour-to-blood ratio.

5.2.5.2 Correlation between plasma miR-210 expression and hyp-PET

In contrast, for miR-210 there was some evidence that baseline plasma levels correlated with some baseline hyp-PET-derived parameters (Figure 5.17). A positive moderate strength correlation was observed between plasma miR-210 and HV ($r_s = 0.45$, $p = 0.006$) and a positive weak correlation with TBR_{peak} ($r_s = 0.36$, $p = 0.042$). Positive weak although not significant correlations were observed between plasma miR-210 expression and HV% ($r_s = 0.29$, $p = 0.086$) and TBR_{mean} ($r_s = 0.31$, $p = 0.062$).

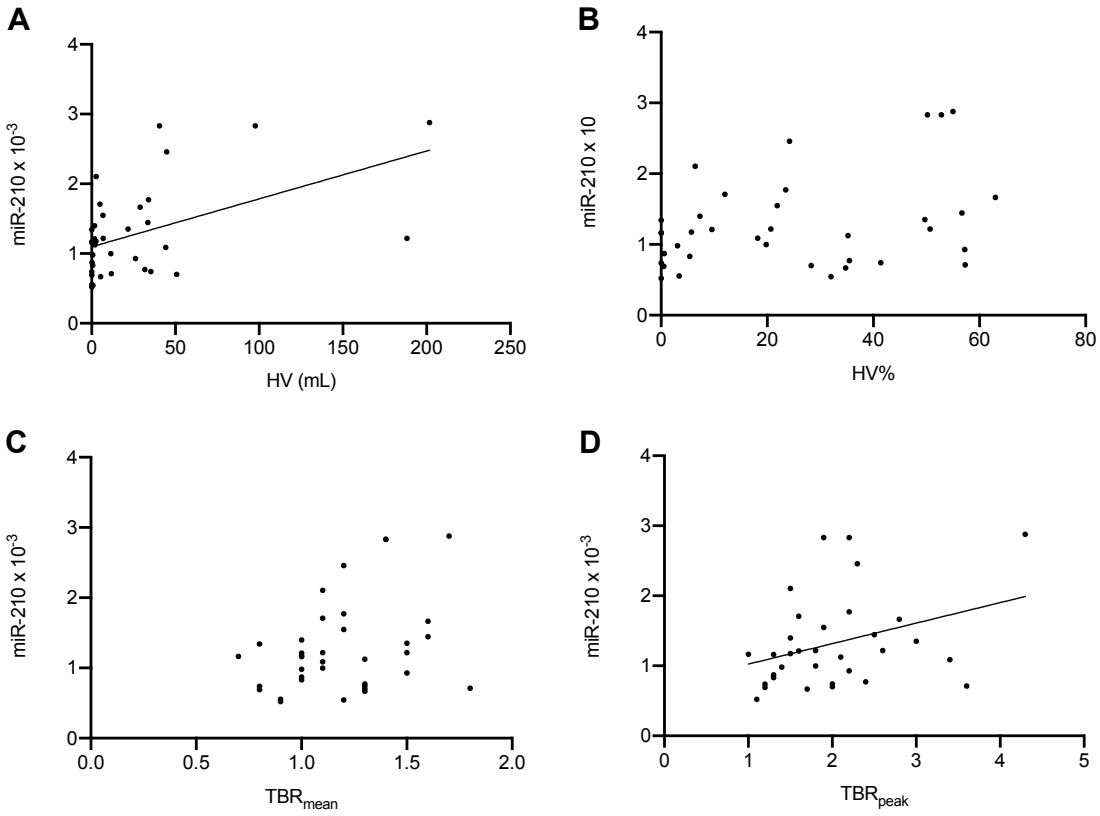


Figure 5.17: Correlation of miR-210 expression with hyp-PET
Scatter plots showing the correlation of baseline plasma miR-210 expression with baseline hyp-PET derived A) HV, B) HV%, C) TBR_{mean} and D) TBR_{peak} for all trial patients. Plasma miR-210 data is reported as an expression ratio relative to internal control miR-16 and only shows patients with non-haemolysed samples. Abbreviations: HV, hypoxic volume; HV%, hypoxic volume percentage; TBR, tumour-to-blood ratio. Line of best fit is shown for correlated data (Spearman's rho correlation coefficient with $p < 0.05$).

As the data provides some evidence that circulating miR-210 correlates with hyp-PET, it was next assessed whether plasma levels could predict whether patients had sufficient baseline hypoxia to reliably measure change in HV, as per the pre-determined minimum 1.5 mL threshold. This data is presented in Figure 5.18 and demonstrates that plasma miR-210 expression was significantly higher in patients with sufficient baseline hypoxia than patients with insufficient hypoxia, median relative expression ratio 1.22 $x10^{-3}$ and 0.83 x 10^{-3}, respectively ($p = 0.002$). Overall, this data suggests that plasma miR-210 may be potentially useful in identifying patients with sufficient hypoxia to reliably measure change using hyp-PET in future studies.

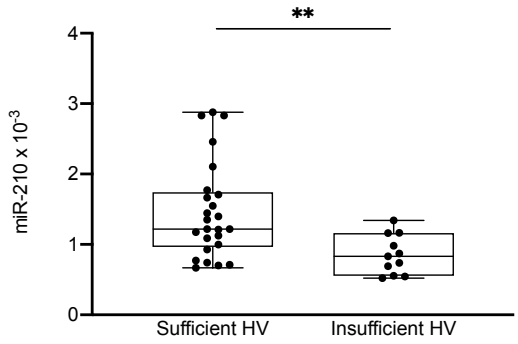


Figure 5.18: Plasma miR-210 expression and the presence of sufficient baseline hypoxia
Box and whisker plots demonstrating the difference in baseline plasma miR-210 expression between patients with sufficient (≥1.5mL) and insufficient (<1.5mL) hypoxia on corresponding hyp-PET. Plasma miR-210 data is reported as an expression ratio relative to internal control miR-16 and only shows patients with non-haemolysed samples. Median levels with interquartile and absolute ranges are shown Abbreviations: HV, hypoxic volume. **p < 0.01 (Mann-Whitney U test).

5.2.6 Tumour pimonidazole and CAIX IHC

As tumours in this study were often very large, immunohistochemical analysis was performed not from a single piece of resected tumour, but rather from whole and also multiple tumour levels. This approach aimed to reduce the risk of sampling error and provide results which were more representative of the whole tumour. Tumour levels were selected from macroscopically viable regions from the top, middle and bottom of tumours in sufficiently large cases. For patients with insufficient baseline hypoxia on hyp-PET who did not continue on the study and have post tumour resection trial-specific specimen processing, IHC was performed from one diagnostic block. As performing IHC on whole and multiple tumour levels generated a very large number of IHC sections (approximately 1250 in total), automated scoring methodology was developed to ensure accurate and consistent scoring throughout, as described in section 2.4.2.2.

Figure 5.19 and Figure 5.20 show representative examples of IHC staining with corresponding automated scoring for pimonidazole and CAIX, respectively. Impressive spatial agreement was observed between IHC staining and the regions identified as

positively stained by the automated classifier. Negative and positive IHC controls are shown in Figure 5.21.

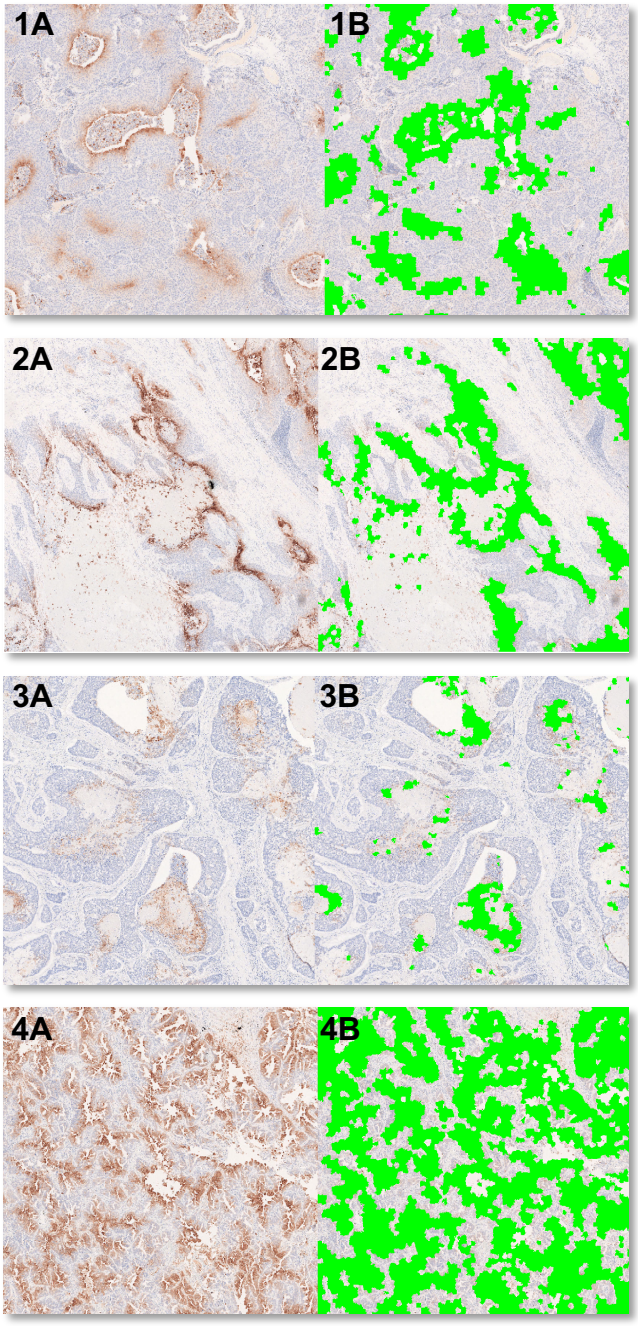


Figure 5.19: Examples of pimonidazole IHC staining and automated scoring
Representative examples of pimonidazole A) IHC staining and B) corresponding scoring by the automated classifier for 1) patient 10043, 2) patient 10041, 3) patient 10010 and 4) patient 10009. Brown regions represent pimonidazole staining and green regions represent regions identified as positively stained by the classifier. Classifier generated tumour percentage scores were: 1) 22.7%, 2) 19.9%, 3) 5.5% and 4) 57.6%. Digital photographs were taken at x 10 magnification.

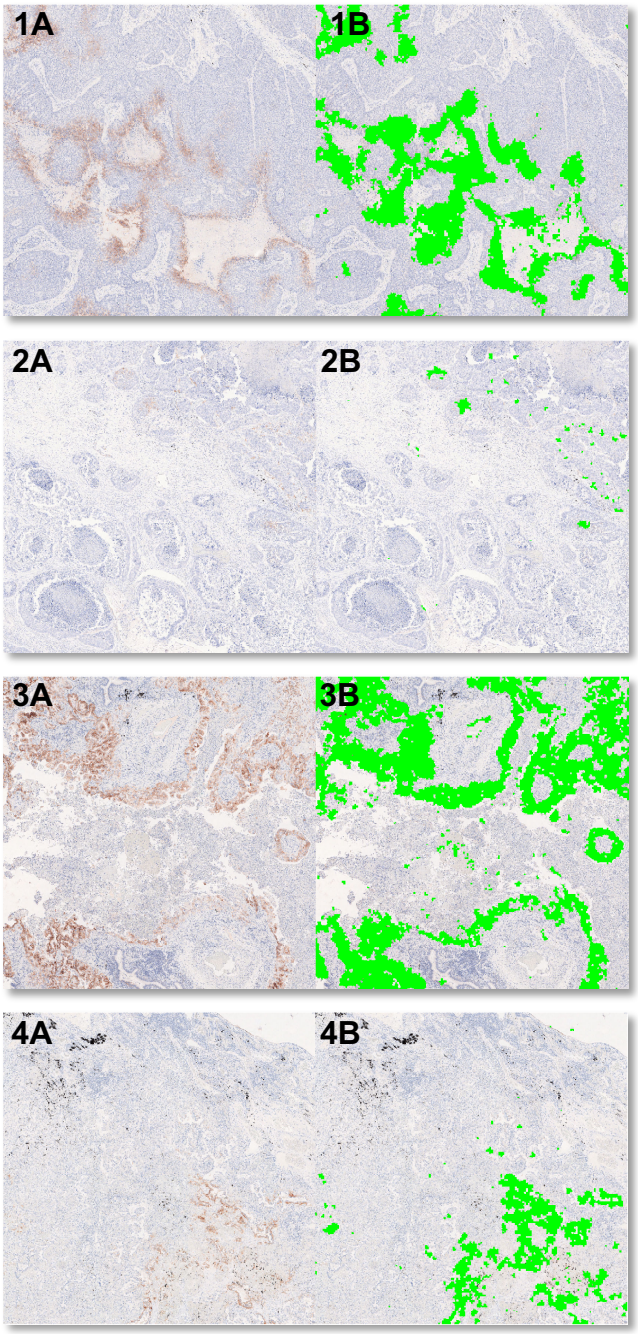


Figure 5.20: Examples of CAIX IHC staining and automated scoring
Representative examples of CAIX A) IHC staining and B) corresponding scoring by the automated classifier for 1) patient 10010, 2) patient 10037, 3) patient 10039 and 4) patient 10022. Brown regions represent CAIX staining and green regions represent regions identified as positively stained by the classifier. Classifier generated tumour staining percentages were: 1) 19.9%, 2) 0.7%, 3) 27.7% and 4) 7.2%. Digital photographs were taken at x 10 magnification.

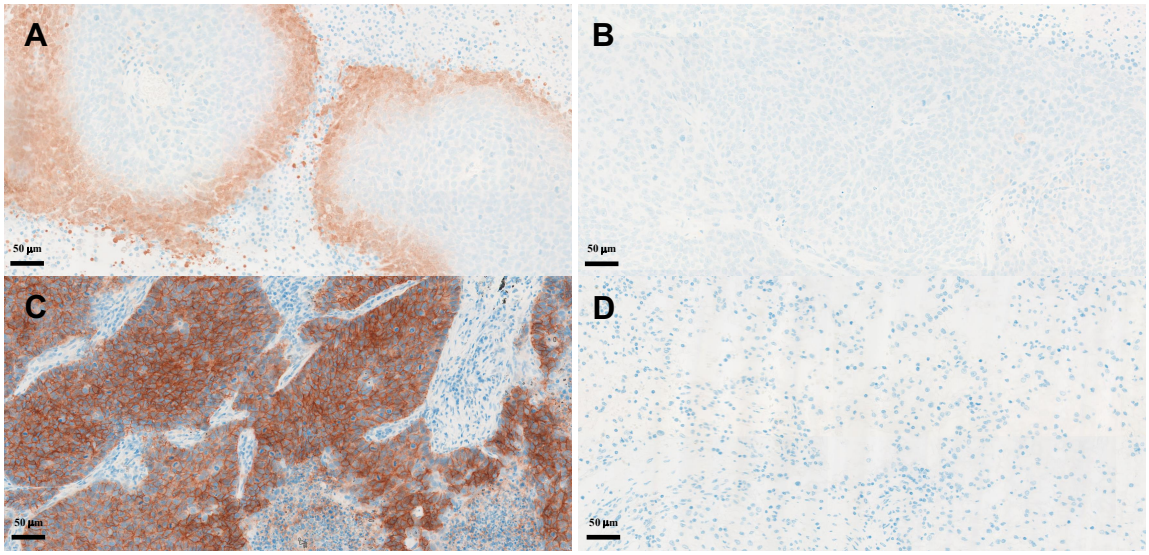


Figure 5.21: Pimonidazole and CAIX positive and negative IHC controls
A) Pimonidazole positive control from Pilot 1 L1 mouse xenograft model treated with pimonidazole (donated by Prof Len Seymour) using Hypoxyprobe-1 MAb1 Anti-pimonidazole mouse IgG1 monoclonal antibody at 1/1000 dilution. B) Pimonidazole negative control from same tumour tissue as positive control with mouse IgG at equivalent positive control primary antibody concentration. C) CAIX positive control from human NSCLC tissue (purchased from ProteoGenex, USA) using rabbit polyclonal CAIX antibody at 1/2000 dilution. D) CAIX negative control from same tumour tissue as positive control with rabbit IgG at equivalent positive control primary antibody concentration. Digital photographs were taken at x 20 magnification.

A strong positive correlation was observed between the histopathologist and automated IHC percentage scores for both pimonidazole ($r_s = 0.83$, $p < 0.001$) and CAIX ($r_s = 0.93$, $p < 0.001$) for test cases (Figure 5.22).

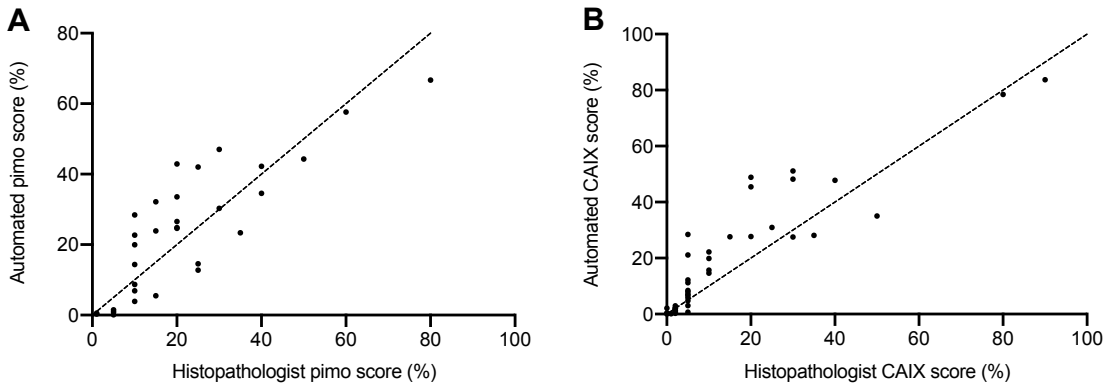


Figure 5.22: Agreement of manual and automated IHC pimonidazole and CAIX scoring
Scattter plots showing very strong positive correlation between tumour percentage staining scores for A) pimonidazole and B) CAIX obtained from manual and automated scoring. Every trial patient is represented. The dotted line is the line of identity. Abbreviations: pimo, pimonidazole; CAIX, carbonic anhydrase IX.

Overall, this data demonstrates that the automated methodology for scoring tumour pimonidazole and CAIX IHC worked well, thus permitting extensive IHC tumour analysis as now presented.

5.2.7 Intra-tumour heterogeneity in pimonidazole and CAIX IHC

The variation in pimonidazole and CAIX IHC percentage scores between tumour levels within individual patients is shown in Figure 5.23 and Figure 5.24, respectively. Notable differences in scores between levels were observed in a significant number of patients with more variability observed in pimonidazole IHC scores as compared with CAIX. In cases with multiple levels, the median range in the tumour percentage score between levels was 6.6% (range 0.7% to 58.5%) for pimonidazole and 4.4% (range 0.0% to 34.9%) for CAIX. The large rage in scores between levels highlights the risk of sampling error when assessing tumour hypoxia by IHC using these markers and justifies the approach of analysing multiple levels used in this study.

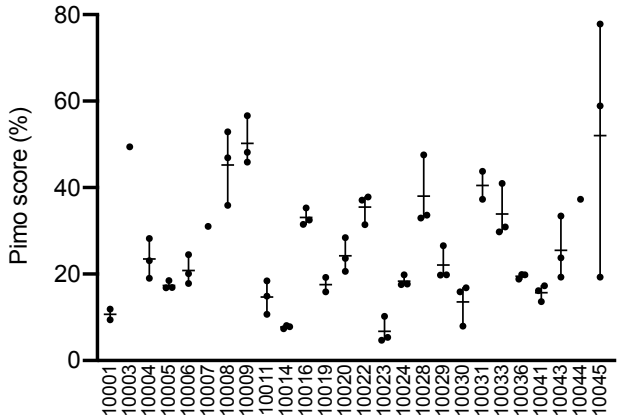


Figure 5.23: Pimonidazole IHC percentage scores per tumour level
Pimonidazole IHC percentage score per tumour level for all trial patients. In cases with multiple levels analysed, the mean score is shown and the percentage scores from each level are joined by a vertical line to demonstrate the range. Patients with just one level analysed are represented by a single data point. Abbreviations: pimo, pimonidazole.

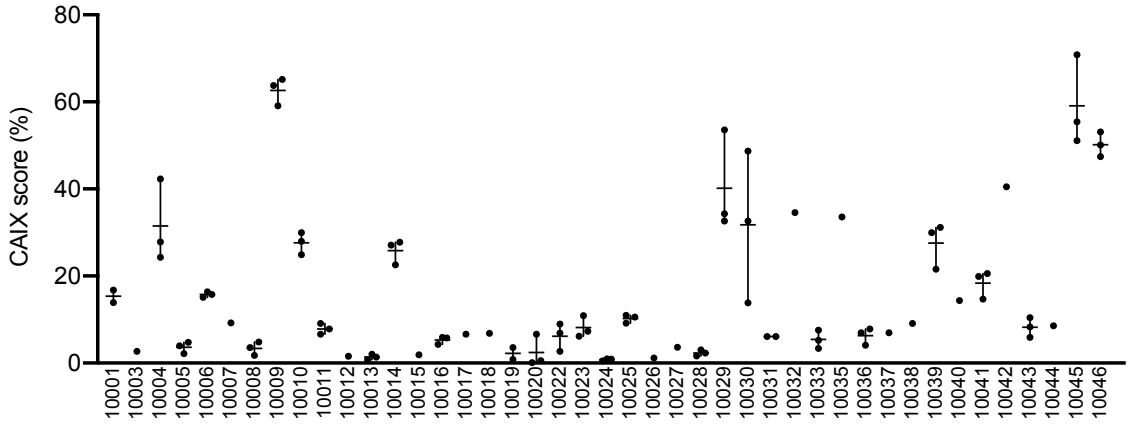


Figure 5.24: CAIX IHC percentage scores per tumour level
CAIX IHC percentage score per tumour level for all trial patients. In cases with multiple levels analysed, the mean score is shown and the percentage scores from each level are joined by a vertical line to illustrate the range. Patients with just one level analysed are represented by a single data point. Abbreviations: CAIX, carbonic anhydrase IX.

5.2.8 Effect of atovaquone on tumour pimonidazole and CAIX IHC

Averaged whole tumour pimonidazole and CAIX IHC percentage scores for atovaquone treated and untreated patients are shown in Table 5.5 and Table 5.6, respectively. The differences in pimonidazole and CAIX scores between atovaquone treated and untreated patients are shown in Figure 5.25 and Figure 5.26, respectively. There was no significant difference in IHC scores between treated and untreated patients for pimonidazole ($p = 0.84$) and CAIX ($p = 0.61$).

Table 5.5: Tumour pimonidazole and CAIX IHC percentage scores for atovaquone treated patients

Patient	Pimonidazole IHC (%)	CAIX IHC (%)
10001	11.0	15.0
10003	49.4	2.7
10004	23.3	30.7
10005	16.3	4.2
10006	20.6	15.6
10007	31.1	9.2
10008	44.8	3.3
10009	50.6	62.6
10010		27.7
10011	15.2	7.8
10013		1.4
10014	7.8	25.9
10016	33.6	5.2
10019	18.0	2.6
10020	24.7	3.1
10022	35.5	6.6
10023	6.2	8.0
Median (IQR)	**23.3** (15.3 – 35.5)	**7.9** (3.2 – 20.8)

Abbreviations: pimo, pimonidazole; CAIX, carbonic anhydrase IX; IQR, interquartile range

Table 5.6: Tumour pimonidazole and CAIX IHC percentage scores for untreated patients

Patient	Pimonidazole IHC (%)	CAIX IHC (%)
10012		1.5
10015		1.9
10017		6.7
10018		6.8
10024	18.4	0.8
10025		10.1
10026		1.2
10027		3.6
10028	35.4	2.5
10029	20.9	36.6
10030	14.0	30.5
10031	40.7	6.1
10032		34.5
10033	32.7	5.6
10035		33.6
10036	19.4	6.5
10037		7.0
10038		9.1
10039		24.7
10040		14.3
10041	16.2	19.3
10042		40.5
10043	22.1	9.2
10044	37.3	8.5
10045	30.4	52.4
10046		49.7
Median (IQR)	**22.2** (18.4 – 35.4)	**8.8** (5.1 – 31.3)

Abbreviations: pimo, pimonidazole; CAIX, carbonic anhydrase IX; IQR, interquartile range

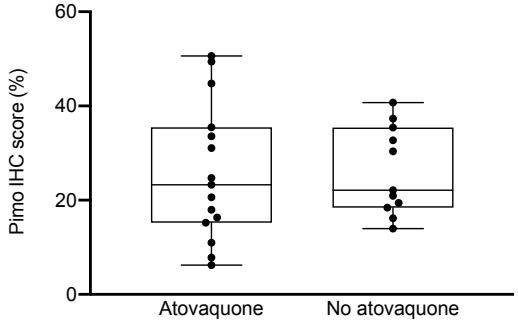


Figure 5.25: Effect of atovaquone on tumour pimonidazole IHC
Box and whisker plots demonstrating the difference in tumour pimonidazole IHC percentage scores between atovaquone treated and untreated patients. Median levels with interquartile and absolute ranges are shown. Abbreviations: pimo, pimonidazole. Difference is not significant (Mann-Whitney U test).

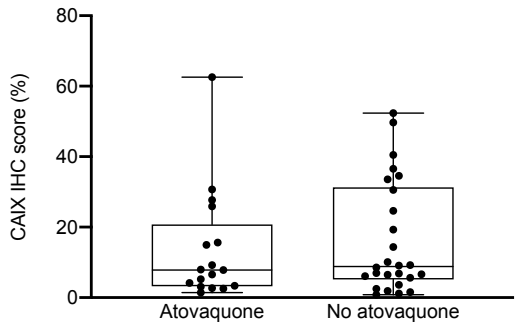


Figure 5.26: Effect of atovaquone on tumour CAIX IHC
Box and whisker plots demonstrating the difference in tumour CAIX IHC percentage scores between atovaquone treated and untreated patients. Median levels with interquartile and absolute ranges are shown. Abbreviations: CAIX, carbonic anhydrase IX. Difference is not significant (Mann-Whitney U test).

When interpreting this data it is important to consider whether both patient groups were balanced in terms of baseline hypoxia. As demonstrated in section 4.2.1, baseline hyp-PET imaging suggested that this was not the case. Patients in the atovaquone-treated group had higher HV than compared with untreated patients. Patients who received atovaquone treatment and were eligible for both pimonidazole and CAIX analysis (n=14), the median HV was 18.6 mL compared with only 4.2 mL for patients who did not receive treatment (n=11). Therefore, it is possible that the equivalence observed between treated and untreated patients in terms of pimonidazole and CAIX IHC may in fact be a meaningful finding.

5.2.9 Correlation between pimonidazole and CAIX IHC

To assess for agreement between pimonidazole and CAIX IHC, correlation was performed between whole tumour percentage scores between both markers in untreated patients (n=11). This data is shown in Figure 5.27 and demonstrates a lack of correlation (r_s = -0.30, p = 0.371).

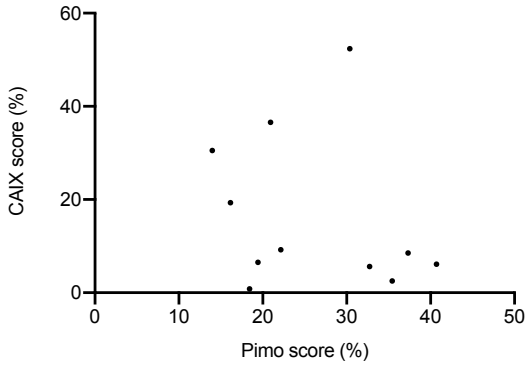


Figure 5.27: Correlation between tumour IHC scores for CAIX and pimonidazole
Scatter plot showing a lack of correlation between tumour percentage scores for CAIX and pimonidazole in untreated patients. Abbreviations: CAIX, carbonic anhydrase IX; pimo, pimonidazole.

5.2.10 Correlation between plasma and tumour CAIX

Visit 2 plasma CAIX levels were correlated with tumour CAIX IHC to assess for agreement (Figure 5.28). A positive moderate strength correlation was observed for untreated patients (n = 14, r_s = 0.56, p = 0.038), as well as for all trial patients (n = 31, r_s = 0.48, p = 0.006).

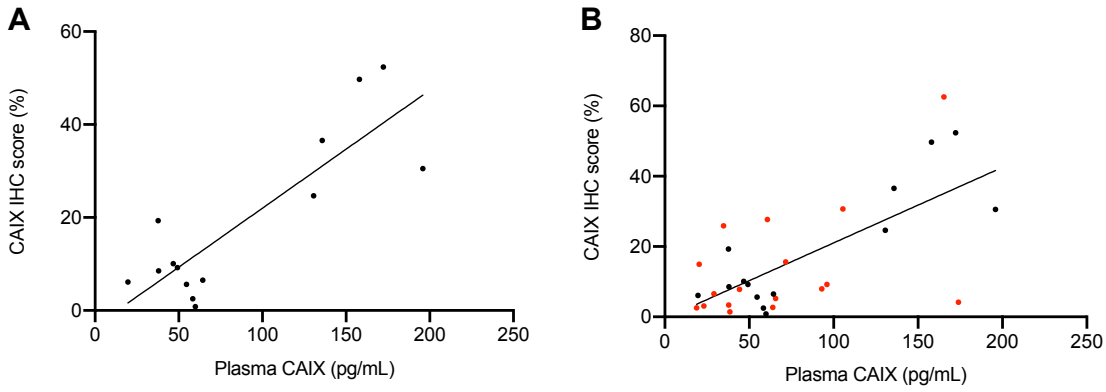


Figure 5.28: Correlation between plasma and tumour CAIX
Scatter plots showing positive correlation between Visit 2 plasma CAIX levels and tumour percentage score for CAIX in A) untreated patients and B) all trial patients. Black data points represent untreated patients and red data points represent atovaquone treated patients. Lines of best fit are shown. Abbreviation: CAIX, carbonic anhydrase IX; IHC, immunohistochemistry.

5.2.11 Correlation between hypoxia IHC with hyp-PET

Lastly, correlation was conducted between pimonidazole and CAIX IHC and hyp-PET parameters obtained from Visit 2, as shown in Figure 5.29 and Figure 5.30, respectively. All patients who took pimonidazole were included (n=25). As CAIX is an endogenous marker which could be affected by drug treatment, only patients who did not take atovaquone were included for CAIX and hyp-PET correlative analysis (n=14).

No correlation was observed between the pimonidazole IHC percentage score and HV (r_s = -0.02, p = 0.942), HV% (r_s = 0.33, p = 0.105), TBR_{mean} (r_s = 0.30, p = 0.152) and TBR_{peak} (r_s = 0.37, p = 0.067). Similarly, there was no correlation observed between the CAIX IHC score and HV (r_s = 0.39, p = 0.170), HV% (r_s = -0.51, p = 0.067), TBR_{mean} (r_s = -0.47, p = 0.091), TBRpeak (r_s = -0.09, p = 0.750).

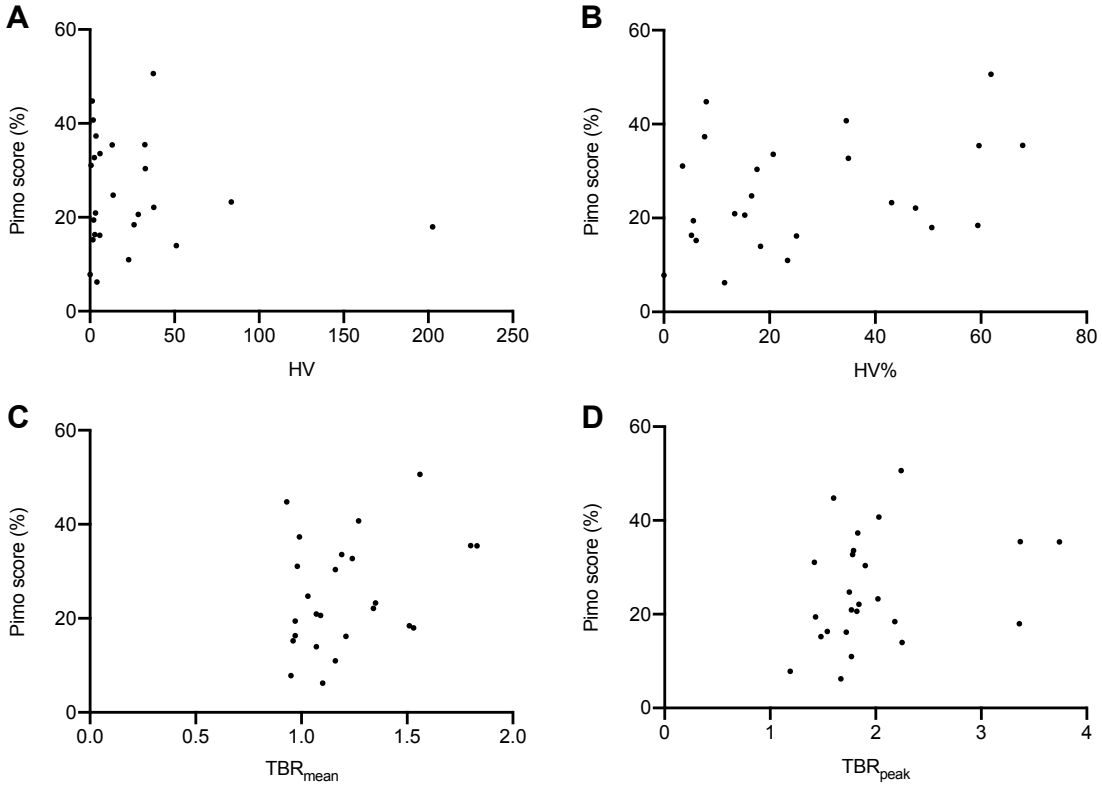


Figure 5.29: Correlation of pimonidazole IHC with hyp-PET
Scatter plots showing a lack of correlation between pimonidazole IHC percentage score and hyp-PET derived A) HV, B) HV%, C) TBR_{mean}, D) TBR_{peak}. Abbreviations: pimo, pimonidazole; HV, hypoxic volume; HV%, hypoxic volume percentage; TBR, tumour-to-blood ratio.

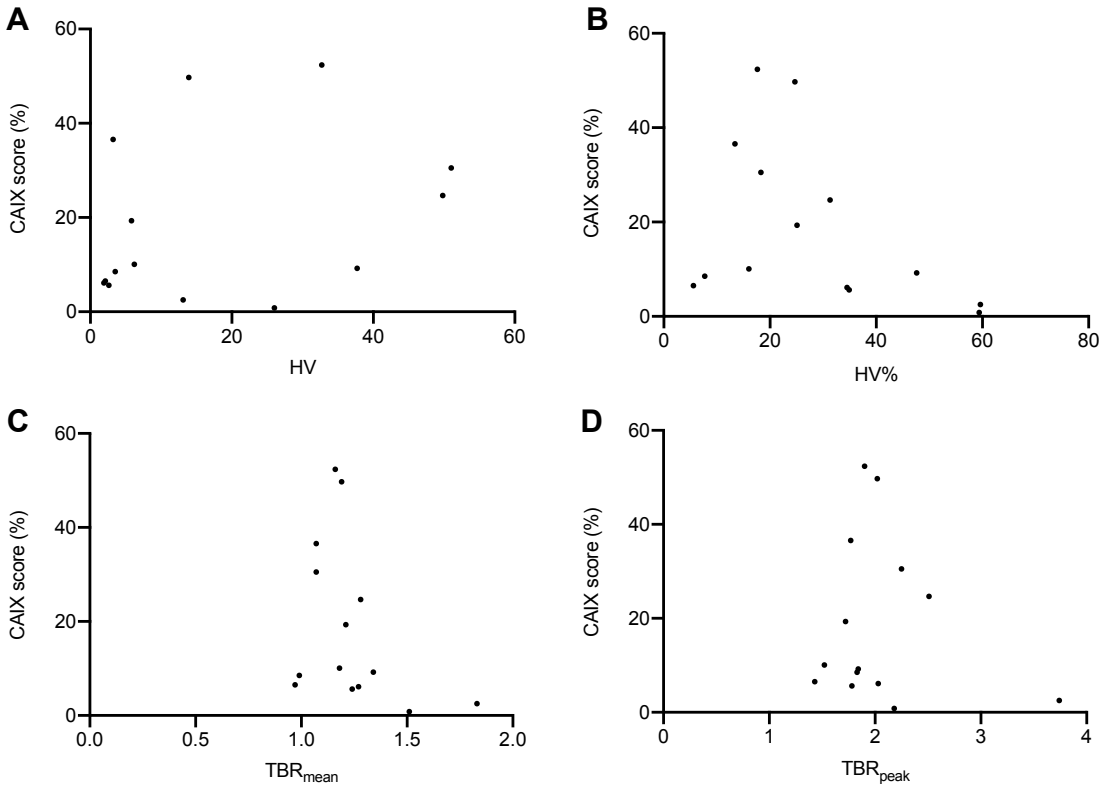


Figure 5.30: Correlation of CAIX IHC with hyp-PET
Scatter plots showing a lack of correlation between CAIX IHC percentage score and hyp-PET derived A) HV, B) HV%, C) TBR_{mean} and D) TBR_{peak}. Abbreviations: CAIX, carbonic anhydrase IX; HV, hypoxic volume; HV%, hypoxic volume percentage; TBR, tumour-to-blood ratio.

5.3 DISCUSSION

5.3.1 Plasma VEGF, CAIX and OPN as hypoxia biomarkers

The data presented in this chapter demonstrates that atovaquone treatment does not significantly alter plasma levels of VEGF, CAIX or OPN in patients with operable NSCLC. Furthermore, no correlation was observed between the levels of these markers and with hyp-PET parameters within individual patients. Initially these were disappointing findings as they do not appear to support the earlier finding that atovaquone reduced tumour hypoxia as measured by hyp-PET as well as also not supporting further development of these markers as hypoxia biomarkers. However, perhaps this finding is not

surprising for a number of reasons when considering the specific patient population in this study.

Circulating VEGF, OPN and CAIX are fairly well-reported diagnostic biomarkers for NSCLC, with higher levels present in patients with NSCLC compared to healthy individuals [142,150,283]. Although considered as 'classic' hypoxia cellular response proteins, VEGF, CAIX and OPN are also known to be involved in tumourigenesis beyond the hypoxia response and to be regulated in a hypoxia-independent manner. In this study, plasma CAIX levels correlated strongly with CAIX tumour IHC, but both CAIX endpoints did not correlate with the exogenous measures of hypoxia such as pimonidazole IHC and hyp-PET parameters, suggesting that plasma CAIX reflects tumour CAIX activity but that this is, at least in part, independent of hypoxia.

Interestingly, in one sizable study of patients with operable NSCLC, as well as in other tumour types [284], HIF-1α expression as detected by IHC did not correlate with CAIX IHC or plasma CAIX levels, demonstrating that HIF-1α- independent regulation of CAIX expression occurs, with mutated VHL and upregulated EGFR signalling as suggested possible mechanisms [142]. In fact, other studies have shown a lack of agreement between CAIX IHC and direct oxygen measurements, leading some to question whether CAIX is an adequate surrogate marker of hypoxia [285]. Further still, others have shown complete absence of immunohistochemical detection of CAIX in HNSCC in regions located far beyond the diffusion capacity of oxygen with relation to vessels [286]. Inconsistent reports of the agreement of pimonidazole and CAIX IHC in numerous tumour types [130,133,287] casts further doubt as to the utility of CAIX as a robust marker of hypoxia.

If doubt exists whether endogenous markers such as CAIX are reliable markers of hypoxia at the tumour tissue level, then whether plasma levels are reflective of tumour hypoxia

should come under ever more scrutiny. Generally, there is a lack of large studies investigating circulating endogenous hypoxia markers with exogenous markers or direct measures of tumour hypoxia, especially in NSCLC. Only small studies have shown correlation of plasma OPN and direct oxygen measurements in HNSCC [149], and NSCLC [49]. With regards to VEGF, there are mixed reports in HNSCC [140,288], with none in NSCLC. Such data is altogether lacking for plasma CAIX.

It is likely that in order to accurately evaluate tumour hypoxia through such endogenous surrogate markers, especially in small studies such as this, the specific tumour type and knowledge of any key driving mutations influencing their expression is of key importance. In recognition of this, tumour exome sequencing for this study has commenced to investigate this.

In view of the lack of correlation between plasma markers and hyp-PET, it was perhaps not surprising that atovaquone treatment did not result in changes for these plasma markers. In addition, as it was shown that atovaquone treatment did not significantly alter tumour growth, changes in these markers due to change in disease activity were not expected either. Previous clinical trials which have reported reductions in the levels of these markers have done so following (chemo)radiotherapy, chemotherapy or surgery which would clearly be expected if these markers reflect disease activity, regardless of their effect on hypoxia. This is the first study to report the effect of a specific hypoxia targeted treatment aimed at reducing tumour OCR on such circulating markers.

It is also important to consider that this was an operable NSCLC cohort and the majority of patients had early stage disease. The majority of previous studies which have investigated changes in circulating levels of VEGF, OPN and CAIX in NSCLC have done so in advanced and inoperable disease with significantly higher baseline levels reported

than observed in this study [141,289]. In fact, in this study a significant number of patients had undetectable VEGF levels, which impeded analysis. Perhaps in early and thus less hypoxic disease, the hypoxic plasma signature may be 'immature' and therefore less likely to demonstrate agreement between markers and be less reliable at detecting change in tumour hypoxia. As any change in analyte level needs to be rather sizable to be considered as meaningful using ELISA, perhaps hoping for large changes in levels in early stage disease was overly ambitious. However, it should be noted that a number of studies have shown no significant change in levels of such markers even following completion of radical radiotherapy during which large reductions in hypoxia would be expected [290,291], demonstrating uncertainty whether circulating markers can reliably detect changes in tumour hypoxia. Clinical data tracking changes in the level of such plasma markers with corresponding changes in tumour hypoxia over time, as measured by direct measurements or hyp-PET, have not been reported.

The lack of correlation of such candidate plasma hypoxia markers with hyp-PET may also be explained by considering differences in the degree of hypoxia which they measure. Imaging hypoxia with nitroimidazole tracers such as FMISO and FAZA relies on accumulation of tracer in severely hypoxic tumour regions (<10 mmHg), whereas endogenous markers of hypoxia, such as CAIX, which are upregulated as a direct consequence of HIF signalling, occurs under less severely hypoxic conditions [292]. Therefore, reduction in severe hypoxia as detected by hyp-PET may not be associated with alterations in less hypoxic regions, especially if redistribution was to occur. Interestingly, in HNSCC, hypoxia imaging with another nitroimidazole PET tracer [^{18}F]-flortanidazole showed no correlation with plasma OPN, CAIX and VEGF [290]. Other studies using other nitroimidazole tracers such as [^{18}F]-fluoroerythronitroimidazole have shown no correlation between tumour uptake and plasma OPN concentration in patients with cervical carcinoma

[293]. FMISO has also been reported not to correlate with HIF-1α and VEGF expression as assed by IHC in gliomas [294], however in another study in glioma patients, agreement between FMISO and these markers as well as CAIX was observed [295]. This was the first clinical study to look at the correlation of these markers with nitroimidazole-based PET imaging in NSCLC.

Lastly, it should not be forgotten that plasma levels of OPN and VEGF can be influenced by non-oncological patient factors. For example, OPN levels can be significantly altered by the immune and stress response and altered by presence of inflammation or infection [296,297].

Overall, the data from this study of patients with operable NSCLC suggests that plasma VEGF, OPN and CAIX have limitations as specific hypoxia biomarkers. Therefore, this data does not support that such markers can replace hyp-PET imaging in future hypoxia clinical trials in NSCLC.

5.3.2 Plasma miR-210 as a potential hypoxia biomarker

In contrast, this study provides some supportive evidence that plasma miR-210 may hold more promise as a hypoxia biomarker. A positive correlation between miR-210 levels and hyp-PET derived HV and TBR_{peak} was observed. Furthermore, plasma miR-210 levels appeared to predict whether patients had sufficient baseline HV for this study and therefore may be potentially useful for selecting patients for future hypoxia imaging trials. This is the first time a correlation between miR-210 and an exogenous measure of hypoxia has been reported and although it represents an exciting finding it clearly requires further confirmation in additional and larger studies.

This study also demonstrated that plasma miR-210 was positively correlated with tumour volume and that mir-210 levels appeared to increase with advancing stage of disease, as previously reported [156,298]. This data therefore provides further support that miR-210 may be a clinically useful diagnostic biomarker in NSCLC.

The results of this study support the important finding of other authors [282] that plasma sample haemolysis is a significant problem when measuring circulating miRNAs, including miR-210 and the most commonly used internal reference miRNA miR-16. Therefore, it must be stressed that careful and possibly multiple blood specimen collections should considered in clinical studies measuring these circulating miRNAs with the rates of haemolysis reported. The identification of suitable endogenous internal reference miRNAs which are not susceptible to haemolysis are likely to be beneficial.

Despite correlation with baseline hypoxia, no significant changes in miR-210 were observed following atovaquone treatment. This raises the question of how quickly does a change in tumour oxygenation translate into an established alteration in hypoxia response protein expression, and subsequently changes in plasma levels of relevant markers? Perhaps only a two-week course of atovaquone treatment may not have been long enough for this to occur. This is in contrast to measuring hypoxia by hyp-PET imaging where theoretically tracer accumulation is independent of the cellular response to hypoxia, but rather, the degree of intracellular retention is reflective of the presence, or absence, of molecular oxygen. Undoubtedly, rapid changes in tumour hypoxia are more detectable using such imaging techniques and perhaps they can be viewed as more ‘real-time’ or dynamic measures of hypoxia, as opposed to waiting for the endogenous hypoxia response to occur, become established and result in meaningful changes in the level of relevant plasma markers.

5.3.3 Tumour tissue IHC based hypoxia biomarkers

With regards to tumour tissue IHC analysis, a major weakness of this study was that no baseline pre-atovaquone treatment tissue was collected and therefore an investigation of the change in hypoxia in individual tumours was not possible. As observed in this study, the majority of patients proceeded to tumour resection on the basis of a radiological and not pathological diagnosis. If diagnostic tissue was obtained pre-surgery, it was often very minimal and in many cases consisted of only a cytological specimen. Also, given the very short window of time available prior to curative surgery, mandating additional biopsies into the study design would have resulted in a delay in surgery, which was clearly not acceptable.

Nevertheless, the finding that pimonidazole and CAIX IHC scores were similar for treated and untreated patients may potentially represent a positive finding. This is because baseline hyp-PET imaging data suggested that patients in the atovaquone treated group had more baseline hypoxia as compared to the untreated group.

Although the lack of agreement between CAIX IHC and hyp-PET can potentially be explained by all the aforementioned challenges of using endogenous surrogate markers of hypoxia, the lack of correlation between pimonidazole IHC and hyp-PET parameters was a surprising finding as both are nitroimidazole-based methods. However, on review of the literature previous reports demonstrating agreement of pimonidazole IHC with FMISO uptake have been primarily conducted in pre-clinical models [120], with equivalent clinical studies lacking to date. Furthermore, any time interval between imaging and tissue resection, on average 48 hours in this study, may result in lack of correlation due to acute changes in hypoxia. In addition, discrepancy between visualising hypoxia at the microscopic level, which is more prone to intra-tumour heterogeneity, and the macroscopic

resolution of the PET voxel are factors which are also likely to limit the accuracy of such comparisons [299].

However, perhaps most important for this study, is the potentially important role that tumour necrosis may have played. A number of patients in this trail had very large tumours with macroscopically visible significant regions of necrosis. Such necrotic regions presented a challenge during tumour processing following resection as they were exceedingly friable and in some cases it was not technically possible to formalin fix and embed this tumour tissue. Tumour levels selected for IHC analysis were from viable tumour regions and thus may not be reflective of the averaged whole tumour hyp-PET parameters, which would have incorporated uptake signal from lost peri-necrotic tissue at the viable/non-viable tumour interface. Work has commenced to investigate the spatial agreement of IHC staining with hyp-PET for each tumour level in order to investigate this further.

Given that pimonidazole is a marker of extreme hypoxia, it was somewhat surprising that generally the pimonidazole IHC percentage scores were higher than for CAIX in the majority of case. On review of the literature, the percentages reported in this study are comparable to that in other NSCLC studies [300]. Perhaps this can be explained by the fact that the majority tumours in this study were adenocarcinomas which are known to have lower staining for CAIX than SCC [142]. An important additional finding in this study, although perhaps less surprising, is the demonstration of significant variation in pimonidazole and CAIX IHC scores between different levels within individual patients. This intra-tumour heterogeneity in hypoxia as measured by IHC highlights the significant risk of sampling error, and thus the limitation of using this technique for the study of tumour hypoxia.

CHAPTER 6: FINAL DISCUSSION AND FUTURE WORK

6.1 GENERAL DISCUSSION

6.1.1 Tumour hypoxia modification past and present

Tumour hypoxia is arguably the best validated target in oncology due to its multifarious role in tumourigenesis and the profound resistance to radiotherapy it confers. In no other tumour type is the need for improving tumour radiation response more evident than in NSCLC where exceptionally poor outcomes following radiotherapy are unfortunately part of everyday clinical practice. Therefore, the development of novel hypoxia modifiers to improve radiation efficacy represents an unmet and urgent clinical need for this patient population.

However, despite decades of clinical research combining promising hypoxia modifiers with radiotherapy, no such agent has been adopted into widespread clinical use. The reasons for this are clear and multifactorial. Although improvement in outcomes has been observed, it has been modest at best and often with concerns regarding toxicity or practical deliverability [157]. However, perhaps of greater importance is that there has been an almost complete absence of proof of principle studies to confirm the ability of such agents to reduce tumour hypoxia in patients. The barrier to conducting such studies has undeniably been a lack of robust, widely available and adequately validated biomarkers for the clinical evaluating tumour hypoxia. This has not only significantly impeded the investigation of the efficacy of hypoxia modifiers, but it has also resulted in an inability to accurately select patients who are likely to benefit most from such treatment. It is likely that only when hypoxia biomarkers are widely available will hypoxia modification enter the well-established era of personalised medicine and significant improvements in outcomes be realised.

Taking into consideration such learnings from the last few decades, the work presented in this thesis represents a complete overhaul of the process of the clinical development of hypoxia modifiers by refocusing on key fundamental translational research principles. Firstly, tackling tumour hypoxia through OCR inhibition represents a truly novel strategy: reducing tumour oxygen demand as opposed to the previous long-standing efforts to increase oxygen supply. Secondly, the ATOM clinical study described here was primarily a proof of principle study to confirm atovaquone reduced tumour hypoxia in patients, prior to embarking on later phase trials. And thirdly, the wide range of techniques utilised for measuring hypoxia not only ensured a thorough assessment of the effect of atovaquone on tumour hypoxia, but also aimed to further develop candidate hypoxia biomarkers and thus contribute to this field of clinical research as a whole. As tempting as it was to simply combine this highly promising agent with radiotherapy and hope for improvement in outcomes, the measured approach undertaken aimed to limit the likelihood that atovaquone would join the long list of previous unsuccessful hypoxia modification treatments.

6.1.2 Clinical proof of principle of atovaquone as a tumour hypoxia modifier and anti-cancer treatment

Therefore, the first aim of this DPhil project was to design and conduct a clinical proof of principle study to investigate the effect of atovaquone on tumour hypoxia in patients with NSCLC. The data presented in this thesis demonstrates this was achieved with a complex and highly ambitious hypoxia-focused window of opportunity study successfully completed. Such window studies are notoriously difficult to conduct with high failure rates [255], however through careful planning and study design, this was effectively delivered with a wealth of clinical data collected.

The exciting finding from this work is that atovaquone treatment significantly and rapidly reduced tumour hypoxia as measured by hyp-PET and did so in the vast majority of patients. As this imaging modality has become the most-widely accepted current standard for measuring changes in hypoxia in the clinical setting [124–128,301], this finding can be viewed as the best available confirmation of clinical proof of principle for this agent as a novel hypoxia modifier. Furthermore, as atovaquone reduces hypoxia by inhibiting OXPHOS and thus OCR, this data supports the efficacy of tackling hypoxia using this approach, a strategy which is gaining momentum [219,220,302].

The lack of significant alteration in tumour perfusion following atovaquone treatment indirectly supports that hypoxia reduction was achieved by decreasing OCR. Recently, Lord *et al*. reported that treatment of breast cancer patients with metformin, which inhibits OXPHOS through complex I rather than complex III inhibition, resulted in a shift in tumour metabolism from OXPHOS to glycolysis [231], therefore supporting that metabolic reprograming is achievable using OXPHOS inhibitors in the clinical setting. In this current study, tumour gene expression signature and metabolomic data aimed at investigating the effect of atovaquone on metabolism is eagerly awaited, with provisionally encouraging gene expression results observed (data not shown).

As glycolysis has long been associated with tumour progression and metastasis [303], some may voice concern that this approach may be detrimental in terms of disease progression. However, retrospective studies have unanimously demonstrated superior outcomes for cancer patients receiving metformin compared to diabetic patients taking alternative medication, with such improvements independent of diabetic control [222–227]. Furthermore, unpublished *in vivo* data from our group has recently shown that atovaquone treatment does not increase tumour metastatic potential. In this study,

atovaquone treated patients had PFS and OS rates comparable with historical data. Perhaps, the re-emergence of the importance of OXPHOS in cancer progression over the last decade [220] may explain, at least in part, why detrimental effects have not been observed with this metabolic reprogramming strategy.

During the undertaking of this project atovaquone was discovered to have a number of anti-cancer properties in addition to hypoxia modification. One such example is the negative effect of atovaquone on the activation of the oncogenic transcription factor signal transducer and activator of transcription 3 (STAT3). STAT3 is frequently upregulated in haematological and solid malignancies and is a key mediator of neoplastic cellular transformation [304]. Xiang *et al.* reported atovaquone to be a potent STAT3 inhibitor [305] and *in vitro* data in haematological cancer cell lines demonstrated that atovaquone at clinically relevant concentrations inhibited STAT3 phosphorylation resulting in death of STAT3-dependant cells, as well as blasts isolated from patients with acute myelogenous leukaemia (AML) and acute lymphocytic leukaemia (ALL). *In vivo* experiments in murine multiple myeloma xenografts resulted in significant tumour growth delay and furthermore, retrospective analysis of outcome data from patients who received atovaquone for *Pneumocystis* prophylaxis following haematopoietic stem cell transplantation for AML showed improved PFS [305]. Separately, in thyroid cancer the inhibition of STAT3 phosphorylation by atovaquone has been shown to be dependent upon its inhibition of mitochondrial complex III and *in vitro* such inhibition significantly increased sensitivity to the commonly used chemotherapeutic agent doxorubicin [306]. Interestingly, in HCC cells, resistance to doxorubicin as well as cisplatin was shown to be mediated by mitochondrial respiration and inhibition of OXPHOS by atovaquone and subsequent increased oxidative stress was able to overcome such resistance [307].

Another example is that a number of recent studies have demonstrated that atovaquone inhibits cancer cell proliferation. For example, atovaquone has been shown to inhibit proliferation and induce apoptosis in renal cell carcinoma cells through a mechanism dependent upon mitochondrial complex III inhibition and increased ROS production [308]. This group also showed that *in vitro* and *in vivo* atovaquone increased the efficacy of 5-fluorouracil (5-FU) and interferon-α (IFN-α) in this tumour type. Further still, in hepatocellular carcinoma (HCC) cells, atovaquone significantly inhibited proliferation through S phase cell cycle arrest with both intrinsic and extrinsic apoptotic pathway induction associated with upregulation of p53 and p21. Further investigation revealed that atovaquone induced double-stranded DNA breaks, leading to sustained activation of ataxia-telangiectasia mutated (ATM) and its downstream molecules such as cell cycle checkpoint kinase-2 (CHK2) and H2AX. Subsequent *in vivo* experiments demonstrated that atovaquone inhibited tumour growth and prolonged survival of tumour-bearing mice [309]. However, in this study atovaquone did not have any significant effect on tumour growth. Furthermore, as previously described Ashton *et al.* did not observe any direct antiproliferative effect of atovaquone in numerous cancer cell types or tumour growth delay in xenograft models [219], thus suggesting that perhaps the antiproliferative effects of atovaquone are dependent on cell type, as well as specific experimental conditions.

Lastly, atovaquone has also recently been shown to have direct activity against cancer stem-like cells (CSCs). In MCF7 breast cancer cells, atovaquone inhibits oxygen-consumption and induces glycolysis as well as oxidative stress. Given that MCF7-derived CSCs are highly-dependant on mitochondrial respiration, atovaquone inhibits CSC proliferation with an IC-50 of just 1 μM. Furthermore, in certain CSC populations, atovaquone induces apoptosis [236].

Overall, there is therefore growing evidence that in addition to hypoxia modification and thus its potential as a radiosensitiser, atovaquone may be a multifunctioning anti-cancer agent. As confirmed in this study, atovaquone is extremely well-tolerated, which is of key importance especially for combining it with toxic therapies such as radiotherapy and chemotherapy where the therapeutic window is often already very narrow. In LA-NSCLC this is of particular importance as radical chemoradiotherapy is associated with significant toxicity in a generally borderline fit patient population. The reason why atovaquone is so well-tolerated is somewhat surprising given that OXPHOS is an integral part of normal cellular function and the main source of energy production. Perhaps the answer lies in the fact that atovaquone has been shown not to alter the metabolic state of normal cells. For example, in normal human fibroblasts no alteration in metabolic function were observed following atovaquone treatment [236]. This apparent cancer-specific inhibition of OXPHOS adds further impetus for developing this agent as an anticancer treatment.

6.1.3 Hypoxia biomarker development

The second aim of this DPhil project was to further develop candidate hypoxia biomarkers to inform the design of future hypoxia modification clinical studies. Although hyp-PET is currently the best available accepted method for studying changes in tumour hypoxia over time with high reproducibility reported, it still has significant shortcomings. Lack of widespread and reliable availability of hypoxic tracers, as well as prohibitively high costs, unfortunately limit the use of this technique to predominantly small single centre studies. In addition, full clinical validation is still required for hyp-PET with crossing of necessary 'translational gaps' as outlined by the imaging biomarker validation roadmap [310].

In this study, correlation of hyp-PET with endogenous cellular hypoxia response proteins was conducted to further validate their use in evaluating hypoxia in NSCLC. In fact, this

was the first study to do so in this tumour type. It was disappointing to observe a lack of agreement between hyp-PET parameters and plasma VEGF, OPN and CAIX, as well as agreement between these markers, as this data does not support their ability to replace hyp-PET imaging.

Using endogenous markers as surrogate measures of hypoxia is challenging as their expression can be regulated by hypoxia-independent processes. In small studies, knowledge of the expression profile of such markers in the specific tumour type and disease stage in question coupled with complete molecular profiling is needed for accurate interpretation of any such results. It is likely that combination of multiple such circulating markers to develop a plasma hypoxia signature is required, as has been attempted by some [141]. In fact, the shift to investigating tumour hypoxia metagene signatures can be viewed as an appreciation that assessment of the wide ranging and complex tumour response to hypoxia is required, as opposed to focusing on a select few markers.

This study did however find that circulating miR-210 may hold some promise as hypoxia biomarker. This 'master hypoxiaMIR' is an increasingly reported diagnostic biomarker in NSCLC and the data from this study does support this further by demonstrating that levels increased with tumour size and stage of disease [156,298]. Furthermore, a positive correlation was observed between miR-210 levels and certain hyp-PET parameters and also that levels appeared predictive of whether patients had sufficient baseline HV for this study. In fact, clinicopathological features such as histology and FDG PET avidity, for example, did not appear to predict whether there was sufficient hypoxia or its degree. This highlights the unpredictability of measuring tumour hypoxia and the development of a hypoxia biomarker which could fulfil this role would be of significant advantage for future studies in this field.

6.2 CURRENT AND FUTURE WORK

6.2.1 Ongoing ATOM trial analysis

A significant amount of work is currently underway to further maximise the data from this study. As previously described, tumour 3' RNA-Seq analysis is in progress to compare both hypoxia and metabolism expression signatures between atovaquone treated and untreated patients, with promising provisional results observed. To further investigate the effect of atovaquone on tumour metabolism, a collaboration has been established with the School of Chemistry to also perform metabolomic profiling of tumour samples. To complete the molecular profiling of tumours and investigate for any key mutations which may influence the hypoxic profile or its modification following atovaquone treatment, whole exome sequencing is also in progress.

To complete the assessment of the effect of atovaquone on tumour perfusion, DCE and DWI MRI as well as dynamic hyp-PET analysis is underway and tumour IHC for the endothelial markers CD31 and CD146 has also been conducted.

Great effort went into carefully orientating resected specimens to ensure that tumour sampling for IHC and gene expression was comparable with hyp-PET imaging at a tumour-by-tumour level. The spatial agreement of such methods is now being investigated to further investigate the validity of such measures in evaluating tumour hypoxia.

6.2.2 A new clinical trial combining atovaquone with chemoradiotherapy in NSCLC

Following this clinical proof of principle that atovaquone modifies tumour hypoxia, the decision was taken to expeditiously further develop this agent as a radiosensitiser and to initiate clinical testing in combination with radiotherapy in NSCLC. As there are no reports

of the safety of combining atovaquone with radiotherapy, and as radical radiotherapy is particularly toxic in this patient population, the safety of this combination first needs to be established. Therefore, the Atovaquone with Radical ChemorADIotherapy in locally advanced NSCLC (ARCADIAN) trial has been developed and is scheduled to open May 2020. This phase I, single arm, open-label, two-centre (Oxford and Edinburgh), 20 patient study will utilise the time-to-event continual reassessment method (TiTE-CRM) to find the optimal and therefore recommended phase II dose of atovaquone in combination with concurrent CRT in patients with LA-NSCLC. The reason why CRT was chosen as opposed to radiotherapy alone is that this is the standard of care treatment for patients with locally advanced disease, which is the patient group most in need of improvement in radiotherapy outcomes. Furthermore, if proven to be safe with this regime, atovaquone could be combined with CRT in many other tumour types thus widening the potential clinical impact of this agent.

The continual reassessment method (CRM) is a Bayesian model-based method for finding the maximum tolerated dose (MTD) under the assumption that toxicity and efficacy increase monotonically with increasing dose, with the aim of finding a dose which causes a specified dose limiting toxicity (DLT) rate. The TiTE-CRM is a modified version of the CRM that accounts for time-to-event of possible later onset toxicities and is therefore particularly advantageous for radiotherapy trials where toxicities are often observed later. A major advantage of the TiTE-CRM is the fact that it uses all current accumulated information to decide which dose to assign to the next patient. The method results in shorter study duration as it is not necessary for a patient to be observed for the full observation period before further recruitment and more patients are treated closer to the MTD [311].

In addition to assessing the safety of this combination, multiple secondary translational endpoints in the ARCADIAN trial capitalise on learnings from the ATOM trial to further confirm the effect of atovaquone on tumour hypoxia, as well as continue to strive to further develop hypoxia biomarkers. The ARCADIAN trial schema is shown in Figure 6.1. This exciting new study represents the next step in the development pipeline of atovaquone as a clinical hypoxia modifier. At every step in this translational research pathway so far, great effort has been taken to further our knowledge of tumour hypoxia biology and validate the methodology used for its study in the clinical setting. It is hoped that by adopting such an approach, this novel and highly promising hypoxia modifier stands the very best chance to become the first hypoxia-targeted treatment to enter routine clinical practice, after a quest spanning more than half a century.

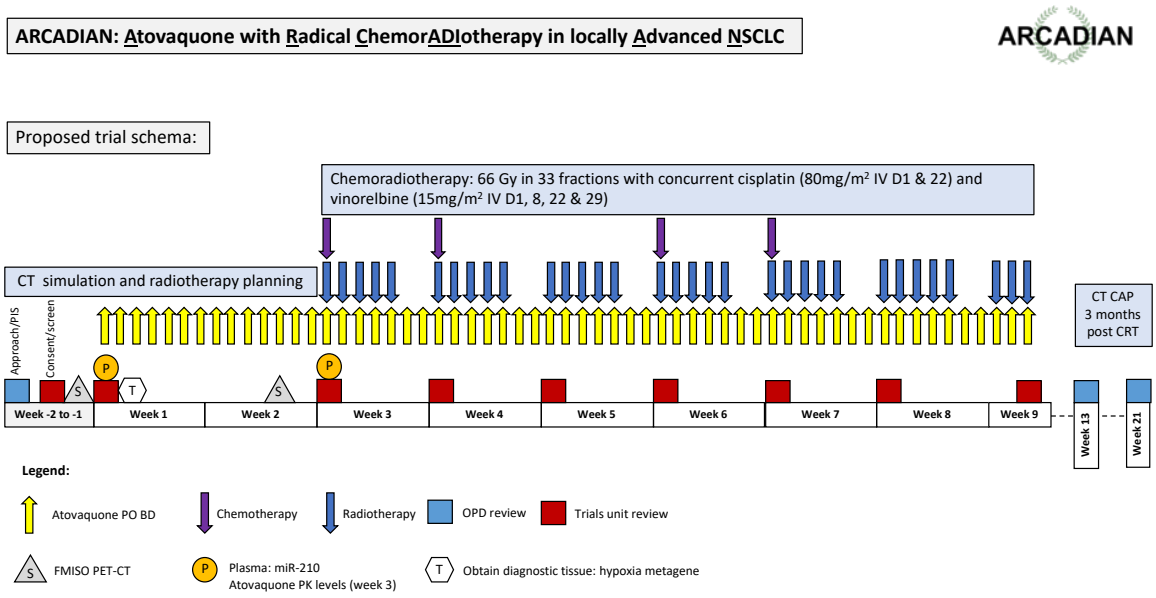


Figure 6.1: ARCADIAN trial schema
Abbreviations: D, day; PIS, patient information sheet; FMISO PET-CT, [18F]-fluoromisonidazole positron emission tomography-computed tomography; CT CAP, computed tomography of chest, abdomen and pelvis.

REFERENCES

[1] Bray F, Ferlay J, Soerjomataram I, Siegel RL, Torre LA, Jemal A. Global cancer statistics 2018: GLOBOCAN estimates of incidence and mortality worldwide for 36 cancers in 185 countries. CA Cancer J Clin 2018;68:394–424.

[2] Cancer Research UK. Lung cancer incidence statistics. https://www.cancerresearchuk.org/health-professional/cancer-statistics/statistics-by-cancer-type/lung-cancer/incidence (accessed September 2, 2019).

[3] Queen's University Belfast and Northern Ireland Cancer Registry http://www.qub.ac.uk/research-centres/nicr/ (accessed September 2, 2019).

[4] ISD Scotland. www.isdscotland.org/Health-Topics/Cancer/Publications/index.asp (accessed September 2, 2019).

[5] Welsh Cancer Intelligence and Surveillance Unit. http://www.wcisu.wales.nhs.uk/home (accessed September 2, 2019).

[6] Office for National Statistics. https://www.ons.gov.uk/peoplepopulationandcommunity/healthandsocialcare/conditionsanddiseases/bulletins/cancerregistrationstatisticsengland/final2016 (accessed September 2, 2019).

[7] Doll R, Hill AB. The Mortality of Doctors in Relation to Their Smoking Habits. Br Med J 1954;1:1451–5.

[8] Deaths from smoking. https://www.deathsfromsmoking.net/countries.html (accessed April 5, 2019).

[9] Agents classified by the IARC monographs. https://monographs.iarc.fr/agents-classified-by-the-iarc/ (accessed April 5, 2019).

[10] Coté ML, Liu M, Bonassi S, Neri M, Schwartz AG, Christiani DC, et al. Increased risk of lung cancer in individuals with a family history of the disease: A pooled analysis from the International Lung Cancer Consortium. Eur J Cancer 2012;48:1957–68.

[11] Travis WD, Brambilla E, Nicholson AG, Yatabe Y, Austin JHM, Beasley MB, et al. The 2015 World Health Organization Classification of Lung Tumors: Impact of Genetic, Clinical and Radiologic Advances Since the 2004 Classification. J Thorac Oncol 2015;10:1243–60.

[12] Devarakonda S, Morgensztern D, Govindan R. Genomic alterations in lung adenocarcinoma. Lancet Oncol 2015;16:e342–51.

[13] Herbst RS, Baas P, Kim D-W, Felip E, Pérez-Gracia JL, Han J-Y, et al. Pembrolizumab versus docetaxel for previously treated, PD-L1-positive, advanced non-small-cell lung cancer (KEYNOTE-010): a randomised controlled trial. Lancet 2016;387:1540–50.

[14] Reck M, Rodríguez-Abreu D, Robinson AG, Hui R, Csőszi T, Fülöp A, et al. Pembrolizumab versus Chemotherapy for PD-L1-Positive Non-Small-Cell Lung Cancer. N Engl J Med 2016;375:1823–33.

[15] Borghaei H, Paz-Ares L, Horn L, Spigel DR, Steins M, Ready NE, et al. Nivolumab versus Docetaxel in Advanced Nonsquamous Non-Small-Cell Lung Cancer. N Engl J Med 2015;373:1627–39.

[16] Antonia SJ, Villegas A, Daniel D, Vicente D, Murakami S, Hui R, et al. Overall Survival with Durvalumab after Chemoradiotherapy in Stage III NSCLC. N Engl J Med 2018;375:2342-50.

[17] Accuracy of Positron Emission Tomography for Diagnosis of Pulmonary Nodules and Mass Lesions: A Meta-analysis. JAMA 2001;285:914-24.

[18] Volpi S, Ali JM, Tasker A, Peryt A, Aresu G, Coonar AS. The role of positron emission tomography in the diagnosis, staging and response assessment of non-small cell lung cancer. Ann Transl Med 2018;6.

[19] Fischer B, Lassen U, Mortensen J, Larsen S, Loft A, Bertelsen A, et al. Preoperative Staging of Lung Cancer with Combined PET–CT. N Engl J Med 2009;361:32–9.

[20] Annema JT, Meerbeeck JP van, Rintoul RC, Dooms C, Deschepper E, Dekkers OM, et al. Mediastinoscopy vs Endosonography for Mediastinal Nodal Staging of Lung Cancer: A Randomized Trial. JAMA 2010;304:2245–52.

[21] Detterbeck FC, Boffa DJ, Kim AW, Tanoue LT. The Eighth Edition Lung Cancer Stage Classification. Chest 2017;151:193–203.

[22] McPhail S, Johnson S, Greenberg D, Peake M, Rous B. Stage at diagnosis and early mortality from cancer in England. Br J Cancer 2015;112:S108–15.

[23] Usman Ali M, Miller J, Peirson L, Fitzpatrick-Lewis D, Kenny M, Sherifali D, et al. Screening for lung cancer: A systematic review and meta-analysis. Prev Med 2016;89:301–14.

[24] National Lung Screening Trial Research Team. Reduced lung-cancer mortality with low-dose computed tomographic screening. N Engl J Med 2011;365:395–409.

[25] Office for National Statistics. https://www.ons.gov.uk/peoplepopulationandcommunity/healthandsocialcare/conditionsanddiseases/bulletins/cancersurvivalbystageatdiagnosisforenglandexperimentalstatistics/adultsdiagnosed20122013and2014andfollowedupto2015 (accessed September 5, 2019).

[26] Cancer Research UK. Lung cancer survival statistics. https://www.cancerresearchuk.org/health-professional/cancer-statistics/statistics-by-cancer-type/lung-cancer/survival (accessed September 5, 2019).

[27] Ginsberg RJ, Rubinstein LV. Randomized trial of lobectomy versus limited resection for T1 N0 non-small cell lung cancer. Ann Thorac Surg 1995;60:615–23.

[28] Fan J, Wang L, Jiang G-N, Gao W. Sublobectomy Versus Lobectomy for Stage I Non-Small-Cell Lung Cancer, A Meta-Analysis of Published Studies. Ann Surg Oncol 2012;19:661–8.

[29] Smith MA, Battafarano RJ, Meyers BF, Zoole JB, Cooper JD, Patterson GA. Prevalence of Benign Disease in Patients Undergoing Resection for Suspected Lung Cancer. Ann Thorac Surg 2006;81:1824–9.

[30] Pignon J-P, Tribodet H, Scagliotti GV, Douillard J-Y, Shepherd FA, Stephens RJ, et al. Lung Adjuvant Cisplatin Evaluation: A Pooled Analysis by the LACE Collaborative Group. J Clin Oncol 2008;26:3552–9.

[31] NSCLC Meta-analyses Collaborative Group. Adjuvant chemotherapy, with or without postoperative radiotherapy, in operable non-small-cell lung cancer: two meta-analyses of individual patient data. The Lancet 2010;375:1267–77.

[32] The Royal College of Radiologists. Radiotherapy dose fractionation third edition. https://www.rcr.ac.uk/publication/radiotherapy-dose-fractionation-third-edition (accessed September 3, 2019).

[33] Senthi S, Lagerwaard FJ, Haasbeek CJ, Slotman BJ, Senan S. Patterns of disease recurrence after stereotactic ablative radiotherapy for early stage non-small-cell lung cancer: a retrospective analysis. Lancet Oncol 2012;13:802–9.

[34] Lagerwaard FJ, Verstegen NE, Haasbeek CJA, Slotman BJ, Paul MA, Smit EF, et al. Outcomes of Stereotactic Ablative Radiotherapy in Patients With Potentially Operable Stage I Non-Small Cell Lung Cancer. Int J Radiat Oncol 2012;83:348–53.

[35] Onishi H, Shirato H, Nagata Y, Hiraoka M, Fujino M, Gomi K, et al. Stereotactic Body Radiotherapy (SBRT) for Operable Stage I Non–Small-Cell Lung Cancer: Can SBRT Be Comparable to Surgery? Int J Radiat Oncol 2011;81:1352–8.

[36] Bradley JD, Paulus R, Komaki R, Masters G, Blumenschein G, Schild S, et al. Standard-dose versus high-dose conformal radiotherapy with concurrent and consolidation carboplatin plus paclitaxel with or without cetuximab for patients with stage IIIA or IIIB non-small-cell lung cancer (RTOG 0617): a randomised, two-by-two factorial phase 3 study. Lancet Oncol 2015;16:187–99.

[37] Saunders M, Dische S, Barrett A, Harvey A, Griffiths G, Palmar M. Continuous, hyperfractionated, accelerated radiotherapy (CHART) versus conventional radiotherapy in non-small cell lung cancer: mature data from the randomised multicentre trial. CHART Steering committee. Radiother Oncol J Eur Soc Ther Radiol Oncol 1999;52:137–48.

[38] O'Rourke N, Roqué I Figuls M, Farré Bernadó N, Macbeth F. Concurrent chemoradiotherapy in non-small cell lung cancer. Cochrane Database Syst Rev 2010:CD002140.

[39] Aupérin A, Le Péchoux C, Rolland E, Curran WJ, Furuse K, Fournel P, et al. Meta-analysis of concomitant versus sequential radiochemotherapy in locally advanced non-small-cell lung cancer. J Clin Oncol 2010;28:2181–90.

[40] Machtay M, Paulus R, Moughan J, Komaki R, Bradley J effrey, Choy H, et al. Defining Local-Regional Control and Its Importance in Locally Advanced Non-small Cell Lung Carcinoma. J Thorac Oncol 2012;7:716–22.

[41] Ohri N. Radiotherapy Dosing for Locally Advanced Non-Small Cell Lung Carcinoma: "MTD" or "ALARA"? Front Oncol 2017;7:205.

[42] Landau DB, Hughes L, Baker A, Bates AT, Bayne MC, Counsell N, et al. IDEAL-CRT: A Phase 1/2 Trial of Isotoxic Dose-Escalated Radiation Therapy and Concurrent Chemotherapy in Patients with Stage II/III Non-Small Cell Lung Cancer. Int J Radiat Oncol Biol Phys 2016;95:1367–77.

[43] Withers HR. The Four R's of Radiotherapy. In: Lett JT, Adler H, editors. Adv. Radiat. Biol 1975;5:241–71.

[44] Pittman RN. Regulation of Tissue Oxygenation. San Rafael (CA): Morgan & Claypool Life Sciences 2011.

[45] Thomlinson RH, Gray LH. The Histological Structure of Some Human Lung Cancers and the Possible Implications for Radiotherapy. Br J Cancer 1955;9:539–49.

[46] Dunwoodie SL. The Role of Hypoxia in Development of the Mammalian Embryo. Dev Cell 2009;17:755–73.

[47] Jungermann K. Oxygen: modulator of metabolic zonation and disease of the liver. Hepatology 2003;31:255-60.

[48] Wang W, Winlove CP, Michel CC. Oxygen partial pressure in outer layers of skin of human fingernail folds. J Physiol 2003;549:855–63.

[49] Le Q-T, Chen E, Salim A, Cao H, Kong CS, Whyte R, et al. An Evaluation of Tumor Oxygenation and Gene Expression in Patients with Early Stage Non–Small Cell Lung Cancers. Clin Cancer Res 2006;12:1507–14.

[50] Müller M, Padberg W, Schindler E, Sticher J, Osmer C, Friemann S, et al. Renocortical tissue oxygen pressure measurements in patients undergoing living donor kidney transplantation. Anesth Analg 1998;87:474–6.

[51] Carreau A, Hafny-Rahbi BE, Matejuk A, Grillon C, Kieda C. Why is the partial oxygen pressure of human tissues a crucial parameter? Small molecules and hypoxia. J Cell Mol Med 2011;15:1239–53.

[52] Semenza GL. Hypoxia-inducible factors: mediators of cancer progression and targets for cancer therapy. Trends Pharmacol Sci 2012;33:207–14.

[53] Goldmann E. The Growth of Malignant Disease in Man and the Lower Animals, with special reference to the Vascular System. Proc R Soc Med 1908;1:1–13.

[54] Carmeliet P, Jain RK. Angiogenesis in cancer and other diseases. Nature 2000;407:249–57.

[55] Hashizume H, Baluk P, Morikawa S, McLean JW, Thurston G, Roberge S, et al. Openings between Defective Endothelial Cells Explain Tumor Vessel Leakiness. Am J Pathol 2000;156:1363–80.

[56] Dvorak HF, Nagy JA, Feng D, Brown LF, Dvorak AM. Vascular permeability factor/vascular endothelial growth factor and the significance of microvascular hyperpermeability in angiogenesis. Curr Top Microbiol Immunol 1999;237:97–132.

[57] Yang W-H, Xu J, Mu J-B, Xie J. Revision of the concept of anti-angiogenesis and its applications in tumor treatment. Chronic Dis Transl Med 2017;3:33–40.

[58] Jain RK. Antiangiogenesis Strategies Revisited: From Starving Tumors to Alleviating Hypoxia. Cancer Cell 2014;26:605–22.

[59] Brown JM. Evidence for acutely hypoxic cells in mouse tumours, and a possible mechanism of reoxygenation. Br J Radiol 1979;52:650–6.

[60] Michiels C, Tellier C, Feron O. Cycling hypoxia: A key feature of the tumor microenvironment. Biochim Biophys Acta BBA - Rev Cancer 2016;1866:76–86.

[61] Bennewith KL, Durand RE. Quantifying transient hypoxia in human tumor xenografts by flow cytometry. Cancer Res 2004;64:6183–9.

[62] Dewhirst MW. Relationships between Cycling Hypoxia, HIF-1, Angiogenesis and Oxidative Stress. Radiat Res 2009;172:653–65.

[63] Nehmeh SA, Lee NY, Schröder H, Squire O, Zanzonico PB, Erdi YE, et al. Reproducibility of Intratumor Distribution of 18F-fluoromisonidazole in Head and Neck Cancer. Int J Radiat Oncol Biol Phys 2008;70:235–42.

[64] Horsman MR, Mortensen LS, Petersen JB, Busk M, Overgaard J. Imaging hypoxia to improve radiotherapy outcome. Nat Rev Clin Oncol 2012;9:674–87.

[65] Vaupel P, Höckel M, Mayer A. Detection and Characterization of Tumor Hypoxia Using pO2 Histography. Antioxid Redox Signal 2007;9:1221–36.

[66] Falk SJ, Ward R, Bleehen NM. The influence of carbogen breathing on tumour tissue oxygenation in man evaluated by computerised p02 histography. Br J Cancer 1992;66:919–24.

[67] Nordsmark M, Bentzen SM, Rudat V, Brizel D, Lartigau E, Stadler P, et al. Prognostic value of tumor oxygenation in 397 head and neck tumors after primary radiation therapy. An international multi-center study. Radiother Oncol 2005;77:18–24.

[68] Movsas B, Chapman JD, Greenberg RE, Hanlon AL, Horwitz EM, Pinover WH, et al. Increasing levels of hypoxia in prostate carcinoma correlate significantly with increasing clinical stage and patient age: an Eppendorf pO(2) study. Cancer 2000;89:2018–24.

[69] Movsas B, Chapman JD, Hanlon AL, Horwitz EM, Greenberg RE, Stobbe C, et al. Hypoxic prostate/muscle pO2 ratio predicts for biochemical failure in patients with prostate cancer: preliminary findings. Urology 2002;60:634–9.

[70] Wang GL, Jiang BH, Rue EA, Semenza GL. Hypoxia-inducible factor 1 is a basic-helix-loop-helix-PAS heterodimer regulated by cellular O2 tension. Proc Natl Acad Sci U S A 1995;92:5510–4.

[71] Ohh M, Park CW, Ivan M, Hoffman MA, Kim TY, Huang LE, et al. Ubiquitination of hypoxia-inducible factor requires direct binding to the beta-domain of the von Hippel-Lindau protein. Nat Cell Biol 2000;2:423–7.

[72] Jaakkola P, Mole DR, Tian YM, Wilson MI, Gielbert J, Gaskell SJ, et al. Targeting of HIF-alpha to the von Hippel-Lindau ubiquitylation complex by O2-regulated prolyl hydroxylation. Science 2001;292:468–72.

[73] Liu W, Shen S-M, Zhao X-Y, Chen G-Q. Targeted genes and interacting proteins of hypoxia inducible factor-1. Int J Biochem Mol Biol 2012;3:165–78.

[74] Lando D, Peet DJ, Gorman JJ, Whelan DA, Whitelaw ML, Bruick RK. FIH-1 is an asparaginyl hydroxylase enzyme that regulates the transcriptional activity of hypoxia-inducible factor. Genes Dev 2002;16:1466–71.

[75] McNeill LA, Hewitson KS, Claridge TD, Seibel JF, Horsfall LE, Schofield CJ. Hypoxia-inducible factor asparaginyl hydroxylase (FIH-1) catalyses hydroxylation at the beta-carbon of asparagine-803. Biochem J 2002;367:571–5.

[76] Dayan F, Roux D, Brahimi-Horn MC, Pouyssegur J, Mazure NM. The oxygen sensor factor-inhibiting hypoxia-inducible factor-1 controls expression of distinct genes through the bifunctional transcriptional character of hypoxia-inducible factor-1alpha. Cancer Res 2006;66:3688–98.

[77] Koivunen P, Hirsilä M, Günzler V, Kivirikko KI, Myllyharju J. Catalytic properties of the asparaginyl hydroxylase (FIH) in the oxygen sensing pathway are distinct from those of its prolyl 4-hydroxylases. J Biol Chem 2004;279:9899–904.

[78] Wiesener MS, Jürgensen JS, Rosenberger C, Scholze CK, Hörstrup JH, Warnecke C, et al. Widespread hypoxia-inducible expression of HIF-2alpha in distinct cell populations of different organs. FASEB 2003;17:271–3.

[79] Ginouvès A, Ilc K, Macías N, Pouysségur J, Berra E. PHDs overactivation during chronic hypoxia “desensitizes” HIFalpha and protects cells from necrosis. Proc Natl Acad Sci U S A 2008;105:4745–50.

[80] Berra E, Benizri E, Ginouvès A, Volmat V, Roux D, Pouysségur J. HIF prolyl-hydroxylase 2 is the key oxygen sensor setting low steady-state levels of HIF-1α in normoxia. EMBO J 2003;22:4082–90.

[81] Dewhirst MW, Cao Y, Moeller B. Cycling hypoxia and free radicals regulate angiogenesis and radiotherapy response. Nat Rev Cancer 2008;8:425–37.

[82] Dengler VL, Galbraith M, Espinosa JM. Transcriptional Regulation by Hypoxia Inducible Factors. Crit Rev Biochem Mol Biol 2014;49:1–15.

[83] Choudhry H, Harris AL. Advances in Hypoxia-Inducible Factor Biology. Cell Metab 2018;27:281–98.

[84] Petrova V, Annicchiarico-Petruzzelli M, Melino G, Amelio I. The hypoxic tumour microenvironment. Oncogenesis 2018;7.

[85] LaGory EL, Giaccia AJ. The Ever-Expanding Role of HIF in Tumour and Stromal Biology. Nat Cell Biol 2016;18:356–65.

[86] Rankin EB, Nam J-M, Giaccia AJ. Hypoxia: Signaling in the Metastatic Cascade. Trends Cancer 2016;2:295–304.

[87] Gray LH, Conger AD, Ebert M, Hornsey S, Scott OCA. The Concentration of Oxygen Dissolved in Tissues at the Time of Irradiation as a Factor in Radiotherapy. Br J Radiol 1953;26:638–48.

[88] Wright EA, Howard-Flanders P. The influence of oxygen on the radiosensitivity of mammalian tissues. Acta Radiol 1957;48:26–32.

[89] Palcic B, Brosing JW, Skarsgard LD. Survival measurements at low doses: oxygen enhancement ratio. Br J Cancer 1982;46:980–4.

[90] Hall E, Giaccia A. Radiobiology for the Radiologist. Seventh edition. Philadelphia: Lippincott Williams & Wilkins; 2011.

[91] Steel G. Basic Clinical Radiobiology. Third edition. London: Oxford University Press; 2002.

[92] Alper T, Howard-Flanders P. Role of oxygen in modifying the radiosensitivity of E. coli B. Nature 1956;178:978–9.

[93] Held KD, Harrop HA, Michael BD. Effects of oxygen and sulphydryl-containing compounds on irradiated transforming DNA. II. Glutathione, cysteine and cysteamine. Int J Radiat Biol Relat Stud Phys Chem Med 1984;45:615–26.

[94] Hutchinson F. Sulfhydryl groups and the oxygen effect on irradiated dilute solutions of enzymes and nucleic acids. Radiat Res 1961;14:721–31.

[95] Chapman JD, Reuvers AP, Borsa J, Greenstock CL. Chemical radioprotection and radiosensitization of mammalian cells growing in vitro. Radiat Res 1973;56:291–306.

[96] Walsh JC, Lebedev A, Aten E, Madsen K, Marciano L, Kolb HC. The Clinical Importance of Assessing Tumor Hypoxia: Relationship of Tumor Hypoxia to Prognosis and Therapeutic Opportunities. Antioxid Redox Signal 2014;21:1516–54.

[97] Scharping NE, Menk AV, Whetstone RD, Zeng X, Delgoffe GM. Efficacy of PD-1 Blockade Is Potentiated by Metformin-Induced Reduction of Tumor Hypoxia. Cancer Immunol Res 2017;5:9–16.

[98] Doktorova H, Hrabeta J, Khalil MA, Eckschlager T. Hypoxia-induced chemoresistance in cancer cells: The role of not only HIF-1. Biomed Pap 2015;159:166–77.

[99] Dische S, Saunders M, Barrett A, Harvey A, Gibson D, Parmar M. A randomised multicentre trial of CHART versus conventional radiotherapy in head and neck cancer. Radiother Oncol 1997;44:123–36.

[100] Koukourakis MI, Bentzen SM, Giatromanolaki A, Wilson GD, Daley FM, Saunders MI, et al. Endogenous markers of two separate hypoxia response pathways (hypoxia inducible factor 2 alpha and carbonic anhydrase 9) are associated with radiotherapy failure in head and neck cancer patients recruited in the CHART randomized trial. J Clin Oncol 2006;24:727–35.

[101] Rischin D, Hicks RJ, Fisher R, Binns D, Corry J, Porceddu S, et al. Prognostic significance of [18F]-misonidazole positron emission tomography-detected tumor hypoxia in patients with advanced head and neck cancer randomly assigned to chemoradiation with or without tirapazamine: a substudy of Trans-Tasman Radiation Oncology Group Study 98.02. J Clin Oncol 2006;24:2098–104.

[102] Eschmann S-M, Paulsen F, Reimold M, Dittmann H, Welz S, Reischl G, et al. Prognostic impact of hypoxia imaging with 18F-misonidazole PET in non-small cell lung cancer and head and neck cancer before radiotherapy. J Nucl Med 2005;46:253–60.

[103] Milosevic M, Warde P, Menard C, Chung P, Toi A, Ishkanian A, et al. Tumor Hypoxia Predicts Biochemical Failure following Radiotherapy for Clinically Localized Prostate Cancer. Clin Cancer Res 2012;18:2108–14.

[104] Kolstad P. Intercapillary distance, oxygen tension and local recurrence in cervix cancer. Scand J Clin Lab Investig Suppl 1968;106:145–57.

[105] Gatenby RA, Kessler HB, Rosenblum JS, Coia LR, Moldofsky PJ, Hartz WH, et al. Oxygen distribution in squamous cell carcinoma metastases and its relationship to outcome of radiation therapy. Int J Radiat Oncol Biol Phys 1988;14:831–8.

[106] Kedderis GL, Miwa GT. The metabolic activation of nitroheterocyclic therapeutic agents. Drug Metab Rev 1988;19:33–62.

[107] Melo T, Ballinger JR, Rauth AM. Role of NADPH:cytochrome P450 reductase in the hypoxic accumulation and metabolism of BRU59-21, a technetium-99m-nitroimidazole for imaging tumor hypoxia. Biochem Pharmacol 2000;60:625–34.

[108] Wang Y, Gray JP, Mishin V, Heck DE, Laskin DL, Laskin JD. Role of cytochrome P450 reductase in nitrofurantoin-induced redox cycling and cytotoxicity. Free Radic Biol Med 2008;44:1169–79.

[109] Prekeges JL, Rasey JS, Grunbaum Z, Krohn KH. Reduction of fluoromisonidazole, a new imaging agent for hypoxia. Biochem Pharmacol 1991;42:2387–95.

[110] McClelland RA. Molecular Interactions and Biological Effects of the Products of Reduction of Nitroimidazoles. In: Adams GE, Breccia A, Fielden EM, Wardman P, editors. Drugs Redox Process. Boston, Springer US; 1990.

[111] Krohn KA, Link JM, Mason RP. Molecular Imaging of Hypoxia. J Nucl Med 2008;49:129S-148S.

[112] Kizaka-Kondoh S, Konse-Nagasawa H. Significance of nitroimidazole compounds and hypoxia-inducible factor-1 for imaging tumor hypoxia. Cancer Sci 2009;100:1366–73.

[113] Dische S. Chemical sensitizers for hypoxic cells: a decade of experience in clinical radiotherapy. Radiother Oncol 1985;3:97–115.

[114] Lord EM, Harwell L, Koch CJ. Detection of hypoxic cells by monoclonal antibody recognizing 2-nitroimidazole adducts. Cancer Res 1993;53:5721–6.

[115] Raleigh JA, Chou SC, Arteel GE, Horsman MR. Comparisons among pimonidazole binding, oxygen electrode measurements, and radiation response in C3H mouse tumors. Radiat Res 1999;151:580–9.

[116] Chapman JD. Hypoxic sensitizers--implications for radiation therapy. N Engl J Med 1979;301:1429–32.

[117] Martin GV, Cerqueira MD, Caldwell JH, Rasey JS, Embree L, Krohn KA. Fluoromisonidazole. A metabolic marker of myocyte hypoxia. Circ Res 1990;67:240–4.

[118] Rasey JS, Martin GV, Krohn KA. Imaging of Hypoxia. Dordrect, Springer; 1999.

[119] Martin GV, Caldwell JH, Graham MM, Grierson JR, Kroll K, Cowan MJ, et al. Noninvasive detection of hypoxic myocardium using fluorine-18-fluoromisonidazole and positron emission tomography. J Nucl Med 1992;33:2202–8.

[120] Dubois L, Landuyt W, Haustermans K, Dupont P, Bormans G, Vermaelen P, et al. Evaluation of hypoxia in an experimental rat tumour model by [(18)F]fluoromisonidazole PET and immunohistochemistry. Br J Cancer 2004;91:1947–54.

[121] Rajendran JG, Krohn KA. Imaging hypoxia and angiogenesis in tumors. Radiol Clin North Am 2005;43:169–87.

[122] Gagel B, Reinartz P, Dimartino E, Zimny M, Pinkawa M, Maneschi P, et al. pO(2) Polarography versus positron emission tomography ([(18)F] fluoromisonidazole, [(18)F]-2-fluoro-2'-deoxyglucose). An appraisal of radiotherapeutically relevant hypoxia. Strahlenther Onkol 2004;180:616–22.

[123] Rajendran J, Krohn K. F18 Fluoromisonidazole for Imaging Tumor Hypoxia: Imaging the Microenvironment for Personalized Cancer Therapy. Semin Nucl Med 2015;45:151–62.

[124] Fleming IN, Manavaki R, Blower PJ, West C, Williams KJ, Harris AL, et al. Imaging tumour hypoxia with positron emission tomography. Br J Cancer 2015;112:238–50.

[125] McGowan DR, Skwarski M, Bradley KM, Campo L, Fenwick JD, Gleeson FV, et al. Buparlisib with thoracic radiotherapy and its effect on tumour hypoxia: A phase I study in patients with advanced non-small cell lung carcinoma. Eur J Cancer 1990 2019;113:87–95.

[126] Koh WJ, Rasey JS, Evans ML, Grierson JR, Lewellen TK, Graham MM, et al. Imaging of hypoxia in human tumors with [F-18]fluoromisonidazole. Int J Radiat Oncol Biol Phys 1992;22:199–212.

[127] Grkovski M, Schwartz J, Rimner A, Schöder H, Carlin SD, Zanzonico PB, et al. Reproducibility of 18F-fluoromisonidazole intratumour distribution in non-small cell lung cancer. EJNMMI Res 2016;6.

[128] Okamoto S, Shiga T, Yasuda K, Ito YM, Magota K, Kasai K, et al. High Reproducibility of Tumor Hypoxia Evaluated by 18F-Fluoromisonidazole PET for Head and Neck Cancer. J Nucl Med 2013;54:201–7.

[129] Pastorek J, Pastoreková S, Callebaut I, Mornon JP, Zelník V, Opavský R, et al. Cloning and characterization of MN, a human tumor-associated protein with a domain homologous to carbonic anhydrase and a putative helix-loop-helix DNA binding segment. Oncogene 1994;9:2877–88.

[130] Wykoff CC, Beasley NJP, Watson PH, Turner KJ, Pastorek J, Sibtain A, et al. Hypoxia-inducible Expression of Tumor-associated Carbonic Anhydrases. Cancer Res 2000;60:7075–83.

[131] Giatromanolaki A, Koukourakis MI, Sivridis E, Pastorek J, Wykoff CC, Gatter KC, et al. Expression of hypoxia-inducible carbonic anhydrase-9 relates to angiogenic pathways and independently to poor outcome in non-small cell lung cancer. Cancer Res 2001;61:7992–8.

[132] Kaluz S, Kaluzová M, Liao S-Y, Lerman M, Stanbridge EJ. Transcriptional control of the tumor- and hypoxia-marker carbonic anhydrase 9: a one transcription factor (HIF-1) show? Biochim Biophys Acta 2009;1795:162–72.

[133] Olive PL, Aquino-Parsons C, MacPhail SH, Liao SY, Raleigh JA, Lerman MI, et al. Carbonic anhydrase 9 as an endogenous marker for hypoxic cells in cervical cancer. Cancer Res 2001;61:8924–9.

[134] Gillies RM, Robinson SP, McPhail LD, Carter ND, Murray JF. Immunohistochemical assessment of intrinsic and extrinsic markers of hypoxia in reproductive tissue: differential expression of HIF1α and HIF2α in rat oviduct and endometrium. J Mol Histol 2011;42:341–54.

[135] Hughes VS, Wiggins JM, Siemann DW. Tumor oxygenation and cancer therapy—then and now. Br J Radiol 2018;92:20170955.

[136] Sobhanifar S, Aquino-Parsons C, Stanbridge EJ, Olive P. Reduced Expression of Hypoxia-Inducible Factor-1α in Perinecrotic Regions of Solid Tumors. Cancer Res 2005;65:7259–66.

[137] Buffa FM, Harris AL, West CM, Miller CJ. Large meta-analysis of multiple cancers reveals a common, compact and highly prognostic hypoxia metagene. Br J Cancer 2010;102:428–35.

[138] Winter SC, Buffa FM, Silva P, Miller C, Valentine HR, Turley H, et al. Relation of a Hypoxia Metagene Derived from Head and Neck Cancer to Prognosis of Multiple Cancers. Cancer Res 2007;67:3441–9.

[139] Harris BHL, Barberis A, West CML, Buffa FM. Gene Expression Signatures as Biomarkers of Tumour Hypoxia. Clin Oncol 2015;27:547–60.

[140] Dunst J, Stadler P, Becker A, Kuhnt T, Lautenschläger C, Molls M, et al. Tumor hypoxia and systemic levels of vascular endothelial growth factor (VEGF) in head and neck cancers. Strahlenther Onkol 2001;177:469–73.

[141] Ostheimer C, Bache M, Güttler A, Kotzsch M, Vordermark D. A pilot study on potential plasma hypoxia markers in the radiotherapy of non-small cell lung cancer. Osteopontin, carbonic anhydrase IX and vascular endothelial growth factor. Strahlenther Onkol 2014;190:276–82.

[142] İlie M, Mazure NM, Hofman V, Ammadi RE, Ortholan C, Bonnetaud C, et al. High levels of carbonic anhydrase IX in tumour tissue and plasma are biomarkers of poor prognostic in patients with non-small cell lung cancer. Br J Cancer 2010;102:1627–35.

[143] Zhao H, Chen Q, Alam A, Cui J, Suen KC, Soo AP, et al. The role of osteopontin in the progression of solid organ tumour. Cell Death Dis 2018;9.

[144] Zhu Y, Denhardt DT, Cao H, Sutphin PD, Koong AC, Giaccia AJ, et al. Hypoxia upregulates osteopontin expression in NIH-3T3 cells via a Ras-activated enhancer. Oncogene 2005;24:6555–63.

[145] Bache M, Reddemann R, Said HM, Holzhausen H-J, Taubert H, Becker A, et al. Immunohistochemical detection of osteopontin in advanced head-and-neck cancer: prognostic role and correlation with oxygen electrode measurements, hypoxia-inducible-factor-1alpha-related markers, and hemoglobin levels. Int J Radiat Oncol Biol Phys 2006;66:1481–7.

[146] Nordsmark M, Eriksen JG, Gebski V, Alsner J, Horsman MR, Overgaard J. Differential risk assessments from five hypoxia specific assays: The basis for biologically adapted individualized radiotherapy in advanced head and neck cancer patients. Radiother Oncol 2007;83:389–97.

[147] Petrik D, Lavori PW, Cao H, Zhu Y, Wong P, Christofferson E, et al. Plasma Osteopontin Is an Independent Prognostic Marker for Head and Neck Cancers. J Clin Oncol 2006;24:5291–7.

[148] Overgaard J, Eriksen JG, Nordsmark M, Alsner J, Horsman MR, Danish Head and Neck Cancer Study Group. Plasma osteopontin, hypoxia, and response to the hypoxia sensitiser nimorazole in radiotherapy of head and neck cancer: results from the DAHANCA 5 randomised double-blind placebo-controlled trial. Lancet Oncol 2005;6:757–64.

[149] Le Q-T, Sutphin PD, Raychaudhuri S, Yu SCT, Terris DJ, Lin HS, et al. Identification of Osteopontin as a Prognostic Plasma Marker for Head and Neck Squamous Cell Carcinomas. Clin Cancer Res 2003;9:59–67.

[150] Wang Y, Yang J, Liu H, Bi J-R, Liu Y, Chen Y-Y, et al. The association between osteopontin and survival in non-small-cell lung cancer patients: a meta-analysis of 13 cohorts. OncoTargets Ther 2015;8:3513–21.

[151] Krol J, Loedige I, Filipowicz W. The widespread regulation of microRNA biogenesis, function and decay. Nat Rev Genet 2010;11:597–610.

[152] Dang K, Myers KA. The Role of Hypoxia-Induced miR-210 in Cancer Progression. Int J Mol Sci 2015;16:6353–72.

[153] Chakraborty C, Das S. Profiling cell-free and circulating miRNA: a clinical diagnostic tool for different cancers. Tumour Biol 2016;37:5705–14.

[154] Madhavan D, Peng C, Wallwiener M, Zucknick M, Nees J, Schott S, et al. Circulating miRNAs with prognostic value in metastatic breast cancer and for early detection of metastasis. Carcinogenesis 2016;37:461–70.

[155] Jiang M, Li X, Quan X, Li X, Zhou B. Clinically Correlated MicroRNAs in the Diagnosis of Non-Small Cell Lung Cancer: A Systematic Review and Meta-Analysis. BioMed Res Int 2018;2018.

[156] Świtlik WZ, Karbownik MS, Suwalski M, Kozak J, Szemraj J. Serum miR-210-3p as a Potential Noninvasive Biomarker of Lung Adenocarcinoma: A Preliminary Study. Genet Test Mol Biomark 2019;23:353–8.

[157] Overgaard J. Hypoxic modification of radiotherapy in squamous cell carcinoma of the head and neck – A systematic review and meta-analysis. Radiother Oncol 2011;100:22–32.

[158] Bennett M, Feldmeier J, Smee R, Milross C. Hyperbaric oxygenation for tumour sensitisation to radiotherapy. Cochrane Database Syst Rev 2005:CD005007.

[159] Harrison LB, Chadha M, Hill RJ, Hu K, Shasha D. Impact of tumor hypoxia and anemia on radiation therapy outcomes. The Oncologist 2002;7:492–508.

[160] Lee WR, Berkey B, Marcial V, Fu KK, Cooper JS, Vikram B, et al. Anemia is associated with decreased survival and increased locoregional failure in patients with locally advanced head and neck carcinoma: a secondary analysis of RTOG 85-27. Int J Radiat Oncol Biol Phys 1998;42:1069–75.

[161] Varlotto J, Stevenson MA. Anemia, tumor hypoxemia, and the cancer patient. Int J Radiat Oncol 2005;63:25–36.

[162] Henke M, Laszig R, Rübe C, Schäfer U, Haase K-D, Schilcher B, et al. Erythropoietin to treat head and neck cancer patients with anaemia undergoing radiotherapy: randomised, double-blind, placebo-controlled trial. Lancet 2003;362:1255–60.

[163] Henke M, Mattern D, Pepe M, Bézay C, Weissenberger C, Werner M, et al. Do erythropoietin receptors on cancer cells explain unexpected clinical findings? J Clin Oncol 2006;24:4708–13.

[164] Kaanders JHAM, Pop LAM, Marres HAM, Bruaset I, van den Hoogen FJA, Merkx MAW, et al. ARCON: experience in 215 patients with advanced head-and-neck cancer. Int J Radiat Oncol Biol Phys 2002;52:769–78.

[165] Hoskin P, Rojas A, Saunders M. Accelerated radiotherapy, carbogen, and nicotinamide (ARCON) in the treatment of advanced bladder cancer: mature results of a Phase II nonrandomized study. Int J Radiat Oncol Biol Phys 2009;73:1425–31.

[166] Janssens GO, Rademakers SE, Terhaard CH, Doornaert PA, Bijl HP, van den Ende P, et al. Accelerated radiotherapy with carbogen and nicotinamide for laryngeal cancer: results of a phase III randomized trial. J Clin Oncol 2012;30:1777–83.

[167] Hoskin PJ, Rojas AM, Bentzen SM, Saunders MI. Radiotherapy With Concurrent Carbogen and Nicotinamide in Bladder Carcinoma. J Clin Oncol 2010.

[168] Qayum N, Muschel RJ, Im JH, Balathasan L, Koch CJ, Patel S, et al. Tumor Vascular Changes Mediated by Inhibition of Oncogenic Signaling. Cancer Res 2009;69:6347–54.

[169] Cerniglia GJ, Pore N, Tsai JH, Schultz S, Mick R, Choe R, et al. Epidermal Growth Factor Receptor Inhibition Modulates the Microenvironment by Vascular Normalization to Improve Chemotherapy and Radiotherapy Efficacy. PLOS ONE 2009;4:e6539.

[170] Fokas E, Im JH, Hill S, Yameen S, Stratford M, Beech J, et al. Dual Inhibition of the PI3K/mTOR Pathway Increases Tumor Radiosensitivity by Normalizing Tumor Vasculature. Cancer Res 2012;72:239–48.

[171] Asquith JC, Watts ME, Patel K, Smithen CE, Adams GE. Electron affinic sensitization. V. Radiosensitization of hypoxic bacteria and mammalian cells in vitro by some nitroimidazoles and nitropyrazoles. Radiat Res 1974;60:108–18.

[172] Mäntylä MJ, Nordman EM, Ruotsalainen PJ, Kylmämaa TT. Misonidazole and radiotherapy in lung cancer: A randomized double-blind trial. Int J Radiat Oncol Biol Phys 1982;8:1719–20.

[173] Bleehen NM, Wiltshire CR, Plowman PN, Watson JV, Gleave JR, Holmes AE, et al. A randomized study of misonidazole and radiotherapy for grade 3 and 4 cerebral astrocytoma. Br J Cancer 1981;43:436–42.

[174] Overgaard J, Bentzen SM, Kolstad P, Kjoerstad K, Davy M, Bertelsen K, et al. Misonidazole combined with radiotherapy in the treatment of carcinoma of the uterine cervix. Int J Radiat Oncol Biol Phys 1989;16:1069–72.

[175] Papavasiliou C, Yiogarakis D, Davillas N, Seretakis L, Pappas J, Licourinas M, et al. Treatment of bladder carcinoma with irradiation combined with misonidazole. Int J Radiat Oncol Biol Phys 1983;9:1631–3.

[176] Overgaard J, Hansen HS, Andersen AP, Hjelm-Hansen M, Jørgensen K, Sandberg E, et al. Misonidazole combined with split-course radiotherapy in the treatment of invasive carcinoma of larynx and pharynx: report from the DAHANCA 2 study. Int J Radiat Oncol Biol Phys 1989;16:1065–8.

[177] Melgaard B, Køhler O, Sand Hansen H, Overgaard J, Munck-Hansen J, Paulson OB. Misonidazole neuropathy. A prospective study. J Neurooncol 1988;6:227–30.

[178] Overgaard J, Hansen HS, Overgaard M, Bastholt L, Berthelsen A, Specht L, et al. A randomized double-blind phase III study of nimorazole as a hypoxic radiosensitizer of primary radiotherapy in supraglottic larynx and pharynx carcinoma. Results of the Danish Head and Neck Cancer Study (DAHANCA) Protocol 5-85. Radiother Oncol 1998;46:135–46.

[179] Bentzen J, Toustrup K, Eriksen JG, Primdahl H, Andersen LJ, Overgaard J. Locally advanced head and neck cancer treated with accelerated radiotherapy, the hypoxic modifier nimorazole and weekly cisplatin. Results from the DAHANCA 18 phase II study. Acta Oncol 2015;54:1001–7.

[180] Metwally MAH, Frederiksen KD, Overgaard J. Compliance and toxicity of the hypoxic radiosensitizer nimorazole in the treatment of patients with head and neck squamous cell carcinoma (HNSCC). Acta Oncol Stockh Swed 2014;53:654–61.

[181] Thomson D, Yang H, Baines H, Miles E, Bolton S, West C, et al. NIMRAD - a phase III trial to investigate the use of nimorazole hypoxia modification with intensity-modulated radiotherapy in head and neck cancer. Clin Oncol 2014;26:344–7.

[182] Zeman EM, Brown JM, Lemmon MJ, Hirst VK, Lee WW. SR-4233: a new bioreductive agent with high selective toxicity for hypoxic mammalian cells. Int J Radiat Oncol Biol Phys 1986;12:1239–42.

[183] DiSilvestro PA, Ali S, Craighead PS, Lucci JA, Lee Y-C, Cohn DE, et al. Phase III randomized trial of weekly cisplatin and irradiation versus cisplatin and tirapazamine and irradiation in stages IB2, IIA, IIB, IIIB, and IVA cervical carcinoma limited to the pelvis: a Gynecologic Oncology Group study. J Clin Oncol 2014;32:458–64.

[184] Rischin D, Peters LJ, O'Sullivan B, Giralt J, Fisher R, Yuen K, et al. Tirapazamine, cisplatin, and radiation versus cisplatin and radiation for advanced squamous cell carcinoma of the head and neck (TROG 02.02, HeadSTART): a phase III trial of the Trans-Tasman Radiation Oncology Group. J Clin Oncol 2010;28:2989–95.

[185] Lunt SY, Vander Heiden MG. Aerobic Glycolysis: Meeting the Metabolic Requirements of Cell Proliferation. Annu Rev Cell Dev Biol 2011;27:441–64.

[186] Kühlbrandt W. Structure and function of mitochondrial membrane protein complexes. BMC Biol 2015;13:89.

[187] Lumen Learning, Metabolic Pathways. Originally from OpenStax Microbiology. https://courses.lumenlearning.com/microbiology/chapter/metabolic-pathways (accessed September 19, 2019).

[188] Jones RG, Thompson CB. Tumor suppressors and cell metabolism: a recipe for cancer growth. Genes Dev 2009;23:537–48.

[189] Hanahan D, Weinberg RA. Hallmarks of Cancer: The Next Generation. Cell 2011;144:646–74.

[190] Koppenol WH, Bounds PL, Dang CV. Otto Warburg's contributions to current concepts of cancer metabolism. Nat Rev Cancer 2011;11:325–37.

[191] DeBerardinis RJ, Lum JJ, Hatzivassiliou G, Thompson CB. The Biology of Cancer: Metabolic Reprogramming Fuels Cell Growth and Proliferation. Cell Metab 2008;7:11–20.

[192] Elstrom RL, Bauer DE, Buzzai M, Karnauskas R, Harris MH, Plas DR, et al. Akt Stimulates Aerobic Glycolysis in Cancer Cells. Cancer Res 2004;64:3892–9.

[193] Osthus RC, Shim H, Kim S, Li Q, Reddy R, Mukherjee M, et al. Deregulation of Glucose Transporter 1 and Glycolytic Gene Expression by c-Myc. J Biol Chem 2000;275:21797–800.

[194] Dang CV, Lewis BC, Dolde C, Dang G, Shim H. Oncogenes in tumor metabolism, tumorigenesis, and apoptosis. J Bioenerg Biomembr 1997;29:345–54.

[195] Dang CV, Semenza GL. Oncogenic alterations of metabolism. Trends Biochem Sci 1999;24:68–72.

[196] Semenza GL. HIF-1: upstream and downstream of cancer metabolism. Curr Opin Genet Dev 2010;20:51–6.

[197] Kim J, Tchernyshyov I, Semenza GL, Dang CV. HIF-1-mediated expression of pyruvate dehydrogenase kinase: A metabolic switch required for cellular adaptation to hypoxia. Cell Metab 2006;3:177–85.

[198] Fukuda R, Zhang H, Kim J, Shimoda L, Dang CV, Semenza GL. HIF-1 regulates cytochrome oxidase subunits to optimize efficiency of respiration in hypoxic cells. Cell 2007;129:111–22.

[199] Orang AV, Petersen J, McKinnon RA, Michael MZ. Micromanaging aerobic respiration and glycolysis in cancer cells. Mol Metab 2019;23:98–126.

[200] Yu M. Generation, function and diagnostic value of mitochondrial DNA copy number alterations in human cancers. Life Sci 2011;89:65–71.

[201] Gaude E, Frezza C. Tissue-specific and convergent metabolic transformation of cancer correlates with metastatic potential and patient survival. Nat Commun 2016;7:13041.

[202] Moreno-Sánchez R, Rodríguez-Enríquez S, Marín-Hernández A, Saavedra E. Energy metabolism in tumor cells. FEBS J 2007;274:1393–418.

[203] Weinberg SE, Chandel NS. Targeting mitochondria metabolism for cancer therapy. Nat Chem Biol 2015;11:9–15.

[204] Zu XL, Guppy M. Cancer metabolism: facts, fantasy, and fiction. Biochem Biophys Res Commun 2004;313:459–65.

[205] Mookerjee SA, Gerencser AA, Nicholls DG, Brand MD. Quantifying intracellular rates of glycolytic and oxidative ATP production and consumption using extracellular flux measurements. J Biol Chem 2017;292:7189–207.

[206] Moreno-Sánchez R, Rodríguez-Enríquez S, Saavedra E, Marín-Hernández A, Gallardo-Pérez JC. The bioenergetics of cancer: Is glycolysis the main ATP supplier in all tumor cells? BioFactors 2009;35:209–25.

[207] Vaupel P, Mayer A. Availability, not respiratory capacity governs oxygen consumption of solid tumors. Int J Biochem Cell Biol 2012;44:1477–81.

[208] Reznik E, Miller ML, Şenbabaoğlu Y, Riaz N, Sarungbam J, Tickoo SK, et al. Mitochondrial DNA copy number variation across human cancers. ELife 2016;5.

[209] Larman TC, DePalma SR, Hadjipanayis AG, Cancer Genome Atlas Research Network, Protopopov A, Zhang J, et al. Spectrum of somatic mitochondrial mutations in five cancers. Proc Natl Acad Sci U S A 2012;109:14087–91.

[210] Birsoy K, Possemato R, Lorbeer FK, Bayraktar EC, Thiru P, Yucel B, et al. Metabolic determinants of cancer cell sensitivity to glucose limitation and biguanides. Nature 2014;508:108–12.

[211] Cavalli LR, Varella-Garcia M, Liang BC. Diminished tumorigenic phenotype after depletion of mitochondrial DNA. Cell Growth Differ Mol Biol 1997;8:1189–98.

[212] Tan AS, Baty JW, Dong L-F, Bezawork-Geleta A, Endaya B, Goodwin J, et al. Mitochondrial Genome Acquisition Restores Respiratory Function and Tumorigenic Potential of Cancer Cells without Mitochondrial DNA. Cell Metab 2015;21:81–94.

[213] Viale A, Corti D, Draetta GF. Tumors and Mitochondrial Respiration: A Neglected Connection. Cancer Res 2015;75:3687–91.

[214] Szatrowski TP, Nathan CF. Production of large amounts of hydrogen peroxide by human tumor cells. Cancer Res 1991;51:794–8.

[215] Ames BN, Shigenaga MK, Hagen TM. Oxidants, antioxidants, and the degenerative diseases of aging. Proc Natl Acad Sci U S A 1993;90:7915–22.

[216] Sullivan LB, Chandel NS. Mitochondrial reactive oxygen species and cancer. Cancer Metab 2014;2.

[217] Secomb TW, Hsu R, Ong ET, Gross JF, Dewhirst MW. Analysis of the effects of oxygen supply and demand on hypoxic fraction in tumors. Acta Oncol 1995;34:313–6.

[218] Grimes DR, Kelly C, Bloch K, Partridge M. A method for estimating the oxygen consumption rate in multicellular tumour spheroids. J R Soc Interface 2014;11:20131124.

[219] Ashton TM, Fokas E, Kunz-Schughart LA, Folkes LK, Anbalagan S, Huether M, et al. The anti-malarial atovaquone increases radiosensitivity by alleviating tumour hypoxia. Nat Commun 2016;7:12308.

[220] Ashton TM, McKenna WG, Kunz-Schughart LA, Higgins GS. Oxidative Phosphorylation as an Emerging Target in Cancer Therapy. Clin Cancer Res 2018;24:2482–90.

[221] Hunter RW, Hughey CC, Lantier L, Sundelin EI, Peggie M, Zeqiraj E, et al. Metformin reduces liver glucose production by inhibition of fructose-1-6-bisphosphatase. Nat Med 2018;24:1395.

[222] Cao X, Wu Y, Wang J, Liu K, Wang X. The Effect of Metformin on Mortality Among Diabetic Cancer Patients: A Systematic Review and Meta-analysis. JNCI Cancer Spectr 2017;1.

[223] Koritzinsky M. Metformin: A Novel Biological Modifier of Tumor Response to Radiation Therapy. Int J Radiat Oncol Biol Phys 2015;93:454–64.

[224] Pernicova I, Korbonits M. Metformin--mode of action and clinical implications for diabetes and cancer. Nat Rev Endocrinol 2014;10:143–56.

[225] Belfiore A, Frasca F, Pandini G, Sciacca L, Vigneri R. Insulin receptor isoforms and insulin receptor/insulin-like growth factor receptor hybrids in physiology and disease. Endocr Rev 2009;30:586–623.

[226] Algire C, Moiseeva O, Deschênes-Simard X, Amrein L, Petruccelli L, Birman E, et al. Metformin reduces endogenous reactive oxygen species and associated DNA damage. Cancer Prev Res 2012;5:536–43.

[227] Dowling RJO, Zakikhani M, Fantus IG, Pollak M, Sonenberg N. Metformin inhibits mammalian target of rapamycin-dependent translation initiation in breast cancer cells. Cancer Res 2007;67:10804–12.

[228] Owen MR, Doran E, Halestrap AP. Evidence that metformin exerts its anti-diabetic effects through inhibition of complex 1 of the mitochondrial respiratory chain. Biochem J 2000;348:607–14.

[229] Zannella VE, Dal Pra A, Muaddi H, McKee TD, Stapleton S, Sykes J, et al. Reprogramming metabolism with metformin improves tumor oxygenation and radiotherapy response. Clin Cancer Res 2013;19:6741–50.

[230] De Bruycker S, Vangestel C, Van den Wyngaert T, Pauwels P, Wyffels L, Staelens S, et al. 18F-Flortanidazole Hypoxia PET Holds Promise as a Prognostic and Predictive Imaging Biomarker in a Lung Cancer Xenograft Model Treated with Metformin and Radiotherapy. J Nucl Med 2019;60:34–40.

[231] Lord SR, Cheng W-C, Liu D, Gaude E, Haider S, Metcalf T, et al. Integrated Pharmacodynamic Analysis Identifies Two Metabolic Adaption Pathways to Metformin in Breast Cancer. Cell Metab 2018;28:679-688.e4.

[232] Tsakiridis T, Hu C, Skinner HD, Santana-Davila R, Lu B, Erasmus JJ, et al. Initial reporting of NRG-LU001 (NCT02186847), randomized phase II trial of concurrent chemoradiotherapy (CRT) +/- metformin in locally advanced Non-Small Cell Lung Cancer (NSCLC). J Clin Oncol 2019;37:8502–8502.

[233] Kirkpatrick DL, Powis G. Clinically Evaluated Cancer Drugs Inhibiting Redox Signaling. Antioxid Redox Signal 2017;26:262–73.

[234] Benej M, Hong X, Vibhute S, Scott S, Wu J, Graves E, et al. Papaverine and its derivatives radiosensitize solid tumors by inhibiting mitochondrial metabolism. Proc Natl Acad Sci U S A 2018;115:10756–61.

[235] Hudson AT, Dickins M, Ginger CD, Gutteridge WE, Holdich T, Hutchinson DB, et al. 566C80: a potent broad spectrum anti-infective agent with activity against malaria and opportunistic infections in AIDS patients. Drugs Exp Clin Res 1991;17:427–35.

[236] Fiorillo M, Lamb R, Tanowitz HB, Mutti L, Krstic-Demonacos M, Cappello AR, et al. Repurposing atovaquone: Targeting mitochondrial complex III and OXPHOS to eradicate cancer stem cells. Oncotarget 2016;7:34084–99.

[237] LaRocque RC, Rao SR, Lee J, Ansdell V, Yates JA, Schwartz BS, et al. Global TravEpiNet: a national consortium of clinics providing care to international travelers--analysis of demographic characteristics, travel destinations, and pretravel healthcare of high-risk US international travelers, 2009-2011. Clin Infect Dis 2012;54:455–62.

[238] Fry M, Pudney M. Site of action of the antimalarial hydroxynaphthoquinone, 2-[trans-4-(4'-chlorophenyl) cyclohexyl]-3-hydroxy-1,4-naphthoquinone (566C80). Biochem Pharmacol 1992;43:1545–53.

[239] Srivastava IK, Rottenberg H, Vaidya AB. Atovaquone, a broad spectrum antiparasitic drug, collapses mitochondrial membrane potential in a malarial parasite. J Biol Chem 1997;272:3961–6.

[240] Birth D, Kao W-C, Hunte C. Structural analysis of atovaquone-inhibited cytochrome bc_1 complex reveals the molecular basis of antimalarial drug action. Nat Commun 2014;5:4029.

[241] Mather MW, Darrouzet E, Valkova-Valchanova M, Cooley JW, McIntosh MT, Daldal F, et al. Uncovering the molecular mode of action of the antimalarial drug atovaquone using a bacterial system. J Biol Chem 2005;280:27458–65.

[242] Painter HJ, Morrisey JM, Mather MW, Vaidya AB. Specific role of mitochondrial electron transport in blood-stage Plasmodium falciparum. Nature 2007;446:88–91.

[243] MEPRON (atovaquone) Suspension GSK Source. https://gsksource.com/pharma/content/gsk/source/us/en/brands/mepron.html (accessed September 5, 2019).

[244] Wellvone 750mg/5ml oral suspension - Summary of Product Characteristics. https://www.medicines.org.uk/emc/product/952/smpc (accessed September 5, 2019).

[245] Cheung TW. Overdose of atovaquone in a patient with AIDS. AIDS 1999;13:1984–5.

[246] Copay AG, Subach BR, Glassman SD, Polly DW, Schuler TC. Understanding the minimum clinically important difference: a review of concepts and methods. Spine 2007;7:541–6.

[247] Yamane T, Aikawa M, Yasuda M, Fukushima K, Seto A, Okamoto K, et al. [18F]FMISO PET/CT as a preoperative prognostic factor in patients with pancreatic cancer. EJNMMI Res 2019;9.

[248] Papież BW, Heinrich MP, Fehrenbach J, Risser L, Schnabel JA. An implicit sliding-motion preserving regularisation via bilateral filtering for deformable image registration. Med Image Anal 2014;18:1299–311.

[249] Sahani DV, Kalva SP, Hamberg LM, Hahn PF, Willett CG, Saini S, et al. Assessing Tumor Perfusion and Treatment Response in Rectal Cancer with Multisection CT: Initial Observations. Radiology 2005;234:785–92.

[250] Song J, Bai Z, Han W, Zhang J, Meng H, Bi J, et al. Identification of suitable reference genes for qPCR analysis of serum microRNA in gastric cancer patients. Dig Dis Sci 2012;57:897–904.

[251] McDermott AM, Kerin MJ, Miller N. Identification and validation of miRNAs as endogenous controls for RQ-PCR in blood specimens for breast cancer studies. PloS One 2013;8:e83718.

[252] Shen J, Todd NW, Zhang H, Yu L, Lingxiao X, Mei Y, et al. Plasma microRNAs as potential biomarkers for non-small-cell lung cancer. Lab Invest 2011;91:579–87.

[253] Fernandez-Mercado M, Manterola L, Larrea E, Goicoechea I, Arestin M, Armesto M, et al. The circulating transcriptome as a source of non-invasive cancer biomarkers: concepts and controversies of non-coding and coding RNA in body fluids. J Cell Mol Med 2015;19:2307–23.

[254] Rademakers SE, Lok J, van der Kogel AJ, Bussink J, Kaanders JH. Metabolic markers in relation to hypoxia; staining patterns and colocalization of pimonidazole, HIF-1α, CAIX, LDH-5, GLUT-1, MCT1 and MCT4. BMC Cancer 2011;11:167.

[255] Schmitz S, Duhoux F, Machiels J-P. Window of opportunity studies: Do they fulfil our expectations? Cancer Treat Rev 2016;43:50–7.

[256] Rasey JS, Koh WJ, Evans ML, Peterson LM, Lewellen TK, Graham MM, et al. Quantifying regional hypoxia in human tumors with positron emission tomography of [18F]fluoromisonidazole: a pretherapy study of 37 patients. Int J Radiat Oncol Biol Phys 1996;36:417–28.

[257] Trinkaus ME, Blum R, Rischin D, Callahan J, Bressel M, Segard T, et al. Imaging of hypoxia with 18F-FAZA PET in patients with locally advanced non-small cell lung cancer treated with definitive chemoradiotherapy. J Med Imaging Radiat Oncol 2013;57:475–81.

[258] Postema EJ, McEwan AJB, Riauka TA, Kumar P, Richmond DA, Abrams DN, et al. Initial results of hypoxia imaging using 1-α-d-(5-deoxy-5-[18F]-fluoroarabinofuranosyl)-2-nitroimidazole (18F-FAZA). Eur J Nucl Med Mol Imaging 2009;36:1565–73.

[259] Graves EE, Vilalta M, Cecic IK, Erler JT, Tran PT, Felsher D, et al. Hypoxia in models of lung cancer: implications for targeted therapeutics. Clin Cancer Res 2010;16:4843–52.

[260] Schwartz LH, Litière S, de Vries E, Ford R, Gwyther S, Mandrekar S, et al. RECIST 1.1—Update and clarification: From the RECIST committee. Eur J Cancer 2016;62:132–7.

[261] National Lung Cancer Audit: Clinical Outcome Publication Report 2018. https://www.hqip.org.uk/resource/national-lung-cancer-audit-clinical-outcome-publication-report-2018/ (accessed September 8, 2019).

[262] Puri T, Greenhalgh TA, Wilson JM, Franklin J, Wang LM, Strauss V, et al. [18F]Fluoromisonidazole PET in rectal cancer. EJNMMI Res 2017;7.

[263] Chu LL, Knebel RJ, Shay AD, Santos J, Badawi RD, Gandara DR, et al. CT perfusion imaging of lung cancer: benefit of motion correction for blood flow estimates. Eur Radiol 2018;28:5069–75.

[264] Bollineni VR, Kerner GSMA, Pruim J, Steenbakkers RJHM, Wiegman EM, Koole MJB, et al. PET Imaging of Tumor Hypoxia Using 18F-Fluoroazomycin Arabinoside in Stage III–IV Non–Small Cell Lung Cancer Patients. J Nucl Med 2013;54:1175–80.

[265] Li X-F, Du Y, Ma Y, Postel GC, Civelek AC. 18F-Fluorodeoxyglucose Uptake and Tumor Hypoxia: Revisit 18F-Fluorodeoxyglucose in Oncology Application. Transl Oncol 2014;7:240–7.

[266] Kinoshita T, Fujii H, Hayashi Y, Kamiyama I, Ohtsuka T, Asamura H. Prognostic significance of hypoxic PET using 18F-FAZA and 62Cu-ATSM in non-small-cell lung cancer. Lung Cancer 2016;91:56–66.

[267] Dierckx RA, Van de Wiele C. FDG uptake, a surrogate of tumour hypoxia? Eur J Nucl Med Mol Imaging 2008;35:1544–9.

[268] Wilson JM, Fokas E, Dutton SJ, Patel N, Hawkins MA, Eccles C, et al. ARCII: A phase II trial of the HIV protease inhibitor Nelfinavir in combination with chemoradiation for locally advanced inoperable pancreatic cancer. Radiother Oncol 2016;119:306–11.

[269] Hill EJ, Roberts C, Franklin JM, Enescu M, West N, MacGregor TP, et al. Clinical Trial of Oral Nelfinavir before and during Radiation Therapy for Advanced Rectal Cancer. Clin Cancer Res 2016;22:1922–31.

[270] Rengan R, Mick R, Pryma D, Rosen MA, Lin L, Maity A, et al. A Phase I Trial of the HIV Protease Inhibitor Nelfinavir with Concurrent Chemoradiotherapy (CT-RT) for Unresectable Stage IIIA/IIIB NSCLC: A Report of Toxicities and Clinical Response. J Thorac Oncol 2012;7:709–15.

[271] Stieb S, Eleftheriou A, Warnock G, Guckenberger M, Riesterer O. Longitudinal PET imaging of tumor hypoxia during the course of radiotherapy. Eur J Nucl Med Mol Imaging 2018;45:2201–17.

[272] Zips D, Zöphel K, Abolmaali N, Perrin R, Abramyuk A, Haase R, et al. Exploratory prospective trial of hypoxia-specific PET imaging during radiochemotherapy in patients with locally advanced head-and-neck cancer. Radiother Oncol 2012;105:21–8.

[273] Löck S, Perrin R, Seidlitz A, Bandurska-Luque A, Zschaeck S, Zöphel K, et al. Residual tumour hypoxia in head-and-neck cancer patients undergoing primary radiochemotherapy, final results of a prospective trial on repeat FMISO-PET imaging. Radiother Oncol 2017;124:533–40.

[274] Mortensen LS, Johansen J, Kallehauge J, Primdahl H, Busk M, Lassen P, et al. FAZA PET/CT hypoxia imaging in patients with squamous cell carcinoma of the head and neck treated with radiotherapy: Results from the DAHANCA 24 trial. Radiother Oncol 2012;105:14–20.

[275] Kimura H, Braun RD, Ong ET, Hsu R, Secomb TW, Papahadjopoulos D, et al. Fluctuations in red cell flux in tumor microvessels can lead to transient hypoxia and reoxygenation in tumor parenchyma. Cancer Res 1996;56:5522–8.

[276] Dewhirst MW, Kimura H, Rehmus SW, Braun RD, Papahadjopoulos D, Hong K, et al. Microvascular studies on the origins of perfusion-limited hypoxia. Br J Cancer 1996;27:S247-251.

[277] Padera TP, Stoll BR, Tooredman JB, Capen D, di Tomaso E, Jain RK. Pathology: cancer cells compress intratumour vessels. Nature 2004;427:695.

[278] Petersson J, Glenny RW. Gas exchange and ventilation–perfusion relationships in the lung. Eur Respir J 2014;44:1023–41.

[279] Win T, Tasker AD, Groves AM, White C, Ritchie AJ, Wells FC, et al. Ventilation-Perfusion Scintigraphy to Predict Postoperative Pulmonary Function in Lung Cancer Patients Undergoing Pneumonectomy. Am J Roentgenol 2006;187:1260–5.

[280] Ostheimer C, Bache M, Güttler A, Kotzsch M, Vordermark D. A pilot study on potential plasma hypoxia markers in the radiotherapy of non-small cell lung cancer. Strahlenther Onkol 2014;190:276.

[281] Ivan M, Huang X. miR-210: Fine-Tuning the Hypoxic Response. Adv Exp Med Biol 2014;772:205–27.

[282] Kirschner MB, Edelman JJB, Kao SC-H, Vallely MP, van Zandwijk N, Reid G. The Impact of Hemolysis on Cell-Free microRNA Biomarkers. Front Genet 2013;4.

[283] Lai Y, Wang X, Zeng T, Xing S, Dai S, Wang J, et al. Serum VEGF levels in the early diagnosis and severity assessment of non-small cell lung cancer. J Cancer 2018;9:1538–47.

[284] Jankovic B, Aquino-Parsons C, Raleigh JA, Stanbridge EJ, Durand RE, Banath JP, et al. Comparison between pimonidazole binding, oxygen electrode measurements, and expression of endogenous hypoxia markers in cancer of the uterine cervix. Cytometry B Clin Cytom 2006;70:45–55.

[285] Mayer A, Höckel M, Vaupel P. Carbonic Anhydrase IX Expression and Tumor Oxygenation Status Do Not Correlate at the Microregional Level in Locally Advanced Cancers of the Uterine Cervix. Clin Cancer Res 2005;11:7220–5.

[286] Mayer A, Zahnreich S, Brieger J, Vaupel P, Schmidberger H. Downregulation of EGFR in hypoxic, diffusion-limited areas of squamous cell carcinomas of the head and neck. Br J Cancer 2016;115:1351–8.

[287] Kaanders JHAM, Wijffels KIEM, Marres HAM, Ljungkvist ASE, Pop LAM, van den Hoogen FJA, et al. Pimonidazole binding and tumor vascularity predict for treatment outcome in head and neck cancer. Cancer Res 2002;62:7066–74.

[288] Le Q-T, Courter D. Clinical Biomarkers for Hypoxia Targeting. Cancer Metastasis Rev 2008;27:351–62.

[289] Ostheimer C, Bache M, Güttler A, Reese T, Vordermark D. Prognostic information of serial plasma osteopontin measurement in radiotherapy of non-small-cell lung cancer. BMC Cancer 2014;14:858.

[290] Zegers CML, Hoebers FJP, van Elmpt W, Bons JA, Öllers MC, Troost EGC, et al. Evaluation of tumour hypoxia during radiotherapy using [18F]HX4 PET imaging and blood biomarkers in patients with head and neck cancer. Eur J Nucl Med Mol Imaging 2016;43:2139–46.

[291] Mok T, Gorbunova V, Juhasz E, Szima B, Burdaeva O, Orlov S, et al. A Correlative Biomarker Analysis of the Combination of Bevacizumab and Carboplatin-Based Chemotherapy for Advanced Nonsquamous Non–Small-Cell

Lung Cancer: Results of the Phase II Randomized ABIGAIL Study (BO21015). J Thorac Oncol 2014;9:848–55.

[292] Beasley NJ, Wykoff CC, Watson PH, Leek R, Turley H, Gatter K, et al. Carbonic anhydrase IX, an endogenous hypoxia marker, expression in head and neck squamous cell carcinoma and its relationship to hypoxia, necrosis, and microvessel density. Cancer Res 2001;61:5262–7.

[293] Vercellino L, Groheux D, Thoury A, Delord M, Schlageter M-H, Delpech Y, et al. Hypoxia imaging of uterine cervix carcinoma with (18)F-FETNIM PET/CT. Clin Nucl Med 2012;37:1065–8.

[294] Kawai N, Lin W, Cao W-D, Ogawa D, Miyake K, Haba R, et al. Correlation between ^{18}F-fluoromisonidazole PET and expression of HIF-1α and VEGF in newly diagnosed and recurrent malignant gliomas. Eur J Nucl Med Mol Imaging 2014;41:1870–8.

[295] Bekaert L, Valable S, Lechapt-Zalcman E, Ponte K, Collet S, Constans J-M, et al. [18F]-FMISO PET study of hypoxia in gliomas before surgery: correlation with molecular markers of hypoxia and angiogenesis. Eur J Nucl Med Mol Imaging 2017;44:1383–92.

[296] Wang KX, Denhardt DT. Osteopontin: role in immune regulation and stress responses. Cytokine Growth Factor Rev 2008;19:333–45.

[297] Vaschetto R, Nicola S, Olivieri C, Boggio E, Piccolella F, Mesturini R, et al. Serum levels of osteopontin are increased in SIRS and sepsis. Intensive Care Med 2008;34:2176–84.

[298] Li Z-H, Zhang H, Yang Z-G, Wen G-Q, Cui Y-B, Shao G-G. Prognostic significance of serum microRNA-210 levels in nonsmall-cell lung cancer. J Int Med Res 2013;41:1437–44.

[299] Mortensen LS, Buus S, Nordsmark M, Bentzen L, Munk OL, Keiding S, et al. Identifying hypoxia in human tumors: A correlation study between 18F-FMISO PET and the Eppendorf oxygen-sensitive electrode. Acta Oncol 2010;49:934–40.

[300] Mandeville HC, Ng QS, Daley FM, Barber PR, Pierce G, Finch J, et al. Operable Non–Small Cell Lung Cancer: Correlation of Volumetric Helical Dynamic Contrast-enhanced CT Parameters with Immunohistochemical Markers of Tumor Hypoxia. Radiology 2012;264:581–9.

[301] Quartuccio N, Asselin M-C. The Validation Path of Hypoxia PET Imaging: Focus on Brain Tumours. Curr Med Chem 2018;25:3074–95.

[302] Coates JT, Skwarski M, Higgins GS. Targeting tumour hypoxia: shifting focus from oxygen supply to demand. Br J Radiol 2018:20170843.

[303] Heiden MGV, DeBerardinis RJ. Understanding the intersections between metabolism and cancer biology. Cell 2017;168:657–69.

[304] Frank DA. STAT3 as a central mediator of neoplastic cellular transformation. Cancer Lett 2007;251:199–210.

[305] Xiang M, Kim H, Ho VT, Walker SR, Bar-Natan M, Anahtar M, et al. Gene expression–based discovery of atovaquone as a STAT3 inhibitor and anticancer agent. Blood 2016;128:1845–53.

[306] Lv Z, Yan X, Lu L, Su C, He Y. Atovaquone enhances doxorubicin's efficacy via inhibiting mitochondrial respiration and STAT3 in aggressive thyroid cancer. J Bioenerg Biomembr 2018;50:263–70.

[307] Sun Y, Xu H, Chen X, Li X, Luo B. Inhibition of mitochondrial respiration overcomes hepatocellular carcinoma chemoresistance. Biochem Biophys Res Commun 2019;508:626–32.

[308] Chen D, Sun X, Zhang X, Cao J. Targeting mitochondria by anthelmintic drug atovaquone sensitizes renal cell carcinoma to chemotherapy and immunotherapy. J Biochem Mol Toxicol 2018;32:e22195.

[309] Gao X, Liu X, Shan W, Liu Q, Wang C, Zheng J, et al. Anti-malarial atovaquone exhibits anti-tumor effects by inducing DNA damage in hepatocellular carcinoma. Am J Cancer Res 2018;8:1697–711.

[310] O'Connor JPB, Aboagye EO, Adams JE, Aerts HJWL, Barrington SF, Beer AJ, et al. Imaging biomarker roadmap for cancer studies. Nat Rev Clin Oncol 2017;14:169–86.

[311] Zhou H, Yuan Y, Nie L. Accuracy, Safety, and Reliability of Novel Phase I Trial Designs. Clin Cancer Res 2018;24:4357–64.

APPENDIX

Appendix Table 1: Baseline hyp-PET data for all patients

Patient	Cohort	Tracer	Tumour volume (mL)	FDG PET SUV_{max}	HV ≥1.5 mL (Y/N)	HV (mL)	HV%	TBR_{mean}	TBR_{max}	TBR_{peak}
10001	1	FMISO	89.5	22.8	Y	31.8	35.5	1.3	2.8	2.4
10004	1	FAZA	184.9	24.5	Y	97.7	52.8	1.4	2.5	2.2
10005	1	FMISO	61.0	11.9	Y	8.2	13.4	1.1	2.5	2.1
10006	1	FMISO	179.5	18	Y	50.8	28.3	1.3	2.3	2.0
10007	1	FMISO	19.4	15.7	N	0.6	3.1	1.0	1.7	1.4
10008	1	FMISO	17.8	12.2	Y	1.7	9.6	1.0	2.1	1.6
10009	1	FMISO	59.3	12.5	Y	33.6	56.7	1.6	2.8	2.5
10010	1	FMISO	371.1	22.9	Y	188.3	50.7	1.5	3.2	2.6
10011	1	FMISO	24.6	21.7	Y	1.8	7.3	1.0	1.9	1.5
10012	1	FMISO	15.2	30	N	0	0.0	0.9	1.3	1.1
10013	1	FMISO	15.5	25.7	Y	5.4	34.8	1.3	2.0	1.7
10014	1	FMISO	42.2	17.2	Y	2.7	6.4	1.1	1.6	1.5
10015	1	FMISO	37.1	3.8	N	0	0.0	0.8	1.3	1.2
10016	1	FMISO	30.6	26.8	Y	6.7	21.9	1.2	2.2	1.9
10017	1	FMISO	24.4	4.5	N	0	0.0	0.7	1.1	1.0
10018	1	FMISO	2.4	15.6	N	0	0.0	0.8	1.4	
10019	1	FMISO	366.9	20.9	Y	201.7	55.0	1.7	6.0	4.3
10020	1	FMISO	85.3	28	Y	35.3	41.4	1.3	2.4	2.0
10022	1	FMISO	45.9	13.7	Y	28.9	63.0	1.6	3.7	2.8
10023	1	FMISO	33.4	11.1	Y	6.9	20.7	1.1	2.3	1.8
10024	2	FMISO	45.8	10.2	Y	26.2	57.2	1.5	2.8	2.2
10025	2	FMISO	40.8	12.8	Y	4.9	12.0	1.1	2.0	1.6
10026	2	FMISO	43.4	7.9	N	0	0.0	1.0	1.4	1.3
10027	2	FMISO	27.9	43.3	N	0	0.0	0.9	1.3	1.1
10028	2	FMISO	20.6	13.9	Y	11.8	57.3	1.8	5.2	3.6
10029	2	FMISO	24.1	6.8	Y	1.6	6.6	0.9	1.7	1.5
10030	2	FMISO	243.0	30.7	Y	44.2	18.2	1.1	4.2	3.4
10031	2	FMISO	5.4	18.9	Y	1.9	35.2	1.3	3.0	2.1
10032	2	FMISO	11.1	9.6	N	0.6	5.4	1.0	1.5	1.3
10033	2	FMISO	6.3	18.1	Y	3.5	55.6	1.5	2.6	2.2
10034	2	FMISO	43.7	19	Y	21.7	49.7	1.5	3.4	3.0
10035	2	FMISO	2.5	18.5	N	0.8	32.0	1.2	2.9	
10036	2	FMISO	35.9	14.4	Y	1.7	4.7	0.9	1.7	1.5
10037	2	FMISO	19.1	12.2	N	0.1	0.5	0.8	1.5	1.2
10038	2	FMISO	32.7	14.3	N	0.2	0.6	1.0	1.5	1.3
10039	2	FMISO	144.8	10.5	Y	34.0	23.5	1.2	3.0	2.2
10040	2	FMISO	2.9	12.7	N	0.1	3.4	0.9	1.5	
10041	2	FMISO	20.0	15.9	Y	4.2	21.0	1.2	2.0	1.7
10042	2	FMISO	7.6	13.8	N	0	0.0	0.7	1.1	0.9
10043	2	FMISO	80.7	25.9	Y	40.5	50.2	1.4	2.1	1.9
10044	2	FMISO	45.3	16	Y	2.6	5.7	1.0	2.0	1.5
10045	2	FMISO	185.4		Y	44.8	24.2	1.2	2.7	2.3
10046	2	FMISO	57.5	15	Y	11.4	19.8	1.1	2.3	1.8

Abbreviations: FMISO, [18F]-fluoromisonidazole; FAZA, [18F]- fluoroazomycin arabinoside; FDG, fluorodeoxyglucose; PET, positron emission tomography; HV, hypoxic volume; HV%, hypoxic volume percentage; TBR, tumour-to-blood ratio; IQR, interquartile range

Appendix Table 2: Cohort 1 perfusion CT data

	Unmatched						Matched					
Patient	**Pre BF**	**Pre BV**	**Pre MTT**	**Post BF**	**Post BV**	**Post MTT**	**Pre BF**	**Pre BV**	**Pre MTT**	**Post BF**	**Post BV**	**Post MTT**
10001	107.9	9.0	6.2	120.2	9.3	7.3	107.9	9.0	6.2	120.2	9.3	7.3
10003*	162.0	6.1	2.6	93.8	4.0	2.5	162.0	6.1	2.6	93.8	4.0	2.5
10004	63.2	6.7	8.7	61.5	7.5	10.1	63.2	6.7	8.7	61.5	7.5	10.1
10005	38.3	2.6	6.0	71.6	4.5	5.8	38.3	2.6	6.0	71.5	4.3	5.7
10006	77.6	5.0	6.8	79.8	4.8	6.3	77.6	5.0	6.8	79.8	4.8	6.3
10007*	87.8	6.7	6.8	80.4	6.3	8.4	87.8	6.7	6.8	80.4	6.3	8.4
10008	115.9	5.6	5.8	133.4	5.6	4.7	115.9	5.6	5.8	133.4	5.6	4.7
10009	105.5	5.1	4.8	132.2	5.8	4.3	105.5	5.1	4.8	132.2	5.8	4.3
10010	24.5	2.7	9.6	27.9	2.6	8.7	23.3	2.7	9.8	26.5	2.5	8.7
10011	111.3	8.4	7.2	104.4	8.1	8.6	111.3	8.4	7.2	104.4	8.1	8.6
10012*	135.1	8.2	5.5									
10014	186.8	7.7	3.6	165.2	7.9	5.2	198.1	7.8	3.2	165.2	7.9	5.2
10015*	109.7	4.8	2.7									
10016	73.9	4.1	5.6	63.9	3.3	5.3	70.5	3.7	5.4	63.9	3.3	5.3
10017*	110.3	4.1	3.7									
10018*	52.1	4.8	7.7									
10019	48.9	7.4	4.9	59.9	7.3	4.9	49.5	7.4	4.9	59.5	7.3	4.9
10020	80.9	6.8	7.0	72.0	5.1	6.7	80.9	6.8	7.0	72.0	5.1	6.7
10022	64.3	5.6	7.6	45.4	5.6	10.9	64.9	5.7	7.7	45.2	5.4	10.7
10023	129.7	8.1	7.6	104.9	6.6	6.6	112.0	7.7	7.9	104.9	6.6	6.6

*Unevaluable for change in hypoxia analysis using hyp-PET
Abbreviations: BF, blood flow; BV, blood volume; MTT, mean transit time; pCT, perfusion CT; IQR, interquartile range

Appendix Table 3: Cohort 2 perfusion CT data

	Unmatched						Matched					
Patient	**Pre BF**	**Pre BV**	**Pre MTT**	**Post BF**	**Post BV**	**Post MTT**	**Pre BF**	**Pre BV**	**Pre MTT**	**Post BF**	**Post BV**	**Post MTT**
10024	33.3	2.5	11.0	30.1	2.6	10.2	33.5	2.5	11.0	30.1	2.6	10.2
10025	59.9	4.0	5.9	41.3	3.0	4.3	48.2	3.5	6.0	44.5	3.3	4.7
10026*	187.3	8.7	4.4									
10027*	40.4	2.6	4.2									
10028	62.8	6.2	8.4	70.8	6.4	7.4	62.8	6.2	8.4	70.8	6.4	7.4
10029	107.6	6.4	5.9									
10030	41.1	3.2	6.9	42.2	3.8	6.7	42.1	3.1	6.7	44.8	3.9	6.5
10031				121.2	4.9	3.3						
10032*	114.9	4.4	3.2									
10033	91.7	4.9	7.1									
10034	43.2	2.3	3.2									
10035*	41.1	2.6	6.4									
10036				38.4	4.0	8.6						
10037*	80.8	8.3	8.7									
10038*	106.0	5.7	4.6									
10039				70.7	3.4	4.9						
10040*	161.0	6.4	3.1									
10041	75.6	4.0	5.1									
10042*	80.0	3.2	4.2									
10043	92.2	6.9	5.9	65.1	6.6	8.6	98.6	6.8	5.3	65.3	6.5	8.5
10044	71.2	7.2	9.0	74.2	7.2	9.1	72.1	7.3	8.9	71.2	7.2	9.3
10045	92.0	4.5	6.0									
10046				68.9	3.1	1.5						

*Unevaluable for change in hypoxia analysis using hyp-PET
Abbreviations: BF, blood flow; BV, blood volume; MTT, mean transit time; pCT, perfusion CT; IQR, interquartile range